# EXPERIMENTAL DETERMINATION OF PRE-ERUPTIVE STORAGE CONDITIONS AND CONTINUOUS DECOMPRESSION OF RHYODACITE MAGMA ERUPTED FROM CHAOS CRAGS, LASSEN VOLCANIC CENTER, CALIFORNIA

By

Erin Todd Quinn

A Thesis Presented to

The Faculty of Humboldt State University

In Partial Fulfillment of the Requirements for the Degree

Master of Science

In Environmental Systems: Geology

Committee Membership

Dr. Brandon E. Schwab, Committee Chair

Dr. Benjamin J. Andrews, Committee Member

Dr. Michael A. Clynne, Committee Member

Dr. Christopher J. Dugaw, Graduate Coordinator

May 2014

## ABSTRACT

EXPERIMENTAL DETERMINATION OF PRE-ERUPTIVE STORAGE CONDITIONS AND CONTINUOUS DECOMPRESSION OF RHYODACITE MAGMA ERUPTED FROM CHAOS CRAGS, LASSEN VOLCANIC CENTER, CALIFORNIA

Erin Todd Quinn

A series of hydrothermal (high-temperature and -pressure) phase equilibrium experiments were performed on a natural rhyodacite pumice from the 1,050 calibrated years B.P. pyroclastic flow from the Chaos Crags, Lassen Volcanic Center, California. The pumice (LQ13-01, collected at the same location as LC84-417 by M.A. Clynne) is from the lower pyroclastic flow member of the group 1 lavas, the most silicic products known of Chaos Crags. Group 1 lavas are homogeneous (bulk rock containing 69-70 wt. % $SiO_2$), petrographically and compositionally similar with rare to sparse mafic inclusions, and comprise the earliest emplaced units of Chaos Crags, the lower, middle, and upper pyroclastic flows, and domes A and B. Group 2 lavas are comparatively heterogeneous (bulk rock containing 67-69 wt. % $SiO_2$), with increasing abundance (10-15%) of mafic inclusions throughout the emplacement sequence, and comprise domes C through F. The phase assemblage in the natural sample used as experimental starting material comprises phenocrysts of quartz, plagioclase feldspar with rims of ~$An_{35}$, biotite, hornblende, and Fe-Ti oxides in a vesiculated glassy matrix. Trace mafic enclaves

are also present, but were removed from experimental starting material. All experiments were performed in cold-seal furnaces at the Smithsonian Institution, under $H_2O$-saturated conditions at pressures of 75 MPa to 200 MPa and temperatures of 750°C to 900°C, at oxygen fugacity ($fO_2$) NNO+1 (±0.5-log-units), for 93 to 142 hours. SEM analyses of experimental products show quartz is stable at ≤200 MPa at 750°C to <175 MPa at 775°C and at 75 MPa at 800°C, and is not stable at temperatures ≥825°C, within the investigated pressure range. Amphibole is stable at >75 MPa at 750°C to >100 MPa at 775°C and at 200 MPa at 825°C, and is not stable at 75 MPa or ≥850°C. Biotite is stable at all investigated pressures at 750°C, stable >125 MPa at 800°C, and is not stable for any pressure at ≥850°C. Pyroxene, not present in the starting material is stable at 200 MPa at ≥800°C and all investigated pressures at ≥825°C. EPMA analyses of 16 titanomagnetite-ilmenite touching pairs have equilibrium temperatures of 760-775°C and $fO_2$ of ~NNO+1.35 (model of Ghiorso and Evans, 2008). FTIR analysis of 34 quartz-hosted melt inclusions contain 3.99±0.40 to 6.48±0.65 wt.% (the bulk of analyses cluster between 3.99±0.40 and 5.42±0.54 wt. %) and up to 361±36 ppm $CO_2$, suggesting saturation pressures of 92-297 MPa (model of Papale et al., 2006). EPMA analyses of amphibole rims show chemical equilibrium (model of Ridolfi et al., 2010) occurred at lower $H_2O_{melt}$ concentrations, lower pressure (71-89 MPa), slightly higher temperature (772-810°C), and more oxidizing (NNO+2.0 to NNO+2.6 log-units) conditions than melt inclusions and titanomagnetite-ilmenite pairs suggest. Comparison of the natural samples with experimental run products suggests $H_2O$-saturated pre-eruptive pressure-temperature storage conditions of 145±25 MPa and 770±10°C.

Continuous decompression experiments were conducted using experimental run product CCPb-34, equilibrated at 120 MPa and 775°C, with sufficient $H_2O$ to ensure $H_2O$-saturated conditions, as a starting material. Decompression rates ranged from 8.5 MPa/hr to 0.35 MPa/hr, corresponding to total decompression times of 16 hours to 54 days. SEM and EPMA textural and geochemical comparisons between continuous decompression experimental run products and natural samples indicate that decompression and ascent of magma producing group 1 lavas was relatively quick, >2.6 MPa/hr (corresponding to minimum ascent velocity of 100 m/hr and total decompression times of <48 hrs), whereas magma that produced group 2 lavas (domes C-F) decompressed and ascended relatively slowly, <2.6 MPa/hr (corresponding to ascent velocity of <100 m/hr and total decompression times >48 hrs).

## ACKNOWLEDGEMENTS

First and foremost, I thank my committee chair, advisor, mentor, and friend, Brandon Schwab for his support, patience, and shared wisdom. I attribute many of my successes, in science and life, to the conversations we have had, and teachings and philosophies he has given me. Thank you, Brandon, for giving me the opportunity and support that would have been hard to find elsewhere.

Thank you very much to Ben Andrews, my advisor and mentor during the SI Predoctoral Fellowship at SI in Washington, DC. Ben provided me the training necessary to use much of the lab equipment, and placed trust in me with the equipment, a brave task for sure. It was an incredible experience for me, and Ben brought me in like family. Thank you, Ben, this was awesome and I look forward to our continued research.

To the most knowledgeable person regarding most aspects Lassen volcanism, Michael Clynne, thank you for everything. From my e-mails as an undergraduate, sample collecting at Chaos Crags, the many conversations throughout the graduate experience, to the thesis and conference abstract reviews, thank you so much. It is unbelievable to have your wealth of knowledge and experience during this process. The geoscience community and I are thankful for your service and research, and we wish there were two of you, one researcher and one university professor.

Though Ben and Mike do not have the official title of Professor, they still take on the duties of Professor. Your shared knowledge and experiences are much appreciated.

To the additional folks during my time in DC, thank you very much for the conversations, trivia nights, beverages, and good times. Rob Dennen, knowing you were

working by my side and our ventures to happy hour made working all those long days much easier. Tim Gooding, I wish I could take you with me everywhere I go. Tim G. also trained me in the lab and answered many of my impractical questions. Tim Rose, Emma Bullock, Stephanie Grocke, Brendan McCormick, Gabrielle Ramirez, and everyone else who I had the pleasure of working with at SI, thank you for making me feel welcome.

Thank you, Jon Castro and Brandon, for sharing your in-prep work on Lassen Peak storage conditions.

Thanks to John Donovan, Dana Johnston, and Julie Barkman of University of Oregon for their welcoming nature and help with EPMA.

A tremendous thanks goes out to all of the folks at Humboldt State University. Thank you to the staff, Laurie Marx, Stephen Tillinghast, Colin Wingfield, and Marty Reed for all your help along the way.

To my professors, William Miller, Susan Cashman, Mark Hemphill-Haley, Andre Lehre, Lori Dengler, Raymond “Bud” Burke, Melanie Michalak, Fred Hochstaedter, and Leslie Turrini-Smith, thank you for sharing the fascinating world of geology with me.

Thank you, Keith Putirka of Fresno State University, for the letters of recommendation. I wish you and your students much success and look forward to seeing your work on Chaos Crags and the Lassen region.

Thank you to the National Park Service for allowing me to collect samples with Dr. Clynne, and Smithsonian Institution Fellowship Program, an NMNH Small Grant, NSF MRI 1126200 awarded to Humboldt State University, and NSF Grant EAR-0510366 awarded to Brandon Schwab, for funding much of this research.

Most importantly, I thank my family and friends for their unwavering support. Grandma, Mom, Dad, Trevor, Kerry, Tony, Antonio, Andrew, Jean, and Dave, I love you all and despite the geographic distance, you are always in my thoughts and I could not have done this without you. Angeline, Harper (the individual who has championed me along the most during this process), and Avery Schwab, thank you for welcoming me into your house, home, and family, and I look forward to the next Calrizian tour. To all of my friends and schoolmates, J. Padgett, Sylvia Nicovich, Anna Hall, Steve Tillinghast, Colin Wingfield, and others, thank you for the wonderful journey.

## TABLE OF CONTENTS

## LIST OF TABLES

## LIST OF FIGURES

## LIST OF APPENDICES

# INTRODUCTION

The Lassen Volcanic Center (LVC, Figure 1) and Lassen region in northern California has hosted at least 70 eruptions in the past 100,000 years (Clynne et al., 2012), including explosive events, ash fall, and emplacement of lava flows and domes, with associated production of lahars. This region poses a major threat to aviation, nearby population centers, and regional infrastructure. The National Volcano Early Warning System (NVEWS) assessment by the United States Geological Survey (USGS) has designated the LVC as a "high threat" that necessitates monitoring, to provide the ability to track detailed changes in real-time and to develop, test, and apply models of ongoing and expected activity (Ewert et al., 2005).

The 1,050 calibrated years B.P. eruptive sequence of the Chaos Crags is the largest recognized LVC eruption in the last 25 k.a. with an erupted volume of ~1.19 $km^3$ (Clynne et al., 2012). Eruptive products from the Chaos Crags and from the nearby 1915 eruption of Lassen Peak have rhyodacite and dacite, respectively, as the dominant rock types. Both sequences contain abundant mafic inclusions, evidence for magma mixing and mingling between host silicic and intruding mafic components (e.g., Heiken and Eichelberger, 1980; Tepley et al., 1999; Clynne, 1993, 1999; Feeley et al., 2008a). Mixing and mingling of mafic and silicic magmas is common in arc settings and may trigger eruption (e.g., Eichelberger et al., 2000).

Despite those observations and numerous investigations of magmatic processes at Chaos Crags and Lassen (Heiken and Eichelberger, 1980; Clynne 1993, 1999; Tepley et al., 1999; Schwab and Castro 2007; Feeley et al., 2008a; Quinn and Schwab, 2012;

Andrews and Manga, 2014; Klemetti and Clynne, in prep), no experimental constraints on pre-eruptive storage conditions of silicic end-member host magmas from the LVC were available until the recent experimental work of Schwab and Castro (2007) who explored pre-eruptive storage conditions of the 1915 Lassen Peak dacite host magma.

This work uses cold-seal hydrothermal experiments to determine pre-eruptive storage conditions and rates of decompression of the rhyodacite host magma erupted from Chaos Crags, to assist in better understanding of the complexities of the LVC and arc volcanism in general.

**Tectonic setting**

The Cascade Volcanic Arc (Figure 1), an arc of nearly twenty major volcanoes and thousands of additional volcanic vents in British Columbia, Washington, Oregon, and California, is the result oblique subduction of the oceanic Explorer, Juan de Fuca, and Gorda Plates beneath the continental North American Plate. At the surface, subduction is terminated by strike-slip faults; the Queen Charlotte Fault on the north and the San Andreas Fault on the south.

**The Lassen region and associated volcanism**

The LVC is located at the southern end of the Cascade Volcanic Arc (Figure 1), ~275 km east of subduction at the surface. Abundant volcanic activity in the Lassen area began at ~7 M.a. (Feeley et al., 2008a). The region hosts regional and local scales of volcanism (Clynne et al., 2012). Regional-scale volcanism built a broad platform that covers the southernmost Cascade Range (Clynne and Muffler, 2010) and consists of hundreds of closely space, small, short-lived volcanoes and a few larger lava cones and

shield volcanoes. These volcanoes are primarily composed of calc-alkaline basalt, associated with Cascade Arc magmatism, as well as tholeiitic basalt, related to the Basin and Range geologic province (Clynne, 1993; Borg et al., 2002). Local-scale volcanism is superimposed on top of the regional volcanism and consists of a few, much larger, long-lived (0.5-1.0 m.y. or longer) volcanic centers, with the LVC the currently active volcanic center. Seismic refraction studies (Berge and Monfort, 1986; Berge and Stauber, 1987) show that the uppermost stratigraphy of the Lassen area consists of volcanic rocks ~4 km thick, and gravity studies (Jachens and Saltus, 1983) and geologic mapping (Williams, 1932; Wilson, 1961; Macdonald, 1963, 1964, 1965; Christiansen et al., 2002; Clynne and Muffler, 2010) infer that rocks underlying the upper ~4km are primarily Paleozoic to Mesozoic igneous and metamorphic basement of the Sierran and Klamath terranes.

The LVC (~825 k.a.-present) consists of three eruptive stages. These include: 1) Rockland caldera complex (~825-609 k.a.), 2) Brokeoff Volcano (~590-385 k.a.), and 3) Lassen domefield (~300 k.a.-present). Within the Lassen domefield stage, three eruptive sequences of Holocene age have been identified at: Chaos Crags 1,050 calibrated years B.P. (Clynne et al., 2012), Cinder Cone 1666 C.E. (Sheppard et al., 2009), and Lassen Peak 1914-1917 (Clynne et al., 1999).

To preserve the landscape, Cinder Cone National Monument and Lassen Peak National Monument were created in 1907. The 1914-1917 eruption at Lassen Peak led to the 1916 establishment of Lassen Volcanic National Park (LVNP, Figure 2), which combined and expanded the two pre-existing national monuments. In 1927, a museum

was opened to educate the public on the region's biological and geological diversity (Loomis, 1926).

**Chaos Crags eruptive history and eruptive products**

Chaos Crags (Figures 3 and 4) consists of a group of six dacitic to rhyodacitic (bulk rock ~67-70 wt. % $SiO_2$; Appendix A) lava domes (labeled A-F) with abundant mafic inclusions and associated pyroclastic deposits, including 3 pyroclastic flows (lower, middle, and upper), located in the northwestern corner of LVNP within the LVC. The eruptions began 1,050 years B.P. with a vent-opening phase followed by explosive eruption and emplacement of the lower and middle pyroclastic flows (Clynne et al., 2008a). The flows were erupted from a vent on the ridge north of Lassen Peak that separates the Lost Creek and Manzanita Creek drainages (Figure 2). Extrusion of a small lava dome (dome A) and cooling of magma in the conduit briefly plugged the vent. Reopening of the conduit and explosive disruption of dome A resulted in emplacement of the upper pyroclastic flow. The upper pyroclastic flow contains the same amount of glass as the lower and middle pyroclastic flows, and breadcrusted pumice, suggesting some volatile loss, but not enough to force crystallization. Subsequently, domes B through F were emplaced (Clynne et al., 2008a).

Chaos Crags eruptive products are categorized into two main compositional groups. Group 1 lavas (Figure 5a-c) are homogeneous, with bulk rock compositions having 69-70 wt. % $SiO_2$ (Appendix A; Clynne et al., 2008b), and are petrographically similar with rare to sparse mafic inclusions. Group 1 comprises the earliest emplaced units of Chaos Crags including the lower, middle, and upper pyroclastic flows, and

domes A and B. Group 2 lavas (Figure 6a-c) are in turn comparatively heterogeneous, with bulk rock compositions having 67-69 wt. % $SiO_2$, (Appendix A; Clynne et al., 2008b), and contain abundant (10-15%) mafic inclusions throughout the emplacement sequence. Group 2 comprises domes C through F. Also contained in both lavas are resorbed mineral phases, and small fragments of disaggregated inclusions (Clynne and Muffler, 2010). These resorbed crystals and fragments of enclaves are much more abundant in group 2 than in group 1 hosts and are the reason that the group 2 lavas are less felsic and more heterogeneous in composition. Mixing between two distinct magmas of silicic and mafic composition is required by these characteristics (e.g., Bacon, 1986; Clynne, 1999; Tepley et al., 1999; Feeley et al., 2008b; Andrews and Manga, 2014).

The present investigation consists of phase-equilibrium and continuous decompression studies, to constrain pre-eruptive storage conditions of the rhyodacite host magma and assess magma decompression and ascent rates. This is done through petrographic analysis of textures, mineral assemblages, and abundances of phenocrysts, with comparisons between natural and experimental samples.

**Motivation/Importance**

Various geological, geochemical, and geophysical aspects of the LVC have been studied for decades (e.g., Williams, 1931; Heiken and Eichelberger, 1980; Tepley et al., 1999; Clynne, 1993, 1999; Schwab and Castro, 2007; Feeley et al., 2008a; Clynne and Muffler, 2010; Andrews and Manga, 2014). In 1976, a network of near-surface seismometers (analog short-period single-component) was installed, with several additional instruments added in each decade since, and as of 2008 (Guffanti et al., 2008),

eleven seismometers were being monitored by the USGS. The USGS also monitors the LVC for horizontal ground deformation, using eight (Guffanti et al., 2008) continuously-recording Global Positioning System sensors (GPS; dual frequency). Current surveys show subsidence is broad and includes the area of the eastern half of LVNP; interpreted to be the result of Basin and Range extension that is impinging on the arc (Poland et al., 2004).

In 1989, a database for potential hazards from future volcanic eruptions for all known California volcanoes was developed (Miller, 1989) and in 2011 the database was digitized (White et al., 2011). The most recent geological mapping of LVC was published in 2002 (Christiansen et al., 2002) and 2010 (Clynne and Muffler, 2010). Eruption probability and hazard assessment for the LVC and region were calculated in 2012 (Nathenson et al., 2012) using 1,050 calibrated years B.P. eruptions of Chaos Crags and 1914-1917 eruption of Lassen Peak as models for the types and magnitude of explosive silicic volcanic activity that can be expected in the future. Volcanic related hazards range from small localized near-vent explosive activity producing downwind ash fallout accompanied by lava flowing a few kilometers from the vent, to large-scale explosive activity sending ash hundreds of kilometers away and producing pyroclastic flows and lahars that could travel tens of kilometers down valleys, causing major destruction. Because of the documented mixing at the Chaos Crags and the potential for future eruptions, it is important to understand the pressure-temperature-composition conditions (as well as other parameters) of the Lassen magmatic system.

With the recent mapping and hazard assessment, there is renewed research interest in the area and multiple research groups are engaged in various projects. There are, however, no published experimental data constraining the high-pressure and high-temperature phase equilibria or decompression rates of the rhyodacite host magma at Chaos Crags. Existing computer models such as MELTS (Ghiorso and Sack, 1995; Asimow and Ghiorso, 1998) do not adequately account for hydrous phases within felsic magmas. Consequently, experimental data are necessary to constrain pre-eruptive storage conditions and decompression rates, and provide context for other ongoing research on the LVC.

# METHODS

## Natural sample bulk composition

The petrography and geochemistry of samples from all Chaos Crags domes and pyroclastic flows indicate group 1 lavas are the most representative of the stored silicic end-member magma. The earliest of these, the lower pyroclastic flow, is likely to be the least contaminated by the mafic magma. Sample LQ13-01 (Figure 7a-g), from the lower pyroclastic flow and with visible mafic enclave fragments removed, to approach the silicic end-member composition, is used as starting material for investigation of pre-eruptive storage conditions and decompression rates of Chaos Crags host magma. Sample LQ13-01 was collected with M. A. Clynne (USGS) and B. E. Schwab (Humboldt State University) on May 25$^{th}$, 2013, from the 1,050 calibrated years B.P. (Clynne et al., 2012) lowest Chaos Crags pyroclastic flow unit and is from the same location (NAD27 UTM Zone 10N 4487570N 0622575E±27 feet) as sample LC84-417 (also from the lower pyroclastic flow) of Clynne et al. (2008b). Hand sample LQ13-01, initially 20 cm x 18 cm x 16 cm in size, was split into two pieces, with one half preserved for future research. The half used in this study was further split and analyzed, and used for phase equilibrium experiments. Backscatter electron (BSE) images (Figures 7b-g) of samples from the lower pyroclastic flow (samples LQ13-01 and LC84-417) show sparse mafic inclusions (Figure 7b) and electron probe microanalysis (EPMA) of glass compositions (Table 1) are identical to LC84-417 and similar to the silicic end-member of Clynne et al. (2008b). As determined by scanning electron microscope (SEM) analysis of polished sections, the hornblende-biotite rhyodacite pumice is crystal-vitric, containing 35% generally ovoid

vesicles, 40% glass (Figure 7b), 15% euhedral twinned zoned plagioclase (Figure 7c), 4% euhedral biotite (Figure 7d), 4% euhedral amphibole (Figure 7e), and 1% quartz (Figure 7f), with minor FeTi-oxides (Figure 7g), apatite and zircon. The glass and mineral assemblage is of similar ratio as the dense rock equivalent from Clynne and Muffler (2010).

Additionally, natural samples from the lower (LC84-417), middle (LC84-418), and upper (LC84-419) pyroclastic flows and domes A (LC84-428), B (LC84-443), C (LC84-434), D (LC84-435), E (LC84-433), and F (LC84-455) collected by M.A. Clynne (bulk rock analyses from Clynne et al. (2008b) in Appendix A), and dome D (ChaosD) collected by B.J. Andrews (from the same hand sample as in Andrews and Manga (2014)) were geochemically and texturally analyzed and are discussed later.

**Natural sample – Preliminary constraints on pre-eruptive storage conditions**

Pumice LQ13-01 was analyzed, by quartz-hosted melt inclusion compositions (e.g., Ihinger et al., 1994; Lowenstern, 2003), magnetite-ilmenite geothermometry (e.g., Bacon and Hirschmann, 1988; LePage, 2003; Blundy and Cashman, 2008; Ghiorso and Evans, 2008) and amphibole chemical equilibrium (e.g., Ridolfi et al., 2010), to constrain volatile concentrations, oxygen fugacity ($fO_2$), equilibration temperature, and equilibrium pressure.

**Melt inclusion sample preparation**

Quartz phenocrysts within the Chaos Crags host rhyodacite are resorbed and contain abundant melt inclusions (Figure 7f). A portion of hand sample LQ13-01 was lightly crushed and quartz phenocrysts extracted from surrounding vesiculated glass

matrix by picking with tweezers under a dissecting microscope. Quartz phenocrysts with visible melt inclusions were single-grain mounted in 10 mm epoxy rounds. Each round was doubly polished (using 1 μm diamond paste and lubricant) to expose one or more melt inclusion(s) with each having a nearly constant thickness ranging from 31 μm to 94 μm (Appendix C). Melt inclusion thicknesses were calculated as the average of two to three repeated measurements of doubly polished host quartz grain, using a flat granite countertop as a base and an electronic drop indicator. Melt inclusions were analyzed by Fourier transform infrared spectroscopy (FTIR) to determine molecular water ($H_2O$), hydroxyl ion ($OH^-$), total water ($H_2O_t$), and $CO_2$ concentrations (Table 2) (e.g., Berlo et al., 2012), then carbon coated and analyzed by EPMA (Table 3).

**Fe-Ti oxides sample preparation**

Euhedral magnetite and ilmenite phenocrysts from sample LQ13-01 were analyzed by EPMA for geothermometry and oxybarometry (e.g., Blundy and Cashman, 2008). Oxide pairs (Figure 7g) were separated from lightly crushed starting material using a neodymium magnet on the exterior of a glass jar to pick up and hold magnetic minerals (titanomagnetite and ilmenite), while less magnetic phases were emptied onto weighing paper. Magnetic phase separates were placed in a thin layer of epoxy on frosted 1-inch round glass slides and polished using a 600-grit silicon-carbide slurry and grinding wheel, followed by 6 μm and 1 μm diamond paste with lubricant, and carbon coated for SEM and EPMA analyses. Titanomagnetite-ilmenite touching pairs were identified through BSE imaging and energy dispersive x-ray spectrometry (EDS), and subsequently analyzed by EPMA.

### Amphibole sample preparation

Euhedral amphiboles (Figure 7e) in pumice LQ13-01 were analyzed by EPMA. Natural pumice was broken into ~1 cm chunks and encased in epoxy in 1-inch rounds then polished using 600-grit then 1500-grit silicon-carbide sand paper followed by 6 μm and 1 μm diamond paste with lubricant until amphibole phenocrysts were exposed. Rounds were carbon coated for EPMA analysis. EPMA calculates total Fe as $Fe^{2+}$. Fe is recalculated to $Fe^{2+}$ and $Fe^{3+}$ by AmpTB (Ridolfi et al., 2010) with the upper bound method of $Fe^{3+}$ placing only Ca and Na in the M(4) site using 23 oxygens per formula and 13 cations per formula (Leake et al., 1997).

## Phase equilibrium experiments

### Starting material

Pumice LQ13-01 was broken into ~1cm size pieces, inspected, and any pieces with visible mafic inclusions discarded. Visible inclusion-free samples were then lightly crushed using an agate mortar and pestle, yielding approximately 50 grams of starting material available for experiments. Phenocrysts were not removed from the crushed sample. This lightly crushed sample was used as starting material for $H_2O$-saturated high-pressure -temperature phase equilibrium experiments.

### Phase equilibrium experimental methods

All experiments were conducted in the Department of Mineral Science's Cold-Seal Hydrothermal Laboratory at the Smithsonian Institution (SI) National Museum of Natural History (NMNH) in Washington, DC. Capsules were constructed from ~1.0 cm lengths of $Ag_{70}$-$Pd_{30}$ tubing with 3-5mm outer diameter and 0.127 mm wall thickness.

One end of the tubes were crimped with pliers and welded under microscope using a Puk3 Professional Welder with neutral Ar gas flow. Capsules were weighed before and after adding 4 to 51 mg of deionized $H_2O$ to each capsule using a microsyringe in order to provide $H_2O$-saturated conditions. Approximately 35 to 262 mg (Table 4) of starting material was added to each capsule and water, and reweighed. The capsules thus contain $H_2O$ and powdered pumice starting material. Loaded capsules were crimped closed and welded shut. Welds were inspected for leaks under a dissecting microscope. Sealed capsules were weighed to identify mass loss and then placed on a ~65°C hot plate for ~10 minutes, and weighed again to ensure capsules were sealed and no $H_2O$ was lost during welding. Capsule $H_2O$ concentrations ranged from 5.1 to 16.1 wt. % (Table 4).

One sealed capsule per experiment, along with nickel filler rod to buffer experiments to NNO+1 log-unit (±0.5 log-units; Matthews et al., 2003), was loaded into a Waspaloy cold-seal pressure vessel (PV) and topped off with water prior to being connected to high-pressure line (Figures 8a-b). The PV was pressurized with water ($P_{H_2O}=P_{total}$) to experimental target pressure (75-200 MPa, Table 4) and held for ~30 minutes to check for leaks. Pressure was monitored using an OMEGA pressure transducer and OMEGA digital meter. A type-k thermocouple was inserted into the end of the PV near the sample location and the PV placed into a horizontal split tube furnace heated to 25°C. Furnace power was computer controlled using a custom proportional-integral controller (developed by T. Gooding of SI) and thermocouple temperatures increased from 25°C to experimental target temperature (ranging 750-900°C; Table 4) over a 120 minute period. During temperature ramping, pressures were monitored and

excess pressure bled using the pressure intensifier and/or the vent line at V5 (Figure 8a). Upon reaching the desired starting conditions and once pressure stabilized, experiments were isolated from the high-pressure line by closing the appropriate valve (V0-V3). Pressure and temperature were computer monitored and recorded at one-minute intervals throughout the experiments, and furnace power adjusted to maintain target temperatures. Experimental start times were identified to be when the set point was reached and pressure stabilized. Run durations were 93-142 hours (Table 4); experiments < 800°C typically ran ~24 hours longer than experiments ≥800°C to account for slower reaction kinetics at lower temperatures. Thirty-two P-T combinations were investigated (Table 4). Twenty-five single-stage (using LQ13-01 as starting material) experiments were performed. An additional nine two-stage (using an experimental run product as starting material) experiments were performed to check for equilibration. Of those, two pairs of melting and crystallization reversal experiments, CCPb-25 and -26, and CCPb-29 and -30, were run to check equilibration.

PVs are isobarically quenched independently and drop below the solidus temperature in <30 seconds. Mainline pressure is adjusted to match the pressure of the PV to be quenched and the appropriate isolation valve (V0-V3) opened to the main high-pressure line. The PV is quickly removed from the furnace and thermocouple detached, sprayed with compressed air for ~5 seconds (to minimize thermal shock and increase the lifespan of the PV), and submerged and swirled in ~20°C water. During quench, pressure is monitored, and the pressure intensifier adjusted as necessary to maintain constant

pressure in the system, minimizing quench effects such as additional vesiculation and quench crystallization.

After quenching, capsules were inspected for leaks and cut open with wire snips, and experimental run products extracted with tweezers. Experimental run products were encased in epoxy in 10-mm rounds then polished using 600-grit and then 1500-grit silicon-carbide sand paper, followed by 6 μm and then 1 μm diamond paste with lubricant, until representative areas were exposed. Rounds were carbon coated for SEM and EPMA analyses.

**Continuous decompression experiments**

Continuous decompression experiments were conducted to constrain magma decompression and ascent rate from the storage depth.

**Starting material**

Preliminary SEM textural analysis of the phase equilibrium experimental run products and FTIR analysis of melt inclusions (detailed below) indicated the Chaos Crags host magma's pre-eruptive storage conditions to be ~775°C and 110-125 MPa. Textures in pumice LQ13-01 were closely reproduced in experimental run product CCPb-18 (775°C, 125 MPa). To verify those conditions and adjust for slightly lower pressures (pressures necessary to reach saturated conditions at $H_2O$ concentrations) as suggested by preliminary FTIR analysis of melt inclusions, and create material for use in decompression experiments, phase equilibrium experiment CCPb-34 was run at 775°C and 120 MPa, with ~10 times greater mass than used in other phase equilibrium experiments. SEM analysis of experimental run product CCPb-34 showed similar texture

to that of both CCPb-18 and LQ13-01 and hence, CCPb-34 was used as starting material for continuous decompression experiments. The post-run CCPb-34 capsule was snipped open with cutters, the sample removed with tweezers, lightly crushed with an agate mortar and pestle, and stored in a glass jar until capsules were constructed for continuous decompression experiments.

Capsules for decompression experiments were prepared using the same procedures as for phase equilibrium experiments. 1 mg of deionized $H_2O$ was added to each capsule, followed by approximately 11 to 21 mg of starting material CCPb-34 (Table 5). This yielded $H_2O$ contents of 4.8 to 7.3 wt. % in addition to the $H_2O$ already within the starting material. Capsules were sealed and inspected for $H_2O$ loss as before.

**Continuous decompression experimental methods**

The SI cold-seal hydrothermal laboratory (Figures 8a-b) has four horizontal split tube furnaces housing four PVs; the use of PV3 and H3 as a pressure actuator provides a maximum of three decompression experimental run products for a single decompression series. Experiments in a single decompression series were quenched at different pressures within a single decompression rate, allowing examination of crystallization processes at discrete times within a single rate or series.

For continuous decompression experiments, pressure was smoothly adjusted with computer control by using one of the furnaces (“H3”) as a pressure actuator; no experiment is loaded in PV3 (housed in H3), instead its temperature is varied up or down to control pressure in the high-pressure line where the specific dependence $P=f(T)$ is determined empirically. Figure 9a shows an example of the pressure-temperature-time

path used in the calibration technique for a two-sample configuration using 3 furnaces in total. In this calibration, there are two samples, one in each PV0 and PV1, and no sample in PV3 (the actuator). In this scenario PV2 is not used and its associated isolation valve, V2, is closed, removing it from the system. For the initial heating period, not shown on Figure 9a, the PVs that will have experiments in them (PV0 and PV1) are brought to their starting temperature (775ºC; Table 5), and allowed to stabilize for ~90 minutes. Then, PV1 is isolated from the system by closing V1. PV3 is ramped up from 25ºC to 250ºC (point A in Figure 9a is at 200ºC in this heating path) in 30 minutes (to point B in Figure 9a), and held for 30 minutes to allow the system to adjust and stabilize to adjustments brought on by thermal expansion in the system. After stabilization (Figure 9a, point C), temperature in PV3 is ramped to 600ºC in 120 minutes. At point D in Figure 9a, the pressure in the system has exceeded that of the desired starting pressure of the decompression experiments (120 MPa; Table 5). Then, PV1 is added to the system by opening its isolation valve (V1). At that point, PV0 and PV1 are part of the system. Using the pressure intensifier, pressure is adjusted to the starting pressure of the decompression experiments (120 MPa), while the 120-minute temperature increase to 600ºC in PV3 is completed (to point E in Figure 9a). After the ramping up cycle is complete, the temperature in PV3 is ramped down to 400ºC in 120 minutes (to point F in Figure 9a). After completion of the ramping down, the experimental rate calibration run is complete. Then, the experimental run data is retrieved from the computer and plotted as in Figure 9a, with each point representing the temperature of PV3 at the system pressure, computer-recorded in one-minute intervals. The slopes of sections of known system

configurations calculate to be the amount of temperature, in ºC, required to change the configuration-specific system pressure by 1.0 MPa. In this example (Figure 9a), the one-sample setup requires temperature change in PV3 of ~2.7ºC to change the system pressure by 1.0 MPa, while the two-sample setup requires temperature change of ~5.3ºC in PV3 to change the system pressure by 1.0 MPa. The desired decompression rate and final pressures of samples within the series are chosen, temperature reduction needed in PV3 to achieve desired pressure drop is calculated for each stage using calibration values. Then, the time to reach the final pressures for each stage is calculated and incorporated into a temperature reduction scheme for each stage, to provide the same overall decompression rate, accounting for the change in system volume. A three-sample configuration adds an additional stage of calibration with PV2 as part of the system, using the same techniques described above.

Once calibration decompression rate curves are established, continuous decompression experiments are ready for setup. Each PV with attached thermocouple was connected to the main pressure line and placed in its own furnace at 25ºC. All PVs were then opened to the main pressure line and brought to experimental starting pressure and held for ~30 minutes to check for leaks. All furnaces were ramped up from 25°C to target temperature (775°C; Table 5) in 120 minutes, with excess pressure bled from the system, ensuring the pressure never exceeds >1.0 MPa more than the experimental starting pressure (120 MPa; Table 5). After target temperature was reached and pressure stabilized, samples were annealed at constant pressure for 60 minutes. After that 60-minute interval, continuous decompression experiments began. PVs with experiments are

held at target temperature, while the temperature of the actuator PV (PV3, without an experiment) is lowered at one-minute intervals (using computer code written by T. Gooding of SI), effectively reducing the pressure in the system at a constant rate. Once the system decompressed to the desired final pressure for the first experiment in the time-series, decompression paused for 10 minutes to permit quenching of the first experiment. Quenching of decompression experiments followed the same procedure as applied to phase equilibrium experiments; in both types of experiments, only the PV to be quenched was open to the pressure line and all other PVs were isolated from the line. After the experiment was quenched, the valve that connects the quenched PV to the mainline is closed, removing that PV from the system, reducing the system's volume, requiring a new temperature reduction rate to achieve the same decompression rate. Pressure to the mainline was then returned to what it was at the initiation of the 10-minute decompression pause (prior to the quenching). The PVs with experiments remaining and the PV acting as a pressure actuator (PV3 in furnace H3) were then opened to the main pressure line allowing communication between all remaining PVs and the main pressure line. The computer was reprogrammed to reduce temperature in H3/PV3, at the rate appropriate for the reduced system volume. This process was repeated until all experiments were quenched at the desired pressures. System pressure and temperature were monitored and recorded throughout the experiments to allow back-calculation of true experimental decompression rate, and to verify that decompression rate and temperature remained constant.

Nine continuous decompression experiments (Table 5) were performed at four different rates from 8.5 to 0.35 MPa/hr with two or three experimental run products per rate. This corresponds to total decompression (120 MPa to one atmosphere) times of 16 hours to 54 days. Decompression paths are plotted in Figure 9b. The signal from diurnal temperature variation within the laboratory is captured by the one-minute interval computer logging and visible as the sawtooth pattern of the slowest rate (0.35 MPa/hr) in Figure 9b. This signal is not observable within the other decompression rates.

Experimental run products were polished and prepared for SEM and EPMA analyses using similar techniques as for phase equilibrium experimental run products.

## Analytical techniques

### FTIR

FTIR absorbance interferograms were obtained for each melt inclusion using a Thermo Scientific Nicolet 6700 Analytical FTIR Spectrometer and Continuum microscope equipped with a liquid nitrogen-cooled MCT detector, KBr beam-splitter, mid-IR source, 10 μm aperture, and OMNIC 8 and Atlus software. Both the bench and sample cache were continuously purged with water- and carbon-dioxide-free air generated with a Whatman pure-gas generator. An NaCl window was used and a background spectrum taken before collection of each sample spectrum. The baseline and maximum peak height were determined using OMNIC 8 software.

Total water concentrations ($H_2O_t$) were calculated as the sum of molecular-$H_2O$ ($H_2O$), using the 5200 $cm^{-1}$ absorption band (e.g., Castro et al., 2013), utilizing a molar absorptivity of 1.61 (±0.05) L/mol·cm (Newman et al., 1986; Ihinger et al., 1994), plus

$OH^-$, using the 4500 $cm^{-1}$ absorption band (e.g., Castro et al., 2013), utilizing a molar absorptivity of 1.73 (±0.02) L/mol·cm (Newman et al., 1986), and a glass density of 2300 $kg/m^3$ (e.g., Larsen, 2006).

$CO_2$ concentrations were calculated using the 2350 $cm^{-1}$ absorption band (e.g., Castro et al., 2013), utilizing a molar absorptivity of 945 (±45) L/mol·cm (Fine and Stolper, 1985; Ihinger et al., 1994), and a glass density of 2300 $kg/m^3$.

The following version of the Beer-Lambert Law was used for calculating $H_2O$ $OH^-$, and $CO_2$ concentrations in glass:

$$concentration(wt.\%) = \frac{100 \times MW \times A}{d\rho\varepsilon}$$

where *MW*=18.02 (g/mol) for water species or 44.01 (g/mol) for $CO_2$, *A*=absorbance (the -log10 of the % transmittance by the sample), *d*=thickness (cm), ρ=density (g/L), and ε= molar absorptivity (L/mol·cm).

The principle challenge with FTIR analysis is that as samples must be very thin (<100 μm for melt inclusions), thickness measurements can introduce substantial error into the volatile determination (Ihinger et al., 1994). Flatness and thickness consistency was checked, and the standard deviation of two to three repeated measurements in addition to the ±1 μm accuracy of the drop indicator sum to < 5.0% of total thicknesses (Appendix C). The errors associated with thickness measurements and extinction coefficients create an average analytical uncertainty of ~10% of the calculated values and that is used here (e.g., Seaman et al., 2006; Castro et al., 2013). Those uncertainties are consistent with Dixon and others (Dixon et al., 1991; Dixon and Clague, 2001) estimates

of accuracy of FTIR total water analyses as ±10% from all variables of the Beer-Lambert Law.

**SEM**

Prepared samples received a 25±5 nm carbon coat in a Cressington EM Coating System with thickness monitor and Evaporation Supply LT750. BSE imaging and *NORAN System 7* energy dispersive X-ray spectroscopy (EDS) analyses were collected at the SI using a FEI Nova NanoSEM 600 SEM operating at 15 kV accelerating voltage, spot size 3.0-4.0, and ~5.0 mm working distance, and at Humboldt State University using a FEI Quanta 250 SEM operating at 15 kV accelerating voltage, spot size 6.0-7.0 and ~10.0 mm working distance.

**EPMA**

Prepared natural samples obtained from M.A. Clynne (samples with prefix LC84, whole rock analyses given in Clynne et al. (2008b), which are reproduced here in Appendix A) were carbon coated at Humboldt State University and analyzed by EPMA in the CAMCOR MicroAnalytical Facility at the University of Oregon (UO), Eugene. Samples received a 30±5 nm carbon coat using a Cressington 208C carbon coater with thickness monitor. Quantitative chemical analyses of minerals and glasses were acquired by a Cameca SX-100 five spectrometer EPMA operating at 15 kV accelerating voltage, 10 nA beam current, ~10 μm spot size, with 10-100 seconds counting time on peak and background. Analysis and automation was performed using *Probe for EPMA* software with natural and synthetic mineral and glass standards. Sodium migration in glasses was

monitored and corrected using the volatile correction routine within the *Probe for EPMA* software.

Prepared natural pumice sample LQ13-01, melt inclusions, Fe-Ti oxide pairs, phase equilibrium experimental run products, and continuous decompression experimental run products were carbon coated and analyzed by EPMA in the SI's Department of Mineral Sciences. Samples received a 25±5 nm carbon coat using a Cressington EM Coating System with thickness monitor and Evaporation Supply LT750. Quantitative chemical analyses of minerals and glasses were acquired by a JEOL JXA-8900R five spectrometer EPMA operating at 15 kV accelerating voltage, 10 nA beam current, beam rastered over a 6×5 μm area, with 10-20 and 5-10 seconds counting time on peak and background, respectively. Analysis and automation was performed using *Probe for EPMA* software with natural minerals and glasses from the Smithsonian's standards collection (Jarosewich, 2002). Sodium migration in glasses was monitored and corrected using the volatile correction routine within the *Probe for EPMA* software. Rhyolite glasses VG568, RLS-132, and MLV-36 were used to monitor drift during glass analyses. Standards used for silicate glasses and minerals were: VG-99, VG-568, Fluorapatite, Ilmenite, Anorthoclase, Augite, Hornblende, Microcline, Scapolite, and Pyrite. Standards used for oxides were: Magnetite, Hornblende, Ti metal, Vanadinite, Chromite, Ilmenite, Manganite.

Minimum detection limits and analytical errors were checked after data collection using *Probe for EPMA*. Compositions of standards were checked to ensure reliability and consistency. Individual raw glass analyses with totals <87.5, or analyses that were clearly

inclusive of other phases (mostly quartz yielding notably high $SiO_2$ totals (>82.0 wt. %) and plagioclase yielding notably low $SiO_2$ (<63.0 wt. %) and high $Al_2O_3$ totals (>18.0 wt. %), were discarded. Individual raw analyses of titanomagnetite and ilmenite phenocrysts with low totals (<88.0 wt. % for titanomagnetite and <92.0 wt. % for ilmenite) or high $SiO_2$ (>1.0 wt. %) were discarded.

# RESULTS

## Natural sample – Preliminary constraints on pre-eruptive storage conditions

### Melt inclusions – FTIR – $H_2O$, $OH^-$, $H_2O_t$ and $CO_2$ concentrations

FTIR analysis of 42 melt inclusions from LQ13-01 (Table 2) yields $H_2O_t$ concentrations ranging 1.09±0.11 to 6.48±0.65 wt. % (the bulk of analyses cluster between 3.99±0.40 and 5.42±0.54 wt. %) and $CO_2$ concentrations ranging 0 to 361±36 ppm (Figure 10). As magma ascends, confining pressure and solubility of volatiles decrease. If a melt inclusion is exposed to lower pressures (through fracturing or resorption of the host phenocryst) it will re-equilibrate to the new solubility levels, and volatile loss may occur. Melt inclusions with $H_2O_t$ <3.0 wt. % were inferred to have leaked (8 of the 42 analyzed by FTIR, most with visible fractures, labeled with suffix "-leak" in Table 2). Upon removing leaked melt inclusions, $H_2O_t$ concentrations range 3.99±0.40 to 6.48±0.65 wt. %, and $CO_2$ concentrations range 44±4 to 361±36 ppm. Figure 11 shows $H_2O$ (blue squares) and $OH^-$ (green diamonds) from preserved melt inclusions plotted against their $H_2O_t$. All melt inclusions have higher $H_2O$ than $OH^-$.

### Melt Inclusions – EPMA – Glass composition

Glass compositions of 30 melt inclusions (all of which were analyzed by FTIR) are converted to anhydrous (by normalizing their totals to 100) and reported as wt. % oxides in Table 3. These anhydrous glass compositions for each melt inclusion along with anhydrous glass compositions (Table 1) from starting material LQ13-01 (lower pyroclastic flow), LC84-417 (lower pyroclastic flow), LC84-418 (middle pyroclastic flow), LC84-428 (dome A), LC84-419 (upper pyroclastic flow), LC84-443 (dome B),

LC84-434 (dome C), ChaosD (dome D), LC84-433 (dome E), and LC84-455 (dome F) are plotted in Harker variation diagrams in Figures 12a-g. Melt inclusions contain 78.06±0.24 to 80.32±0.28 wt. % $SiO_2$ (Figure 12a), and plot at the upper end of the range (or greater than) shown by the natural pyroclastic flow and dome glasses (Figure 12a). $K_2O$ (Figure 12a) ranges 3.96±0.02 to 4.32±0.07 wt. %, decreasing as $SiO_2$ increases, opposite to the trend of the pyroclastic flows and domes where $K_2O$ increases as $SiO_2$ increases. $Al_2O_3$ (Figure 12b), $Na_2O$ (Figure 12c), CaO (Figure 12d), FeO (Figure 12e), MgO (Figure 12f), and $TiO_2$ (Figure 12g) generally decrease as $SiO_2$ increases and plot less than or at the lower end of the respective ranges shown by the natural pyroclastic flow and dome glasses.

**Melt inclusions – Saturation pressures**

In a review of saturation models, Moore (2008) determined the $H_2O+CO_2$ solubility model of Papale et al. (2006) best resolves saturation pressures for rhyolitic-dacitic compositions at pressures ranging 100-250 MPa. Using the $H_2O$ and $CO_2$ concentrations determined by FTIR (Table 2) and anhydrous glass compositions (as required by the model), determined by EPMA (Table 3), of melt inclusions from LQ13-01, the model of Papale et al. (2006) calculates saturation pressures of 92-297 MPa.

**Titanomagnetite-ilmenite pairs – Temperature and $fO_2$**

Compositions of 16 titanomagnetite and ilmenite touching mineral pairs from LQ13-01 are reported as wt. % oxides in Table 6 and plotted in Figure 13. EPMA results report total Fe as FeO. Fe is recalculated (e.g., Spencer and Lindsley, 1981; Stormer, 1983) by normalizing cations to a stoichiometric formula and balancing the number of

cation charges by varying the $Fe^{2+}/Fe^{3+}$ ratio, ultimately providing concentrations of $Fe_2O_3$ and FeO. Iron recalculation is performed using ILMAT (LePage, 2003) and OxideGeothrm (Ghiorso and Evans, 2008). Mg/Mn partitioning (Table 7) in titanomagnetite and ilmenite, of all pairs, pass the Bacon and Hirschmann (1988) test for equilibrium between coexisting Fe-Ti oxides (Figure 14).

Figure 15 shows equilibration temperature and $fO_2$ results (Table 7), using titanomagnetite-ilmenite pairs (Table 6), from the Fe-Ti geothermometer/oxybarometer OxideGeothrm (Ghiorso and Evans, 2008). The model calculates equilibration at $fO_2$ of ~NNO+1.35 log-units and a clustering at temperature between 760-775°C with individual pairs as high as 807°C.

**Amphiboles – $fO_2$, Temperature, $H_2O_{melt}$, Pressure**

Amphiboles in LQ13-01 are not zoned, however, SEM analysis shows some phenocrysts exhibit cores that are of different composition than their rims. Amphibole rim compositions from LQ13-01 are reported as wt. % oxides in Table 8. All analyses calculate by AmpTB (Ridolfi et al., 2010) to be calcic amphiboles, with most as magnesiohornblende, and one a tschermakitic-pargasite. Most of the experiments used in calibration of the Ridolfi et al. (2010) model were fluid-saturated with initial $H_2O/(H_2O+CO_2)$ in the experimental charges of 0.8–1.0, conducted at controlled and/or buffered $fO_2$ of NNO-1 to NNO+4.8 log-units, and fixed pressure-temperature conditions of 750–1075°C and 100–960 MPa, using different types of gas vessels. Some experiments used in the calibration were obtained using piston-cylinder apparatus with

temperatures of 800–1120°C at relatively high pressures of 800–1200 MPa on intermediate-basic calc-alkaline rocks.

Phenocryst amphibole compositions from LQ13-01 meet the criteria for the Ridolfi et al. (2010) model given in Table 9 and shown in Figures 16a-c. According to the model, magnesiohornblende rims equilibrated at $fO_2$ of ~NNO+2.1 log-units (Figure 16a), temperatures 772-810°C (Figures 16a-c), 4.3-4.8 wt. % $H_2O$ in melt (Figure 16b) and pressures 71-89 MPa (Figure 16c). The lone tschermakitic-pargasite analysis (blue square) plots at slightly less oxidizing $fO_2$ of NNO+1.3 log-units and higher temperature of 874°C, pressure of 188 MPa, and 5.6 wt. % $H_2O$ in melt. It is likely that the tschermakitic-pargasite analysis includes a higher-temperature earlier-formed core and is not representative of the final pre-eruptive equilibrium storage conditions of the host rhyodacite magma chamber (e.g., Clynne, 1999). The tschermakitic-pargasite has notably higher $TiO_2$, $Al_2O_3$, FeO, and $Na_2O$, and lower $SiO_2$, MnO, and MgO than the magnesiohornblendes analyzed here, and the same trend of higher $Al_2O_3$ and lower $SiO_2$ in core vs. rim for representative amphibole from group 1 lavas of Tepley et al. (1999).

**Phase equilibrium experiments**

**Phase assemblage**

SEM analysis (Figures 17a-h) of phase equilibrium experimental run product textures shows the P-T stability range for each phase (Figure 18). Quartz is stable from ≤200 MPa at 750°C to <175 MPa at 775°C and at 75 MPa at 800°C, and is not stable at temperatures >800°C, within the investigated pressure range. Amphibole is stable from >75 MPa at 750°C to >100 MPa at 775°C and at 200 MPa at 825°C, and is not stable at

75 MPa or ≥850°C. Biotite is stable at all investigated pressures at 750°C, stable >125 MPa at 800°C, and is not stable for any pressure at ≥850°C. Pyroxene, not present in the starting material is stable at 200 MPa at ≥800°C and all investigated pressures at ≥825°C. The phase stability diagram overlays phase equilibrium experimental run product glass oxide composition contour plots in Figures 19a-h.

**Phase compositions**

EPMA analyses of glass in all experimental run products were collected and are presented below. Biotite, amphibole, pyroxene, and plagioclase in subsets of experiments were measured, but the small rim sizes presented analytical challenges, thus those data are not reported here.

***Glass compositions and calculated/modeled $H_2O$ concentrations***

Glass compositions of experimental run products are reported as wt. % oxides in Table 10, and contoured as colors and plotted in P-T-x plots in Figures 19a-h. Target compositions (LQ13-01-glass average compositions from Table 1) are plotted as bold lines with associated ±1σ uncertainties (thin lines) for each oxide. There are visible trends in the data. $SiO_2$ (Figure 19a) and $K_2O$ (Figure 19b) decrease with increasing pressure and/or temperature, while $Na_2O$ (Figure 19c), CaO (Figure 19d), $Al_2O_3$ (Figure 19e), $TiO_2$ (Figure 19f), FeO (Figure 19g), and MgO (Figure 19h) decrease as pressure and/or temperature decreases. All oxide compositions from LQ13-01 overlap experimental run products, with most overlap in the range between 175 to 200 MPa at 750°C to 75 MPa at 800-850°C.

Dissolved $H_2O$ concentrations calculated as volatiles by difference (VBD) through EPMA are reported as wt. % in Table 11 and contoured as gray lines in Figure 20. There is no obvious pattern from the plot. However, there are solubility models (e.g., Moore et al., 1998), which calculate solubility and dissolved water concentration from pressure, temperature, and composition of a silicate melt or glass. Phase equilibrium experimental run product glass compositions (Table 10) are input into the model of Moore et al. (1998), at each experimental P-T combination (Table 4), and concentrations contoured as black lines at 0.5 wt. % increments in Figure 20. The calculated model solubility from Moore et al. (1998) indicates that the effect of pressure dominates volatile solubility, and increasing pressure and decreasing temperature yield greater solubility within the investigated range. CCPb phase equilibrium experimental run products have dissolved water concentrations ranging ~3.5 wt. % at 75 MPa to ~6.0 wt. % at 200 MPa. These water concentrations are overlain as gray lines on the experimentally determined phase stability diagram (Figure 18) and phase equilibrium experimental run product glass composition plots (Figures 19a-h).

**Continuous decompression experiments**

**Phase assemblage**

All decompression experimental run products contain glass, plagioclase, quartz, amphibole, and biotite, with minor amounts of Fe-Ti oxides and apatite. BSE images of continuous decompression experimental run products are presented in Figures 21a-j.

Continuous decompression experimental run products CCPb-39 (Figure 21d), CCPb-35 (Figure 21e), and CCPb-37 (Figure 21g) show contamination from the mafic

magma, either through the presence of mafic enclaves or olivine xenocrysts. Therefore, the starting material for all continuous decompression experiments (phase equilibrium experimental run product CCPb-34) is also contaminated. The total exposed surface area of the experiments that comprise the mafic magma is however, <1% of the total exposed surfaces of experimental run products CCPb-34 thru CCPb-43, and it appears texturally (Figure 21e) that minimal mixing occurred.

**Phase compositions**

***Biotite***

SEM analysis of experimental decompression products indicates biotite does not breakdown at any pressure for any rate within the investigated range. Biotite often appears to be in contact with vesicles, such as in Figures 21f and 21i. No grains show dehydration breakdown rims, such as those observed in group 2 eruptive products (Figure 6b).

***Amphibole***

SEM analysis of experimental run products indicates amphibole does not breakdown for the fastest rates, 8.5 MPa/hr (Figures 21a-b). Amphibole does not breakdown for the second fastest rate, 2.6 MPa/hr (Figures 21c-d), but there is a compositional change at the rim as seen in the BSE image in Figure 21c. Amphibole breaks down at the slower rates, 1.0 MPa/hr (Figures 21e-h) and 0.35 MPa/hr (21i-j). No phenocrysts show dehydration breakdown rims such as those observed in group 2 eruptive products (Figure 6c).

***Glass***

Continuous decompression experimental run product glass compositions (Table 12) and modeled $H_2O$-concentrations (using Moore et al., 1998; Table 11) are plotted on pressure (and approximate crustal depth using a lithostatic pressure gradient and 2650 $kg/m^3$ crustal density) vs. wt. % oxide (or $H_2O$) diagrams, with compositions of natural pyroclastic flows and domes (Table 1) for reference, in Figures 22a-i. Different decompression rates are plotted as separate lines. Glass $SiO_2$ concentrations (Figure 22a) generally increase as decompression continues. $Al_2O_3$ (Figure 22b) decreases, $K_2O$ (Figure 22c) increases, and $Na_2O$ (Figure 22d) remains constant with decompression. CaO (Figure 22e) decreases with decompression. CaO is the most linear of this plot type and shows most distinction between decompression rates. FeO (Figure 22f), $TiO_2$ (Figure 22g), and MgO (Figure 22h) show little to no variation with decompression within the investigated range. Extent of volatile ($H_2O$) loss is the same for all decompression rates and pressure regions (Figure 22i). $H_2O$ concentrations (Table 11) of domes and pyroclastic flows calculated using the VBD by EPMA method for comparison in Figures 22i and 23i. However, the reliability and significance of these values is questionable, as discussed earlier.

Continuous decompression experimental run product glass compositions and modeled $H_2O$-concentrations (using Moore et al., 1998) are plotted in Figures 23a-i as wt. % oxide (or $H_2O$) vs. decompression time, with glass compositions of natural samples (pyroclastic flows and domes) for reference. These plots in effect stretch the plots of

Figures 22a-i along the pressure axis, incorporating and emphasizing variation with time. Trends are identical to those in Figures 22a-i.

There are systematic differences in oxide concentrations with respect to decompression rate. $SiO_2$ and $Al_2O_3$ concentrations differ between the fastest rate (8.5 MPa/hr) and slower rates (2.6 MPa/hr and 0.35 MPa/hr). $K_2O$ concentrations differ between the fastest rate (8.5MPa/hr) and all slower rates (2.6 MPa/hr, 1.0 MPa/hr and 0.35 MPa/hr). CaO concentrations differ between the fastest rate (8.5 MPa/hr) and intermediate rates (2.6 MPa/hr and 1.0 MPa/hr) and the slowest rate (0.35 MPa/hr).

The longest duration decompression experiments within each rate were all quenched at ~50 MPa. At the lowest final pressure (~50 MPa) most glass oxide concentrations of the pyroclastic flows and domes A and B overlap with those of the fastest rate (8.5 MPa/hr), while glass oxide concentrations of domes C-E overlap with those of intermediate rates (2.6 MPa/hr and 1.0 MPa/hr), and glass oxide concentrations of dome F overlap with the slowest rate (0.35 MPa/hr).

# INTERPRETATION

## Constraints on pre-eruptive storage conditions from natural samples

### $H_2O$ concentration, Pressure, Temperature, $fO_2$

Preserved melt inclusions from LQ13-01 show dissolved $H_2O$ concentrations range 3.99±0.40 to 6.48±0.65 wt. %; the bulk of analyses cluster between 3.99±0.40 and 5.42±0.54 wt. %. The titanomagnetite-ilmenite pairs and the model of Ghiorso and Evans (2008) show equilibration at temperatures of 760-775°C at $fO_2$ of NNO+1.35 log-units, with one pair equilibrated at hotter temperature of 807°C. This suggests much of the magma equilibrated at a small temperature range, with a lesser amount heated by as much as ~50°C just prior to eruption. It could also be the case that magma was heated very rapidly, faster than most of the Fe-Ti oxides were able to record. In any case, the host magma was at or near to ~760-775°C and $fO_2$ ~NNO+1.35 log-units just prior to eruption. Amphibole chemical equilibrium (Ridolfi et al., 2010) shows close agreement with the aforementioned models in the host magma's water concentration, pressure, temperature, and $fO_2$. According to the model of Ridolfi et al. (2010), amphibole rims last equilibrated at lower $H_2O_{melt}$ concentrations (4.3 to 4.8 wt %), lower pressure (71-89 MPa), slightly higher temperature (772-810°C), and more oxidizing (NNO+2.0 to NNO+2.6 log-units) conditions than melt inclusions and titanomagnetite-ilmenite pairs suggest.

## Phase equilibrium experiments

### Storage conditions

Comparison of natural samples and experimental run products suggests pre-eruptive P-T storage conditions of the Chaos Crags rhyodacite host magma at 145±25 MPa and 770±10°C. This is represented by the shaded region in Figures 18 and 19a-g, and thus if $H_2O$-saturated ~5.2 wt. %.

## Continuous decompression experiments

No amphibole or biotite phenocrysts observed from group 1 lavas (pyroclastic flows and domes A and B) show dehydration breakdown reaction rims. Amphibole does however show a rim composition change at 2.6 MPa/hr and breakdown texture for decompression rates <2.6 MPa/hr. Textural and geochemical comparisons of experimental run products and natural samples indicate decompression and ascent of the magma producing group 1 lavas was relatively quick, >2.6 MPa/hr (corresponding to minimum ascent velocity of >100 m/hr and total decompression times of <48 hrs), whereas the magma that produced group 2 lavas (domes C-F) decompressed relatively slowly, <2.6 MPa/hr (corresponding to ascent velocity of <100 m/hr and total decompression times >48 hrs).

# DISCUSSION

## Storage conditions

The experimentally determined pre-eruptive pressure-temperature storage conditions (145±25 MPa and 770±10˚C) of Chaos Crags provide new physical constraints on the host rhyodacite magma chamber. Crustal depths of 5.6±1.0 km are required to achieve confining pressures of 145±25 MPa, assuming a lithostatic pressure gradient and crustal density of 2650 kg/m$^3$ (e.g., Schwab and Castro, 2007; Castro et al., 2013).

Klemetti and Clynne (in-prep) determined that zircon saturation temperature in LVC magmas is 750-775˚C (method of Watson and Harrison, 1983) and Ti in zircon temperatures (method of Ferry and Watson, 2007) range ~700-760˚C (average 725˚C) for Chaos Crags. Maximum zircon saturation temperature of Chaos Crags using a new model from Boehnke et al. (2013) is calculated to be ~705˚C (Klemetti and Clynne, in-prep) which is inconsistent with the phase equilibrium experiments here, Ti in zircon using the Watson and Harrison (1983) method, and Ti in quartz data of M.A. Clynne (personal communication).

The experimentally determined pressure-temperature storage conditions (145±25 MPa and 770±10˚C) determined here are comparable to some dacites, rhyodacites and rhyolites of other systems.

Chaos Crags storage conditions are of slightly greater pressure (and depth) and cooler temperature than the 50-100 MPa (2.0-4.5 km) and 825-875˚C as determined by Schwab and Castro (2007) of the 1915 Lassen Peak host dacite magma chamber

proposed by Clynne (1999). Refinement of those 1915 Lassen Peak storage conditions is currently in-progress (Schwab, personal communication), but are unlikely to change significantly.

Rutherford et al. (1985) estimate the top of the 1980 Mount St. Helens (MSH) dacite magma chamber resided at 220±30 MPa (~8.5 km depth) with temperature of 930±10˚C. Blundy et al. (2008) determined the May 18, 1980, blast deposit of MSH tapped magma from just below the edifice to ~5 km below sea level, the subsequent Plinian eruption involved magma that last equilibrated 5-11 km below sea level, and following episodes in 1980 tapped magma down to 10 km below sea level. The tapping of deeper magma stopped abruptly at the end of 1980, coincident with the onset of shallow pre-eruptive seismicity and the transition to purely effusive activity. All subsequent 1981-86 eruptive episodes tapped exclusively shallowly-stored (at or above sea level) magma. Rutherford and Hill (1993) determined the October 1986 dome forming dacite had storage temperature of 860±10˚C. Rutherford and Devine (2008) determined 2004-2006 MSH dacite magma last equilibrated at temperature of 820-890˚C and 3.5-4 km depth. Chaos Crags equilibrated at cooler temperature and a similar depth as magmas that produced the 1980 initial blast deposit and subsequent effusive activity, and the 2004-2006 eruption of MSH.

Castro and Dingwell (2009) determined the rhyolitic magma that erupted explosively on May 1$^{st}$, 2008, from Chaitén was stored at temperatures 780-840˚C and pressures 120-190 MPa, with the minimum pressure corresponding to depth of ~5 km

(using a bubble-free magma overburden density of ~2300 kg/$m^3$). These are similar pressures and depths, and slightly hotter temperatures to those of Chaos Crags.

Larsen (2006) determined storage conditions of rhyodacite magma erupted 3430 years B.P. (a caldera-forming eruption) at Aniakchak volcano, Alaska, to be at temperatures of 870–880°C and pressures of 95–150 MPa, with a likely depth of 4.5–5.4 km. These are similar pressures (and depths) to and significantly hotter temperatures than those of Chaos Crags.

Rhyodacite storage at Chaos Crags was slightly deeper and cooler than the dacite erupted at Novarupta, AK in 1912, which was presumably stored at 850-880˚C very shallowly (>2 km) prior to eruption, as determined by Hammer et al. (2002).

Venezky and Rutherford (1997) determined dacite magma erupted 2.2 k.a. at Mount Rainier was stored at ~2.4 km depth and temperature of 930±10˚C, slightly shallower and significantly hotter than Chaos Crags.

The inferred (by earthquake swarms) shallow magma chamber of Mount Dutton, Alaska volcano resides at ~3-5 km depth (Miller et al., 1999), similar to that of Chaos Crags.

Scruggs et al. (2014) determined that ~50% of mafic enclaves from Chaos Crags are concentrically zoned with respect to vesicularity, composition, and texture, and enclaves are similar, except that a few define a distinct K-enrichment trend. The mafic magma contained olivine, plagioclase, and clinopyroxene, with origination temperature of 1100±50°C and pressure of 11.8±1.4 kbar prior to mixing (Scruggs et al., 2014), and ascent to pressures of ~1-2 kbar.

**Decompression and ascent**

Assuming textural variation is primarily due to decompression, comparison of continuous decompression experimental run products and natural samples of Chaos Crags indicates ascent of the magma that produced the group 1 lavas was relatively quick, >2.6 MPa/hr (corresponding to ascent velocity of >100 m/hr and total decompression times of <48 hrs), and that producing group 2 lavas (domes C-F) was relatively slow, <2.6 MPa/hr (corresponding to ascent velocity of <100 m/hr and total decompression times >48 hrs). This can be seen through comparison of groundmass textures and glass compositions in experimental run products and domes C-F. Change in %-crystallinity of plagioclase is the dominant textural change in the experimental run products and domes C-F. Plagioclase crystallinity increases throughout the dome emplacement sequence and decompression experiments. Glass compositions of decompression experimental run products mimic the glass composition of pyroclastic flows and domes through stratigraphic succession, showing increased $SiO_2$ and $K_2O$, and decreased $Al_2O_3$, CaO, and $Na_2O$ over time.

Rutherford and Hill (1993) determined variable average ascent velocities for the MSH May 18, 1980 eruption of >66 m/hr for amphiboles with no dehydration rims, 35-50 m/hr for thin-rimmed amphiboles (probably erupted from the ~8km depth storage), and 15-30 m/hr for thick rimmed amphiboles (probably erupted from along the conduit margin), with the average ranging 10-50 m/hr. Seismic data (Endo et al., 1990) suggests ascent rate of 25-40 m/hr for post May 18, 1980 MSH magmas. Magma ascent rates estimated from surface deformation studies range from 1-5 m/hr in the days before an eruption to 150 m/hr as extrusion begins (Chadwick et al., 1988), bracketing average

ascent rates based on amphibole reaction rim measurements. These are comparable ascent rates to those of Chaos Crags.

Castro and Dingwell (2009) determined ascent rate of >40 MPa/hr (corresponding to velocity of >0.5 m/s or 1800 m/hr) for the 2008 rhyolite of Chaitén, much greater (one or more orders of magnitude) than that of magma producing the group 2 lavas of Chaos Crags.

## Uncertainties

### Model dissimilarity and potential magma evolution

The results from the saturation model of Papale et al. (2006) using quartz-hosted melt inclusions, the FeTi-oxide geothermometer/oxybarometer of Ghiorso and Evans (2008) using titanomagnetite-ilmenite pairs, and the amphibole chemical equilibrium model of Ridolfi et al. (2010), broadly agree, but show slight variations. Amphibole rims last equilibrated at lower $H_2O_{melt}$ concentrations, lower pressure, slightly higher temperature, and more oxidizing conditions than melt inclusions and titanomagnetite-ilmenite pairs suggest. Melt inclusions formed earlier than the amphibole, titanomagnetite, and ilmenite rims, as seen by the presence of melt inclusions of lesser mixed and more evolved compositions than the silica end-member, within resorbed quartz phenocrysts. There is no evidence to suggest magma descended or convected and overturned as it did at Lassen Peak (Clynne, 1999). It is possible that melt inclusions are recording the crystallization of magma at a slightly cooler temperature, ~750°C as suggested by textures of the phase equilibrium experimental run products and zircon saturation temperatures (Klemetti and Clynne, in prep). This is followed by warming of

the chamber, as seen by the resorbed quartz, and slight mixing, as seen by the more mafic compositions of early eruptive products compared to compositions of melt inclusions. The warming episode lowers the host magma's density, bringing it closer to the surface and to slightly lower pressure, increasing the stability of quartz, and lowering saturation levels of volatiles. Magma is then stored at these conditions as recorded in the titanomagnetite-ilmenite pairs. Then, intrusion of the mafic magma occurs, ultimately leading to eruption, with the amphibole phenocryst compositions recording the heating, decompression, and ascent associated with eruption.

**Storage**

All experiments were conducted at $H_2O$-saturated conditions. The assumption of $H_2O$-saturation is reasonable for phase equilibrium experiments determining equilibrium storage conditions. The natural sample contains stable hydrous minerals, such as biotite and amphibole, and preserved melt inclusions, which have $H_2O$-concentrations that overlap with modeled saturations of experimental run products in the experimentally determined storage region, along with minor $CO_2$ concentrations up to ~350 ppm. In the event that storage conditions were $H_2O$-undersaturated the storage pressure range would elevate to greater pressures (e.g., Larsen, 2006).

**Decompression**

Browne and Gardner (2006) conducted single-step and multi-step isothermal decompression experiments on 1992 eruptive products from Redoubt, Alaska. They determined the dehydration breakdown of amphibole and found that the rate and width of rim-formation varies with pressure, decompression rate, and decompression path. In their

experiments, rim formation rate is a maximum at lower pressure for multi-step, as compared to single-step decompressions. For single-step, and to a lesser degree for multi-step decompression experiments, each step provides a shock to the system that may help overcome kinetic barriers to crystal nucleation and growth or breakdown reactions (e.g., Brugger and Hammer, 2010a, 2010b; Brugger, 2011); those shocks are not present in continuous decompression experiments. It may be the case that maximum rate of rim formation for continuous decompression experiments is at even lower pressures, outside of the investigated range.

These decompression experiments assume $H_2O$-saturated conditions, which may be reasonable for most of group 1, but less reasonable for group 2. These experiments also assume, despite some contamination from mafic enclaves, no mixing occurred with the mafic source. EPMA analyses of the silicic and mafic glasses (Heiken and Eichelberger, 1980) show the two glasses are different, but with only minimal compositional variation (slightly higher $K_2O$ and FeO, and lower $Na_2O$ in the mafic enclave glass) between the two.

It may be the case that temperature plays a significant role in the formation of dehydration breakdown rims, surrounding biotite and amphibole. The rims may record a mixing intensity of sorts, related to degree of heating, and duration and degree of mixing. It is likely that formation of dehydration rims is a complex process involving several magmatic properties in addition to decompression rate, such as decompression path, crystallization kinetics, temperature, and volatile concentrations.

It is important to obtain more information regarding the evolution of magmatic parameters within the Chaos Crags system, such as volatile concentrations, temperatures, viscosity changes, glass transitions, mafic magma evolution, and more, in order to further understand the complexities. Determination of $H_2O$-concentrations of all pyroclastic flow and dome sample glasses, geothermometry using titanomagnetite-ilmenite pairs, and chemical equilibrium conditions for amphibole phenocrysts from all pyroclastic flows and domes would provide additional constraints for decompression experiments and the evolution of Chaos Crags.

# CONCLUSION

Eruptive products from the explosive and effusive 1050 calibrated years B.P. eruption of Chaos Crags displays evidence for magma mixing between a silicic rhyodacite host magma and an intruding mafic magma. Pumice from the initial, explosive eruption (the lower pyroclastic flow), contains the nearest-to-end-member rhyodacite with only minor mafic enclaves. Pre-eruptive pressure-temperature storage conditions of the rhyodacite host magma are 145±25 MPa and 770±10ºC, as determined by SEM textural and EPMA geochemical analyses of cold-seal hydrothermal phase equilibrium experimental run products, combined with constraints on $H_2O$ concentration, $fO_2$, pressure, and temperature from natural sample melt inclusions, titanomagnetite-ilmenite pairs, and amphibole chemical equilibrium. Textural and geochemical comparisons of continuous decompression experimental run products and natural samples indicate that decompression and ascent of magma producing group 1 lavas was relatively quick, >2.6 MPa/hr (corresponding to minimum ascent velocity of 100m/hr and total decompression times of <48 hrs), whereas that producing group 2 lavas (domes C-F) was relatively slow, <2.6 MPa/hr (corresponding to ascent velocity of <100m/hr and total decompression times >48 hrs).

## REFERENCES

Andrews, B.J. and Manga, M., 2014, Thermal and rheological controls on the formation of mafic enclaves or banded pumice, Contributions to Mineralogy and Petrology, 167, 961.

Asimow, P.D. and Ghiorso, M.S., 1998, Algorithmic modifications extending MELTS to calculate subsolidus phase relations, American Mineralogist, 83: 1127-1131.

Bacon, C., 1986, Magmatic inclusions in silicic and intermediate volcanic rocks, Journal of Geophysical Research, v. 91, p. 6091-6112.

Bacon, C. and Hirschmann, M., 1988, Mg/Mn partitioning as a test for equilibrium between coexisting Fe-Ti oxides. American Mineralogist 73: 57-61.

Berge, P. and Monfort, M., 1986, Teleseismic residual study of the Lassen Volcanic National Park region in California. USGS Open-File Report: 86-252.

Berge, P.A., and Stauber, D.A., 1987, Seismic refraction study of upper crustal structure in the Lassen Peak area, northern California: Journal of Geophysical Research, v. 92, p. 10571–10579.

Berlo, K., Stix, J., Roggensack, K., and Ghaleb, B., 2012, A tale of two magmas, Fuego, Guatemala, Bulletin of Volcanology, v. 74, p. 377-390.

Blundy, J. and Cashman, K., 2008, Petrologic reconstruction of magmatic system variables and processes. Reviews in Mineralogy: Minerals, inclusions, and volcanic processes, 69, 179-239.

Blundy, J., Cashman, K., and Berlo, K., 2008, Evolving magma storage conditions beneath Mount St. Helens inferred from chemical variations in melt inclusions from the 1980-1986 and current (2004-2006) eruptions, US Geological Survey Professional Paper 1750, p. 755-790.

Boehnke, P., Watson, E., Trail, D., Harrison, T., and Schmitt, A., 2013, Zircon saturation re-visited, Chemical Geology, v. 351, p. 324-334.

Borg, L.E., Blichert-Toft, Janne, and Clynne, M.A., 2002, Ancient and modern subduction zone contributions to the mantle sources of lavas from the Lassen Region of California inferred from Lu–Hf isotopic systematics: Journal of Petrology, v. 43, p. 705–723.

Browne, B. and Gardner, J., 2006, The influence of magma ascent path on the texture, mineralogy, and formation of hornblende reaction rims, Earth and Planetary Science Letters, v. 246, p. 161-176.

Brugger, C., 2011, Crystallization of hydrous rhyodacite magma during continuous decompression, Ph. D. Dissertation, University of Hawai'i at Manoa.

Brugger, C. and Hammer, J., 2010a, Crystal size distribution of plagioclase in experimentally decompressed hydrous rhyodacite magma, Earth and Planetary Science Letters, v. 300, p. 246-254.

Brugger, C. and Hammer, J., 2010b, Crystallization kinetics in continuous decompression experiments: Implications for interpreting natural magma ascent processes, Journal of Petrology, v. 51, no. 9, p. 1941-1965.

Castro, J. and Dingwell, D., 2009, Rapid ascent of rhyolitic magma at Chaiten volcano, Chile, Nature, v. 461.

Castro, J.M., Schipper, C.I., Mueller, S.P., Militzer, A.S., Amigo, A., Silva Parejas, C., Jacob, D., 2013, Storage and eruption of near-liquidus rhyolite magma at Cordon Caulle, Chile, Bulletin of Volcanology, 75, 4, 1-17.

Chadwick, W., Archuleta, R., and Swanson, D., 1988, The mechanics of ground deformation precursory to dome-building extrusions at Mount St. Helens 1981-1982, Journal of Geophysical Research, v. 93, no. B5, p. 4351-4366.

Christiansen, R., Clynne, M., and Muffler, P., 2002, Geologic map of the Lassen Peak, Chaos Crags, and Upper Hat Creek area, California. U.S. Geological Survey, I-2723. [http://pubs.usgs.gov/imap/i2723/]

Clynne, M.A., 1993, Geologic studies of the Lassen Volcanic Center, Cascade Range, California. Ph. D. Dissertation, University of California, Santa Cruz.

Clynne, M.A., 1999, A complex magma mixing origin for rocks erupted in 1915, Lassen Peak, California, Journal of Petrology, 40: 105-132.

Clynne, M.A., Christiansen, R.L., Felger, T.J., Stauffer, P.H., and Hendley II, J.W., 1999, US Geological Fact Sheet FS173-98.

Clynne, M.A., Christiansen, R.L., Trimble, D.A., and McGeehin, J.P., 2008a, Radiocarbon dates from volcanic deposits of the Chaos Crags and Cinder Cone eruptive sequences and other deposits, Lassen Volcanic National Park and

vicinity, California: U.S. Geological Survey Open-file Report 02-290, 18 p. [http://pubs.usgs.gov/of/2002/of02-290/].

Clynne, M.A. and Muffler, L.J.P., 2010, Geologic map of Lassen Volcanic National Park and vicinity, California: U.S. Geological Survey Scientific Investigations Map 2899, scale 1:50,000.

Clynne, M.A., Muffler, L.J.P., Siems, D.F., Taggart, J.E. Jr., and Bruggman, Peggy, 2008b, Major and EDXRF trace element chemical analyses of volcanic rocks from Lassen Volcanic National Park and vicinity: U.S. Geological Survey Open-File Report 2008-1091, 11p. and .xls table [http://pubs.usgs.gov/of/2008/1091/].

Clynne, M.A., Robinson, J.E., Nathenson, M., Muffler, L.J.P., 2012, Volcano hazards assessment for the Lassen region, northern California, U.S. Geological Survey Scientific Investigations Report 2012-5176-A.

Dixon, J. and Clague, D., 2001, Volatiles in basaltic glass from Loihi Seamount, Hawaii: evidence for a relatively dry plume component, Journal of Petrology, v. 42, p. 627-654.

Dixon, J., Clague, D., and Stolper, E., 1991, Degassing history of water, sulfur, and carbon in submarine lavas from Kilauea volcano, Hawaii, Journal of Geology, v. 99, p. 371-394.

Eichelberger, J., Chertkoff, D., Dreher, S. and Nye, C., 2000, Magmas in collision: Rethinking chemical zonation in silicic magmas, Geology, v. 28, no. 7, p. 603-606.

Endo, E., Dzurisin, D. and Swanson, D., 1990, Geophysical and observational constraints for ascent rates of dacitic magma at Mount Saint Helens, Magma Transport and Storage, p. 317-334.

Ewert, J., Guffanti, M., and Murray, T., 2005, An assessment of volcanic threat and monitoring capabilities in the United States; framework for a national volcano early warning system, US Geological Survey Open-file Report OFR 2005-1164.

Feeley, T.C., Clynne, M.A., Winer, G.S., and Grice, W.C., 2008a, Oxygen isotope geochemistry of the Lassen Volcanic Center, California: Resolving crustal and mantle contributions to continental arc magmatism, Journal of Petrology, 49: 971-997.

Feeley, T.C., Wilson, L.F., and Underwood, S.J., 2008b, Distribution and compositions of magmatic inclusions in the Mount Helen dome, Lassen Volcanic Center, California: Insights into magma chamber processes, Lithos, 106: 173-189.

Ferry, J., and Watson, E., 2007, New thermodynamic models and revised calibrations for the Ti-in-zircon and Zr-in-rutile thermometers, Contributions to Mineralogy and Petrology, v. 154, no. 4, p. 429-437.

Fine, G. and Stolper, E., 1985, The speciation of carbon dioxide in sodium aluminosilicate glasses, Contributions to Mineralogy and Petrology, v. 92, no. 2, p. 105-121.

Ghiorso, M. and Evans, B., 2008, Thermodynamics of rhombohedral oxide solid solutions and a revision of the Fe-Ti two-oxide geothermometer and oxygen-barometer, American Journal of Science, v. 308, p. 957-1039.

Ghiorso, M.S. and Sack, R.O., 1995, Chemical mass transfer in magmatic process. IV. A revised and internally consistent thermodynamic model for the interpolation and extrapolation of liquid-solid equilibria in magmatic systems at elevated temperatures and pressures, Contributions to Mineralogy and Petrology, 119: 197-212.

Guffanti, M., Diefenbach, A., Ewert, J., Ramsey, D., Cervelli, P., and Schilling, S., 2008, Volcano-monitoring instrumentation in the United States, 2008. U.S. Geological Survey Open-file Report OFR 2009-1165.

Haas, J. and Robie, R., 1973, Thermodynamic data for wustite, $Fe_{0.947}O$, magnetite, $Fe_3O_4$, and hematite, $Fe_2O_3$, Eos, Transactions, American Geophysical Union, 54, 4, 483.

Hammer, J., Rutherford, M., and Hildreth, W., 2002, Magma storage prior to the 1912 eruption at Novarupta, Alaska, Contributions to Mineralogy and Petrology, v. 144, no. 2, p. 144-162.

Heiken, G., and Eichelberger, J.C., 1980, Eruptions at Chaos Crags, Lassen Volcanic National Park, Journal of Volcanology and Geothermal Research, 7: 443-481.

Heubner, J., 1971, Buffering techniques for hydrostatic systems at elevated pressure, Research Techniques for High Pressure and High Temperature, p. 123-177.

Heubner, J. and Sato, M., 1970, The oxygen fugacity-temperature relationships of manganese oxide and nickel oxide buffers, American Mineralogist, v. 55, p. 934-952.

Hewitt, A., 1978, A redetermination of the fayalite-magnetite-quartz equilibrium between 650° and 850°C, American Journal of Science, v. 278, p. 715-724.

Ihinger P., Hervig, R., and McMillan, P., 1994 Analytical methods for volatiles in glasses. Reviews in Mineralogy: Volatiles in Magmas, 30, 67–112.

Jachens, R. and Saltus, R., 1983, Precision gravity network for monitoring the Lassen geothermal system, northern California: U.S. Geological Survey Open-File Report 83-193, 16 p.

Jarosewich, G., 2002, Smithsonian Microbeam Standards. Journal of Research of the National Institute of Standards and Technology, 107, 681–685.

Klemetti, E. and Clynne, M., in prep, Localized rejuvenation of a crystallizing pluton captured in volcanic zircon from Lassen Volcanic Center, California.

Larsen, J., 2006, Rhyodacite magma storage conditions prior to the 3430 yBP caldera-forming eruption of Aniakchak volcano, Alaska. Contributions to Mineralogy and Petrology, 152, 523-540.

Leake, B.E., Woolley, A.R., Arps, C.E.S., Birch, W.D., Gilbert, M.C., Grice, J.D., Hawthorne, F.C., Kato, A., Kisch, H.J., Krivovichev, V.G., Linthout, K., Laird, J., Mandarino, J.A., Maresch, W.V., Nickel, E.H., Rock, N.M.S., Schumacher, J.C., Smith, D.C., Stephenson, N.C.N., Ungaretti, L., Whittaker, E.J.W., and Youzhi, G.,1997, Nomenclature of amphiboles: Report of the Subcommittee on Amphiboles of the International Mineralogical Association, Commission on New Minerals and Mineral Names, American Mineralogist, v. 82, p. 1019-1037.

LePage, L.D., 2003, ILMAT: An Excel worksheet for ilmenite-magnetite geothermometry and geobarometry. Computers & geosciences, 29, 5, 673-678.

Loomis, B., 1926, Pictoral history of the Lassen Volcano, California.

Lowenstern, J., 2003, Melt inclusions come of age: Volatiles, Volcanoes, and Sorby's Legacy, In: B. De Vivo and R.J. Bodnar (eds). Melt Inclusions in Volcanic Systems: Methods, Applications and Problems. Developments in Volcanology 5, Elsevier Press, Amsterdam, pp. 1-22.

Macdonald, G.A., 1963, Geologic map of the Manzanita Lake quadrangle, California: U.S. Geological Survey Geologic Quadrangle Map GQ-248, scale 1:62,500.

Macdonald, G.A., 1964, Geologic map of the Prospect Peak quadrangle, California: U.S. Geological Survey Geologic Quadrangle Map GQ-345, scale 1:62,500.

Macdonald, G.A., 1965, Geologic map of the Harvey Mountain quadrangle, California: U.S. Geological Survey Geologic Quadrangle Map GQ-443, scale 1:62,500.

Matthews, W., Linnen, R., and Guo, Q., 2003, A filler-rod technique for controlling redox conditions in cold-seal pressure vessels. American Mineralogist, 88: 701-707.

McBirney, A., 1968, Petrochemistry of the Cascade andesite volcanoes, Oregon Department of Geology and Mineralogy Industry Bulletin, v. 62, p. 101-107.

Miller, D., 1989, Potential Hazards from Future Volcanic Eruptions in California: U.S. Geological Survey Bulletin 1847.

Miller, T., Chertkoff, D., Eichelberger, J., and Coombs, M., 1999, Mount Dutton volcano, Alaska: Aleutian arc analog to Unzen volcano, Japan, Journal of Volcanology and Geothermal Research, v. 89, p. 275-301.

Moore, G., 2008, Interpreting $H_2O$ and $CO_2$ contents in melt inclusions: Constraints from solubility experiments and modeling. Reviews in Mineralogy: Minerals, inclusions, and volcanic processes, 69, 331-361.

Moore, G., Vennemann, T., and Carmichael, I., 1998, An empirical model for the solubility of $H_2O$ in magmas to 3 kilobars, American Mineralogist, v. 83, no. 1-2, p. 36-42.

Nathenson, M., Clynne, M., and Muffler, P., 2012, Eruption Probabilities for the Lassen Volcanic Center and Regional Volcanism, Northern California, and Probabilities for Large Explosive Eruptions in the Cascade Range. U.S. Geological Survey Scientific Investigations Report 2012–5176-B.

Newman, S., Stolper, E., and Epstein, S., 1986, Measurement of water in rhyolitic glasses: Calibration of an infrared spectroscopic technique. American Mineralogist, 71, 1527–1541.

Papale, P., Moretti, R., and Barbato, D., 2006, The compositional dependence of the saturation of $H_2O + CO_2$ fluids in silicate melts, Chemical Geology, v. 229, p. 78-95.

Poland, M., Bawden, G., Lisowski, M., Dzurisin, D., 2004, Newly discovered subsidence at Lassen Peak, southern Cascade Range, California, from InSAR and GPS, Eos,

Transactions, American Geophysical Union, 85, 47, Suppl., AGU 2004 Fall Meeting.

Quinn, E.T. and Schwab, B.E., 2012, Experimental determination of one-atmosphere phase relations of rhyodacite pumice erupted from Chaos Crags, Lassen Volcanic Center, California, Abstract V11C-2766 presented at 2012 Fall Meeting, AGU, San Francisco, Calif., 3-7 Dec.

Ridolfi, F., Renzulli, A., and Puerini, M., 2010, Stability and chemical equilibrium of amphibole in calc-alkaline magmas; an overview, new thermobarometric formulations an application to subduction-related volcanoes. Contributions to Mineralogy and Petrology, 160, 1, 45-66.

Robinson, J. and Clynne, M., 2012, Lahar hazard zones for eruption-generated lahars in the Lassen Volcanic Center, California, U.S. Geological Survey Scientific Investigations Report 2012–5176–C.

Rutherford, M. and Devine, J., 2008, Magmatic conditions and processes in the storage zone of the 2004-2006 Mount St. Helens dacite, US Geological Survey Professional Paper 1750, p. 703-725.

Rutherford, M. and Hill, P., 1993, Magma ascent rates from amphibole breakdown: an experimental study applied to the 1980-1986 Mount St. Helens eruptions, Journal of Geophysical Research, v. 98, no. B11, p. 19667-19685.

Rutherford, M., Sigurdsson, H., Carey, S., and Davis, A., 1985, The May 18, 1980 eruption of Mount St. Helens; 1, Melt composition and experimental phase equilibria, Journal of Geophysical Research, v. 90, no. B4, p. 2929-2947.

Schwab, B.E. and Castro, J.M., 2007, Pre-eruptive storage conditions of the 1915 Lassen Peak dacite, Geol. Soc. Amer. Abstract with Programs, Vol. 39, No. 6. 143-4.

Scruggs, M., Putirka, K., and Clynne, M., 2014, Enclave formation and magma mixing at Chaos Crags, California, Goldschmidt 2014, Abstract 2241.

Seaman, S., Dyar, M., Marinkovic, N., Dunbar, N., 2006, An FTIR study of hydrogen in anorthoclase and associated melt inclusions, American Mineralogist, v. 91, no. 1, p. 12-20.

Sheppard, P., Ort, M., Anderson, K., Clynne, M., and May, E., 2009, Multiple dendrochronological responses to the eruption of Cinder Cone, Lassen Volcanic National Park, California. Dendrochronologia, 27: 213–221.

Spencer, K., and Lindsley, D., 1981, A solution model for coexisting iron-titanium oxides, American Mineralogist, v. 66, p. 1189-1201.

Stormer, J., 1983, The effects of recalculation on estimates of temperature and oxygen fugacity from analyses of multicomponent iron-titanium oxides, American Mineralogist, v. 68, no. 5-6, p. 586-594.

Tepley III, F.J., Davidson, J.P., and Clynne, M.A., 1999, Magmatic interactions as recorded in plagioclase phenocrysts of Chaos Crags, Lassen Volcanic Center, California, Journal of Petrology, 40: 787-806.

Venezky, D. and Rutherford, M., 1997, Preeruption conditions and timing of dacite-andesite magma mixing in the 2.2 ka eruption at Mount Rainier, Journal of Geophysical Research, v. 102, p. 20069-20086.

Watson, E. and Harrison, T., 1983, Zircon saturation revisited; temperature and composition effects in a variety of crustal magma types, Earth and Planetary Science Letters, v. 64, no. 2, p. 295-304.

White, M., Ramsey, D., and Miller, D., 2011, Database for Potential Hazards from Future Volcanic Eruptions in California. U.S. Geological Survey Data Series 661. [http://pubs.usgs.gov/ds/661/]

Williams, H., 1931, The dacites of Lassen Peak and vicinity, California, and their basic inclusions, American Journal of Science, 22: 385-403.

Williams, H., 1932, Geology of Lassen Volcanic National Park, California: Berkeley, University of California Department of Geological Sciences Bulletin, v. 21, p. 195–385.

Wilson, T.A., 1961, The geology near Mineral, California: Berkeley, University of California, M.S. thesis, 92 p.

**Table 1.** Natural sample glass compositions (wt. %).

| Sample | Unit | $SiO_2$ | $TiO_2$ | $Al_2O_3$ | $FeO^*$ | MnO | MgO | CaO | $Na_2O$ | $K_2O$ | Cl |
|---|---|---|---|---|---|---|---|---|---|---|---|
| LQ13-01-glass-ave (n=7) | lower pf | 77.97 (46) | 0.17 (3) | 12.23 (38) | 0.94 (10) | 0.06 (3) | 0.16 (6) | 0.90 (18) | 3.39 (14) | 4.07 (16) | 0.09 (1) |
| LC84-417-glass-ave (n=8) | lower pf | 77.48 (21) | 0.17 (2) | 12.45 (14) | 0.78 (5) | 0.03 (1) | 0.15 (1) | 0.87 (2) | 3.88 (10) | 4.11 (4) | 0.08 (1) |
| LC84-418-glass-ave (n=9) | middle pf | 77.45 (29) | 0.16 (2) | 12.45 (8) | 0.77 (6) | 0.04 (1) | 0.16 (1) | 0.85 (4) | 3.96 (23) | 4.07 (12) | 0.08 (1) |
| LC84-428-glass-ave (n=8) | dome A | 77.99 (53) | 0.16 (2) | 11.75 (41) | 0.67 (5) | 0.03 (1) | 0.10 (1) | 0.71 (5) | 4.25 (39) | 4.29 (25) | 0.06 (1) |
| LC84-419-glass-ave (n=7) | upper pf | 78.18 (41) | 0.20 (2) | 11.39 (28) | 0.90 (12) | 0.03 (1) | 0.25 (11) | 0.67 (15) | 3.82 (42) | 4.49 (19) | 0.06 (1) |
| LC84-443-glass-ave (n=15) | dome B | 77.73 (19) | 0.15 (2) | 12.35 (16) | 0.71 (4) | 0.03 (1) | 0.14 (1) | 0.81 (2) | 3.79 (17) | 4.20 (12) | 0.07 (1) |
| LC84-434-glass-ave (n=9) | dome C | 78.56 (99) | 0.17 (6) | 11.93 (68) | 0.63 (30) | MDL | 0.08 (4) | 0.67 (54) | 3.31 (70) | 4.61 (1.64) | 0.02 (1) |
| ChaosD-glass-ave (n=82) | dome D | 77.89 (3.05) | 0.08 (7) | 12.50 (1.75) | 0.32 (24) | MDL | MDL | 0.90 (50) | 3.81 (76) | 4.33 (1.19) | MDL |
| LC84-435-glass | dome D | N/A | N/A | N/A | N/A | N/A | N/A | N/A | N/A | N/A | N/A |
| LC84-433-glass-ave (n=10) | dome E | 78.05 (75) | 0.27 (3) | 11.75 (56) | 0.89 (7) | 0.03 (1) | 0.07 (3) | 0.62 (22) | 3.70 (28) | 4.52 (25) | 0.08 (1) |
| LC84-455-glass-ave (n=17) | dome F | 78.38 (59) | 0.26 (3) | 11.49 (34) | 0.91 (16) | 0.03 (1) | 0.08 (5) | 0.41 (12) | 3.32 (28) | 5.05 (17) | 0.08 (1) |

Notes:

Determined by electron probe microanalysis (EPMA).

All compositions converted to anhydrous and totals normalized to 100.

Numbers in parens are 1sigma uncertainties on mean compositions in terms of least units cited, i.e., 77.97(46)=77.97±0.46.

All analyses for glass in LC84-435 were contaminated by plagioclase.

Raw individual analyses in Appendix B.

* Total Fe reported as FeO as determined by EPMA.

Values marked MDL were below the minimum detection limit.

**Table 2.** Melt inclusion $H_2O$, $OH^-$, $H_2O_t$, and $CO_2$ concentrations from FTIR analysis.

| Melt Inclusion | $H_2O$ (wt. %)[a] | $OH^-$ (wt. %)[b] | $H_2O_t$ (wt. %)[c] | $CO_2$ (ppm)[d] | Saturation Pressure (MPa)[e] |
|---|---|---|---|---|---|
| LQ13-01-mi-01-02 | 5.07 (51) | 1.12 (11) | 6.19 (62) | 258 (26) | 276 |
| LQ13-01-mi-02-01 | 4.05 (41) | 0.45 (5) | 4.50 (45) | 44 (5) | 125 |
| LQ13-01-mi-03-01* | 3.03 (30) | 1.48 (15) | 4.52 (45) | 285 (29) | N/A |
| LQ13-01-mi-04-01 | 3.34 (33) | 1.06 (11) | 4.41 (44) | 204 (20) | 115 |
| LQ13-01-mi-04-02 | 2.85 (29) | 1.14 (11) | 3.99 (40) | 190 (19) | 92 |
| LQ13-01-mi-05-01 | 3.50 (35) | 1.27 (13) | 4.77 (48) | 190 (19) | 134 |
| LQ13-01-mi-06-01 | 3.70 (37) | 1.72 (17) | 5.42 (54) | 312 (31) | 190 |
| LQ13-01-mi-07-01 | 3.56 (36) | 1.22 (12) | 4.78 (48) | 300 (30) | 139 |
| LQ13-01-mi-07-02 | 3.65 (37) | 1.22 (12) | 4.87 (49) | 175 (18) | 145 |
| LQ13-01-mi-07-03 | 3.18 (32) | 1.22 (12) | 4.40 (44) | 140 (14) | 116 |
| LQ13-01-mi-10-03* | 2.95 (30) | 1.48 (15) | 4.44 (44) | 209 (21) | N/A |
| LQ13-01-mi-11-01 | 4.33 (43) | 2.12 (21) | 6.45 (65) | 285 (29) | 286 |
| LQ13-01-mi-12-01 | 3.86 (39) | 2.01 (20) | 5.87 (59) | 191 (19) | 229 |
| LQ13-01-mi-13-01 | 3.89 (39) | 1.48 (15) | 5.38 (54) | 191 (19) | 183 |
| LQ13-01-mi-14-01 | 3.83 (38) | 1.55 (16) | 5.38 (54) | 243 (24) | 190 |
| LQ13-01-mi-14-02* | 3.36 (34) | 1.26 (13) | 4.62 (46) | 74 (7) | N/A |
| LQ13-01-mi-14-03 | 2.68 (27) | 1.32 (13) | 4.00 (40) | 91 (9) | 96 |
| LQ13-01-mi-15-01 | 3.71 (37) | 1.40 (14) | 5.11 (51) | 302 (30) | 162 |
| LQ13-01-mi-16-01 | 3.63 (36) | 1.52 (15) | 5.16 (52) | 249 (25) | 173 |
| LQ13-01-mi-17-01 | 3.76 (38) | 1.25 (13) | 5.01 (50) | 156 (16) | 154 |
| LQ13-01-mi-18-01 | 3.30 (33) | 1.13 (11) | 4.42 (44) | 176 (18) | 116 |
| LQ13-01-mi-18-02 | 3.57 (36) | 1.26 (13) | 4.82 (48) | 223 (22) | 142 |
| LQ13-01-mi-19-02* | 3.34 (33) | 1.24 (12) | 4.58 (46) | 143 (14) | N/A |
| LQ13-01-mi-20-01 | 3.56 (36) | 1.22 (12) | 4.78 (48) | 338 (34) | 135 |
| LQ13-01-mi-21-01 | 3.40 (34) | 1.24 (12) | 4.63 (46) | 348 (35) | 124 |
| LQ13-01-mi-23-02 | 3.63 (36) | 1.17 (12) | 4.80 (48) | 286 (29) | 137 |
| LQ13-01-mi-23-03 | 3.36 (34) | 1.38 (14) | 4.74 (47) | 263 (26) | 135 |
| LQ13-01-mi-24-01* | 3.31 (33) | 1.12 (11) | 4.43 (44) | 121 (12) | N/A |
| LQ13-01-mi-25-01 | 3.09 (31) | 1.05 (11) | 4.14 (41) | 44 (4) | 97 |
| LQ13-01-mi-26-02 | 3.32 (33) | 1.18 (12) | 4.50 (45) | 199 (20) | 120 |
| LQ13-01-mi-27-01 | 5.32 (53) | 1.17 (12) | 6.48 (65) | 139 (14) | 297 |
| LQ13-01-mi-28-01 | 3.02 (30) | 1.09 (11) | 4.11 (41) | 209 (21) | 98 |
| LQ13-01-mi-28-02 | 3.40 (34) | 1.17 (12) | 4.56 (46) | 361 (36) | 121 |
| LQ13-01-mi-29-01 | 3.06 (31) | 1.06 (11) | 4.12 (41) | 159 (16) | 100 |

**Table 2, continued.**

| Melt Inclusion | $H_2O$ (wt. %)[a] | $OH^-$ (wt. %)[b] | $H_2O_t$ (wt. %)[c] | $CO_2$ (ppm)[d] | Saturation Pressure (MPa)[e] |
|---|---|---|---|---|---|
| LQ13-01-mi-01-01-leak | 1.45 (15) | 0.97 (10) | 2.42 (24) | 36 (4) | N/A |
| LQ13-01-mi-02-02-leak | 2.79 (28) | 0 | 2.79 (28) | 104 (10) | N/A |
| LQ13-01-mi-10-01-leak | 1.19 (12) | 1.48 (15) | 2.67 (27) | 0 | N/A |
| LQ13-01-mi-15-02-leak | 1.22 (12) | 0.61 (6) | 1.83 (18) | 48 (5) | N/A |
| LQ13-01-mi-18-03-leak | 1.80 (18) | 0.66 (7) | 2.45 (25) | 53 (5) | N/A |
| LQ13-01-mi-19-01-leak | 1.47 (15) | 0.54 (5) | 2.01 (20) | 145 (15) | N/A |
| LQ13-01-mi-24-02-leak | 0.84 (8) | 0.25 (3) | 1.09 (11) | 48 (5) | N/A |
| LQ13-01-mi-26-01-leak | 1.84 (18) | 0.68 (7) | 2.52 (25) | 20 (2) | N/A |

Notes:

[*]Not analyzed by EPMA.

[**]Average and median taken from preserved melt inclusions only.

[a]using 5200 $cm^{-1}$ band and $\varepsilon$=1.61 l $mol^{-1}$ $cm^{-1}$ (Newman et al., 1986)

[b]using 4500 $cm^{-1}$ band and $\varepsilon$=1.73 l $mol^{-1}$ $cm^{-1}$ (Newman et al., 1986)

[c]totals are sum of $H_2O$ and $OH^-$

[d]using 2350 $cm^{-1}$ band and $\varepsilon$=945 l $mol^{-1}$ $cm^{-1}$ (Fine and Stolper, 1985)

[e]using saturation model of Papale et al. (2006) with temperature at 775°C.

Numbers in parens are 10% uncertainties on totals in terms of least units cited, i.e., 5.07(51)=5.07±0.51.

Thicknesses and absorbances in Appendix C.

**Table 3.** Melt inclusion glass compositions (wt. %).

| Melt Inclusion | $SiO_2$ | $TiO_2$ | $Al_2O_3$ | FeO* | MnO | MgO | CaO | $Na_2O$ | $K_2O$ | Cl |
|---|---|---|---|---|---|---|---|---|---|---|
| LQ13-01-mi-01-02 (n=3) | 78.06 (24) | 0.12 (3) | 12.35 (16) | 0.64 (8) | MDL | 0.14 (2) | 0.83 (1) | 3.41 (18) | 4.31 (10) | 0.11 (2) |
| LQ13-01-mi-02-01 (n=4) | 78.31 (26) | 0.12 (4) | 12.14 (23) | 0.79 (11) | MDL | 0.14 (2) | 0.74 (3) | 3.32 (12) | 4.32 (7) | 0.09 (1) |
| LQ13-01-mi-04-01 (n=4) | 79.52 (14) | 0.08 (3) | 11.49 (8) | 0.64 (4) | MDL | 0.11 (2) | 0.70 (4) | 3.22 (20) | 4.10 (4) | 0.11 (1) |
| LQ13-01-mi-04-02 (n=3) | 79.56 (35) | 0.09 (4) | 11.45 (22) | 0.62 (26) | MDL | 0.07 (2) | 0.69 (3) | 3.30 (9) | 4.06 (2) | 0.10 (1) |
| LQ13-01-mi-05-01 (n=6) | 79.83 (52) | 0.08 (2) | 11.33 (29) | 0.56 (9) | 0.05 (2) | 0.05 (2) | 0.55 (4) | 3.35 (13) | 4.06 (9) | 0.11 (1) |
| LQ13-01-mi-06-01 (n=5) | 79.07 (22) | 0.09 (2) | 11.69 (8) | 0.54 (11) | 0.05 (2) | 0.08 (2) | 0.73 (4) | 3.49 (22) | 4.12 (7) | 0.11 (2) |
| LQ13-01-mi-07-01 (n=5) | 79.18 (29) | 0.08 (3) | 11.68 (25) | 0.58 (11) | MDL | 0.07 (3) | 0.64 (1) | 3.51 (13) | 4.11 (3) | 0.11 (1) |
| LQ13-01-mi-07-02 (n=5) | 79.16 (38) | 0.07 (1) | 11.76 (15) | 0.68 (34) | MDL | 0.07 (4) | 0.61 (3) | 3.33 (13) | 4.16 (2) | 0.12 (2) |
| LQ13-01-mi-07-03 (n=6) | 79.06 (18) | 0.08 (2) | 11.82 (10) | 0.62 (9) | 0.06 (3) | 0.06 (2) | 0.65 (6) | 3.37 (14) | 4.17 (3) | 0.09 (1) |
| LQ13-01-mi-11-01 (n=1) | 79.49 | 0.10 | 11.46 | 0.63 | MDL | 0.08 | 0.70 | 3.46 | 3.97 | 0.11 |
| LQ13-01-mi-12-01 (n=7) | 79.53 (24) | 0.09 (2) | 11.49 (17) | 0.63 (10) | 0.05 (3) | 0.08 (2) | 0.69 (3) | 3.20 (8) | 4.11 (4) | 0.11 (1) |
| LQ13-01-mi-13-01 (n=5) | 79.86 (23) | 0.07 (2) | 11.39 (12) | 0.45 (9) | 0.06 (5) | 0.07 (2) | 0.59 (2) | 3.35 (11) | 4.04 (3) | 0.11 (2) |
| LQ13-01-mi-14-01 (n=7) | 79.17 (27) | 0.12 (3) | 11.83 (8) | 0.54 (9) | 0.05 (3) | 0.07 (2) | 0.76 (6) | 3.24 (14) | 4.12 (4) | 0.11 (2) |
| LQ13-01-mi-14-03 (n=13) | 78.80 (37) | 0.11 (4) | 11.98 (20) | 0.67 (18)` | 0.04 (3) | 0.10 (4) | 0.74 (11) | 3.33 (13) | 4.12 (18) | 0.10 (2) |
| LQ13-01-mi-15-01 (n=4) | 79.32 (21) | 0.09 (3) | 11.60 (16) | 0.70 (17) | MDL | 0.07 (2) | 0.70 (3) | 3.34 (15) | 4.06 (7) | 0.10 (2) |
| LQ13-01-mi-16-01 (n=5) | 78.99 (52) | 0.09 (2) | 11.97 (22) | 0.65 (25) | MDL | 0.08 (4) | 0.74 (3) | 3.14 (46) | 4.16 (2) | 0.10 (2) |
| LQ13-01-mi-17-01 (n=8) | 79.17 (24) | 0.09 (3) | 11.59 (25) | 0.69 (17) | MDL | 0.08 (2) | 0.68 (3) | 3.34 (14) | 4.19 (3) | 0.11 (2) |
| LQ13-01-mi-18-01 (n=6) | 79.49 (14) | 0.07 (2) | 11.64 (20) | 0.46 (12) | 0.03 (2) | 0.06 (1) | 0.59 (3) | 3.52 (29) | 4.02 (5) | 0.12 (2) |
| LQ13-01-mi-18-02 (n=9) | 79.04 (28) | 0.08 (2) | 11.78 (15) | 0.62 (15) | 0.07 (5) | 0.07 (3) | 0.65 (4) | 3.50 (13) | 4.07 (2) | 0.11 (1) |
| LQ13-01-mi-20-01 (n=6) | 79.60 (20) | 0.08 (2) | 11.33 (20) | 0.62 (20) | 0.04 (3) | 0.08 (2) | 0.71 (4) | 3.41 (11) | 4.00 (6) | 0.12 (2) |
| LQ13-01-mi-21-01 (n=2) | 80.00 (9) | 0.08 (1) | 11.06 (1) | 0.53 (23) | 0.07 (5) | 0.05 (2) | 0.67 (1) | 3.49 (7) | 3.96 (2) | 0.09 (2) |
| LQ13-01-mi-23-02 (n=2) | 80.32 (28) | 0.07 (1) | 11.18 (9) | 0.51 (15) | MDL | MDL | 0.64 (2) | 3.17 (5) | 3.98 (7) | 0.09 (1) |
| LQ13-01-mi-23-03 (n=6) | 79.27 (35) | 0.10 (2) | 11.55 (13) | 0.62 (9) | 0.05 (3) | 0.06 (2) | 0.72 (2) | 3.42 (17) | 4.08 (3) | 0.12 (1) |
| LQ13-01-mi-25-01 (n=5) | 79.06 (39) | 0.08 (2) | 11.09 (26) | 0.54 (7) | 0.05 (1) | 0.08 (1) | 0.59 (4) | 3.49 (13) | 4.00 (4) | 0.11 (1) |
| LQ13-01-mi-26-02 (n=2) | 79.38 (2) | 0.13 (4) | 11.40 (25) | 0.55 (16) | MDL | 0.12 (1) | 0.71 (6) | 3.50 (2) | 4.04 (3) | 0.10 (2) |
| LQ13-01-mi-27-01 (n=4) | 78.62 (39) | 0.08 (2) | 11.96 (15) | 0.64 (10) | 0.06 (5) | 0.07 (1) | 0.63 (3) | 3.49 (15) | 4.31 (22) | 0.12 (1) |
| LQ13-01-mi-28-01 (n=6) | 79.35 (22) | 0.08 (2) | 11.50 (13) | 0.58 (15) | MDL | 0.08 (3) | 0.71 (1) | 3.38 (16) | 4.15 (3) | 0.10 (1) |
| LQ13-01-mi-28-02 (n=2) | 79.45 (24) | 0.13 (5) | 11.30 (3) | 0.77 (3) | 0.03 (1) | 0.07 (2) | 0.70 (2) | 3.40 (15) | 4.04 (2) | 0.10 (1) |
| LQ13-01-mi-29-01 (n=6) | 79.13 (20) | 0.08 (2) | 11.75 (11) | 0.54 (14) | MDL | 0.05 (3) | 0.60 (2) | 3.48 (18) | 4.22 (3) | 0.11 (1) |

Notes:

Determined by electron probe microanalysis (EPMA).

All compositions converted to anhydrous and totals normalized to 100.

Numbers in parens are 1sigma uncertainties on mean compositions in terms of least units cited, i.e., 78.06(24)=78.06±0.24.

Raw individual analyses in Appendix D.

*Total Fe reported as FeO as determined by EPMA.

Values marked MDL were below the minimum detection limit.

**Table 4.** Phase equilibrium experimental run conditions.

| Sample | Run Duration (hr) | Temperature (°C) | Pressure (MPa) | $H_2O$ (g) | Starting Material (g) | $H_2O$ (wt. %) | Phases[a] | Furnace | Starting Material |
|---|---|---|---|---|---|---|---|---|---|
| CCPb-01 | 95.3 | 775 | 150 | 0.004 | 0.035 | 9.7 | qz, bt, am | H0 | LQ13-01 |
| CCPb-02 | 95.3 | 850 | 150 | 0.006 | 0.036 | 13.8 | px | H1 | LQ13-01 |
| CCPb-03 | 95.3 | 825 | 100 | 0.005 | 0.041 | 10.5 | px | H2 | LQ13-01 |
| CCPb-04 | 95.3 | 875 | 100 | 0.005 | 0.045 | 9.6 | px | H3 | LQ13-01 |
| CCPb-05 | 94.1 | 850 | 200 | 0.005 | 0.095 | 5.1 | px | H0 | LQ13-01 |
| CCPb-06 | 94.2 | 825 | 150 | 0.005 | 0.052 | 9.1 | px | H1 | LQ13-01 |
| CCPb-07 | 94.3 | 875 | 150 | 0.005 | 0.055 | 8.4 | px | H2 | LQ13-01 |
| CCPb-08 | 94.3 | 900 | 100 | 0.005 | 0.062 | 7.6 | px | H3 | LQ13-01 |
| CCPb-09 | 96.1 | 800 | 200 | 0.006 | 0.054 | 9.3 | px, am, bt | H0 | LQ13-01 |
| CCPb-10 | 96.3 | 800 | 175 | 0.005 | 0.051 | 9.5 | am, bt | H1 | LQ13-01 |
| CCPb-11 | 96.4 | 850 | 125 | 0.005 | 0.066 | 7.1 | px | H2 | LQ13-01 |
| CCPb-12 | 98.2 | 800 | 125 | 0.005 | 0.061 | 7.9 | am | H3 | LQ13-01 |
| CCPb-13 | 97.7 | 750 | 100 | 0.005 | 0.048 | 9.9 | qz, bt, am | H0 | LQ13-01 |
| CCPb-14 | 97.7 | 850 | 75 | 0.005 | 0.052 | 9.4 | px | H1 | LQ13-01 |
| CCPb-15 | 97.8 | 800 | 75 | 0.006 | 0.068 | 7.9 | qz | H2 | LQ13-01 |
| CCPb-16 | 96.1 | 900 | 75 | 0.005 | 0.053 | 9.2 | px | H3 | LQ13-01 |
| CCPb-17 | 96.1 | 825 | 125 | 0.006 | 0.064 | 8.1 | px | H0 | LQ13-01 |
| CCPb-18 | 96.3 | 775 | 125 | 0.005 | 0.059 | 8.6 | qz, bt, am | H1 | LQ13-01 |
| CCPb-19 | 96.4 | 800 | 100 | 0.006 | 0.052 | 9.7 | -- | H2 | LQ13-01 |
| CCPb-20 | 93.1 | 750 | 125 | 0.005 | 0.054 | 9.2 | qz, bt, am | H3 | LQ13-01 |
| CCPb-21 | 119.6 | 750 | 150 | 0.006 | 0.052 | 9.9 | qz, bt, am | H0 | LQ13-01 |
| CCPb-22 | 95.8 | 825 | 200 | 0.006 | 0.049 | 10.4 | px, am | H1 | LQ13-01 |
| CCPb-23 | 132.2 | 750 | 75 | 0.006 | 0.067 | 7.5 | qz, bt | H2 | LQ13-01 |
| CCPb-24 | 132.2 | 750 | 200 | 0.001 | 0.014 | 5.9 | qz, bt, am | H3 | CCPb-09 |

**Table 4, continued.**

| Sample | Run Duration (hr) | Temperature (°C) | Pressure (MPa) | $H_2O$ (g) | Starting Material (g) | $H_2O$ (wt. %) | Phases[a] | Furnace | Starting Material |
|---|---|---|---|---|---|---|---|---|---|
| CCPb-25 | 119.8 | 775 | 100 | 0.001 | 0.021 | 5.3 | qz, bt | H1 | CCPb-13 |
| CCPb-26 | 119.8 | 775 | 100 | 0.002 | 0.019 | 7.7 | qz, bt | H1 | CCPb-08 |
| CCPb-27 | 120.0 | 775 | 75 | 0.002 | 0.017 | 12.0 | qz, bt | H0 | CCPb-13 |
| CCPb-28 | 116.3 | 775 | 200 | 0.001 | 0.014 | 4.1 | am, bt | H2 | CCPb-09 |
| CCPb-29 | 96.1 | 800 | 150 | 0.002 | 0.018 | 7.7 | am | H3 | CCPb-01 |
| CCPb-30 | 96.1 | 800 | 150 | 0.002 | 0.035 | 5.1 | am | H3 | CCPb-06 |
| CCPb-31 | 121.0 | 750 | 175 | 0.002 | 0.019 | 7.2 | qz, bt, am | H1 | CCPb-10 |
| CCPb-32 | 118.7 | 775 | 175 | 0.001 | 0.017 | 6.7 | am, bt | H0 | CCPb-10 |
| CCPb-33 | 99.9 | 825 | 75 | 0.006 | 0.054 | 9.2 | px | H3 | LQ13-01 |
| CCPb-34 | 141.8 | 775 | 120 | 0.051 | 0.262 | 16.1 | qz, bt, am | H0 | LQ13-01 |

Notes:

[a] Stable phases in experimental run products determined to be quartz (qz), biotite (bt), amphibole (am), pyroxene (px). All runs also contain glass, plagioclase, Fe-Ti oxides, and apatite.

**Table 5.** Continuous decompression experimental run conditions.

| Sample | Run duration (hr) | Total decompression time (hr) | Temperature (°C) | Initial pressure (MPa) | Final pressure (MPa) | Initial depth (km)* | Final depth (km)* | Decompression rate (MPa/hr) | $H_2O$ (g)** | Starting Material (g) | $H_2O$ (wt. %)** | Furnace | Starting Material |
|---|---|---|---|---|---|---|---|---|---|---|---|---|---|
| CCPb-35 | 24.0 | 144.0 | 775 | 120.0 | 96.3 | 4.6 | 3.7 | 1.0 | 0.001 | 0.015 | 7.3 | H0 | CCPb-34 |
| CCPb-36 | 48.0 | 144.0 | 775 | 120.0 | 72.5 | 4.6 | 2.8 | 1.0 | 0.001 | 0.016 | 6.6 | H1 | CCPb-34 |
| CCPb-37 | 72.0 | 144.0 | 775 | 120.0 | 50.0 | 4.6 | 1.9 | 1.0 | 0.001 | 0.018 | 6.3 | H2 | CCPb-34 |
| CCPb-38 | 16.0 | 48.0 | 775 | 120.0 | 78.3 | 4.6 | 3.0 | 2.6 | 0.001 | 0.021 | 5.0 | H0 | CCPb-34 |
| CCPb-39 | 24.0 | 48.0 | 775 | 120.0 | 57.6 | 4.6 | 2.2 | 2.6 | 0.001 | 0.017 | 7.0 | H1 | CCPb-34 |
| CCPb-40 | 5.3 | 16.0 | 775 | 120.0 | 74.6 | 4.6 | 2.9 | 8.5 | 0.001 | 0.016 | 4.8 | H0 | CCPb-34 |
| CCPb-41 | 8.0 | 16.0 | 775 | 120.0 | 51.8 | 4.6 | 2.0 | 8.5 | 0.001 | 0.011 | 6.9 | H1 | CCPb-34 |
| CCPb-42 | 145.0 | 432.0 | 775 | 120.0 | 69.0 | 4.6 | 2.7 | 0.35 | 0.001 | 0.017 | 6.1 | H0 | CCPb-34 |
| CCPb-43 | 213.8 | 432.0 | 775 | 120.0 | 47.3 | 4.6 | 1.8 | 0.35 | 0.001 | 0.020 | 5.1 | H1 | CCPb-34 |

Notes:

* Approximate depths calculated using a lithostatic pressure gradient and overburden density of 2650 $kg/m^3$.

** Water in addition to that already in experimental run product CCPb-34.

**Table 6.** Titanomagnetite and ilmenite compositions (wt. %) as determined by EPMA from touching pairs in LQ13-01.

| Sample | $SiO_2$ | $TiO_2$ | $Al_2O_3$ | $Cr_2O_3$ | $FeO^*$ | MnO | MgO | CaO | $Na_2O$ | Total |
|---|---|---|---|---|---|---|---|---|---|---|
| LQ13-01-ox-01-03-mag-ave (n=2) | 0.02 (1) | 5.09 (21) | 1.75 (7) | 0.07 (0) | 80.33 (39) | 0.67 (8) | 1.22 (4) | MDL | MDL | 89.23 (39) |
| LQ13-01-ox-01-03-ilm-ave (n=1) | MDL | 38.86 | 0.25 | MDL | 51.11 | 0.83 | 2.25 | 0.04 | 0.03 | 93.36 |
| LQ13-01-ox-01-06-mag-ave (n=3) | MDL | 5.45 (7) | 1.78 (9) | 0.10 (3) | 81.72 (72) | 0.72 (6) | 1.21 (1) | MDL | MDL | 91.00 (65) |
| LQ13-01-ox-01-06-ilm-ave (n=1) | 0.03 | 36.03 | 0.34 | MDL | 53.63 | 0.99 | 2.09 | 0.13 | MDL | 93.23 |
| LQ13-01-ox-01-08-mag-ave (n=2) | MDL | 5.28 (7) | 1.80 (4) | 0.07 (1) | 81.56 (12) | 0.69 (8) | 1.18 (0) | 0.05 (0) | MDL | 90.63 (2) |
| LQ13-01-ox-01-08-ilm-ave (n=2) | MDL | 38.48 (12) | 0.18 (0) | MDL | 52.32 (50) | 0.79 (11) | 2.20 (1) | 0.02 (1) | MDL | 94.04 (45) |
| LQ13-01-ox-01-09-mag-ave (n=3) | MDL | 5.21 (12) | 1.77 (6) | 0.08 (1) | 81.16 (57) | 0.69 (7) | 1.22 (2) | 0.07 (5) | MDL | 90.19 (71) |
| LQ13-01-ox-01-09-ilm-ave (n=2) | MDL | 38.87 (65) | 0.16 (2) | 0.05 (2) | 51.34 (1.08) | 0.89 (0.12) | 2.12 (2) | MDL | 0.02 (0) | 93.56 (1.44) |
| LQ13-01-ox-01-10-mag-ave (n=3) | MDL | 5.28 (10) | 1.74 (8) | 0.09 (2) | 82.27 (40) | 0.67 (4) | 1.18 (6) | MDL | MDL | 91.27 (0.52) |
| LQ13-01-ox-01-10-ilm-ave (n=2) | MDL | 38.80 (52) | 0.18 (2) | MDL | 51.92 (14) | 0.85 (5) | 2.16 (1) | 0.01 (0) | MDL | 93.93 (60) |
| LQ13-01-ox-01-12-mag-ave (n=3) | MDL | 5.18 (3) | 1.75 (1) | 0.07 (2) | 81.23 (77) | 0.65 (3) | 1.27 (6) | 0.13 (4) | MDL | 90.31 (74) |
| LQ13-01-ox-01-12-ilm-ave (n=1) | 0.01 | 38.44 | 0.23 | 0.01 | 50.75 | 0.92 | 2.30 | 0.06 | MDL | 92.72 |
| LQ13-01-ox-01-13-mag-ave (n=2) | MDL | 5.10 (4) | 1.69 (4) | 0.08 (5) | 82.52 (26) | 0.71 (0) | 1.22 (5) | 0.01 (0) | MDL | 91.38 (10) |
| LQ13-01-ox-01-13-ilm-ave (n=3) | MDL | 38.23 (6) | 0.15 (2) | MDL | 52.97 (37) | 0.90 (5) | 2.15 (7) | MDL | MDL | 94.48 (56) |
| LQ13-01-ox-01-14-mag-ave (n=4) | MDL | 5.27 (3) | 1.79 (7) | 0.09 (4) | 81.74 (38) | 0.68 (7) | 1.21 (5) | MDL | MDL | 90.87 (37) |
| LQ13-01-ox-01-14-ilm-ave (n=2) | MDL | 38.76 (43) | 0.18 (1) | MDL | 51.63 (20) | 0.88 (4) | 2.27 (3) | 0.06 (4) | MDL | 93.78 (18) |
| LQ13-01-ox-01-16-mag-ave (n=2) | MDL | 5.38 (28) | 1.89 (13) | 0.05 (1) | 82.02 (52) | 0.65 (7) | 1.25 (2) | 0.02 (1) | MDL | 91.26 (27) |
| LQ13-01-ox-01-16-ilm-ave (n=4) | MDL | 37.48 (20) | 0.19 (3) | 0.03 (2) | 53.63 (49) | 0.85 (7) | 2.06 (4) | MDL | MDL | 94.28 (0.39) |
| LQ13-01-ox-01-17-mag-ave (n=4) | MDL | 5.26 (7) | 1.73 (5) | 0.10 (2) | 82.63 (68) | 0.74 (6) | 1.21 (7) | MDL | MDL | 91.68 (73) |
| LQ13-01-ox-01-17-ilm-ave (n=4) | MDL | 38.95 (50) | 0.17 (3) | 0.02 (1) | 52.44 (32) | 0.87 (12) | 2.22 (8) | MDL | MDL | 94.70 (65) |
| LQ13-01-ox-01-18-mag-ave (n=4) | MDL | 5.24 (6) | 1.74 (10) | 0.04 (2) | 82.59 (59) | 0.63 (6) | 1.20 (6) | 0.03 (1) | MDL | 91.51 (58) |
| LQ13-01-ox-01-18-ilm-ave (n=4) | MDL | 38.95 (50) | 0.17 (3) | 0.02 (1) | 52.44 (32) | 0.87 (12) | 2.22 (8) | MDL | MDL | 94.70 (65) |
| LQ13-01-ox-02-01-mag-ave (n=6) | MDL | 5.21 (7) | 1.70 (5) | 0.07 (2) | 83.33 (62) | 0.68 (7) | 1.17 (5) | MDL | MDL | 92.19 (61) |
| LQ13-01-ox-02-01-ilm-ave (n=3) | MDL | 39.06 (32) | 0.16 (2) | 0.04 (1) | 52.73 (33) | 0.81 (10) | 2.13 (6) | 0.04 (3) | MDL | 95.03 (7) |
| LQ13-01-ox-02-02-mag-ave (n=6) | MDL | 5.21 (7) | 1.70 (5) | 0.07 (2) | 83.33 (62) | 0.68 (7) | 1.17 (5) | MDL | MDL | 92.19 (61) |
| LQ13-01-ox-02-02-ilm-ave (n=1) | MDL | 39.05 | 0.16 | 0.04 | 52.62 | 0.87 | 2.05 | MDL | MDL | 94.80 |
| LQ13-01-ox-02-03-mag-ave (n=6) | MDL | 5.21 (7) | 1.70 (5) | 0.07 (2) | 83.33 (62) | 0.68 (7) | 1.17 (5) | MDL | MDL | 92.19 (61) |
| LQ13-01-ox-02-03-ilm-ave (n=1) | 0.03 | 38.47 | 0.12 | 0.06 | 53.21 | 0.82 | 2.01 | 0.07 | 0.03 | 94.83 |
| LQ13-01-ox-02-04-mag-ave (n=3) | MDL | 6.10 (31) | 1.92 (4) | 0.03 (2) | 81.88 (15) | 0.72 (2) | 1.23 (3) | 0.02 (0) | 0.03 (1) | 91.93 (47) |
| LQ13-01-ox-02-04-ilm-ave (n=5) | MDL | 37.51 (31) | 0.26 (3) | MDL | 54.06 (45) | 0.81 (9) | 1.95 (7) | MDL | MDL | 94.63 (72) |
| LQ13-01-ox-02-05-mag-ave (n=2) | MDL | 5.20 (1) | 1.68 (2) | 0.09 (1) | 83.67 (62) | 0.71 (1) | 1.09 (2) | 0.02 (0) | MDL | 92.47 (62) |
| LQ13-01-ox-02-05-ilm-ave (n=2) | MDL | 38.86 (11) | 0.13 (0) | 0.02 (1) | 53.99 (1.09) | 0.88 (0) | 2.06 (2) | MDL | MDL | 95.97 (1.27) |

Notes:

* Total Fe reported as FeO as determined by EPMA.

Numbers in parens are 1sigma uncertainties on mean compositions in terms of least units cited, i.e., 0.02(1)=0.02±0.01.

Each touching pair consists of one titanomagnetite and one ilmenite. Pairs separated by horizontal lines.

Individual analyses in Appendix E.

Values marked MDL were below the minimum detection limit.

**Table 7.** LQ13-01 titanomagnetite-ilmenite equilibrium.

| Touching Pair | Temperature (°C)[a] | log fO2 (log-units)[a] | Δ+NNO (log- | Magnetite log(Mg/Mn)[c] | Ilmenite log(Mg/Mn)[c] |
|---|---|---|---|---|---|
| LQ13-01-ox-01-03 | 760 | -13.44 | 1.35 | 0.51 | 0.68 |
| LQ13-01-ox-01-06 | 790 | -12.68 | 1.41 | 0.47 | 0.57 |
| LQ13-01-ox-01-08 | 769 | -13.19 | 1.37 | 0.48 | 0.69 |
| LQ13-01-ox-01-09 | 761 | -13.40 | 1.34 | 0.49 | 0.62 |
| LQ13-01-ox-01-10 | 764 | -13.33 | 1.35 | 0.49 | 0.65 |
| LQ13-01-ox-01-12 | 763 | -13.36 | 1.35 | 0.54 | 0.65 |
| LQ13-01-ox-01-13 | 760 | -13.36 | 1.41 | 0.48 | 0.63 |
| LQ13-01-ox-01-14 | 766 | -13.28 | 1.35 | 0.50 | 0.66 |
| LQ13-01-ox-01-16 | 779 | -12.94 | 1.41 | 0.53 | 0.63 |
| LQ13-01-ox-01-17 | 763 | -13.33 | 1.37 | 0.46 | 0.65 |
| LQ13-01-ox-01-18 | 762 | -13.35 | 1.37 | 0.53 | 0.65 |
| LQ13-01-ox-02-01 | 758 | -13.45 | 1.38 | 0.48 | 0.67 |
| LQ13-01-ox-02-02 | 757 | -13.47 | 1.37 | 0.48 | 0.62 |
| LQ13-01-ox-02-03 | 760 | -13.37 | 1.40 | 0.48 | 0.64 |
| LQ13-01-ox-02-04 | 807 | -12.40 | 1.33 | 0.48 | 0.63 |
| LQ13-01-ox-02-05 | 761 | -13.36 | 1.40 | 0.43 | 0.62 |

Notes:

[a] Calculated using OxideGeothrm (Moore et al., 1998).

[b] Calculated using NNO relationship of Huebner and Sato (1970).

[c] Calculated using ILMAT (LePage, 2006).

All pass the Bacon and Hirschmann (1988) test for equilibrium.

**Table 8.** Natural sample LQ13-01 amphibole compositions (wt. %).

| | $SiO_2$ | $TiO_2$ | $Al_2O_3$ | $FeO^*$ | MnO | MgO | CaO | $Na_2O$ | $K_2O$ | Total |
|---|---|---|---|---|---|---|---|---|---|---|
| LQ13-01-am-mghbl-01 | 49.45 | 0.98 | 5.40 | 12.38 | 0.69 | 15.65 | 11.71 | 0.97 | 0.39 | 97.69 |
| LQ13-01-am-mghbl-02 | 49.56 | 0.97 | 5.66 | 12.03 | 0.65 | 16.65 | 11.17 | 0.95 | 0.30 | 98.05 |
| LQ13-01-am-mghbl-03 | 48.87 | 1.11 | 6.27 | 12.88 | 0.55 | 15.56 | 11.67 | 1.07 | 0.44 | 98.46 |
| LQ13-01-am-mghbl-04 | 48.73 | 1.18 | 6.30 | 10.89 | 0.44 | 16.06 | 11.37 | 1.02 | 0.34 | 96.38 |
| LQ13-01-am-mghbl-05 | 49.05 | 1.03 | 6.20 | 11.84 | 0.53 | 15.83 | 11.69 | 1.08 | 0.38 | 97.69 |
| LQ13-01-am-mghbl-06 | 48.74 | 1.13 | 6.28 | 11.76 | 0.56 | 15.57 | 11.48 | 0.96 | 0.39 | 96.93 |
| LQ13-01-am-mghbl-07 | 48.84 | 1.18 | 6.33 | 12.49 | 0.54 | 15.88 | 11.43 | 0.83 | 0.41 | 98.04 |
| LQ13-01-am-mghbl-08 | 48.57 | 1.08 | 6.06 | 11.69 | 0.45 | 15.91 | 11.36 | 1.09 | 0.36 | 96.62 |
| LQ13-01-am-tschprg-01 | 45.43 | 1.90 | 9.45 | 13.66 | 0.39 | 14.39 | 11.37 | 1.60 | 0.42 | 98.66 |

Notes:

Determined by EPMA.

* Total Fe reported as FeO as determined by EPMA.

**Table 9.** Amphibole equilibrium conditions from LQ13-01 amphiboles using Ridolfi et al. (2006) model.

| Sample | Temperature (°C)[a] | Pressure (MPa) | Pressure error (MPa) | Δ+NNO (log-units) | log $fO_2$[b] (log-units) | $H_2O_{melt}$ (wt. %)[c] |
|---|---|---|---|---|---|---|
| LQ13-01-am-mghbl-01 | 772 | 71 | 8 | 2.1 | -12.4 | 4.3 |
| LQ13-01-am-mghbl-02 | 810 | 74 | 8 | 2.6 | -11.1 | 4.5 |
| LQ13-01-am-mghbl-03 | 793 | 87 | 10 | 2.0 | -12.0 | 4.4 |
| LQ13-01-am-mghbl-04 | 789 | 89 | 10 | 2.1 | -12.0 | 4.7 |
| LQ13-01-am-mghbl-05 | 788 | 86 | 9 | 2.0 | -12.1 | 4.6 |
| LQ13-01-am-mghbl-06 | 786 | 89 | 10 | 2.0 | -12.2 | 4.8 |
| LQ13-01-am-mghbl-07 | 802 | 88 | 10 | 2.2 | -11.7 | 4.6 |
| LQ13-01-am-mghbl-08 | 786 | 84 | 9 | 2.1 | -12.1 | 4.4 |
| LQ13-01-am-mghbl ave (n=8) | 791 (11) | 88 (7) | 9 (1) | 2.1 (2) | -11.9 (4) | 4.5 (2) |
| LQ13-01-am-tschprg-01 | 874 | 188 | 21 | 1.3 | -11.0 | 5.6 |

Notes:

[a] Ridolfi model calculates ±22°C uncertainty for all samples.

[b] Ridolfi model calculates ±0.4 log-units uncertainty for all samples.

[c] Ridolfi model calculates ±0.4 wt. % uncertainty for all mghbl and 0.84 wt. % for tschprg.

Numbers in parens are 1sigma uncertainties on mean totals in terms of least units cited, i.e., 791(11)=791±11.

**Table 10.** Phase equilibrium experimental run product glass compositions (wt. %).

| Sample | $SiO_2$ | $TiO_2$ | $Al_2O_3$ | $FeO^*$ | MnO | MgO | CaO | $Na_2O$ | $K_2O$ |
|---|---|---|---|---|---|---|---|---|---|
| CCPb-01-ave (n=7) | 77.49 (59) | 0.09 (6) | 13.28 (24) | 0.81 (11) | 0.05 (3) | 0.18 (3) | 1.07 (7) | 3.24 (21) | 3.76 (55) |
| CCPb-02-ave (n=14) | 74.71 (47) | 0.21 (5) | 14.04 (30) | 1.58 (28) | MDL | 0.36 (3) | 1.77 (8) | 3.72 (18) | 3.52 (4) |
| CCPb-03-ave (n=7) | 76.85 (32) | 0.20 (5) | 12.88 (13) | 1.28 (15) | MDL | 0.26 (7) | 1.12 (6) | 3.45 (17) | 3.88 (27) |
| CCPb-04-ave (n=12) | 74.89 (29) | 0.25 (6) | 13.84 (20) | 1.52 (22) | MDL | 0.39 (4) | 1.65 (7) | 3.75 (16) | 3.60 (7) |
| CCPb-05-ave (n=13) | 73.53 (99) | 0.25 (4) | 14.78 (54) | 1.66 (30) | MDL | 0.43 (4) | 2.00 (18) | 3.97 (16) | 3.27 (8) |
| CCPb-06-ave (n=7) | 75.88 (71) | 0.17 (4) | 13.74 (25) | 1.15 (17) | 0.05 (4) | 0.22 (3) | 1.34 (8) | 3.74 (24) | 3.69 (46) |
| CCPb-07-ave (n=7) | 72.74 (66) | 0.27 (3) | 14.90 (38) | 1.83 (15) | 0.04 (2) | 0.51 (4) | 2.13 (13) | 4.00 (12) | 3.55 (5) |
| CCPb-08-ave (n=10) | 74.50 (84) | 0.25 (5) | 13.74 (54) | 1.77 (16) | MDL | 0.40 (4) | 1.63 (17) | 3.96 (19) | 3.70 (4) |
| CCPb-09-ave (n=7) | 75.91 (27) | 0.16 (4) | 13.84 (38) | 1.22 (14) | 0.07 (6) | 0.24 (2) | 1.62 (10) | 3.41 (21) | 3.46 (47) |
| CCPb-10-ave (n=6) | 76.53 (56) | 0.16 (1) | 13.30 (39) | 0.98 (11) | MDL | 0.21 (3) | 1.32 (10) | 3.65 (18) | 3.80 (3) |
| CCPb-11-ave (n=13) | 75.11 (67) | 0.25 (5) | 13.78 (32) | 1.65 (18) | MDL | 0.33 (5) | 1.66 (11) | 3.50 (40) | 3.62 (6) |
| CCPb-12-ave (n=7) | 77.01 (38) | 0.17 (2) | 12.97 (30) | 1.19 (17) | MDL | 0.18 (3) | 1.18 (6) | 3.41 (8) | 3.80 (36) |
| CCPb-13-ave (n=7) | 78.42 (14) | 0.09 (2) | 12.48 (9) | 0.72 (7) | MDL | 0.12 (4) | 0.83 (5) | 3.13 (11) | 4.12 (3) |
| CCPb-14-ave (n=7) | 77.23 (53) | 0.21 (4) | 12.72 (23) | 1.06 (18) | MDL | 0.26 (10) | 1.03 (6) | 3.35 (19) | 4.08 (22) |
| CCPb-15-ave (n=7) | 78.53 (29) | 0.15 (3) | 12.18 (27) | 0.79 (10) | 0.04 (3) | 0.18 (4) | 0.80 (8) | 3.12 (14) | 4.19 (24) |
| CCPb-16-ave (n=9) | 75.36 (89) | 0.27 (6) | 13.39 (40) | 1.52 (23) | MDL | 0.38 (5) | 1.59 (11) | 3.67 (17) | 3.72 (11) |
| CCPb-17-ave (n=7) | 75.95 (33) | 0.20 (3) | 13.34 (18) | 1.39 (15) | MDL | 0.24 (4) | 1.42 (7) | 3.43 (18) | 3.91 (2) |
| CCPb-18-ave (n=7) | 77.12 (45) | 0.12 (1) | 13.39 (27) | 0.86 (8) | 0.05 (3) | 0.19 (4) | 1.38 (6) | 3.33 (20) | 3.52 (57) |
| CCPb-19-ave (n=10) | 78.25 (46) | 0.16 (4) | 12.93 (26) | 0.90 (22) | MDL | 0.18 (3) | 0.95 (4) | 2.70 (34) | 3.85 (8) |
| CCPb-20-ave (n=9) | 78.34 (53) | 0.12 (4) | 12.22 (50) | 0.74 (11) | MDL | 0.13 (4) | 0.76 (8) | 3.17 (13) | 4.42 (8) |
| CCPb-21-ave (n=5) | 78.54 (99) | 0.09 (3) | 12.08 (71) | 0.60 (16) | 0.06 (4) | 0.10 (5) | 0.73 (19) | 3.09 (20) | 4.70 (21) |
| CCPb-22-ave (n=12) | 73.89 (60) | 0.21 (3) | 14.80 (30) | 1.48 (19) | MDL | 0.33 (5) | 1.81 (10) | 3.93 (19) | 3.45 (7) |
| CCPb-23-ave (n=7) | 78.05 (39) | 0.11 (1) | 12.73 (29) | 0.75 (12) | MDL | 0.13 (2) | 0.95 (4) | 3.32 (14) | 3.89 (5) |
| CCPb-24-ave (n=7) | 77.66 (32) | 0.14 (2) | 12.67 (28) | 0.96 (17) | MDL | 0.15 (2) | 0.96 (5) | 3.34 (12) | 4.01 (5) |

**Table 10, continued.**

| Sample | $SiO_2$ | $TiO_2$ | $Al_2O_3$ | FeO* | MnO | MgO | CaO | $Na_2O$ | $K_2O$ |
|---|---|---|---|---|---|---|---|---|---|
| CCPb-25-ave (n=7) | 78.71 (41) | 0.14 (3) | 12.26 (16) | 0.74 (5) | MDL | 0.12 (1) | 0.80 (9) | 3.13 (7) | 4.03 (32) |
| CCPb-26-ave (n=4) | 76.73 (1.47) | 0.12 (3) | 13.10 (37) | 1.07 (34) | MDL | 0.19 (10) | 0.76 (3) | 3.49 (29) | 4.52 (83) |
| CCPb-25-26-ave[a] (n=2) | 77.72 (1.40) | 0.13 (2) | 12.68 (60) | 0.90 (23) | MDL | 0.15 (5) | 0.78 (3) | 3.31 (26) | 4.28 (35) |
| CCPb-27-ave (n=6) | 79.08 (89) | 0.12 (2) | 11.63 (41) | 0.85 (56) | 0.06 (3) | 0.16 (12) | 0.60 (10) | 3.00 (18) | 4.45 (26) |
| CCPb-28-ave (n=7) | 76.94 (31) | 0.10 (3) | 13.51 (35) | 0.95 (10) | MDL | 0.19 (7) | 1.33 (4) | 3.43 (27) | 3.49 (54) |
| CCPb-29-ave (n=7) | 76.41 (62) | 0.16 (2) | 13.37 (34) | 1.11 (20) | 0.04 (2) | 0.20 (1) | 1.27 (4) | 3.60 (20) | 3.82 (43) |
| CCPb-30-ave (n=7) | 76.38 (77) | 0.19 (2) | 13.27 (39) | 1.10 (13) | 0.06 (3) | 0.17 (1) | 1.19 (8) | 3.79 (18) | 3.82 (54) |
| CCPb-29-30-ave[a] (n=2) | 76.39 (2) | 0.18 (2) | 13.32 (7) | 1.11 (1) | 0.05 (1) | 0.19 (2) | 1.23 (6) | 3.69 (14) | 3.82 (1) |
| CCPb-31-ave (n=7) | 77.44 (20) | 0.18 (12) | 12.81 (12) | 0.85 (15) | 0.09 (4) | 0.12 (1) | 1.02 (4) | 3.41 (14) | 4.06 (4) |
| CCPb-32-ave (n=12) | 77.62 (57) | 0.18 (4) | 12.51 (31) | 0.96 (24) | MDL | 0.16 (4) | 0.84 (13) | 3.45 (24) | 4.21 (8) |
| CCPb-33-ave (n=18) | 76.42 (46) | 0.13 (3) | 13.49 (20) | 1.02 (21) | MDL | 0.17 (4) | 1.21 (4) | 3.66 (21) | 3.84 (6) |
| CCPb-34-ave (n=24) | 77.93 (33) | 0.13 (4) | 12.58 (23) | 0.86 (18) | MDL | 0.13 (3) | 0.93 (6) | 3.29 (19) | 4.06 (10) |

Notes:

Determined by electron probe microanalysis (EPMA).

All compositions converted to anhydrous and totals normalized to 100.

Numbers in parens are 1sigma uncertainties on mean compositions in terms of least units cited, i.e., 77.49(59)=77.49±0.59.

Raw individual analyses in Appendix F.

* Total Fe reported as FeO as determined by EPMA.

[a] Experiments CCPb-25/-26 have same P-T conditions and compositions are averaged. Similarly done for CCPb-29/-30.

**Table 11.** Water concentrations of experimental run products.

| Sample | Temperature (°C) | Pressure (MPa) | $H_2O$ (wt. %) VBD EPMA[a] | $H_2O$ (wt. %) CCPb[b] |
|---|---|---|---|---|
| CCPb-01 | 775 | 150 | 8.11 | 5.18 |
| CCPb-02 | 850 | 150 | 6.33 | 4.97 |
| CCPb-03 | 825 | 100 | 6.18 | 4.10 |
| CCPb-04 | 875 | 100 | 4.62 | 3.94 |
| CCPb-05 | 850 | 200 | 7.46 | 5.80 |
| CCPb-06 | 825 | 150 | 7.85 | 5.07 |
| CCPb-07 | 875 | 150 | 8.31 | 4.88 |
| CCPb-08 | 900 | 100 | 5.85 | 3.89 |
| CCPb-09 | 800 | 200 | 10.18 | 5.93 |
| CCPb-10 | 800 | 175 | 8.92 | 5.60 |
| CCPb-11 | 850 | 125 | 6.42 | 4.50 |
| CCPb-12 | 800 | 125 | 8.17 | 4.68 |
| CCPb-13 | 750 | 100 | 7.94 | 4.32 |
| CCPb-14 | 850 | 75 | 5.47 | 3.45 |
| CCPb-15 | 800 | 75 | 6.89 | 3.59 |
| CCPb-16 | 900 | 75 | 7.59 | 3.31 |
| CCPb-17 | 825 | 125 | 8.20 | 4.58 |
| CCPb-18 | 775 | 125 | 9.39 | 4.73 |
| CCPb-19 | 800 | 100 | 5.53 | 4.13 |
| CCPb-20 | 750 | 125 | 8.29 | 4.84 |
| CCPb-21 | 750 | 150 | 7.02 | 5.31 |
| CCPb-22 | 825 | 200 | 7.64 | 5.85 |
| CCPb-23 | 750 | 75 | 7.82 | 3.73 |
| CCPb-24 | 750 | 200 | 7.88 | 6.15 |
| CCPb-25-26-ave | 775 | 100 | 8.24 | 4.24 |
| CCPb-27 | 775 | 75 | 6.05 | 3.67 |
| CCPb-28 | 775 | 200 | 9.09 | 6.03 |
| CCPb-29-30-ave | 800 | 150 | 9.49 | 5.16 |
| CCPb-31 | 750 | 175 | 10.15 | 5.73 |
| CCPb-32 | 775 | 175 | 5.37 | 5.70 |
| CCPb-33 | 825 | 75 | 7.75 | 3.50 |
| CCPb-34 | 775 | 120 | 8.07 | 4.66 |

**Table 11, continued.**

| Sample | Temperature (°C) | Pressure (MPa) | $H_2O$ (wt. %) VBD EPMA[a] | $H_2O$ (wt. %) CCPb[b] |
|---|---|---|---|---|
| CCPb-35 | 775 | 96.3 | 6.32 | 4.17 |
| CCPb-36 | 775 | 72.5 | 5.88 | 3.61 |
| CCPb-37 | 775 | 50.0 | 3.85 | 2.95 |
| CCPb-38 | 775 | 78.3 | 5.17 | 3.75 |
| CCPb-39 | 775 | 57.6 | 3.94 | 3.19 |
| CCPb-40 | 775 | 74.6 | 6.42 | 3.65 |
| CCPb-41 | 775 | 51.8 | 5.11 | 3.01 |
| CCPb-42 | 775 | 69.0 | 4.20 | 3.50 |
| CCPb-43 | 775 | 47.3 | 4.59 | 2.86 |

Notes:

[a] Using volatiles by difference (VBD) from raw EPMA averages, forcing totals to 100.

[b] Using Moore et al. (1998) model with CCPb glass compositions (Tables 10 and 12) and P-T run conditions.

**Table 12.** Continuous decompression experimental run product glass compositions (wt. %).

| Sample | $SiO_2$ | $TiO_2$ | $Al_2O_3$ | $FeO^*$ | MnO | MgO | CaO | $Na_2O$ | $K_2O$ |
|---|---|---|---|---|---|---|---|---|---|
| CCPb-35-glass-ave (n=13) | 77.79 (75) | 0.13 (4) | 12.59 (29) | 0.95 (21) | MDL | 0.18 (15) | 0.96 (27) | 3.30 (28) | 4.03 (15) |
| CCPb-36-glass-ave (n=13) | 78.38 (74) | 0.12 (4) | 12.19 (46) | 0.81 (16) | MDL | 0.11 (3) | 0.73 (22) | 3.38 (33) | 4.16 (19) |
| CCPb-37-glass-ave (n=10) | 78.61 (45) | 0.14 (4) | 12.18 (20) | 0.76 (26) | MDL | 0.10 (5) | 0.68 (9) | 3.24 (35) | 4.23 (14) |
| CCPb-38-glass-ave (n=10) | 77.98 (45) | 0.12 (3) | 12.44 (23) | 0.84 (18) | MDL | 0.13 () | 0.79 (10) | 3.49 (20) | 4.11 (8) |
| CCPb-39-glass-ave (n=12) | 78.33 (35) | 0.12 (3) | 12.37 (18) | 0.70 (19) | MDL | 0.09 (2) | 0.66 (6) | 3.46 (25) | 4.16 (8) |
| CCPb-40-glass-ave (n=9) | 77.79 (47) | 0.13 (4) | 12.55 (20) | 0.99 (28) | MDL | 0.19 (15) | 0.84 (6) | 3.36 (30) | 4.04 (14) |
| CCPb-41-glass-ave (n=10) | 78.20 (25) | 0.10 (4) | 12.29 (10) | 0.78 (14) | MDL | 0.11 (1) | 0.84 (2) | 3.45 (18) | 4.15 (4) |
| CCPb-42-glass-ave (n=8) | 78.42 (24) | 0.12 (4) | 12.31 (27) | 0.85 (17) | MDL | 0.09 (3) | 0.59 (6) | 3.26 (17) | 4.23 (4) |
| CCPb-43-glass-ave (n=9) | 79.48 (67) | 0.14 (3) | 11.50 (39) | 0.70 (21) | MDL | 0.08 (3) | 0.43 (3) | 3.07 (19) | 4.55 (15) |

Notes:

Determined by electron probe microanalysis (EPMA).

All compositions converted to anhydrous and totals normalized to 100.

Numbers in parens are 1sigma uncertainties on mean compositions in terms of least units cited, i.e., 77.79(75)=77.79±0.75.

Raw individual analyses in Appendix G.

* Total Fe reported as FeO as determined by EPMA.

Values marked MDL were below the minimum detection limit.

## FIGURE CAPTION LIST

**Figure 1.** Tectonic map of the Cascade Range showing areas of late Cenozoic volcanic rocks in stippled patterns after McBirney (1968). Letters next to dots refer to major composite volcanoes and centers: LVC, Lassen Volcanic Center; MS, Mount Shasta; MLV, Medicine Lake Volcano; MMc, Mount McLoughlin; CLV, Crater Lake Volcano; NV, Newberry Volcano; TS, Three Sisters; MJ, Mount Jefferson; MH, Mount Hood; SVF, Simcoe Volcanic Field; MSH, Mount Saint Helens; MA, Mount Adams; MR, Mount Rainier; GP, Glacier Peak; MB, Mount Baker; MG, Mount Garibaldi; MC, Mount Cayley; MM, Meager Mountain. [modified after Feeley et al. (2008b; figure 2)].

**Figure 2.** Map of Lassen region with boundary of Lassen Volcanic National Park (LVNP). Chaos Crags in the northwest corner of LVNP. [modified after Robinson and Clynne (2012)].

**Figure 3.** Geologic map of Chaos Crags and surrounding area showing pyroclastic flows, dome sequence, and sample locations. Created using online-accessible data files from Clynne and Muffler (2010).

**Figure 4.** View of Chaos Crags domes looking northeast from Loomis Peak. Composite tuff cones formed by initial pyroclastic eruptions of Chaos Crags visible at the right. The small dome above the tuff cones is dome A. Large coulee sloping from upper right to lower left is dome B. High, craggy dome at left (with oxidized patch) is dome D. Dome E is visible between domes D and B. Domes C and F are not visible in this view. Photograph by Michael A. Clynne (Clynne and Muffler, 2010).

**Figure 5a-c.** Images of group 1 lavas. **(a)** Photograph of hand sample from upper pyroclastic flow from same location as LC84-419. BSE images of **(b)** biotite (Bt) and **(c)** amphibole (Am) in dome A (LC84-428).

**Figure 6a-c.** Images of group 2 lavas. **(a)** Photograph of hand sample from dome C, primarily composed of rhyodacite, with a mafic inclusion. BSE images of **(b)** biotite (Bt) and **(c)** amphibole (Am), both exhibiting dehydration reaction rims, in dome F (LC84-455).

**Figure 7a-g.** Images of samples from the lower pyroclastic flow. **(a)** Photograph of hand sample LQ13-01. BSE images of: **(b)** glass (Gl) and mafic inclusion, **(c)** plagioclase (Pl) with complexly zoned rim, **(d)** biotite (Bt), **(e)** amphibole (Am), and **(f)** quartz (Qz) with melt inclusion (MI) from sample LC84-417, and **(g)** an extracted titanomagnetite-ilmenite (Mag-Ilm) touching pair from LQ13-01.

**Figure 8a-b. (a**) Schematic and **(b)** photograph of the hydrothermal cold-seal experimental petrology laboratory at Smithsonian Institution, Department of Mineral

Sciences. Samples and nickel filler rod are loaded into Waspaloy pressure vessels ("PV0"-"PV3"; light gray rectangles) and PVs are filled with deionized water and connected to the high-pressure line via pressure heads (dark-gray boxes). The high-pressure line maintains pressure throughout the system. Individual PVs can be isolated from the high-pressure line via 3-way valves ("V0"-"V3"). Temperature for each experiment is controlled by horizontal split-tube furnaces ("H0"-"H3"), into which the PVs are loaded. Temperature is monitored using K-type thermocouples ("T0"-"T3") that fit into the base of each pressure vessel near the sample location; those temperatures are monitored and logged by computer and used to control sample temperature. Pressure is monitored with a pressure transducer ("P") connected by serial port to a data-logging computer. Pressure in the high-pressure line (and any experiments open to the line) can be manually controlled using an air-actuated wall pump at V4 (2-way valve) or vent line at V5 (2-way valve) (coarse adjustments >10 MPa) or with a pressure intensifier (fine adjustments). For continuous decompression experiments, pressure can be smoothly adjusted with computer control by using one of the furnaces ("H3") as a pressure actuator; no experiment is loaded in PV3/H3, instead its temperature is varied up or down to control pressure in the high-pressure line where the specific dependence P=f(T) is determined empirically. Courtesy B.J. Andrews (SI), with modification.

**Figures 9a-b. (a)** Example of rate calibration plot for continuous decompression experiments using a maximum of two experiments. The slopes of best fit lines between points G-H for two PVs and points B-C for one PV as part of the system equate to change in temperature (ºC) of actuator PV (PV3) required to change system pressure by 1.0 MPa. The smaller system volume during B-C compared to G-H results in a smaller slope and lesser temperature required to achieve equal amounts of pressure change. (See text for further discussion). **(b)** Experimental decompression paths. Each experiment (CCPb-35 through CCPb-43; Table 5) started at 775ºC and 120 MPa and decompressed along the plotted path until it was quenched (marked by **x**). The signal from diurnal temperature fluctuation is visible as the sawtooth pattern in the slowest rate (0.35 MPa/hr) path.

**Figure 10.** Concentrations of dissolved $CO_2$ and $H_2O$ in LQ13-01 melt inclusion glass as determined by Fourier transform infrared spectroscopy (FTIR). Preserved melt inclusions plotted as black circles and those inferred to have leaked (< 3.99 wt. % $H_2O_t$) plotted as red circles. Values reported in Table 2. Error bars represent 10% uncertainties on totals.

**Figure 11.** Speciation of dissolved $H_2O$, as hydroxyl ion ($OH^-$) and molecular water ($H_2O$), versus total dissolved water ($H_2O_t$) in LQ13-01 preserved melt inclusions (black circles from Figure 10). $OH^-$ plotted as green diamonds and $H_2O$ plotted as blue squares. Values reported in Table 2. Error bars represent 10% uncertainties on totals.

**Figure 12a-h.** Glass composition as determined by EPMA plotted in Harker variation diagrams as wt. % oxide vs. wt. % $SiO_2$ for individual melt inclusions (light gray), pyroclastic flows, and domes. **(a)** $K_2O$ **(b)** $Al_2O_3$; **(c)** $Na_2O$; **(d)** CaO; **(e)** FeO; **(f)** MgO;

**(g)** $TiO_2$. In comparison to domes and pyroclastic flows, the melt inclusions plot at the high-$SiO_2$ end and low end of all other oxides. Totals are converted to anhydrous, error bars represent 1σ uncertainties on mean compositions, and are reported in Tables 1 and 3.

**Figure 13.** $FeO$-$TiO_2$-$Fe_2O_3$ ternary diagram, with join-lines for the cubic (magnetite-ulvospinel) and rhombohedral (ilmenite-ferric oxide) phases as solid solutions, of titanomagnetite-ilmenite touching pairs (connected by lines) as determined by EPMA with Fe recalculation computed by ILMAT (LePage, 2003) using method of Stormer (1983). Compositions are reported in Table 6.

**Figure 14.** Mg/Mn partitioning for titanomagnetite-ilmenite pairs from LQ13-01 plotted as titanomagnetite log(Mg/Mn) vs. ilmenite log(Mg/Mn) with Bacon and Hirschmann (1988) test for equilibrium curve (middle line) and the two 10% 2σ lower and upper boundaries. Pairs that plot within the upper and lower bounds are considered to be in equilibrium. Values reported in Table 7.

**Figure 15.** Geothermometer/oxybarometer results plotted as $fO_2$ vs. T from titanomagnetite-ilmenite touching pairs using OxideGeothrm (Ghiorso and Evans, 2008) with buffer curves for hematite-magnetite (HM) (Spencer and Lindsley, 1981), nickel-nickel oxide (NNO) (Heubner and Sato, 1970), fayalite-magnetite-quartz (FMQ) (Hewitt, 1978), and magnetite-wustite (MW) (Heubner, 1971; Haas and Robie, 1973). Values reported in Table 7.

**Figure 16a-c.** LQ13-01 amphibole EPMA analyses input, producing amphibole stability plots using Amp-TB model (Ridolfi et al., 2010). Most amphiboles plot compositionally as magnesiohornblende (light gray circles) with the magnesiohornblende average plotted as a black circle and one as tschermakitic-pargasite (blue square; analysis from a core and unrepresentative of equilibrated conditions with the melt). Magnesiohornblendes equilibrated at: **(a)** temperatures 774-808ºC and fO2 NNO+2.0 to NNO+2.6 log-units (showing NNO+0 to +3 log-unit buffer curves); **(b)** temperatures 774-808ºC and 4.3-4.9 wt. % $H_2O$ in melt; and **(c)** temperatures 774-808ºC and pressures 84-89 MPa. Error bars represent associated uncertainties as calculated by Amp-TB (Ridolfi et al., 2010). Values reported in Tables 8 and 9.

**Figure 17a-h**. BSE images of phase equilibrium experimental run products with phases labeled: amphibole (Am), biotite (Bt), glass (Gl), plagioclase (Pl), pyroxene (px), quartz (Qz). Experimental run number and P-T conditions noted on each figure. **(a)** CCPb-18 and **(b)** CCPb-34 match starting material, showing euhedral amphibole. **(c)** CCPb-31, crystallization of plagioclase and biotite dominates the groundmass; **(d)** CCPb-17, amphibole breaking down and pyroxene crystallizing; **(e)** CCPb-13, crystallization of quartz and plagioclase dominate the groundmass; **(f)** CCPb-16, crystallization of pyroxene; **(g)** CCPb-07, pyroxene rims surrounding amphibole and biotite, and

plagioclase rims becoming for anorthitic; **(h)** CCPb-08, pyroxene rim surrounding amphibole.

**Figure 18.** Phase stability P-T diagram determined from CCPb experiments. Pre-eruptive storage region (shaded) determined to be 145±25 MPa and 770±10ºC. Thirty-two P-T combinations were investigated (Table 4). Twenty-five single-stage (using LQ13-01 as starting material) experiments were performed (squares). An additional nine two-stage (using an experimental run product as starting material) experiments were performed to check for equilibration (single-arrows, pointing away from starting material and toward final experimental P-T conditions). Of those, two pairs of melting and crystallization reversal experiments (double-arrows), CCPb-25 and -26, and CCPb-29 and -30, were run to check equilibration. Dissolved $H_2O$ concentrations (wt. %) superimposed as labeled gray lines (also shown as gray lines in Figures 19a-h and black lines in Figure 20).

**Figure 19a-h.** Phase equilibrium experimental run product glass compositions as wt. % oxides of **(a)** $SiO_2$; **(b)** $K_2O$; **(c)** $Na_2O$; **(d)** CaO; **(e)** $Al_2O_3$; **(f)** $TiO_2$; **(g)** FeO; **(h)** MgO, as determined by EPMA plotted as contoured colors with target natural sample LQ13-01 composition (black bold line) and associated $\pm 1\sigma$ uncertainties (thin lines). Phase stability diagram, dissolved $H_2O$ concentrations, and storage region (shaded) from Figure 19 superimposed. Totals are converted to anhydrous and reported in Table 10.

**Figure 20.** Dissolved $H_2O$ concentrations in phase equilibrium experimental run product glasses as determined by volatiles by difference from EPMA totals (light gray isopleths), and the model of Moore et al. (1998) (black isopleths). Values reported in Table 11.

**Figure 21a-j.** BSE images of continuous decompression experimental run products with phases labeled: amphibole (Am), biotite (Bt), glass (Gl), plagioclase (Pl), pyroxene (px), quartz (Qz), olivine (Ol), with mafic enclave contamination noted where applicable. Experiment number, decompression rate, run duration, and final pressure noted on each figure. Each experiment used CCPb-34 as starting material and decompressed isothermally (775ºC) from 120 MPa. Decompression rates of 8.5 MPa/hr: **(a)** CCPb-40, plagioclase from mafic enclave in center of view and all other phases similar to starting material, and **(b)** CCPb-41, biotite and amphibole stable and phases in similar proportion to starting material; 2.6 MPa/hr: **(c)** CCPb-38, upper right of amphibole phenocryst shows change in composition similar to that of amphibole grains to right edge of view, and **(d)** CCPb-39, quartz grain at center of view and plagioclase from mafic enclave at lower right; 1.0 MPa/hr: **(e)** CCPb-35, contamination from mafic enclave dominates upper right quadrant, **(f)** CCPb-36, crystallization of plagioclase in groundmass, and amphibole and biotite in contact with vesicles, **(g)** CCPb-37, olivine xenocryst in center of view and plagioclase crystallization to its right, and **(h)** CCPb-37, amphibole breaking down; and 0.35 MPa/hr: **(i)** CCPb-42, amphibole resorbed and plagioclase crystallizing in

groundmass, biotite and amphibole in contact with vesicles, and **(j)** CCPb-43, amphibole breaking down and plagioclase dominating the groundmass.

**Figure 22a-i.** Continuous decompression experimental run product glass compositions plotted as wt. % oxide (or $H_2O$) vs. final quench pressure. **(a)** $SiO_2$, **(b)** $Al_2O_3$, **(c)** $K_2O$, **(d)** $Na_2O$, **(e)** CaO, **(f)** FeO, **(g)** $TiO_2$, **(h)** MgO, and **(i)** $H_2O$. Each decompression rate of 8.5 MPa/hr (red, upward triangles), 2.6 MPa/hr (pink, diamonds), 1.0 MPa/hr (green, circles), and 0.35 MPa/hr (blue, downward triangles) is connected by a line showing the advancement of decompression. Mean glass composition of natural pyroclastic flows and domes plotted at the top. Compositional evolution of experimental run product glass mimicks that of the natural samples; nominally due to crystallization of plagioclase (see text for discussion). Error bars represent associated ±1σ uncertainties on mean compositions. Oxide totals are converted to anhydrous and are reported in Table 12, and $H_2O$ totals are reported in Table 11.

**Figure 23a-i.** Continuous decompression experimental run product glass compositions plotted as wt. % oxide (or $H_2O$) vs. decompression duration. **(a)** $SiO_2$, **(b)** $Al_2O_3$, **(c)** $K_2O$, **(d)** $Na_2O$, **(e)** CaO, **(f)** FeO, **(g)** $TiO_2$, **(h)** MgO, and **(i)** $H_2O$. Each decompression rate of 8.5 MPa/hr (red, upward triangles), 2.6 MPa/hr (pink, diamonds), 1.0 MPa/hr (green, circles), and 0.35 MPa/hr (blue, downward triangles) is connected by a line, showing the advancement of decompression. These plots are essentially those in Figures 22a-i, but are stretched out, displaying the progression with time. Glass composition of natural pyroclastic flows and domes plotted at the top. Compositional evolution of experimental run product glass mimicks that of the natural samples; nominally due to crystallization of plagioclase (see text for discussion). Error bars represent associated ±1σ uncertainties on mean compositions. Oxide totals are converted to anhydrous and are reported in Table 12, and $H_2O$ totals are reported in Table 11.

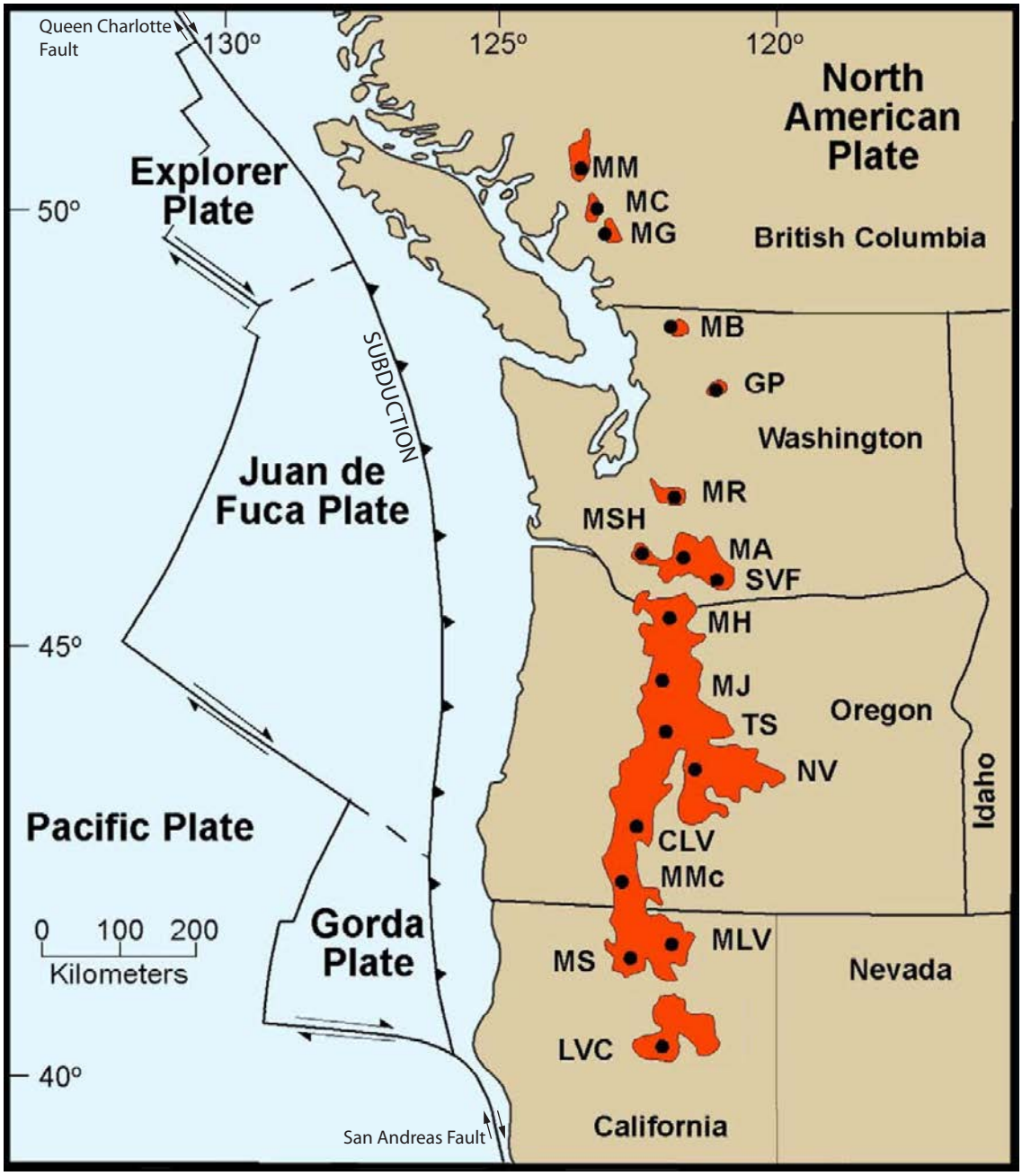
Queen Charlotte Fault
130°
125°
120°
North American Plate
Explorer Plate
50°
MM
MC
MG
British Columbia
MB
GP
Washington
SUBDUCTION
Juan de Fuca Plate
MR
MSH
MA
SVF
MH
45°
MJ
TS
Oregon
NV
Idaho
Pacific Plate
CLV
MMc
0 100 200
Kilometers
Gorda Plate
MLV
MS
Nevada
LVC
40°
San Andreas Fault
California

**Figure 1.**

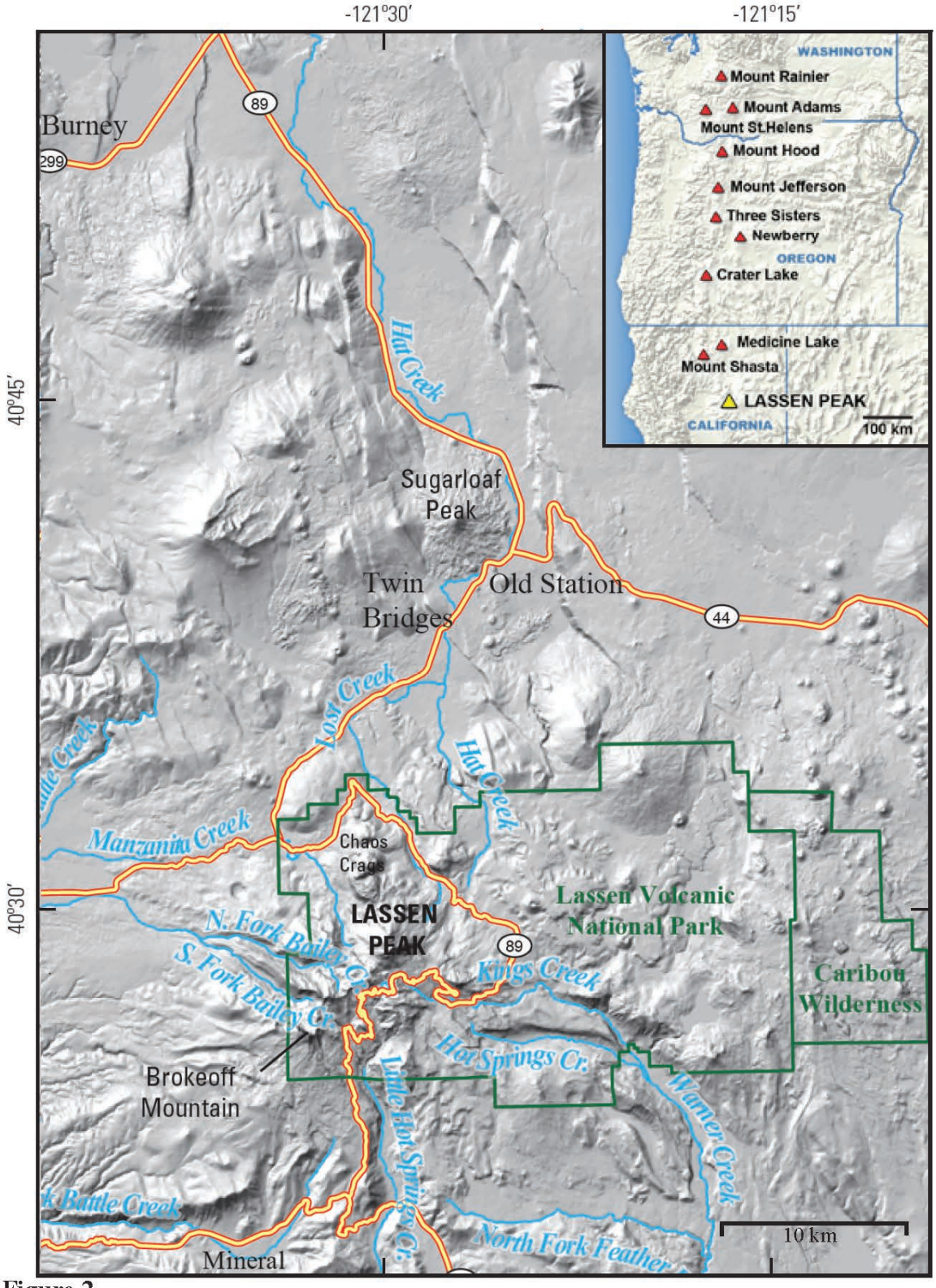
-121°30′
-121°15′
40°45′
40°30′
Burney
89
299
Hat Creek
Sugarloaf Peak
Twin Bridges
Old Station
44
Lost Creek
Manzanita Creek
Chaos Crags
LASSEN PEAK
89
N. Fork Bailey Cr.
S. Fork Bailey Cr.
Kings Creek
Lassen Volcanic National Park
Caribou Wilderness
Hot Springs Cr.
Warner Creek
Little Hot Springs Cr.
Brokeoff Mountain
Battle Creek
Mineral
North Fork Feather
10 km
WASHINGTON
Mount Rainier
Mount Adams
Mount St.Helens
Mount Hood
Mount Jefferson
Three Sisters
Newberry
OREGON
Crater Lake
Medicine Lake
Mount Shasta
LASSEN PEAK
CALIFORNIA
100 km

**Figure 2.**

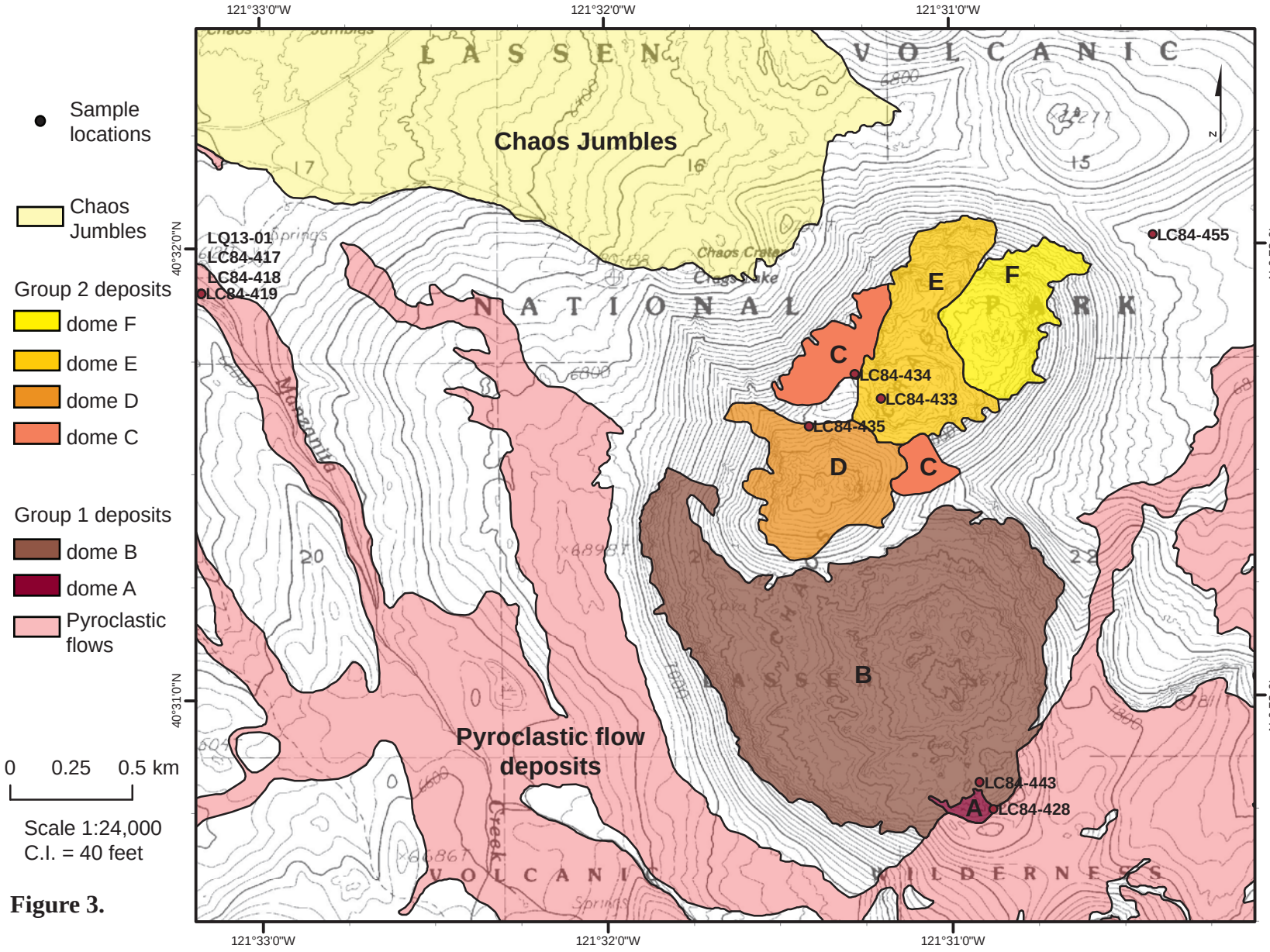
Sample locations
Chaos Jumbles
Group 2 deposits
dome F
dome E
dome D
dome C
Group 1 deposits
dome B
dome A
Pyroclastic flows
0 0.25 0.5 km
Scale 1:24,000
C.I. = 40 feet
121°33'0"W
121°32'0"W
121°31'0"W
40°32'0"N
40°31'0"N
LASSEN VOLCANIC NATIONAL PARK
Chaos Jumbles
LQ13-01
LC84-417
LC84-418
LC84-419
LC84-455
LC84-434
LC84-433
LC84-435
LC84-443
LC84-428
Pyroclastic flow deposits
Morgan Mtn
Chaos Crags
Crags Lake
Lassen Peak
Creek
WILDERNESS

**Figure 3.**

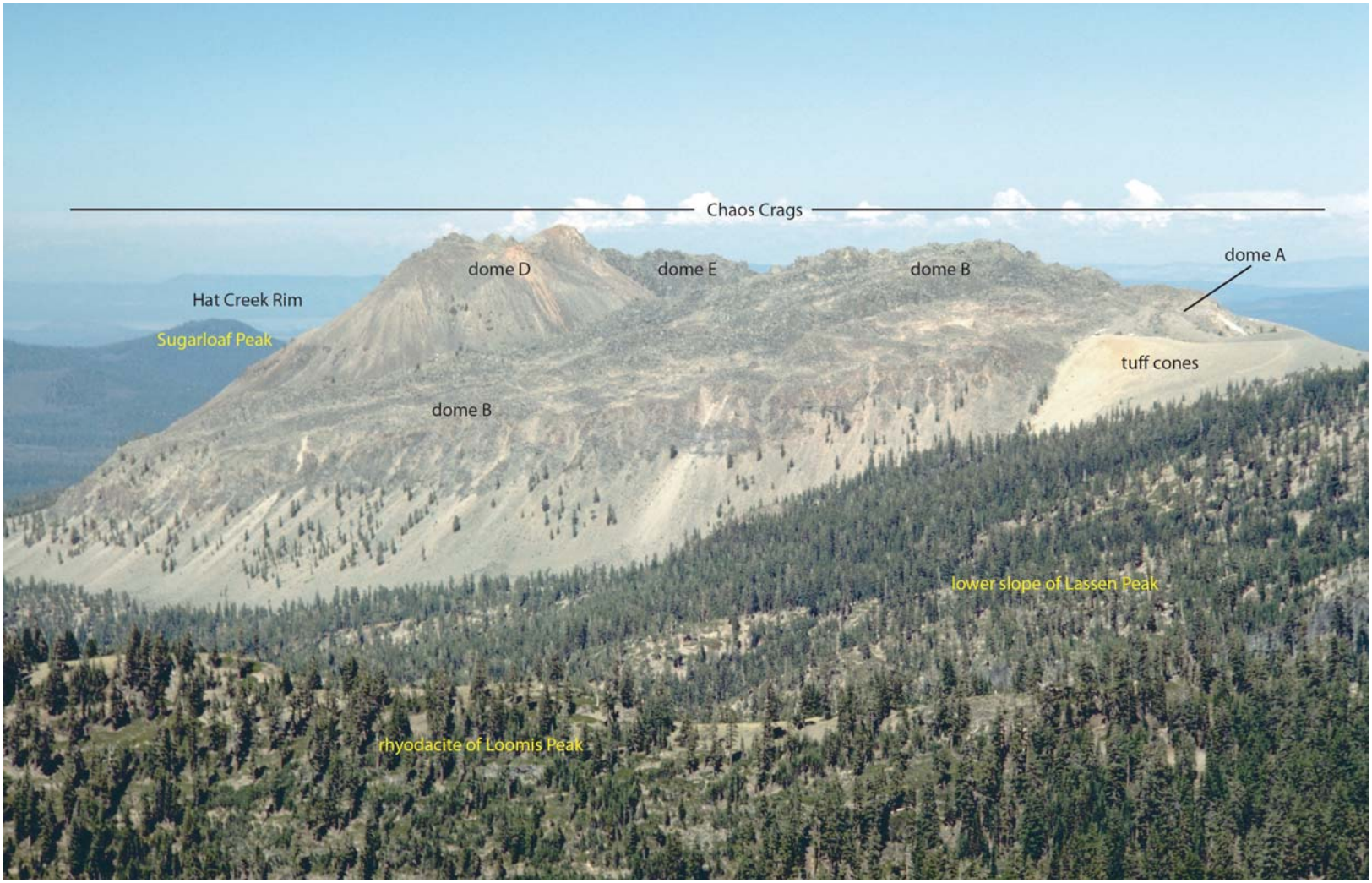
Chaos Crags
dome D
dome E
dome B
dome A
Hat Creek Rim
Sugarloaf Peak
tuff cones
dome B
lower slope of Lassen Peak
rhyodacite of Loomis Peak

**Figure 4.**

Group 1

Rhyodacite of upper pyroclastic flow


**Figure 5a.**

Group 1

Dome A
LC84-428

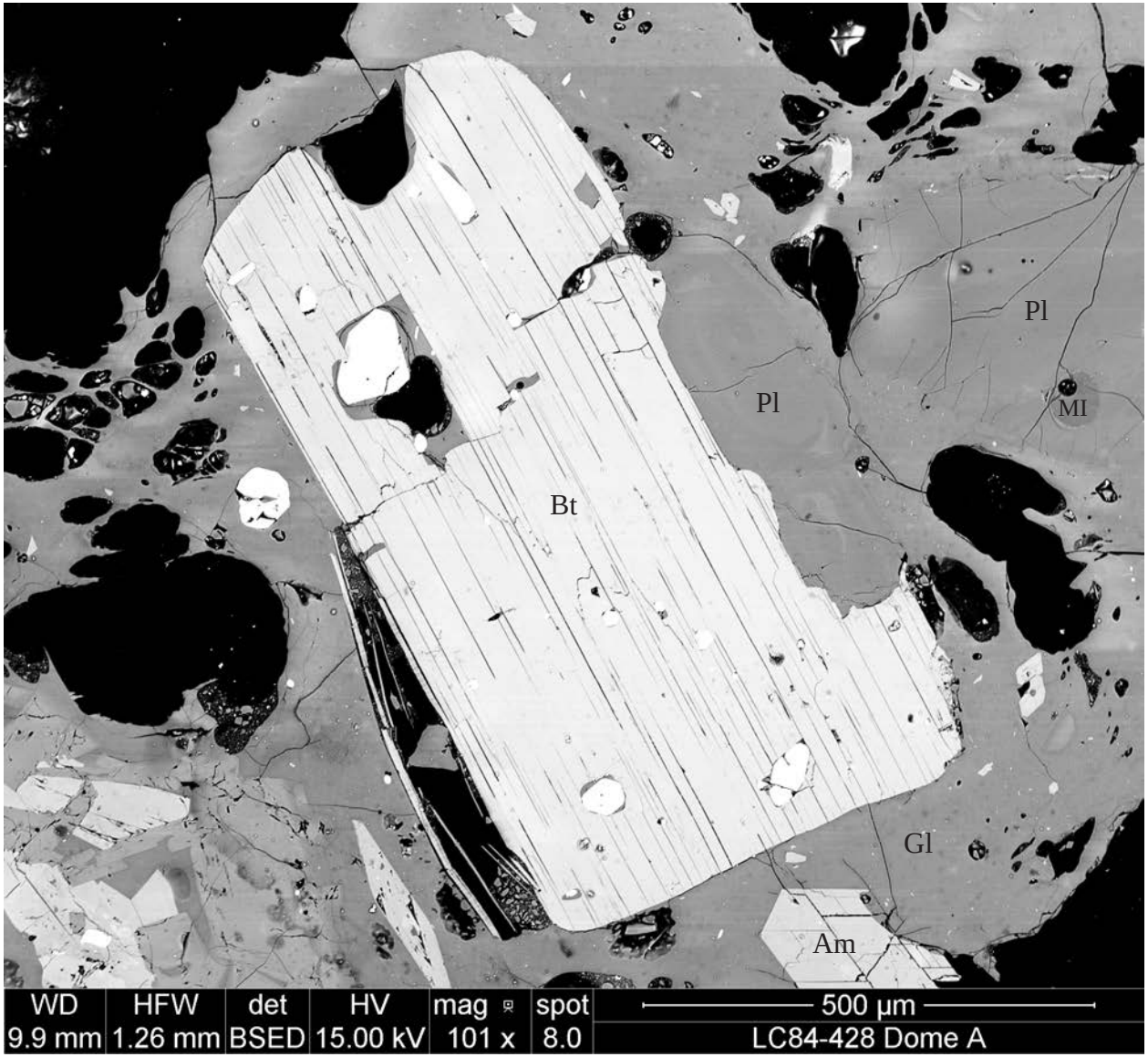


**Figure 5b.**

Group 1

Dome B
LC84-443

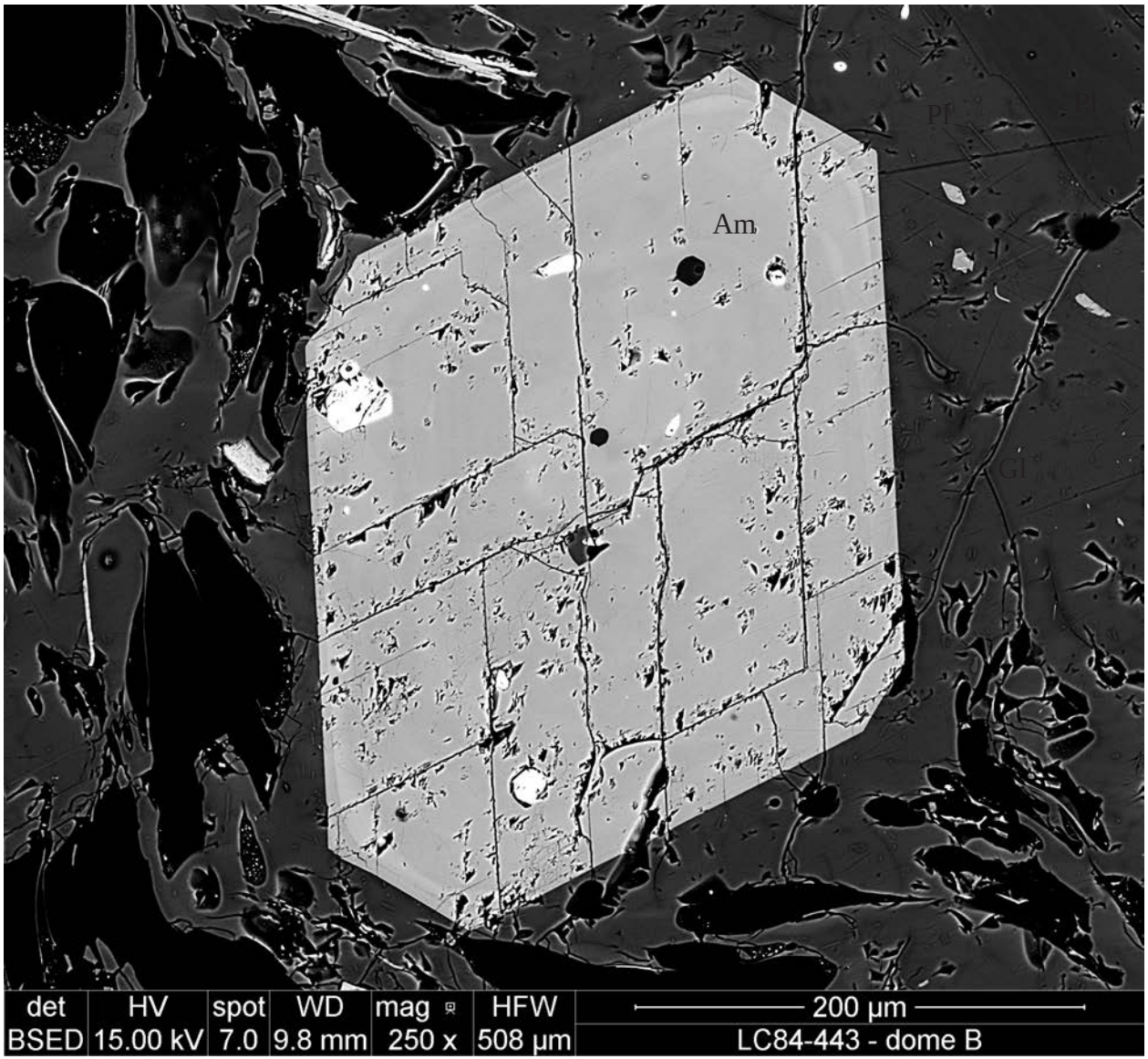


**Figure 5c.**

Group 2

Hand sample
Dome C


**Figure 6a.**

Group 2

Dome F
LC84-455

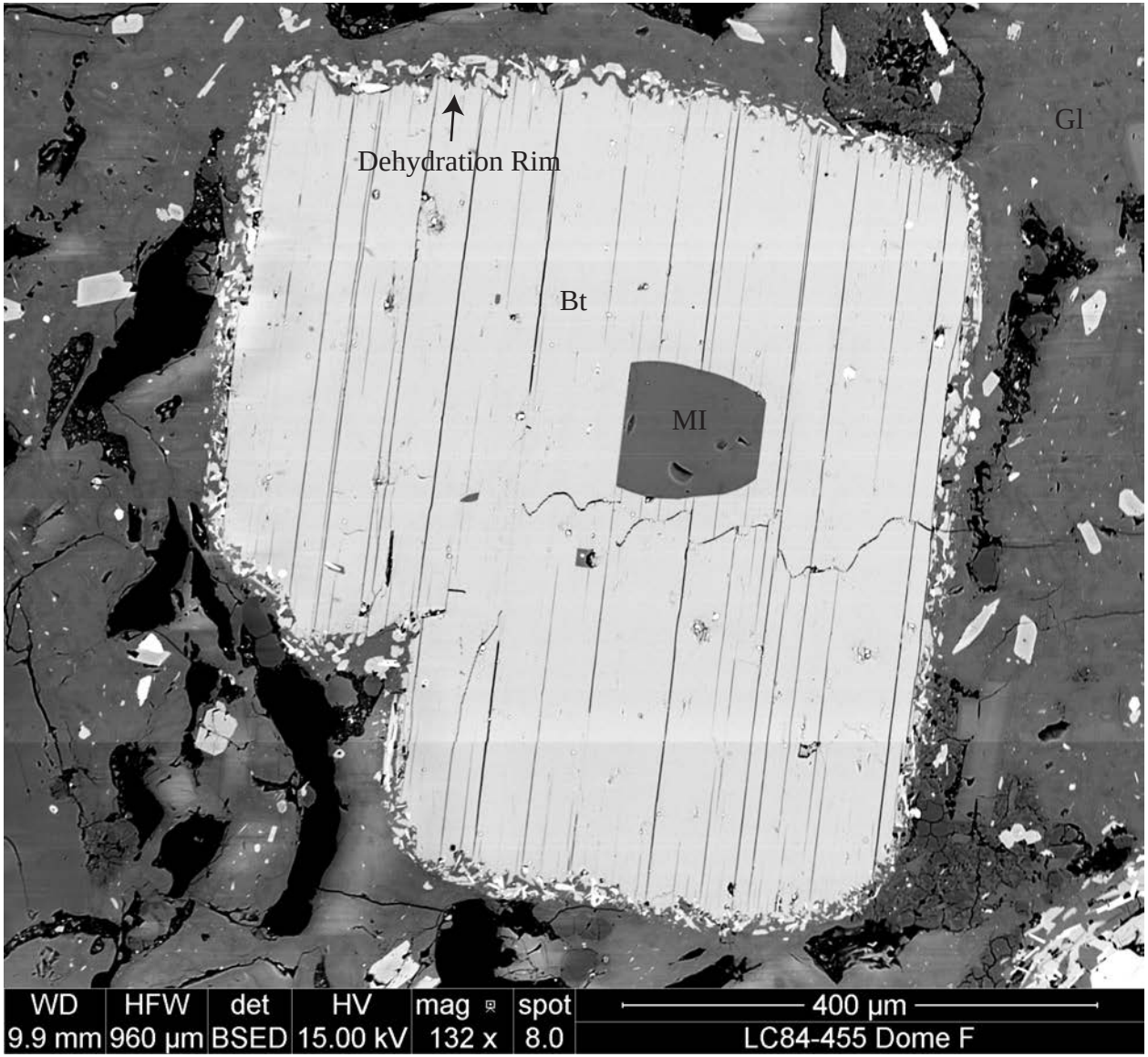


**Figure 6b.**

Group 2

Dome F
LC84-455

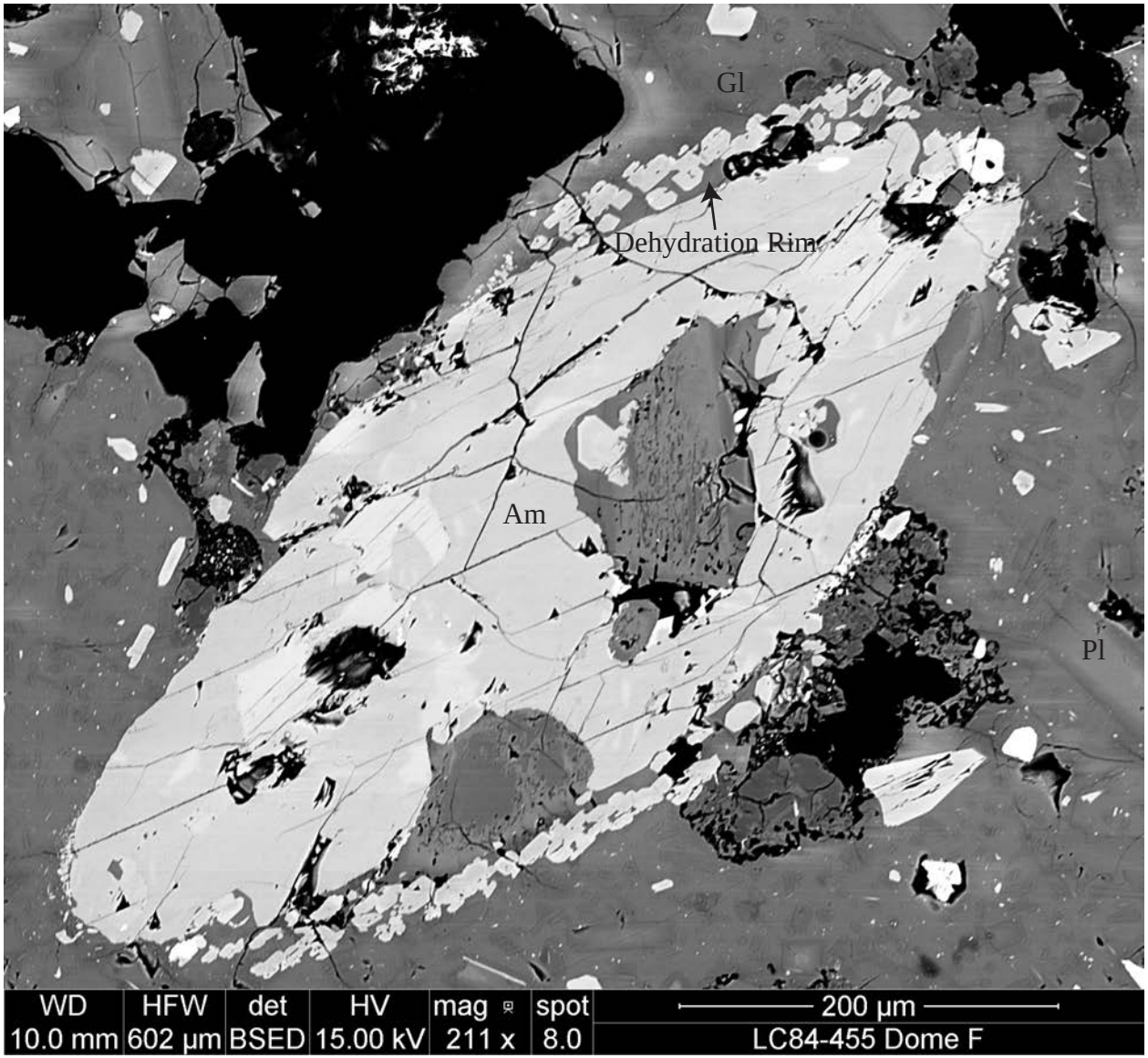


**Figure 6c.**

Group 1

Hand sample LQ13-01
lower pyroclastic flow


**Figure 7a.**

Group 1

lower pyroclastic flow

LC84-417

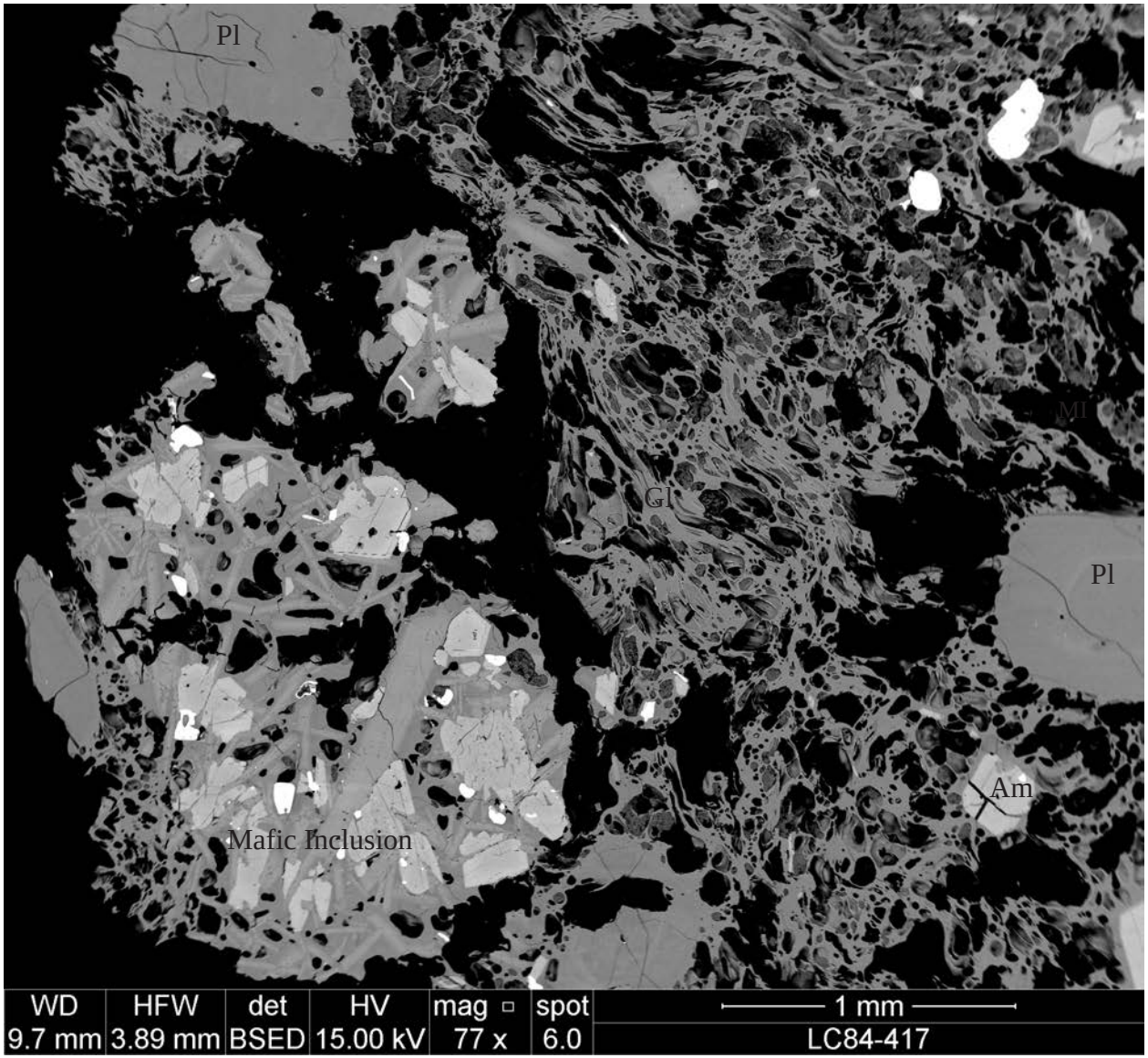


**Figure 7b.**

Group 1

lower pyroclastic flow

LC84-417

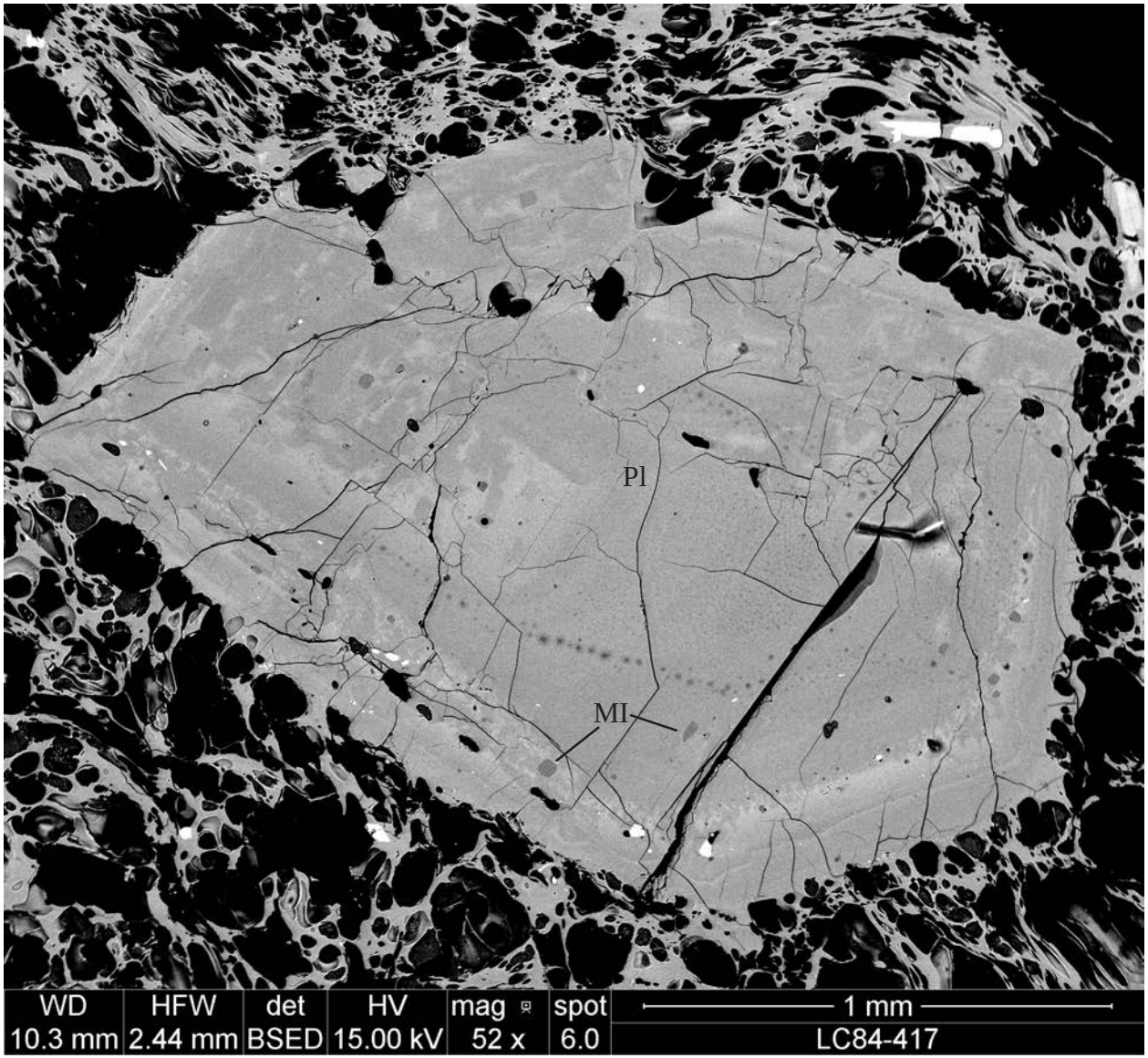


**Figure 7c.**

Group 1

lower pyroclastic flow

LC84-417

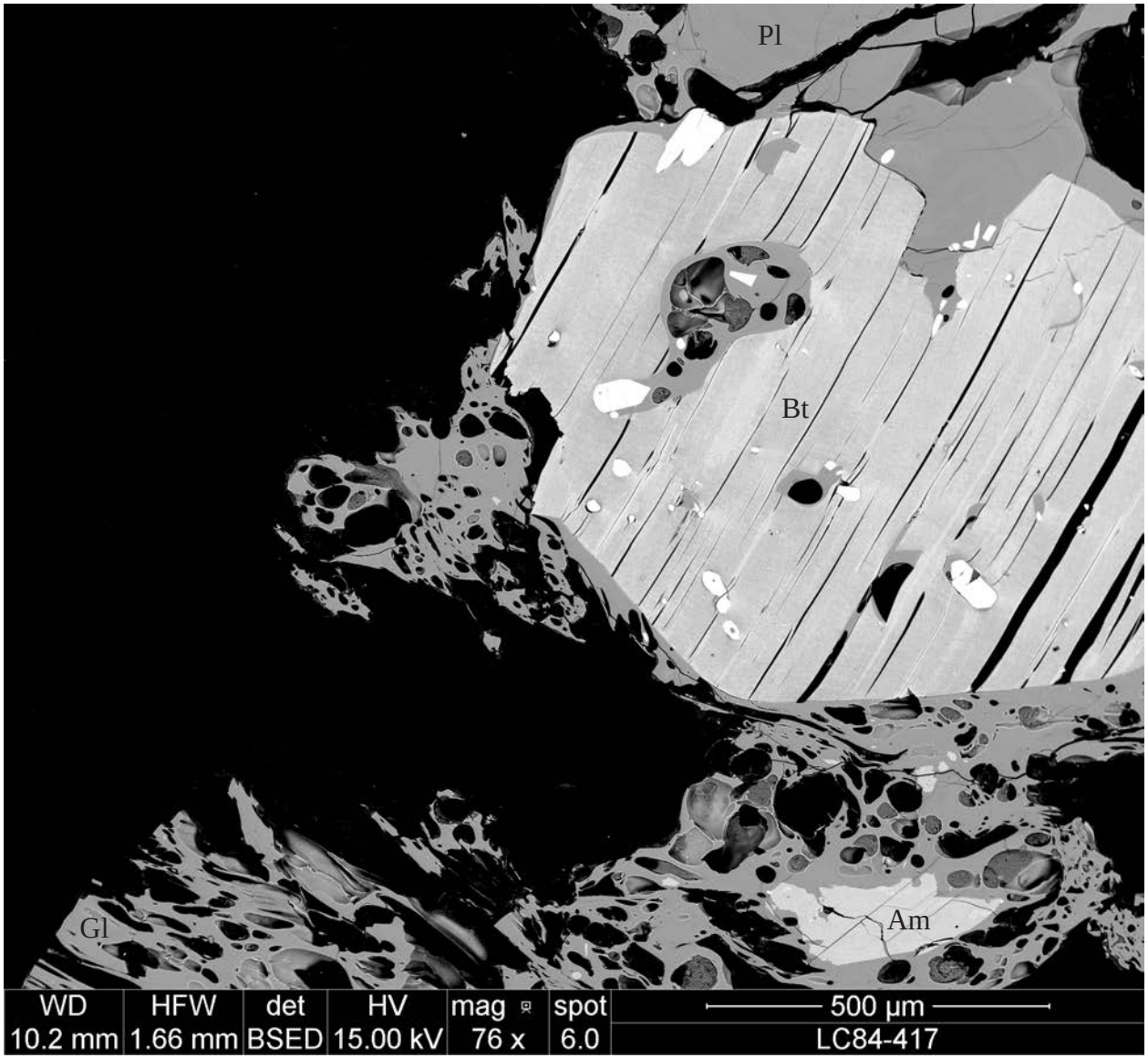


**Figure 7d.**

Group 1

lower pyroclastic flow

LC84-417

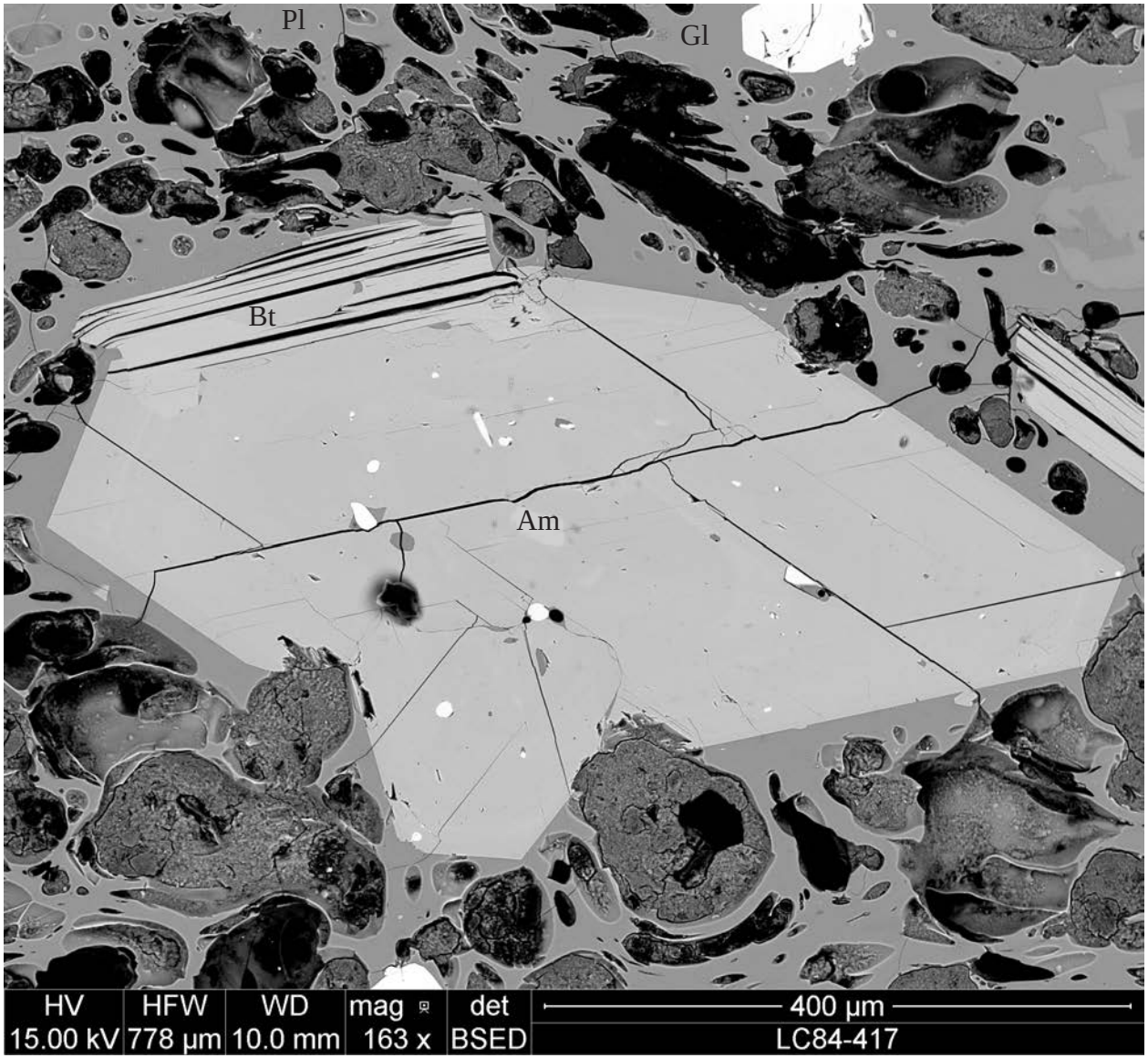


**Figure 7e.**

Group 1

lower pyroclastic flow

LC84-417

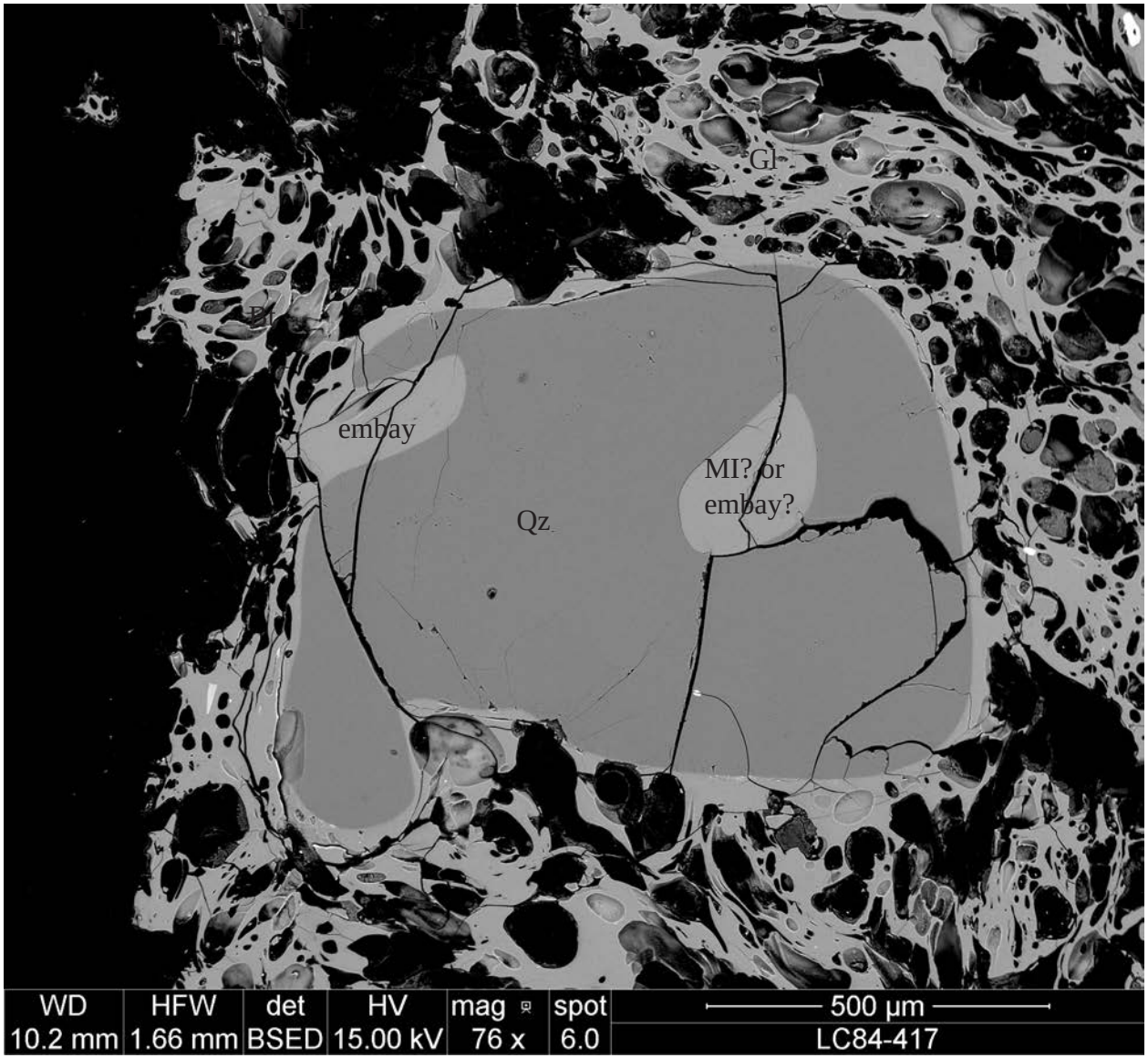


**Figure 7f.**

Group 1

lower pyroclastic flow

LQ13-01

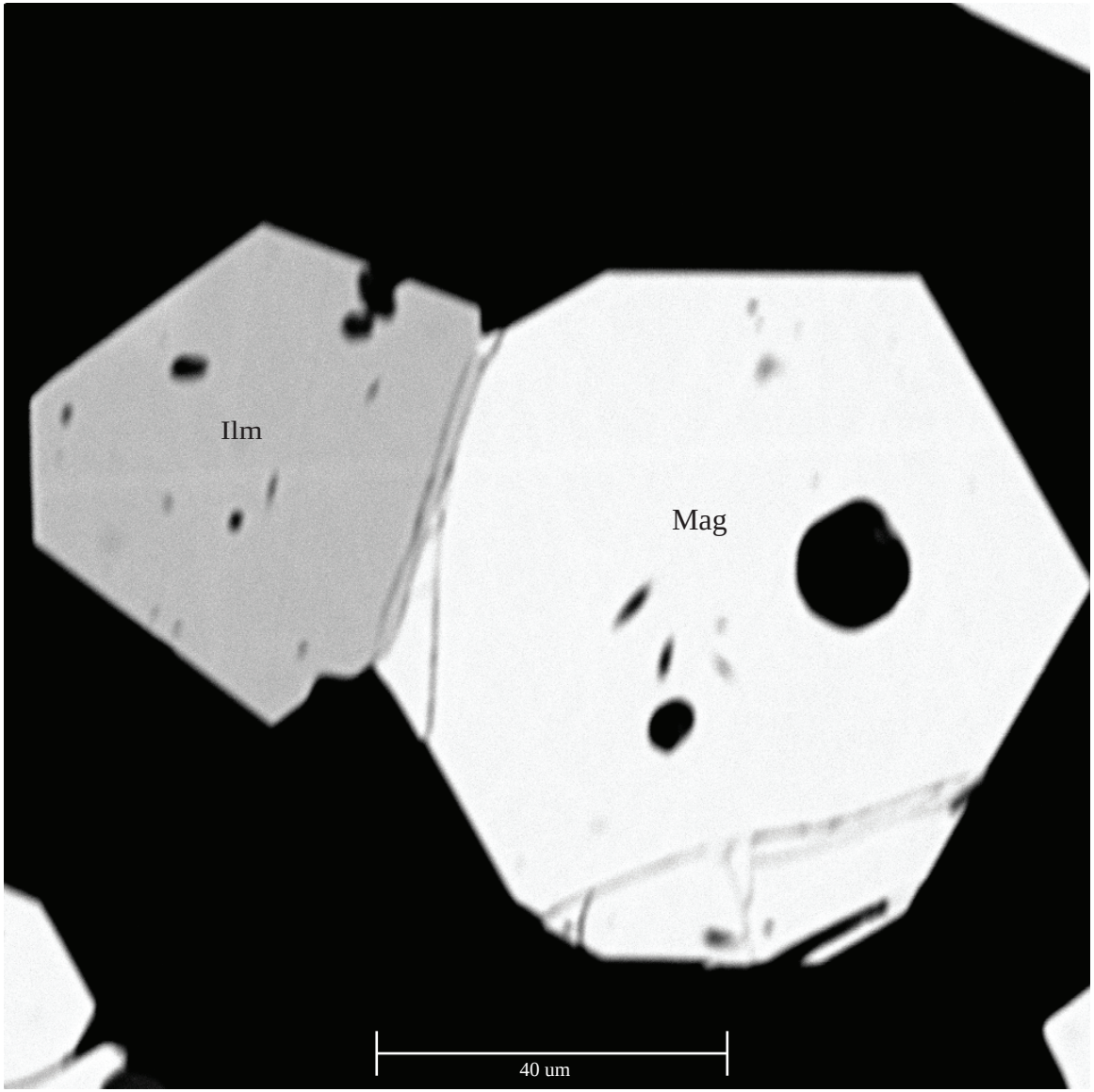


**Figure 7g.**

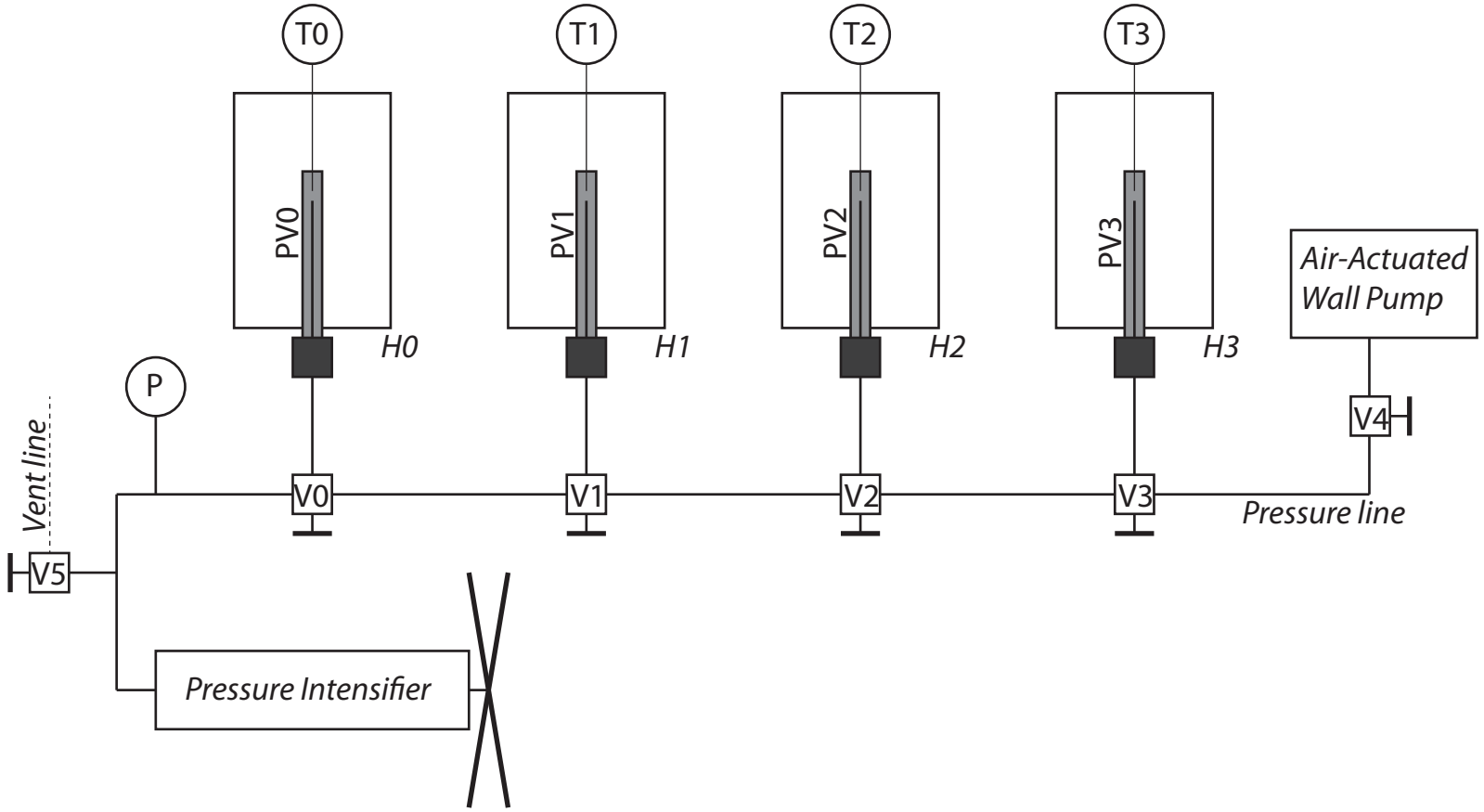
T0
T1
T2
T3
PV0
PV1
PV2
PV3
H0
H1
H2
H3
Air-Actuated
Wall Pump
P
V4
Vent line
V0
V1
V2
V3
Pressure line
V5
Pressure Intensifier

**Figure 8a.**

**Figure 8b.**

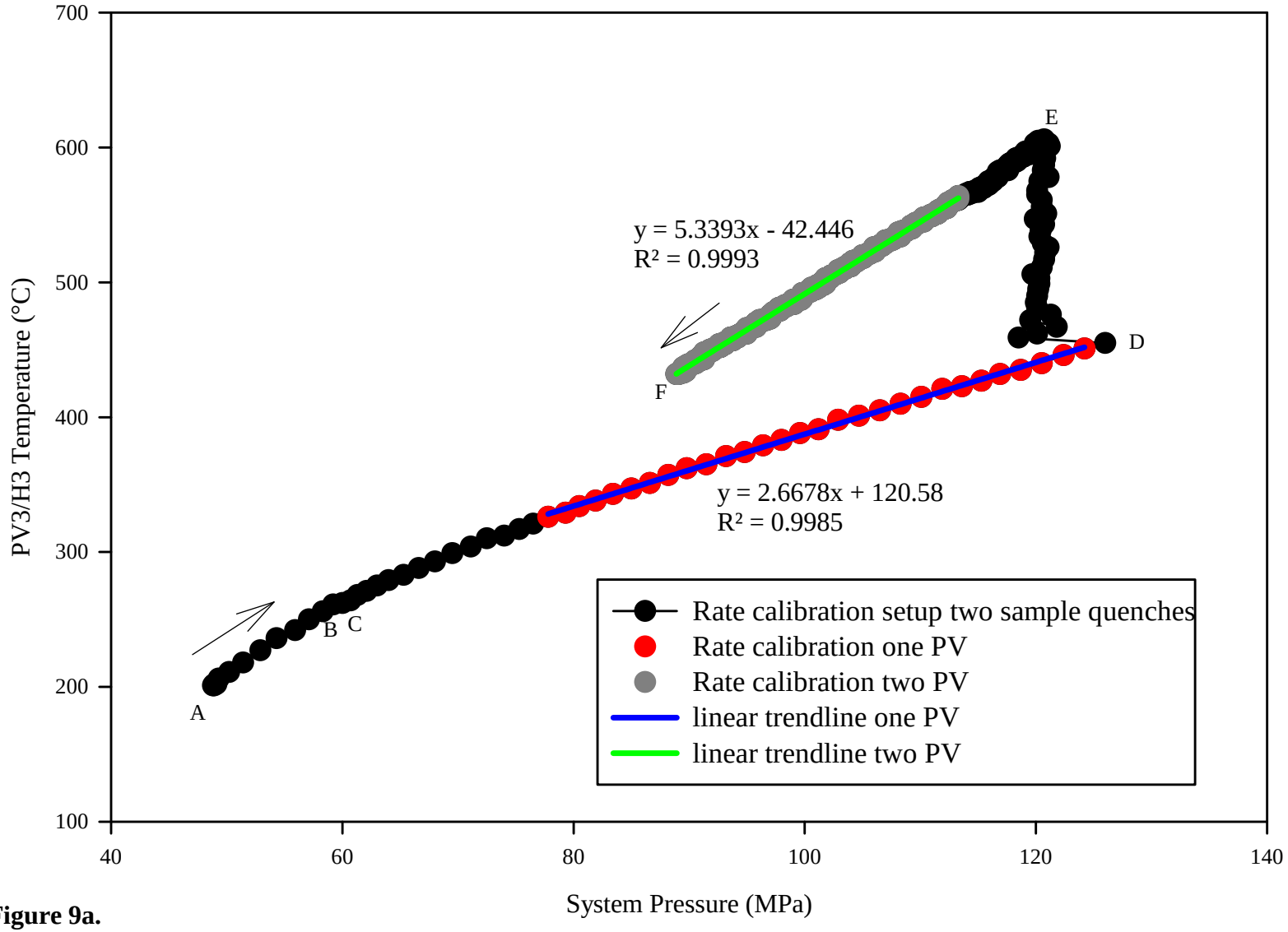
700
600
500
400
300
200
100
40
60
80
100
120
140
PV3/H3 Temperature (°C)
System Pressure (MPa)
y = 5.3393x - 42.446
R² = 0.9993
y = 2.6678x + 120.58
R² = 0.9985
A
B
C
D
E
F
Rate calibration setup two sample quenches
Rate calibration one PV
Rate calibration two PV
linear trendline one PV
linear trendline two PV

**Figure 9a.**

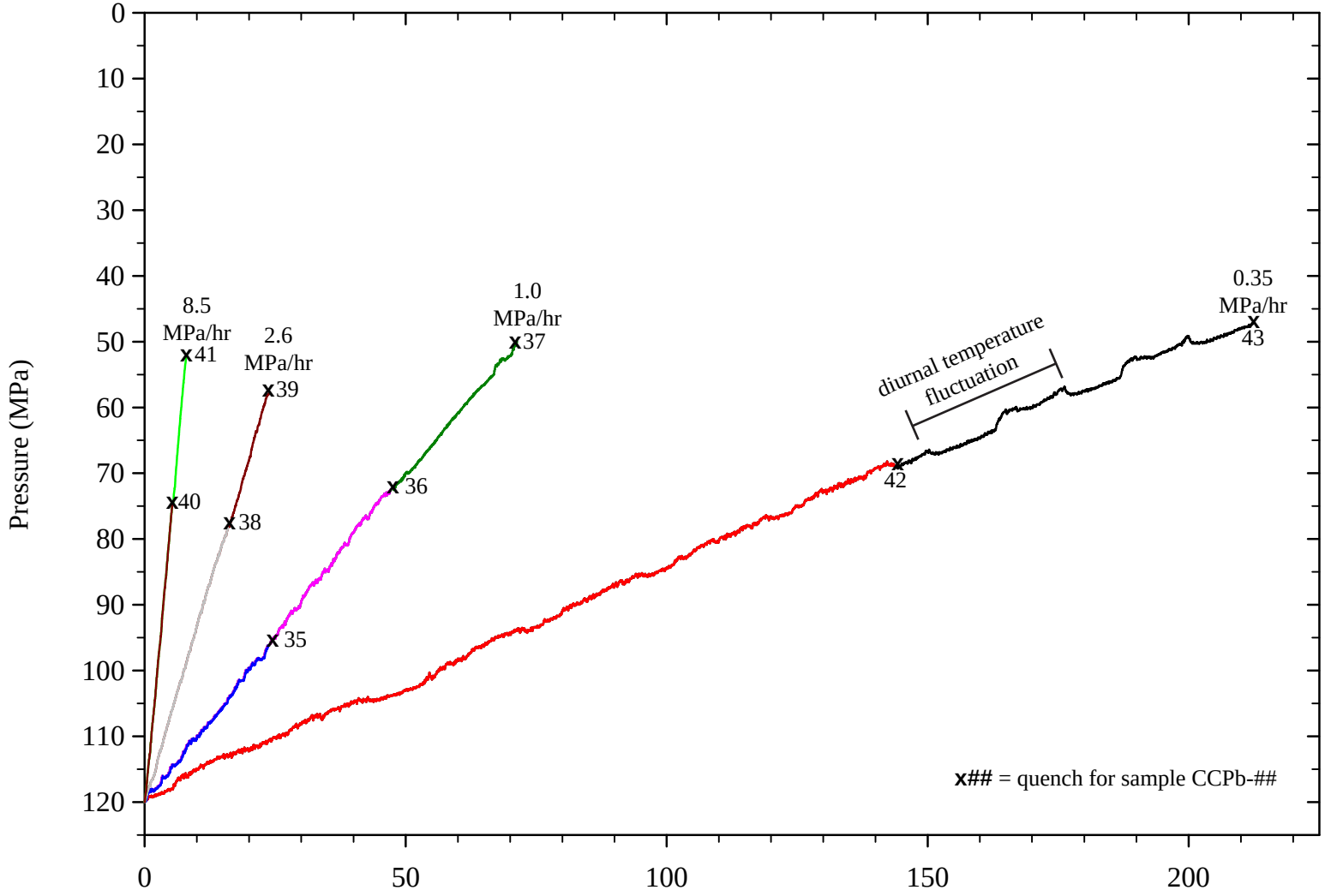
Pressure (MPa)
Decompression duration (hours)
0
10
20
30
40
50
60
70
80
90
100
110
120
0
50
100
150
200
8.5
MPa/hr
2.6
MPa/hr
1.0
MPa/hr
0.35
MPa/hr
x41
x40
x39
x38
x37
x36
x35
x42
x43
diurnal temperature
fluctuation
x## = quench for sample CCPb-##

**Figure 9b.**

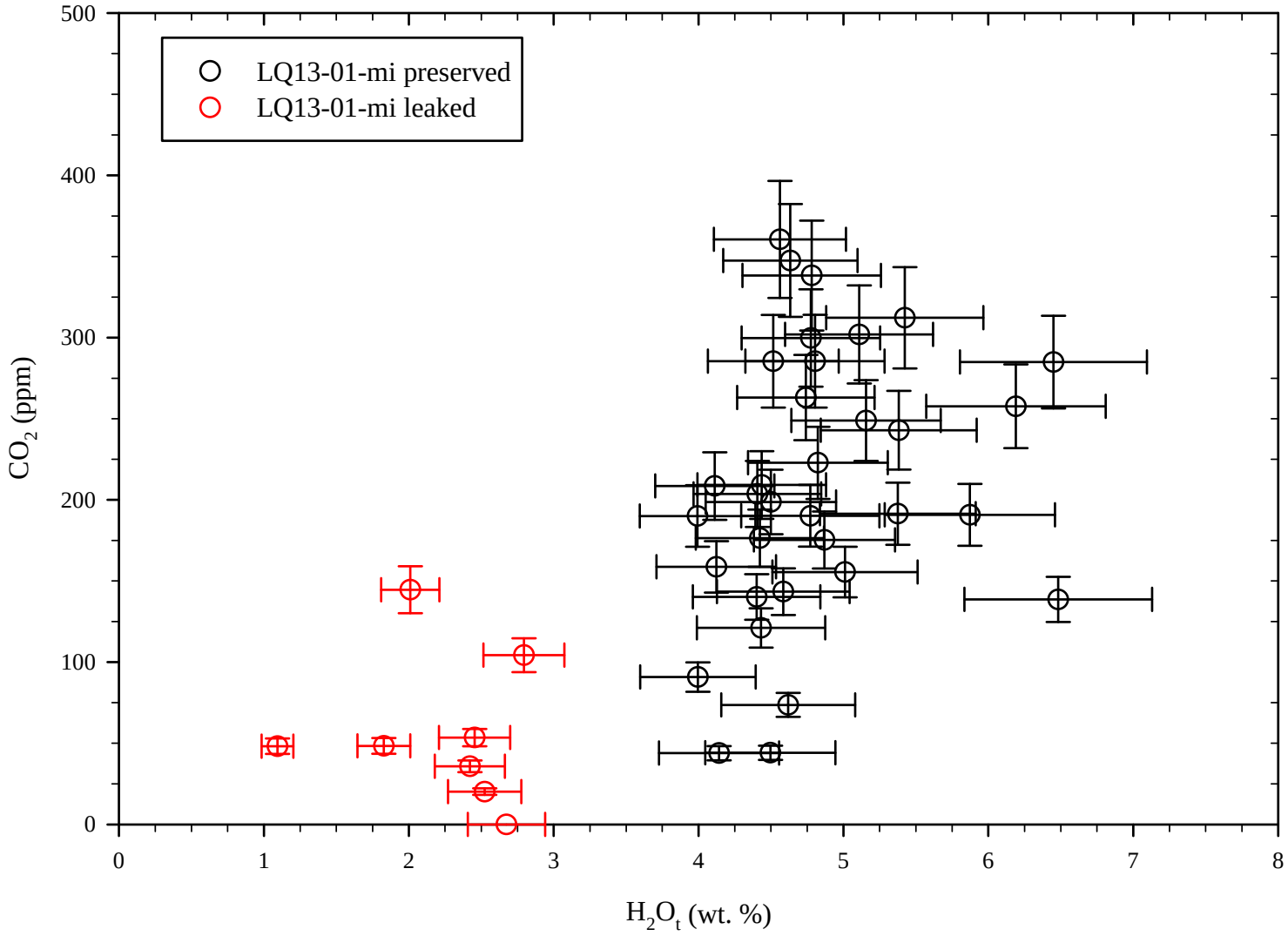
LQ13-01-mi preserved
LQ13-01-mi leaked
CO2 (ppm)
H2Ot (wt. %)
0
100
200
300
400
500
0
1
2
3
4
5
6
7
8

**Figure 10.**

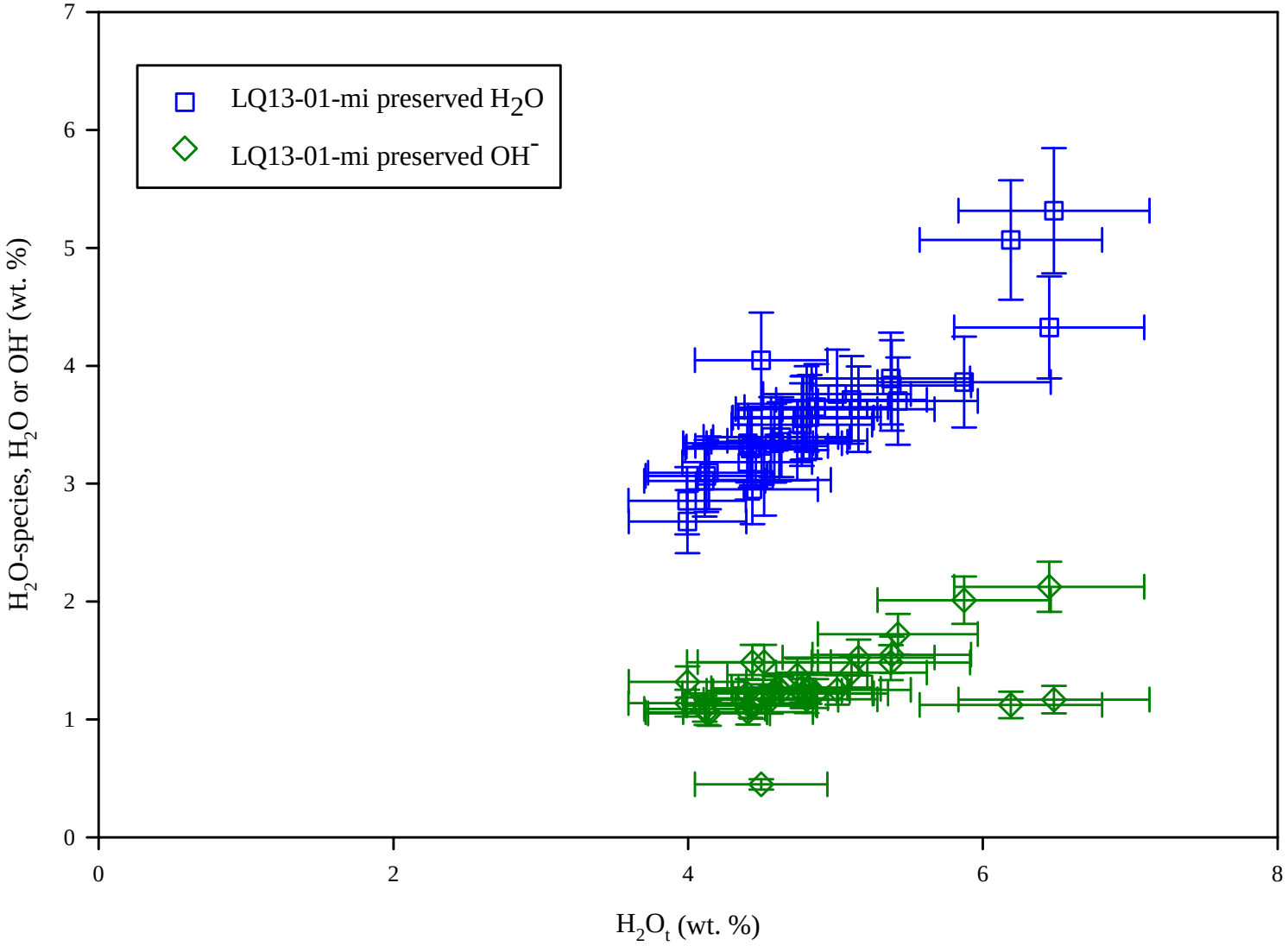
LQ13-01-mi preserved H2O
LQ13-01-mi preserved OH-
H2O-species, H2O or OH- (wt. %)
H2Ot (wt. %)
0
1
2
3
4
5
6
7
0
2
4
6
8

**Figure 11.**

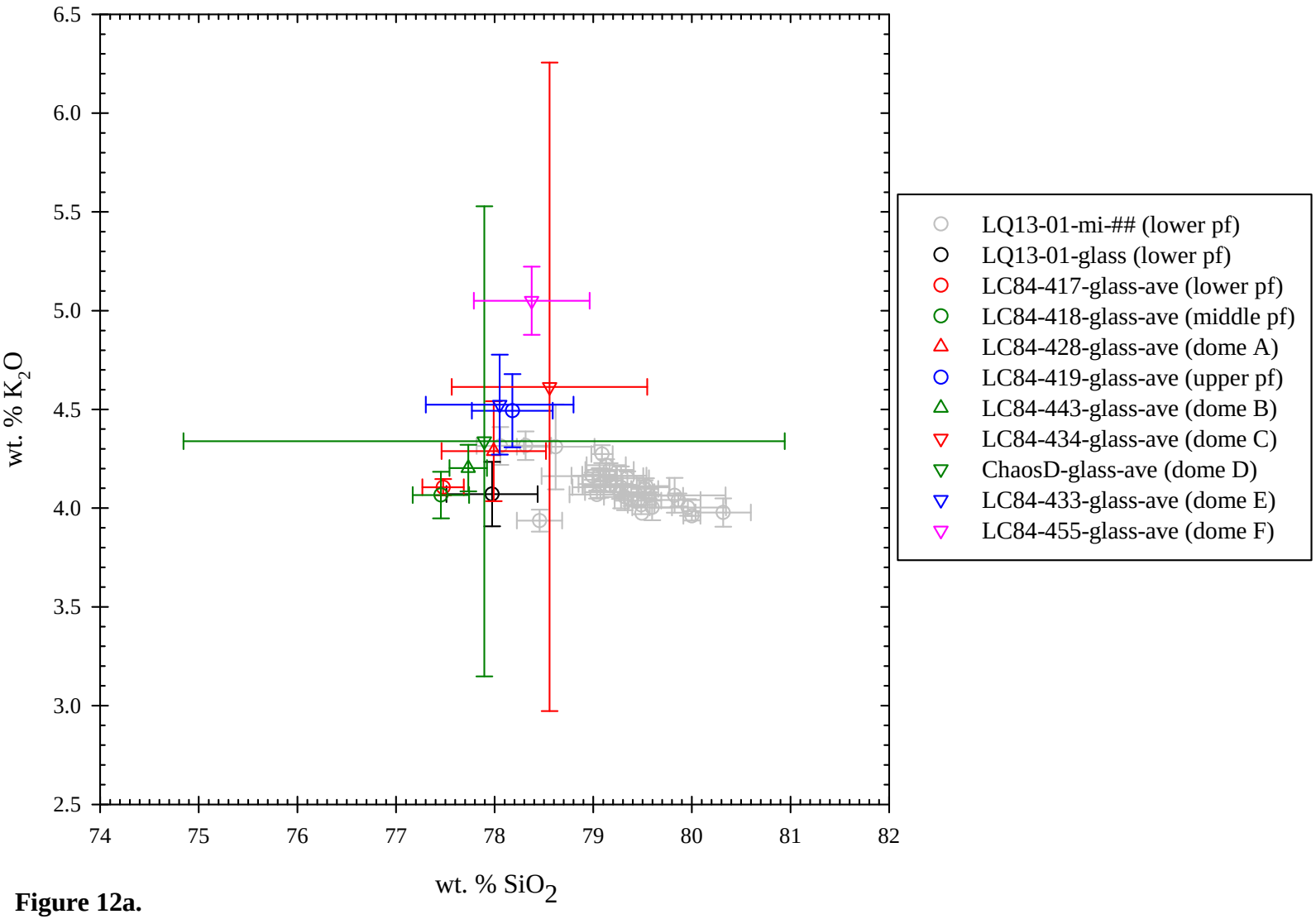
6.5
6.0
5.5
5.0
4.5
4.0
3.5
3.0
2.5
wt. % $K_2O$
74
75
76
77
78
79
80
81
82
wt. % $SiO_2$
LQ13-01-mi-## (lower pf)
LQ13-01-glass (lower pf)
LC84-417-glass-ave (lower pf)
LC84-418-glass-ave (middle pf)
LC84-428-glass-ave (dome A)
LC84-419-glass-ave (upper pf)
LC84-443-glass-ave (dome B)
LC84-434-glass-ave (dome C)
ChaosD-glass-ave (dome D)
LC84-433-glass-ave (dome E)
LC84-455-glass-ave (dome F)

**Figure 12a.**

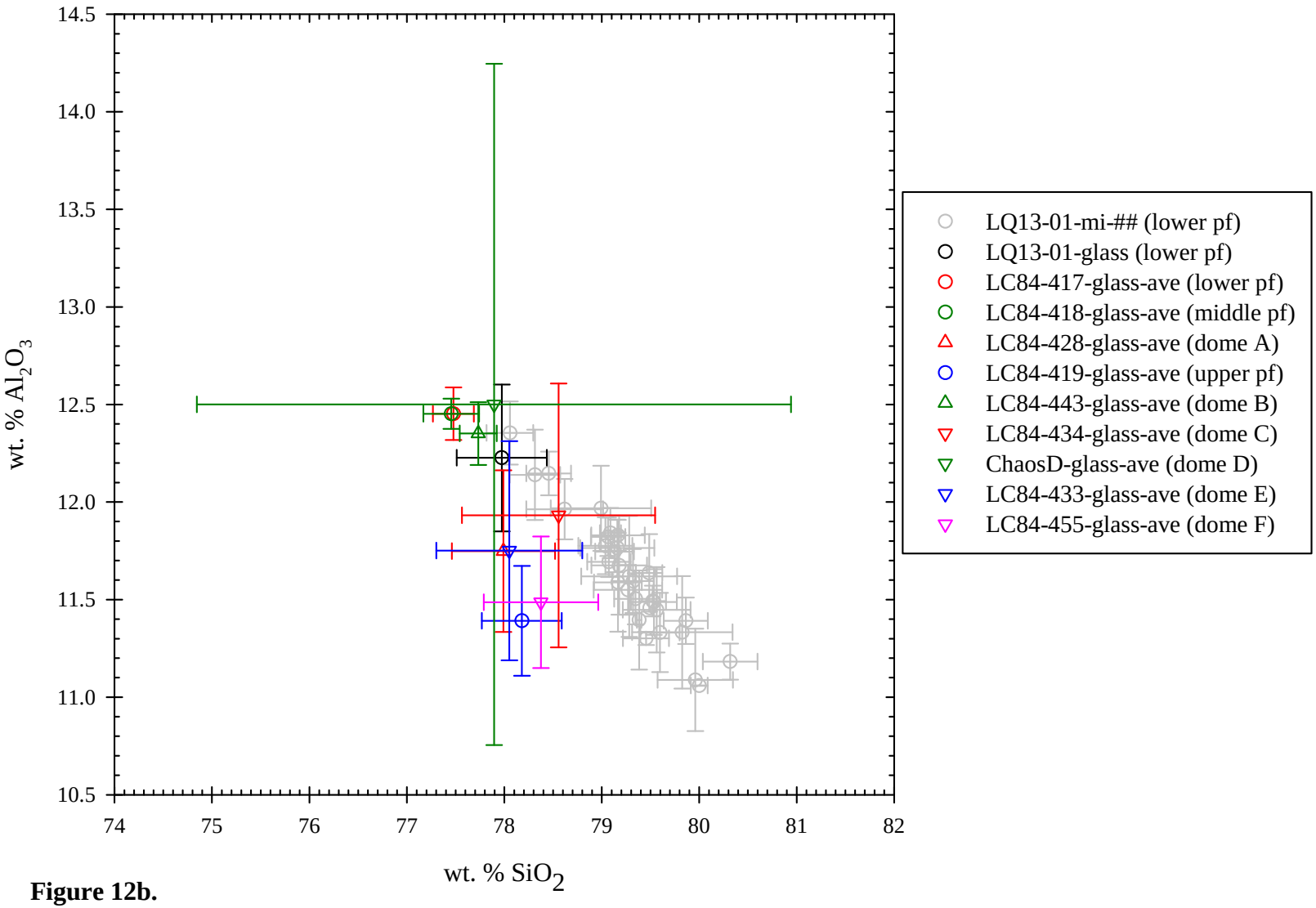
14.5
14.0
13.5
13.0
12.5
12.0
11.5
11.0
10.5
wt. % Al2O3
74
75
76
77
78
79
80
81
82
wt. % SiO2
LQ13-01-mi-## (lower pf)
LQ13-01-glass (lower pf)
LC84-417-glass-ave (lower pf)
LC84-418-glass-ave (middle pf)
LC84-428-glass-ave (dome A)
LC84-419-glass-ave (upper pf)
LC84-443-glass-ave (dome B)
LC84-434-glass-ave (dome C)
ChaosD-glass-ave (dome D)
LC84-433-glass-ave (dome E)
LC84-455-glass-ave (dome F)

**Figure 12b.**

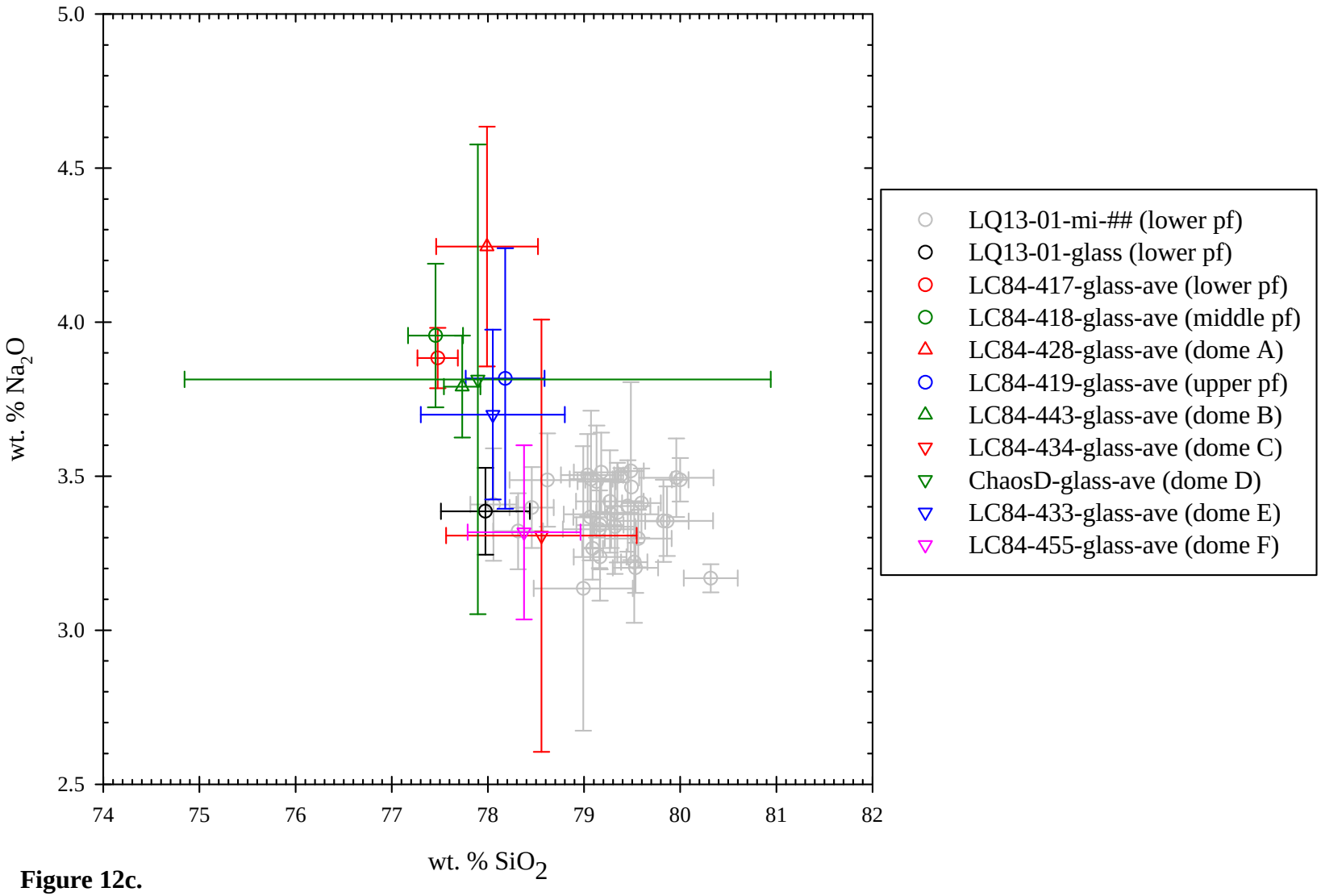
5.0
4.5
4.0
3.5
3.0
2.5
wt. % Na2O
74
75
76
77
78
79
80
81
82
wt. % SiO2
LQ13-01-mi-## (lower pf)
LQ13-01-glass (lower pf)
LC84-417-glass-ave (lower pf)
LC84-418-glass-ave (middle pf)
LC84-428-glass-ave (dome A)
LC84-419-glass-ave (upper pf)
LC84-443-glass-ave (dome B)
LC84-434-glass-ave (dome C)
ChaosD-glass-ave (dome D)
LC84-433-glass-ave (dome E)
LC84-455-glass-ave (dome F)

**Figure 12c.**

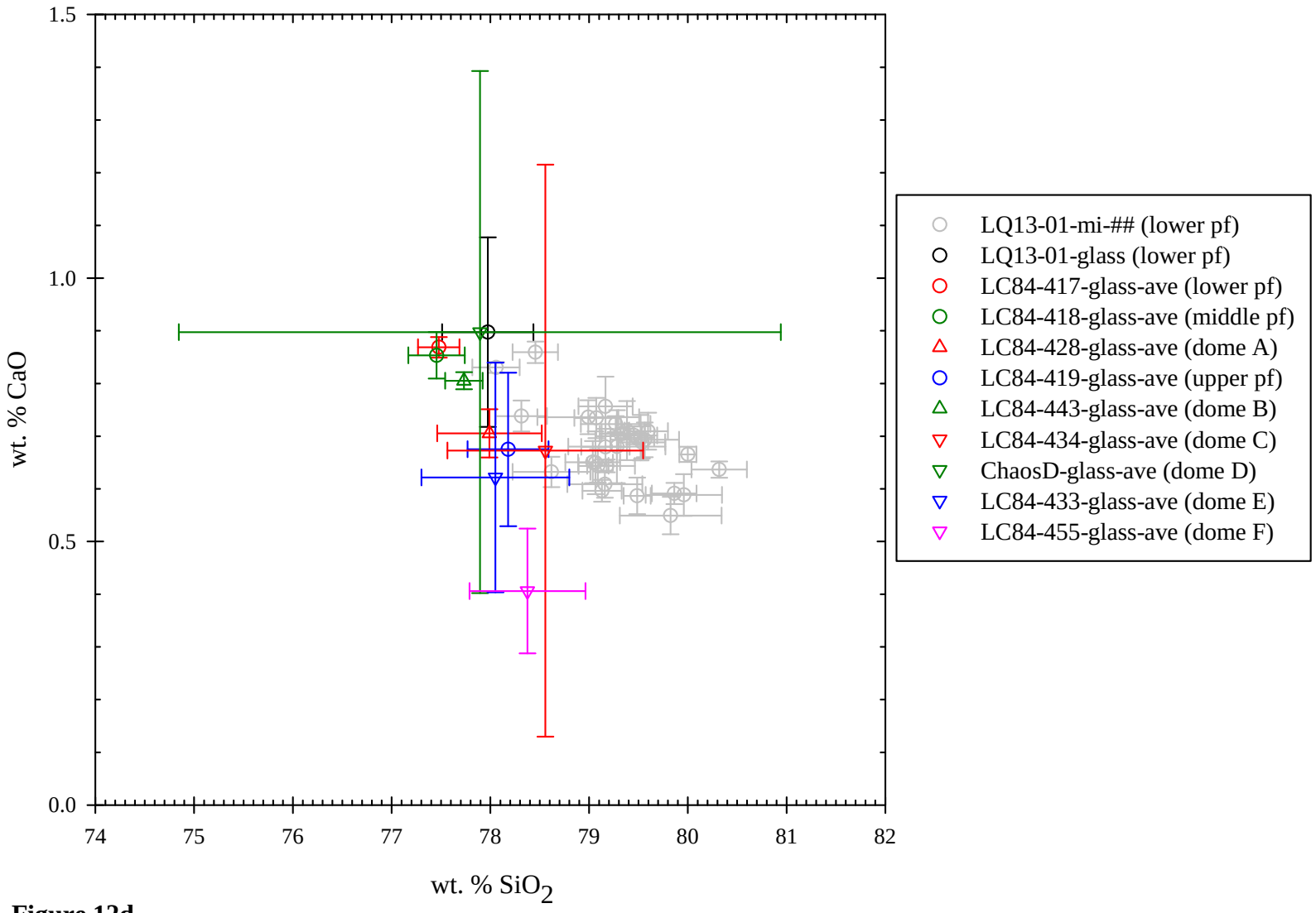
1.5
1.0
0.5
0.0
wt. % CaO
74
75
76
77
78
79
80
81
82
wt. % SiO2
LQ13-01-mi-## (lower pf)
LQ13-01-glass (lower pf)
LC84-417-glass-ave (lower pf)
LC84-418-glass-ave (middle pf)
LC84-428-glass-ave (dome A)
LC84-419-glass-ave (upper pf)
LC84-443-glass-ave (dome B)
LC84-434-glass-ave (dome C)
ChaosD-glass-ave (dome D)
LC84-433-glass-ave (dome E)
LC84-455-glass-ave (dome F)

**Figure 12d.**

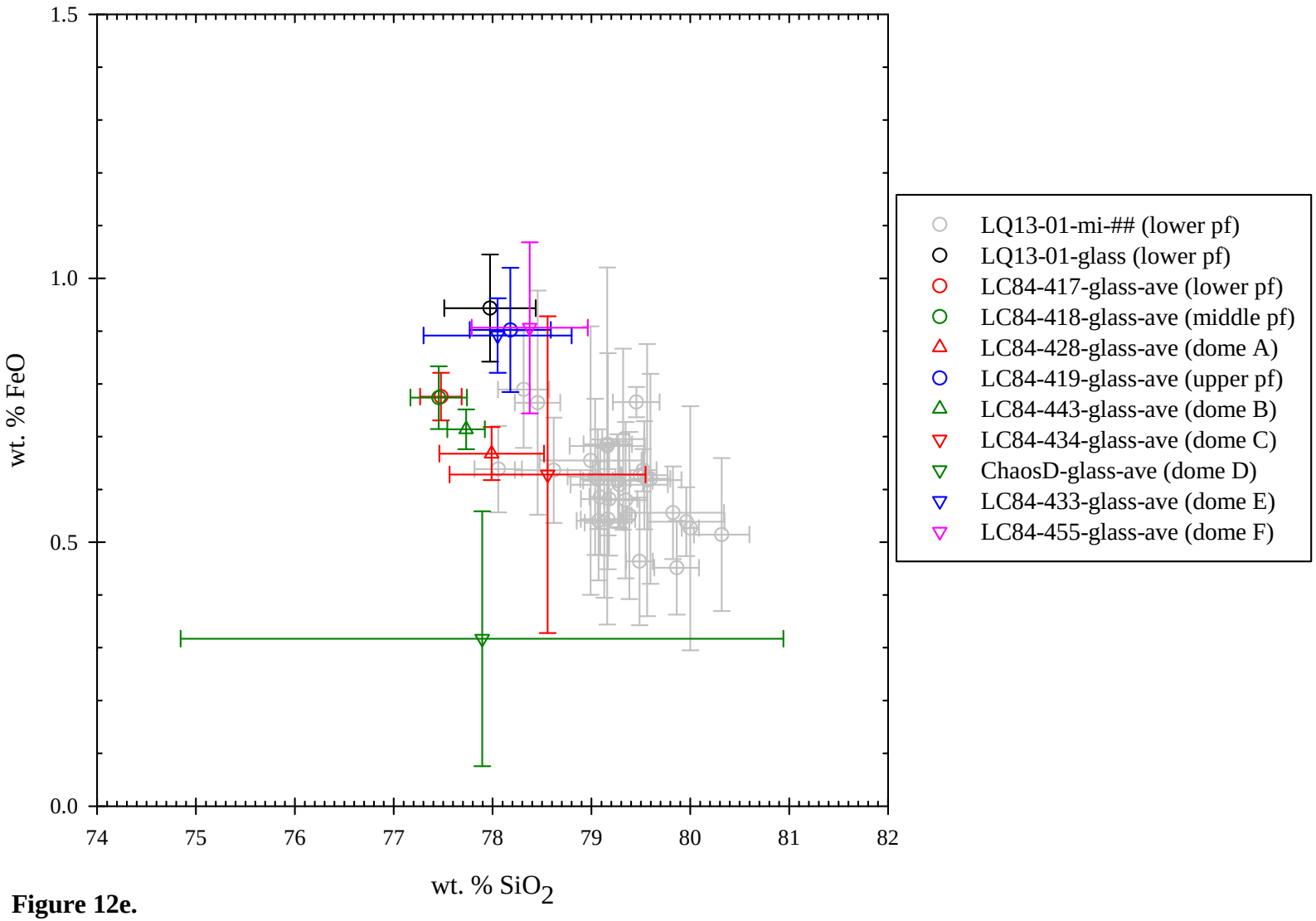
1.5
1.0
0.5
0.0
wt. % FeO
74
75
76
77
78
79
80
81
82
wt. % SiO2
LQ13-01-mi-## (lower pf)
LQ13-01-glass (lower pf)
LC84-417-glass-ave (lower pf)
LC84-418-glass-ave (middle pf)
LC84-428-glass-ave (dome A)
LC84-419-glass-ave (upper pf)
LC84-443-glass-ave (dome B)
LC84-434-glass-ave (dome C)
ChaosD-glass-ave (dome D)
LC84-433-glass-ave (dome E)
LC84-455-glass-ave (dome F)

**Figure 12e.**

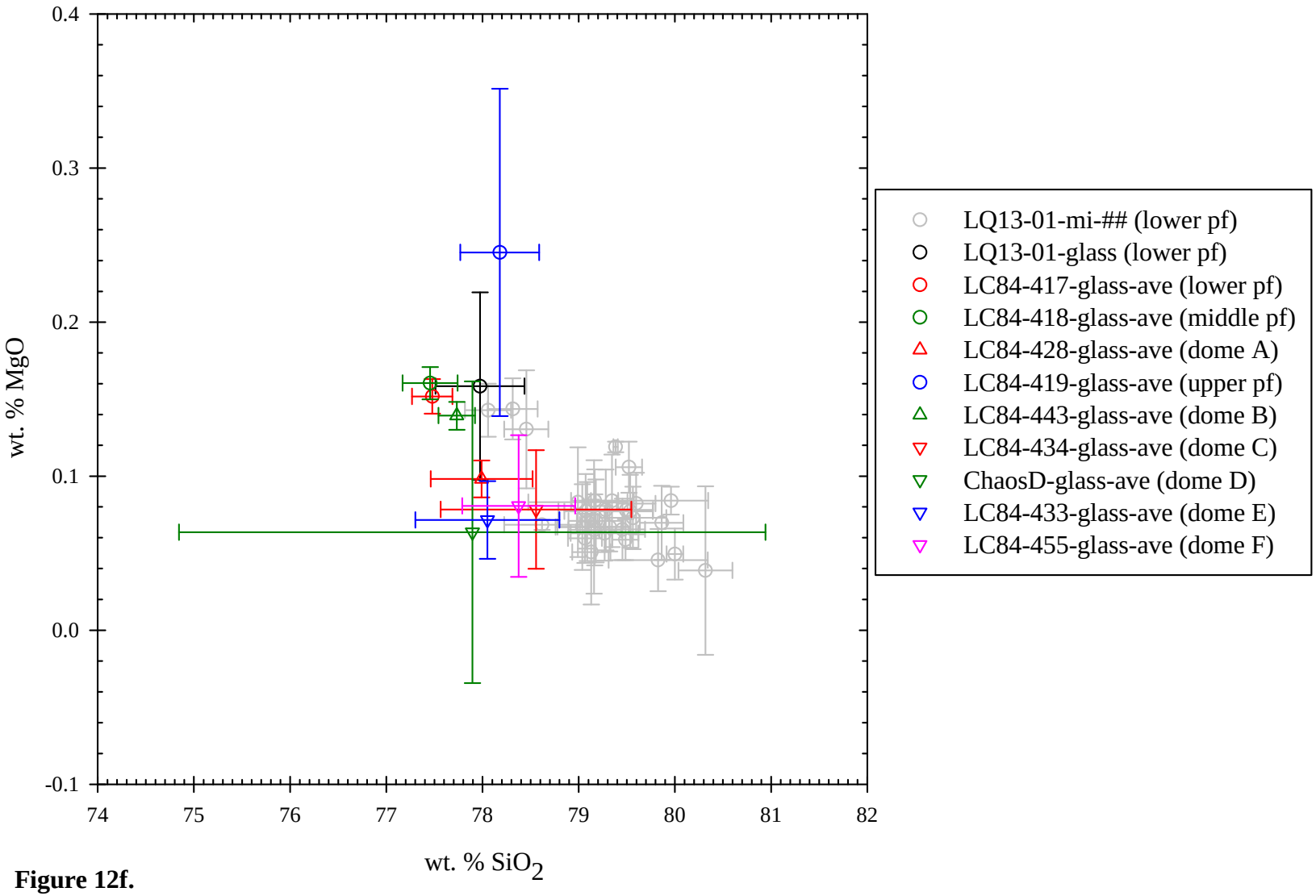
0.4
0.3
0.2
0.1
0.0
-0.1
wt. % MgO
74
75
76
77
78
79
80
81
82
wt. % SiO2
LQ13-01-mi-## (lower pf)
LQ13-01-glass (lower pf)
LC84-417-glass-ave (lower pf)
LC84-418-glass-ave (middle pf)
LC84-428-glass-ave (dome A)
LC84-419-glass-ave (upper pf)
LC84-443-glass-ave (dome B)
LC84-434-glass-ave (dome C)
ChaosD-glass-ave (dome D)
LC84-433-glass-ave (dome E)
LC84-455-glass-ave (dome F)

**Figure 12f.**

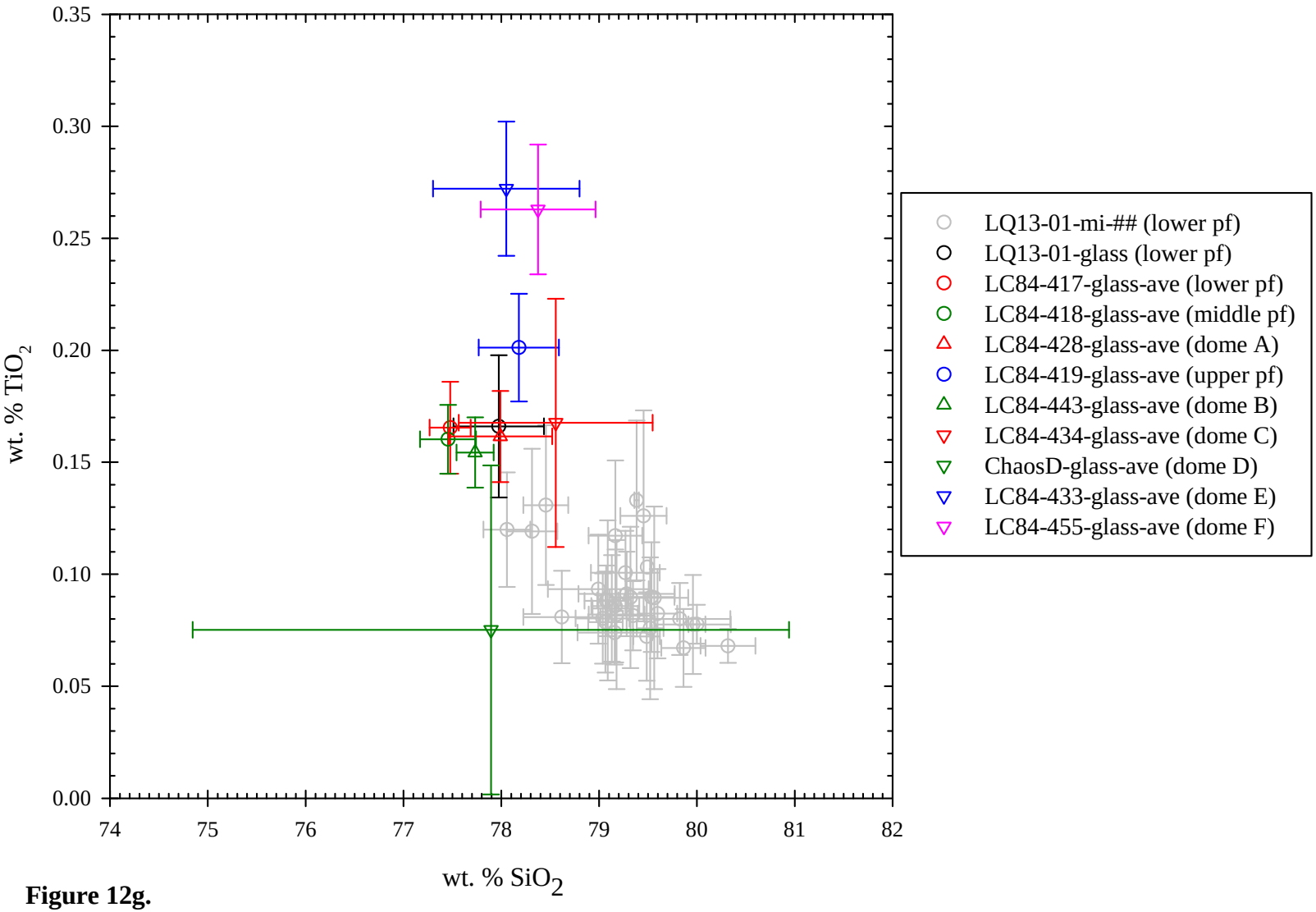
0.35
0.30
0.25
0.20
0.15
0.10
0.05
0.00
wt. % TiO2
74
75
76
77
78
79
80
81
82
wt. % SiO2
LQ13-01-mi-## (lower pf)
LQ13-01-glass (lower pf)
LC84-417-glass-ave (lower pf)
LC84-418-glass-ave (middle pf)
LC84-428-glass-ave (dome A)
LC84-419-glass-ave (upper pf)
LC84-443-glass-ave (dome B)
LC84-434-glass-ave (dome C)
ChaosD-glass-ave (dome D)
LC84-433-glass-ave (dome E)
LC84-455-glass-ave (dome F)

**Figure 12g.**

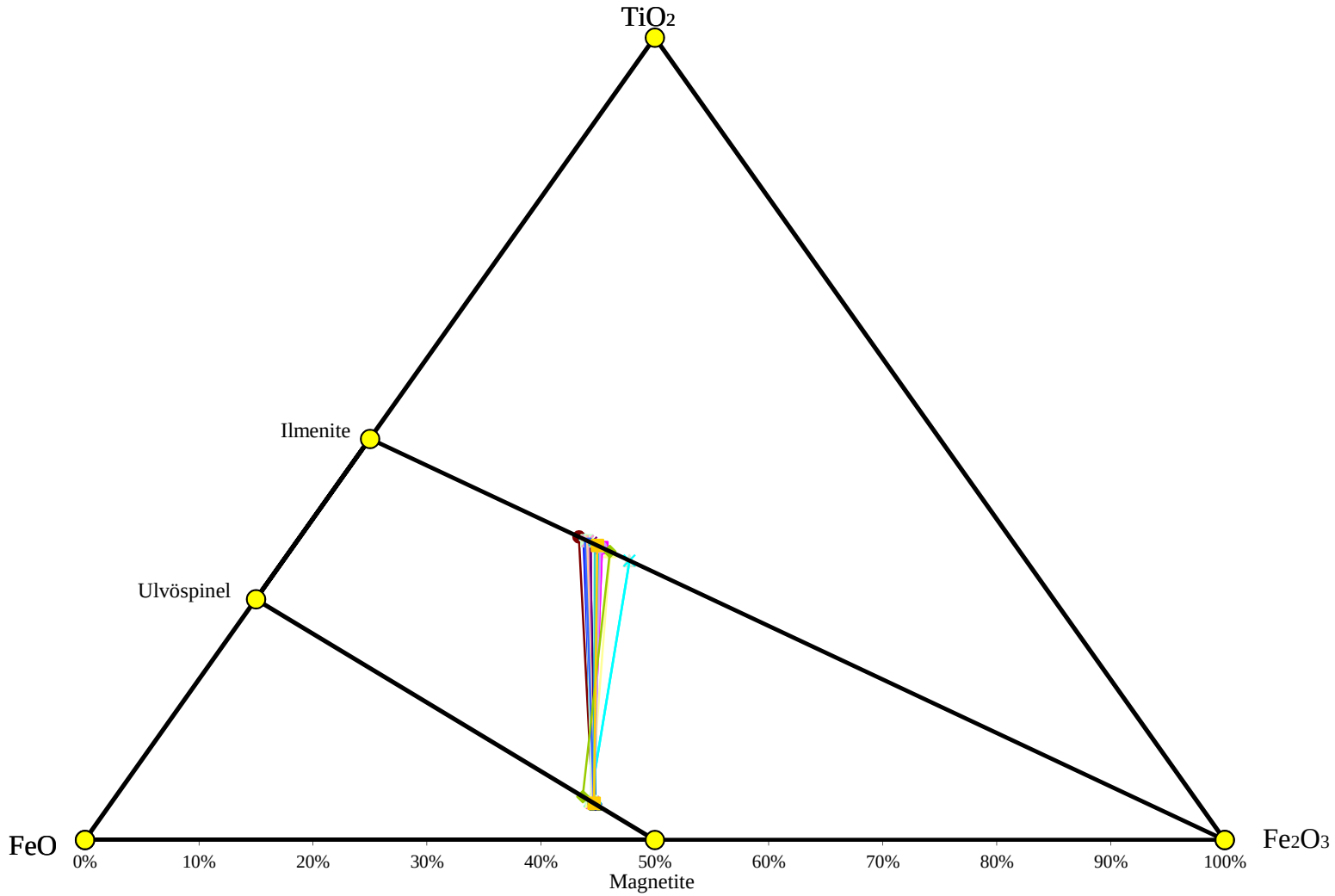
TiO2
Ilmenite
Ulvöspinel
FeO
Fe2O3
0%
10%
20%
30%
40%
50%
60%
70%
80%
90%
100%
Magnetite

**Figure 13.**

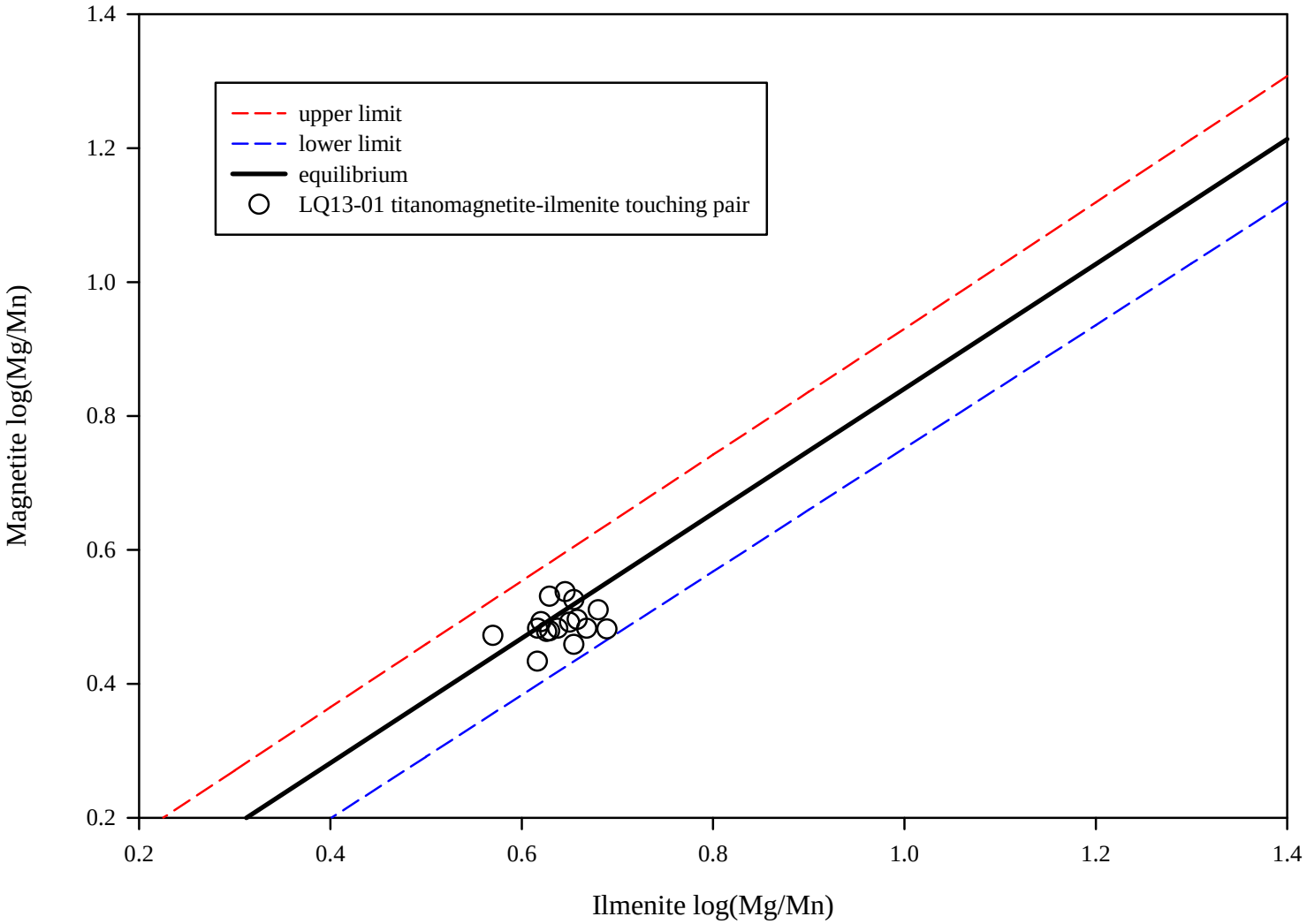
upper limit
lower limit
equilibrium
LQ13-01 titanomagnetite-ilmenite touching pair
Magnetite log(Mg/Mn)
Ilmenite log(Mg/Mn)
0.2
0.4
0.6
0.8
1.0
1.2
1.4

**Figure 14.**

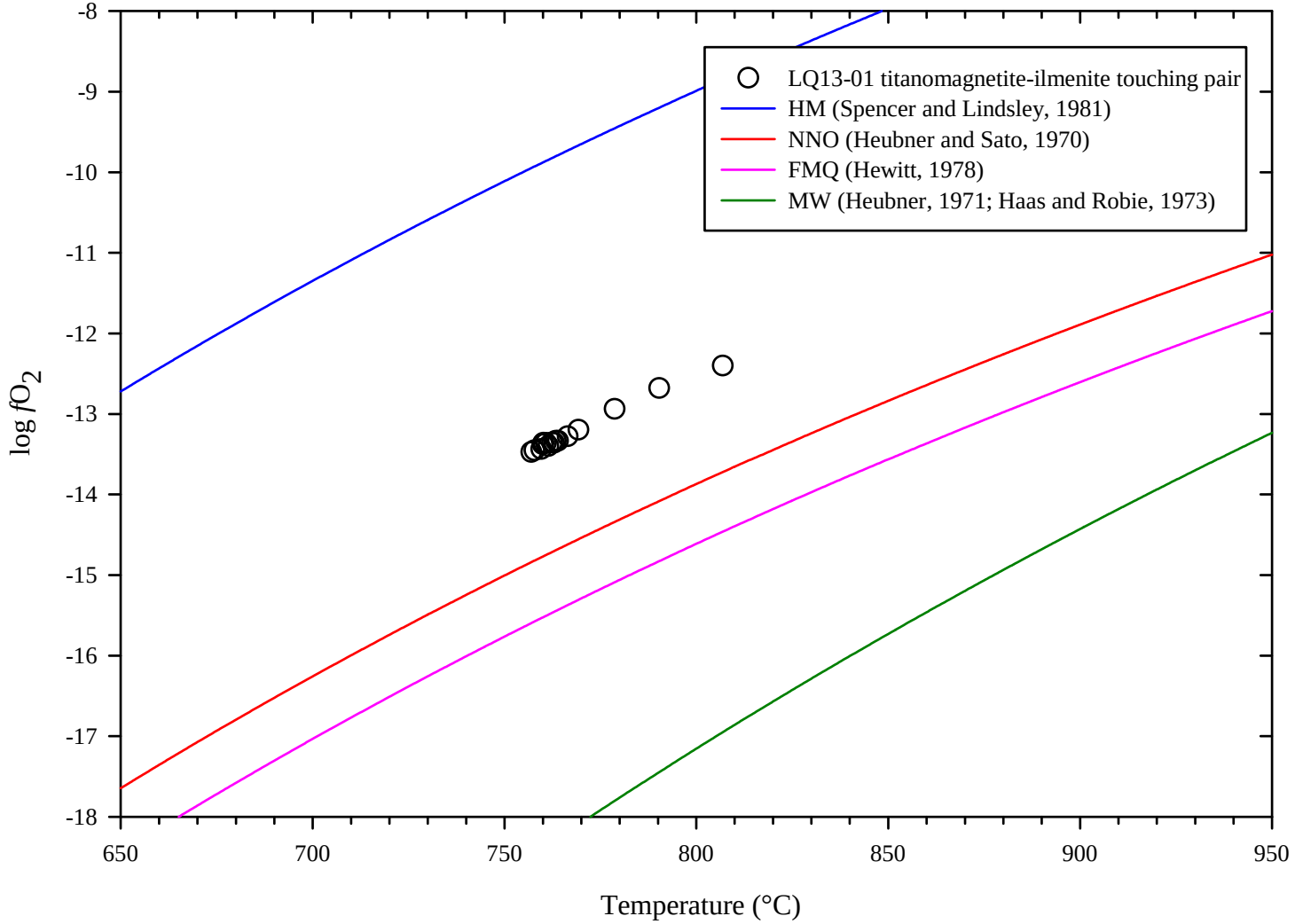
LQ13-01 titanomagnetite-ilmenite touching pair
HM (Spencer and Lindsley, 1981)
NNO (Heubner and Sato, 1970)
FMQ (Hewitt, 1978)
MW (Heubner, 1971; Haas and Robie, 1973)
log fO2
Temperature (°C)
-8
-9
-10
-11
-12
-13
-14
-15
-16
-17
-18
650
700
750
800
850
900
950

**Figure 15.**

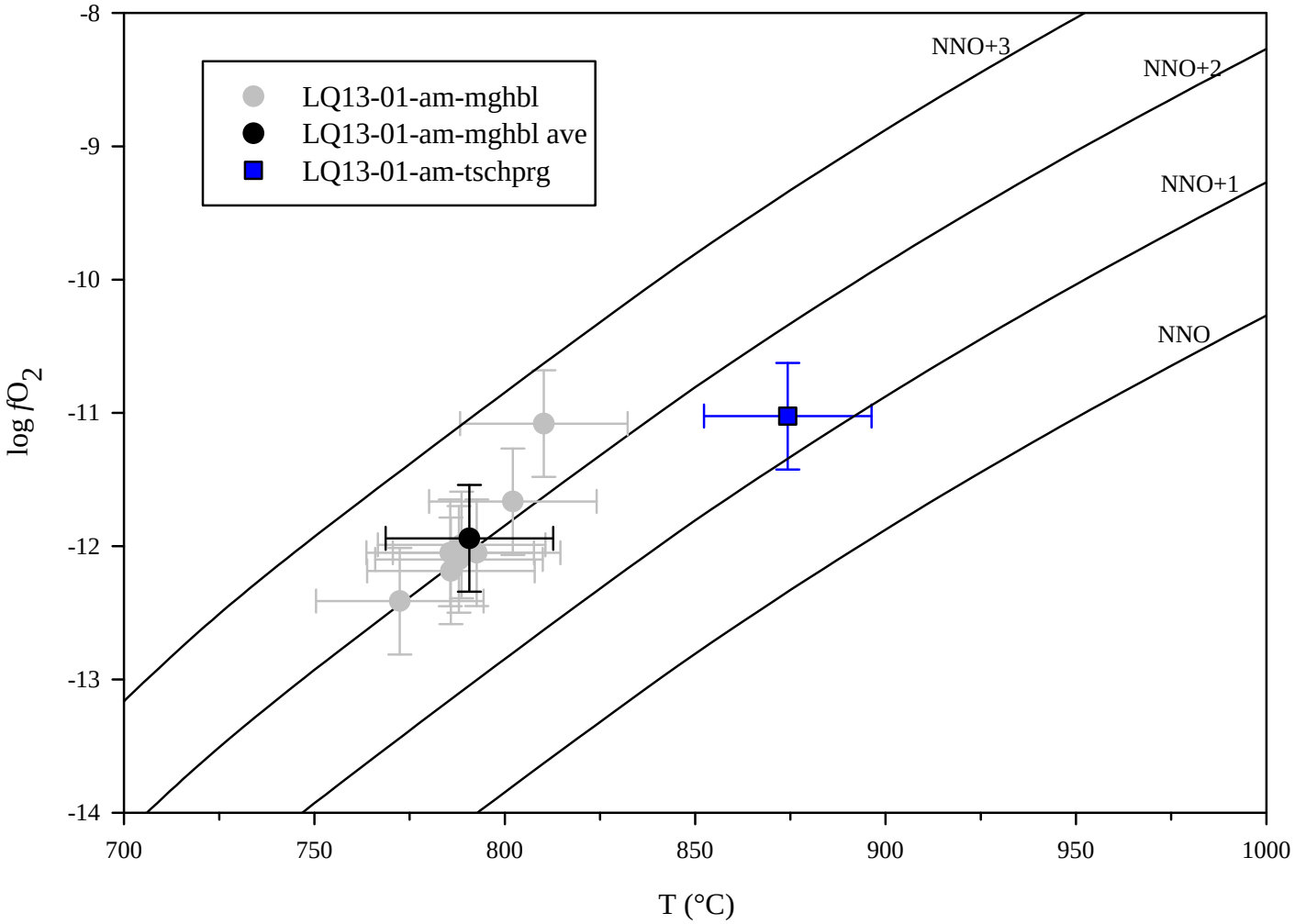
LQ13-01-am-mghbl
LQ13-01-am-mghbl ave
LQ13-01-am-tschprg
NNO+3
NNO+2
NNO+1
NNO
log fO2
T (°C)
-8
-9
-10
-11
-12
-13
-14
700
750
800
850
900
950
1000

**Figure 16a.**

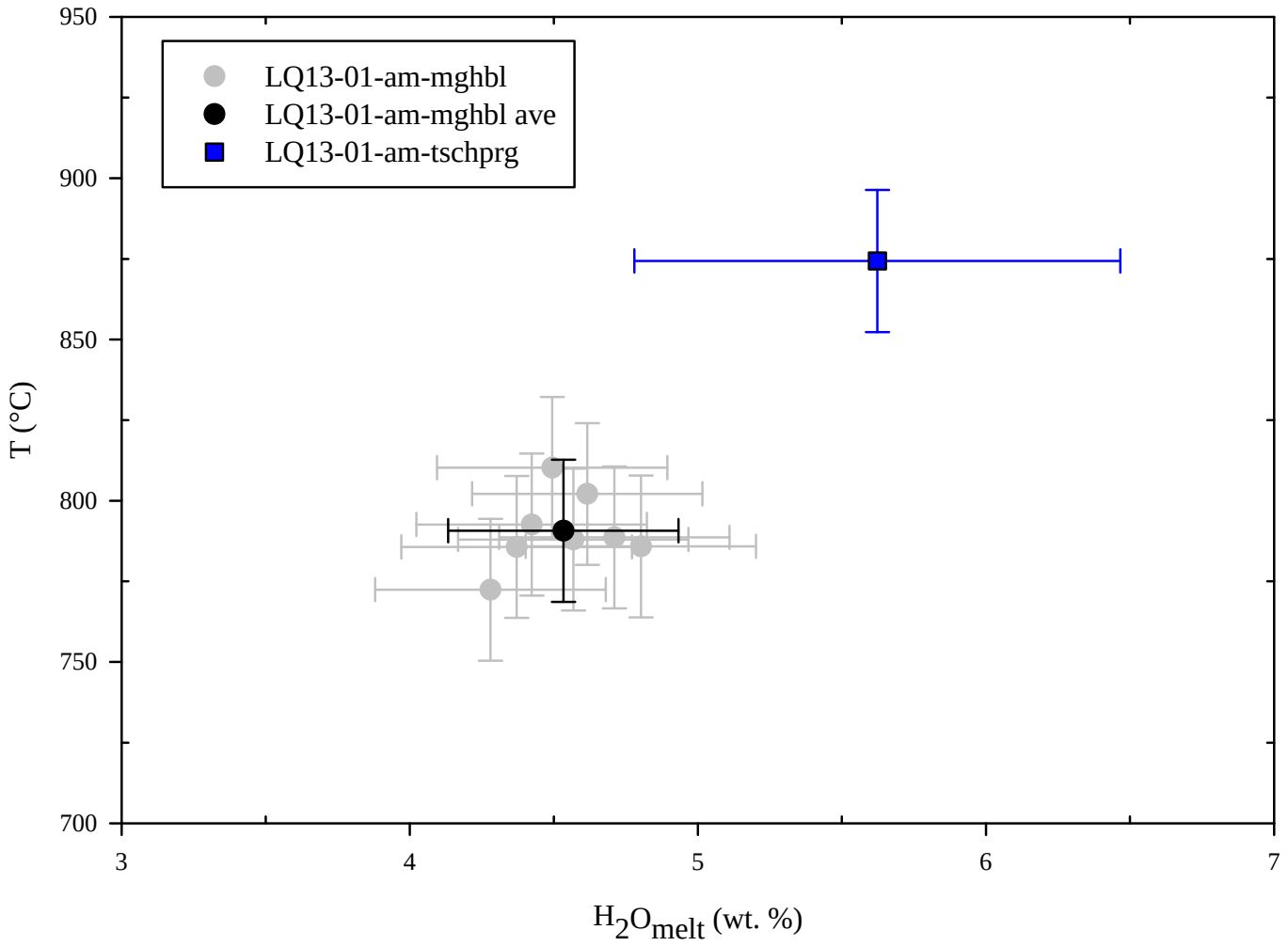
LQ13-01-am-mghbl
LQ13-01-am-mghbl ave
LQ13-01-am-tschprg
950
900
850
800
750
700
T (°C)
3
4
5
6
7
H2Omelt (wt. %)

**Figure 16b.**

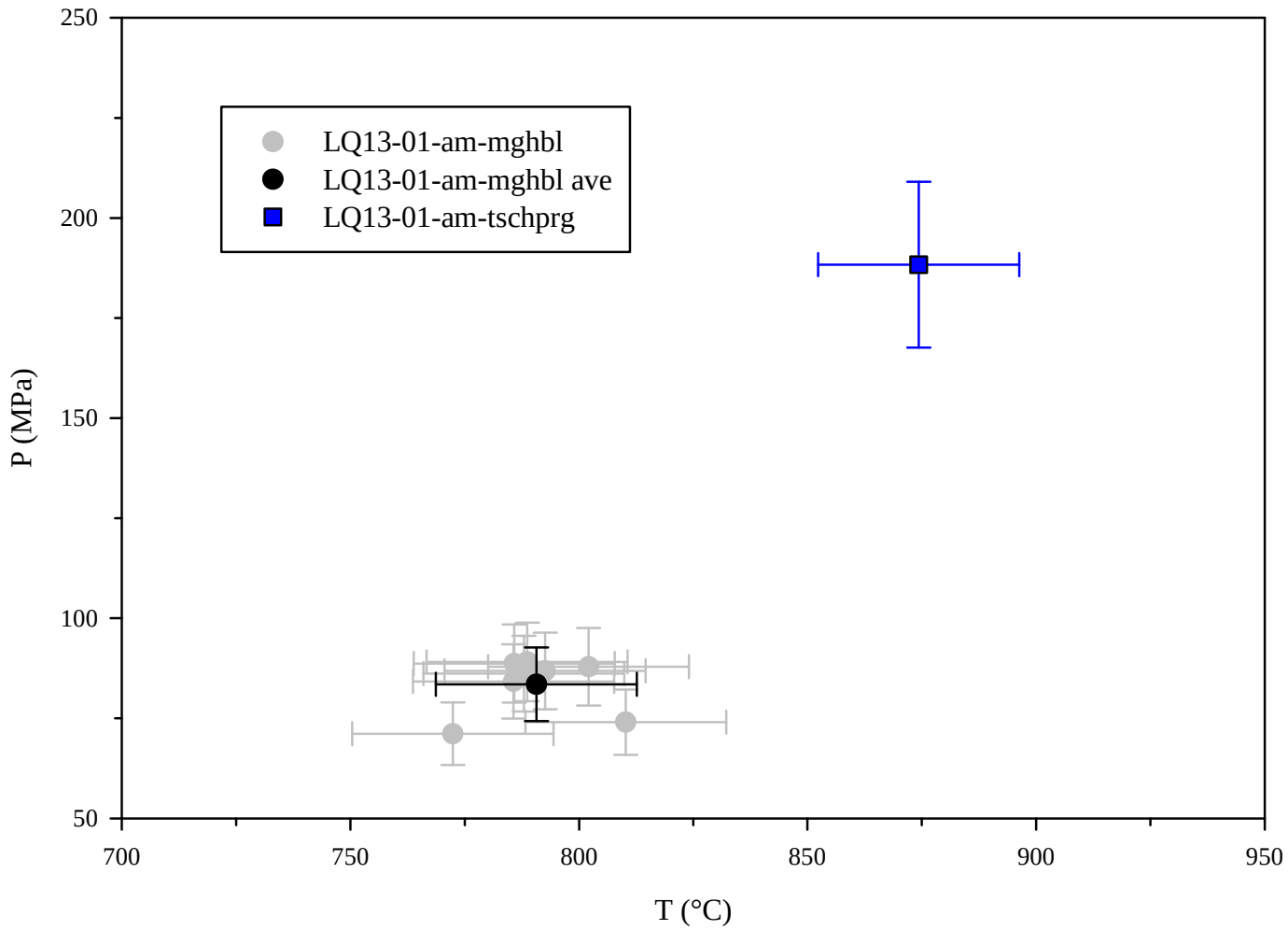
LQ13-01-am-mghbl
LQ13-01-am-mghbl ave
LQ13-01-am-tschprg
P (MPa)
T (°C)
250
200
150
100
50
700
750
800
850
900
950

**Figure 16c.**

CCPb-18

Pressure:
125 MPa

Temperature:
775°C

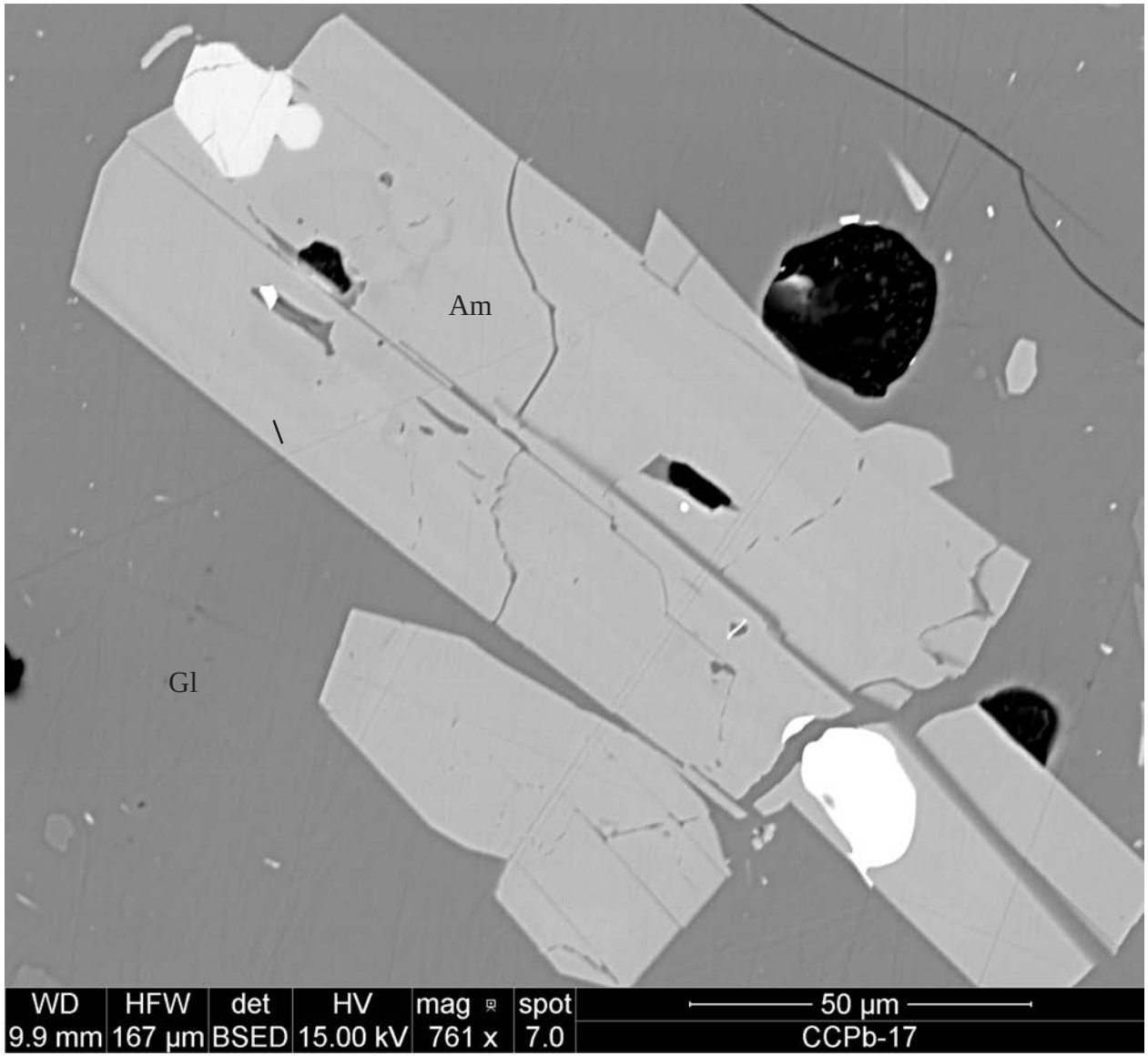


**Figure 17a.**

CCPb-34

Pressure:
120 MPa

Temperature:
775°C

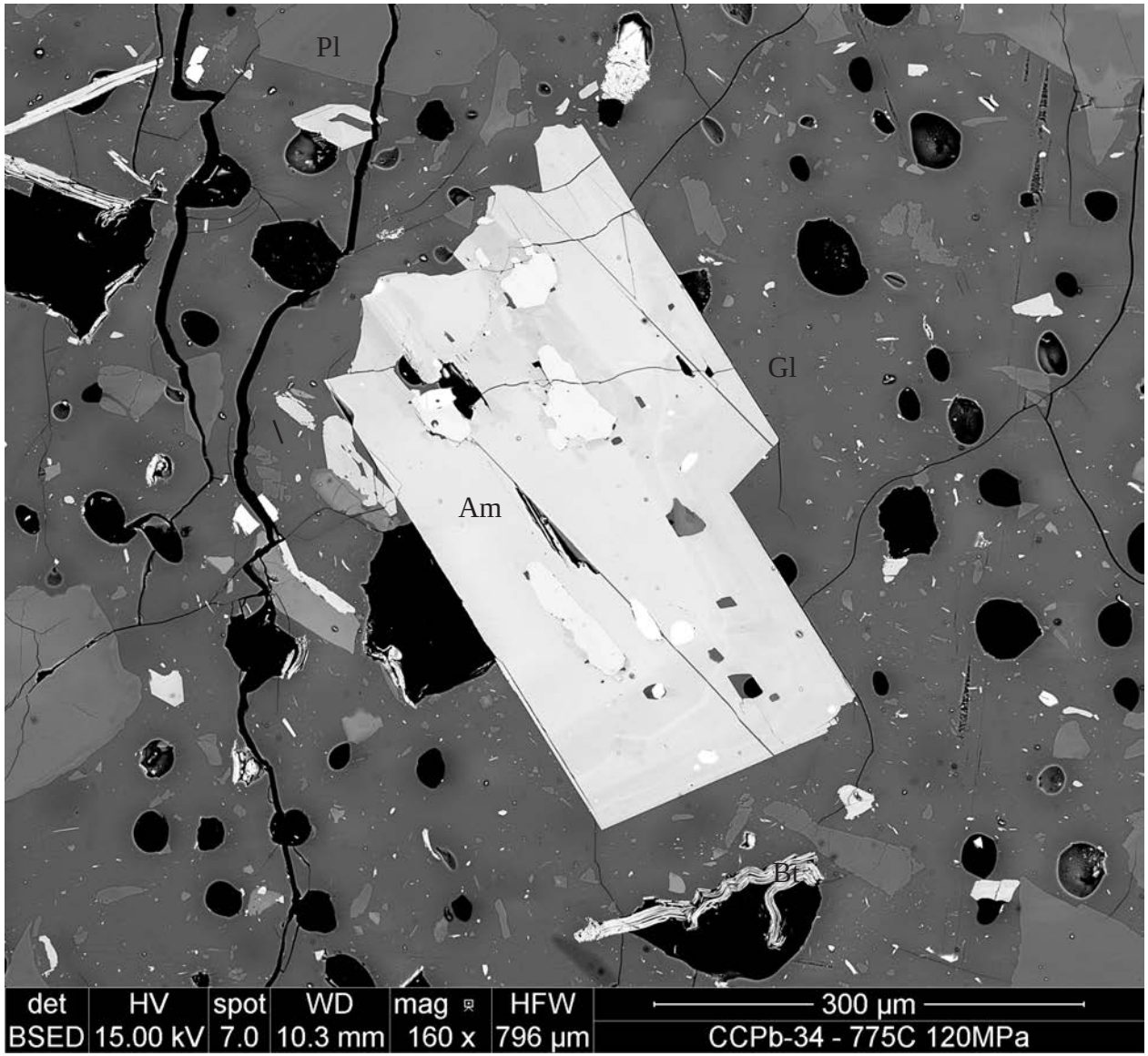


**Figure 17b.**

CCPb-31

Pressure:
175 MPa

Temperature:
750°C

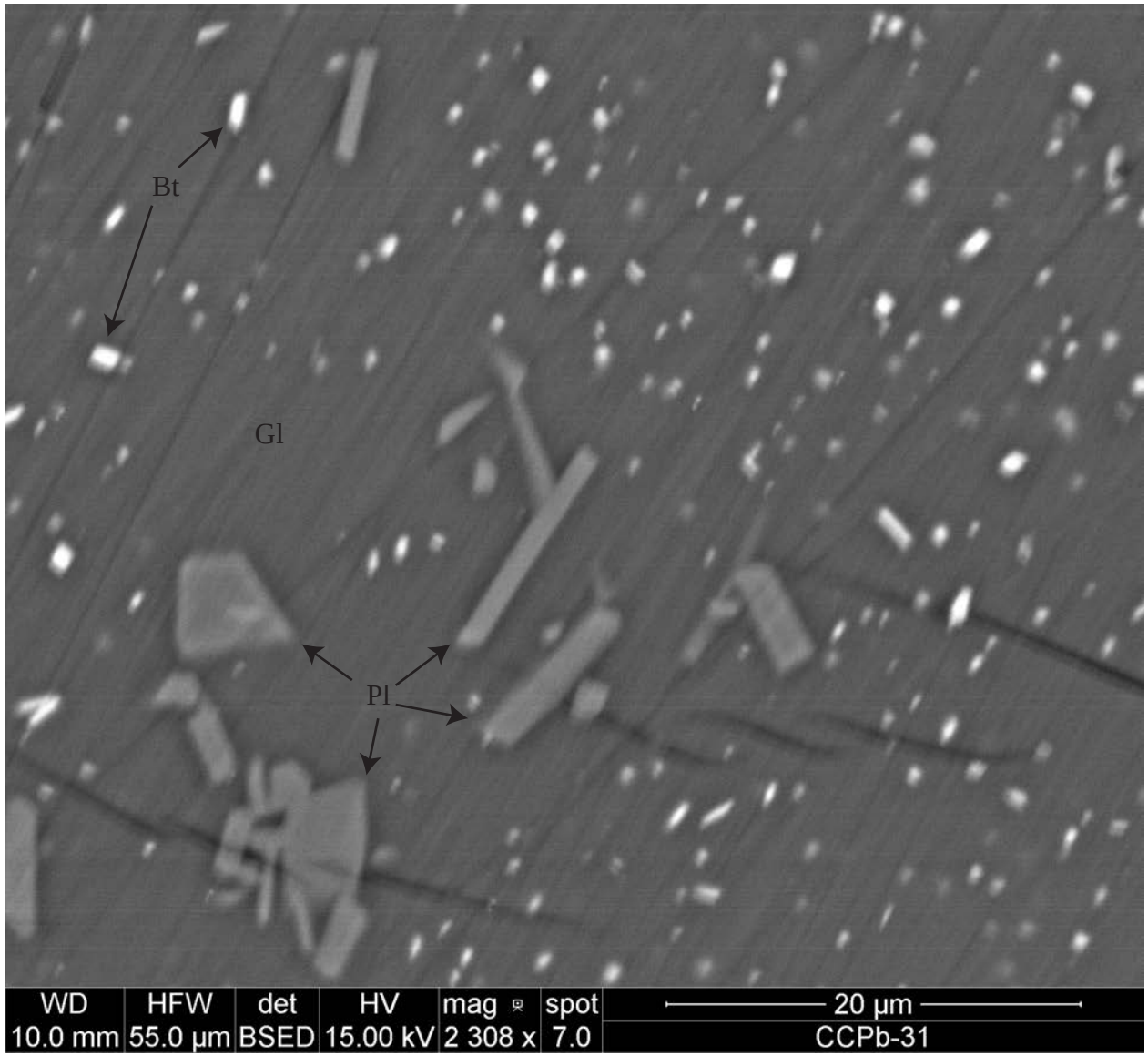


**Figure 17c.**

CCPb-17

Pressure:
125 MPa

Temperature:
825°C

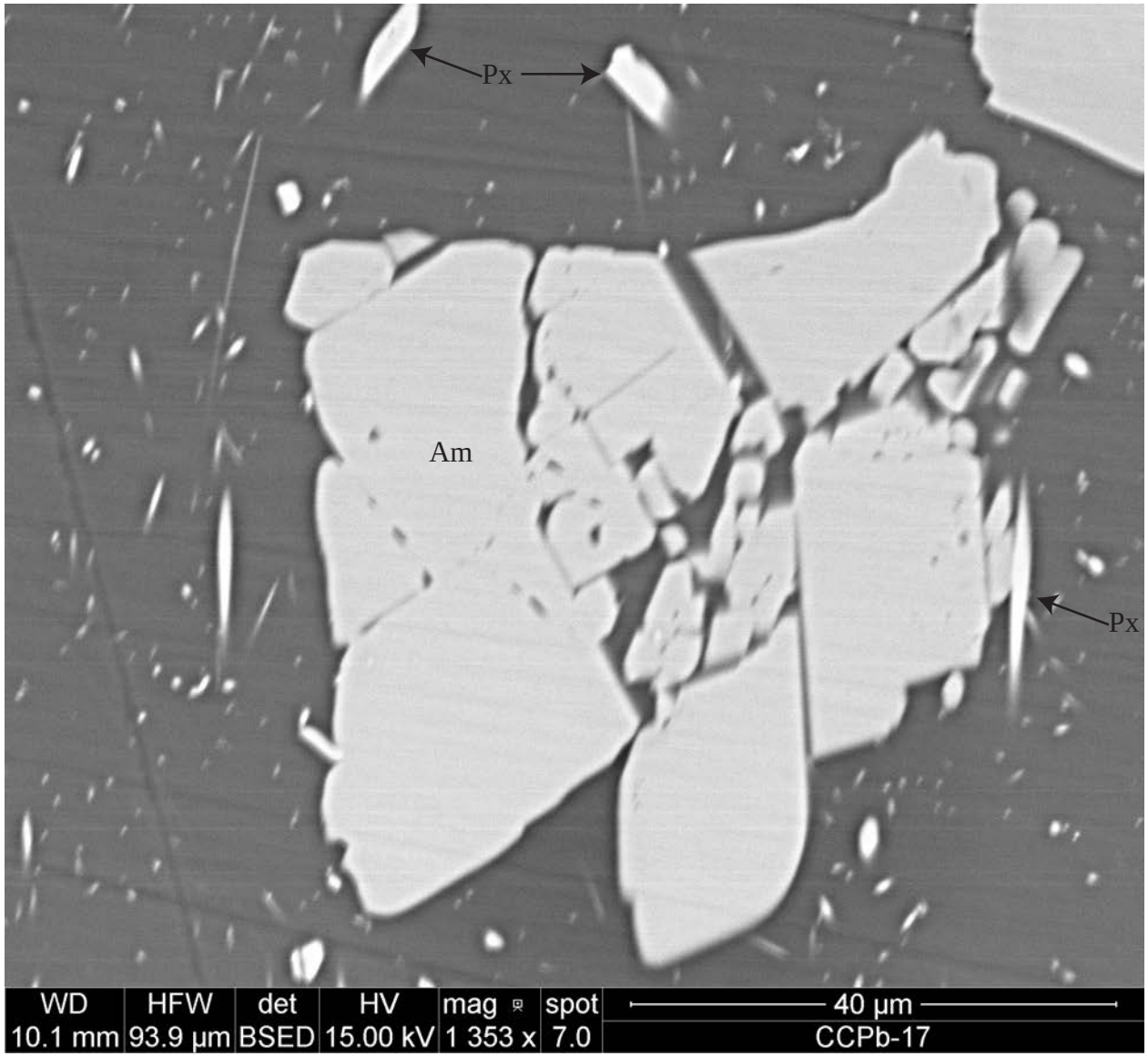


**Figure 17d.**

CCPb-13

Pressure:
100 MPa

Temperature:
750°C

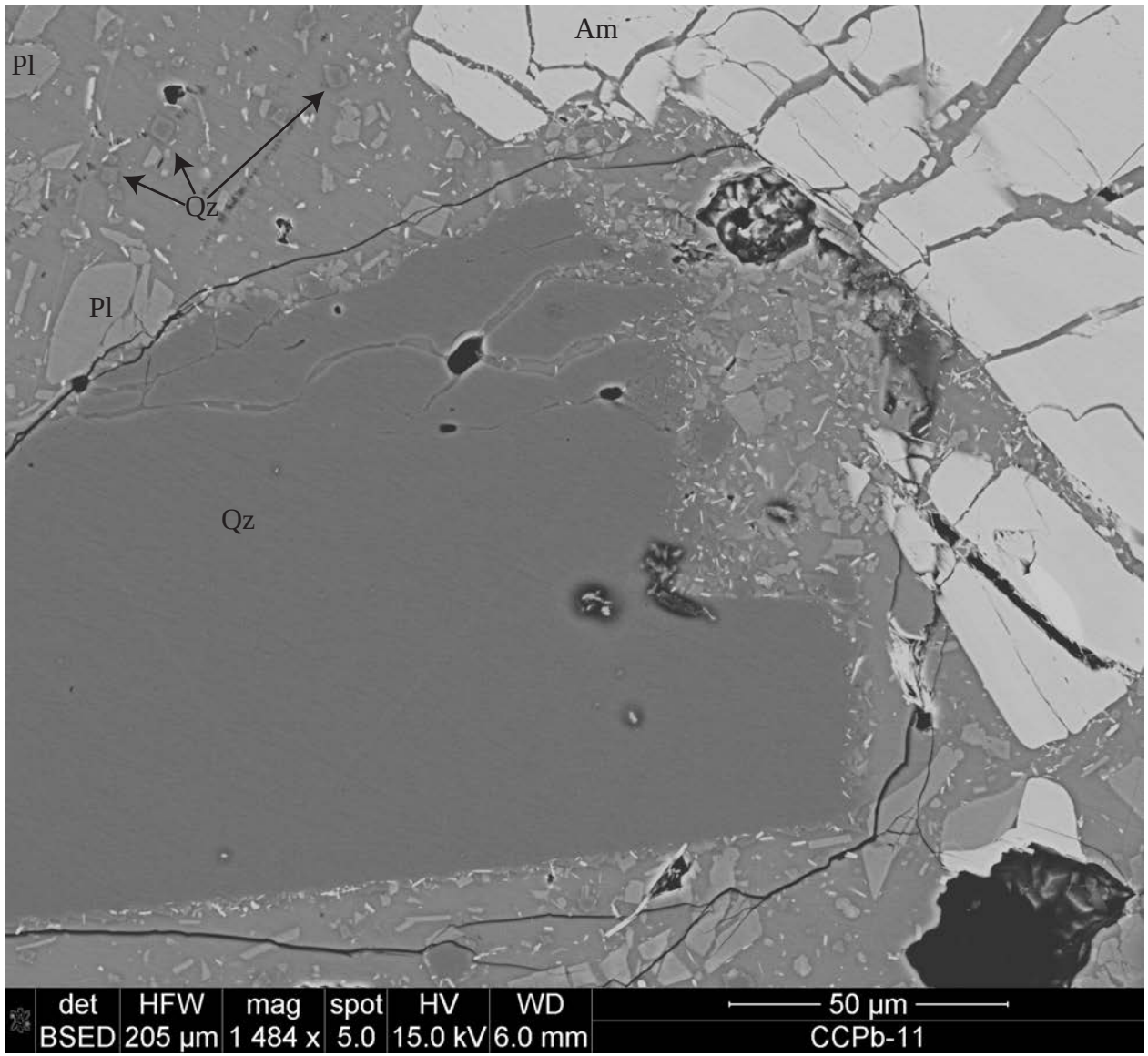


**Figure 17e.**

CCPb-16

Pressure:
75 MPa

Temperature:
900°C

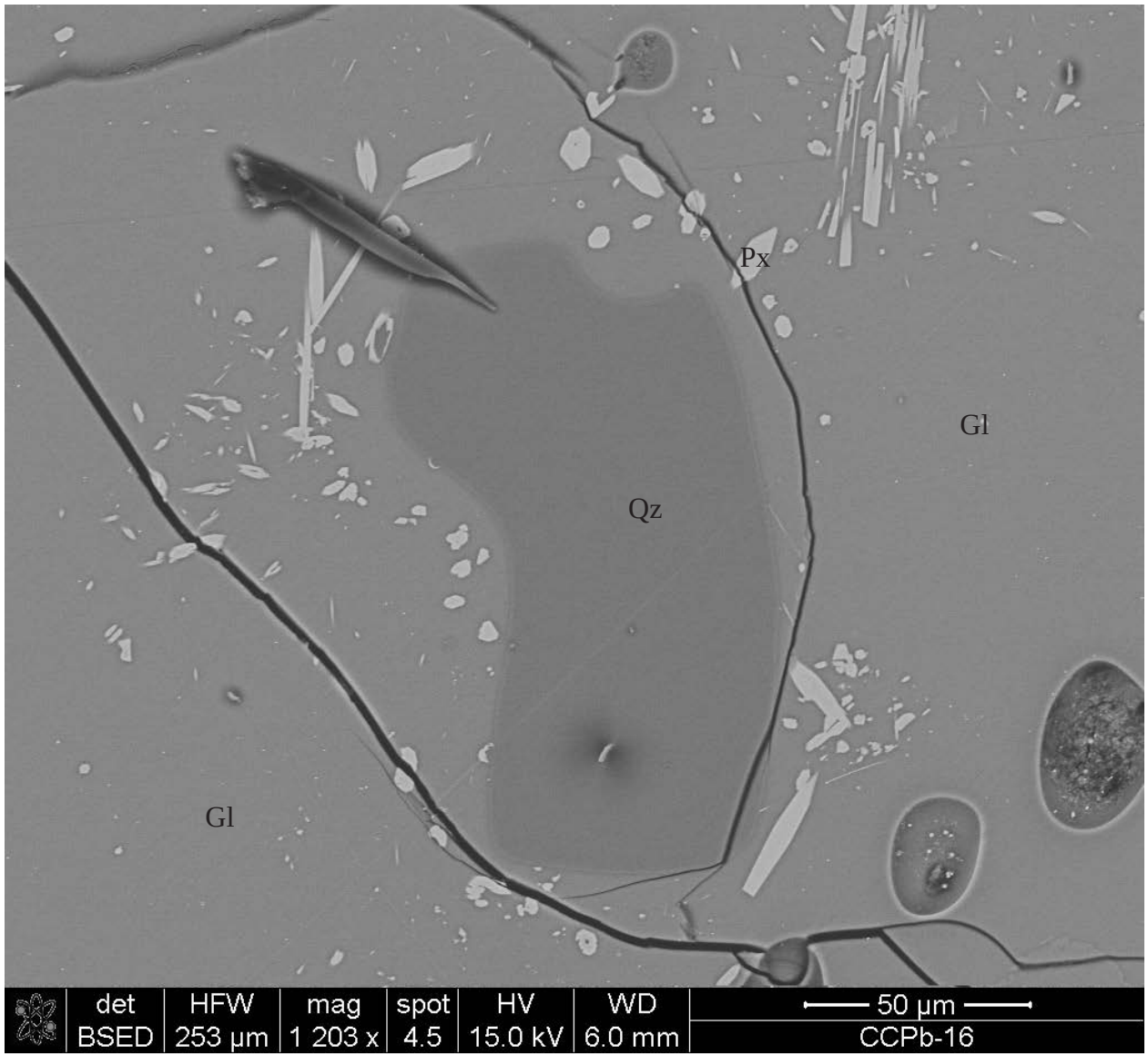


**Figure 17f.**

CCPb-07

Pressure:
150 MPa

Temperature:
875°C

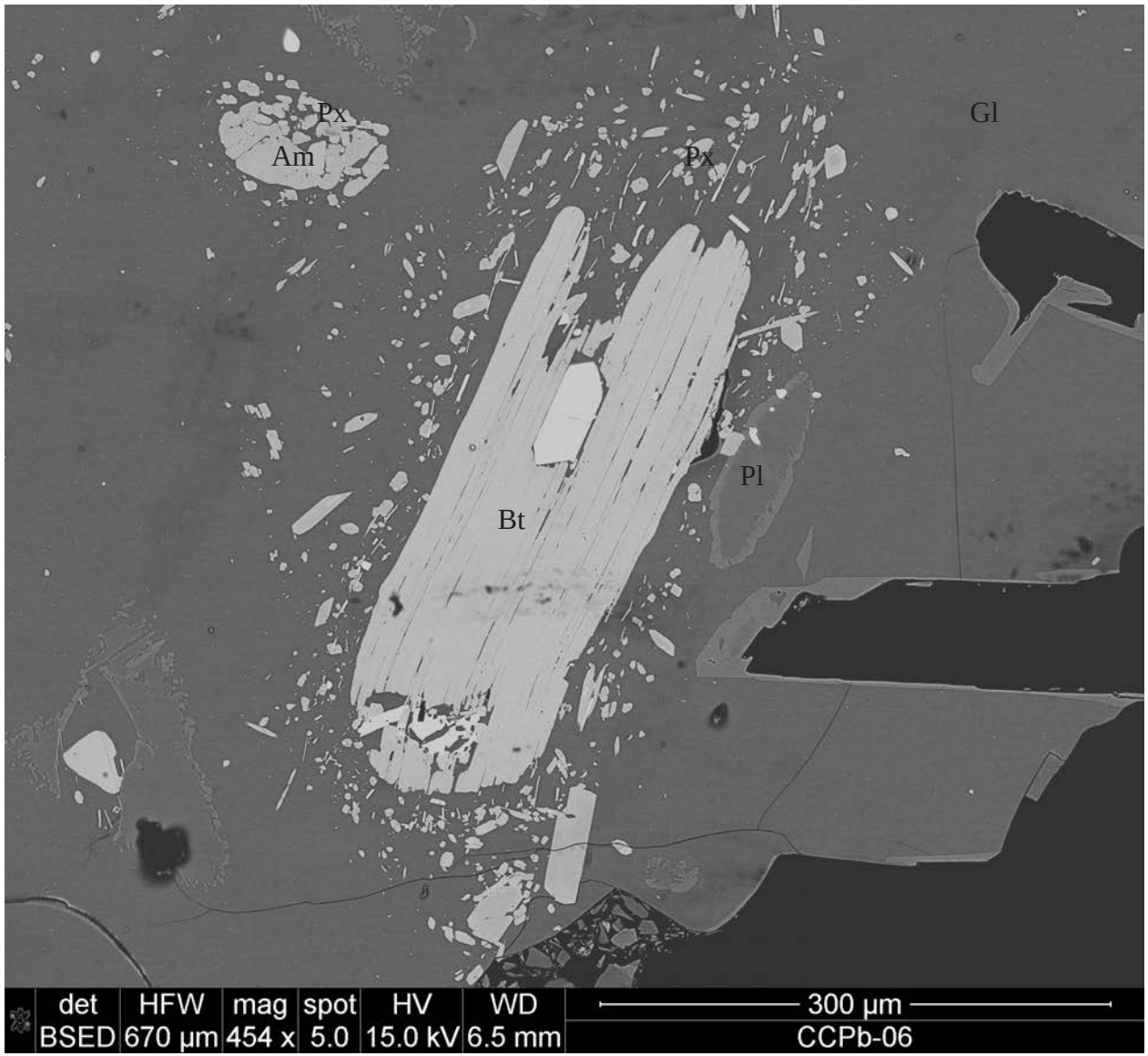


**Figure 17g.**

CCPb-08

Pressure:
100 MPa

Temperature:
900°C

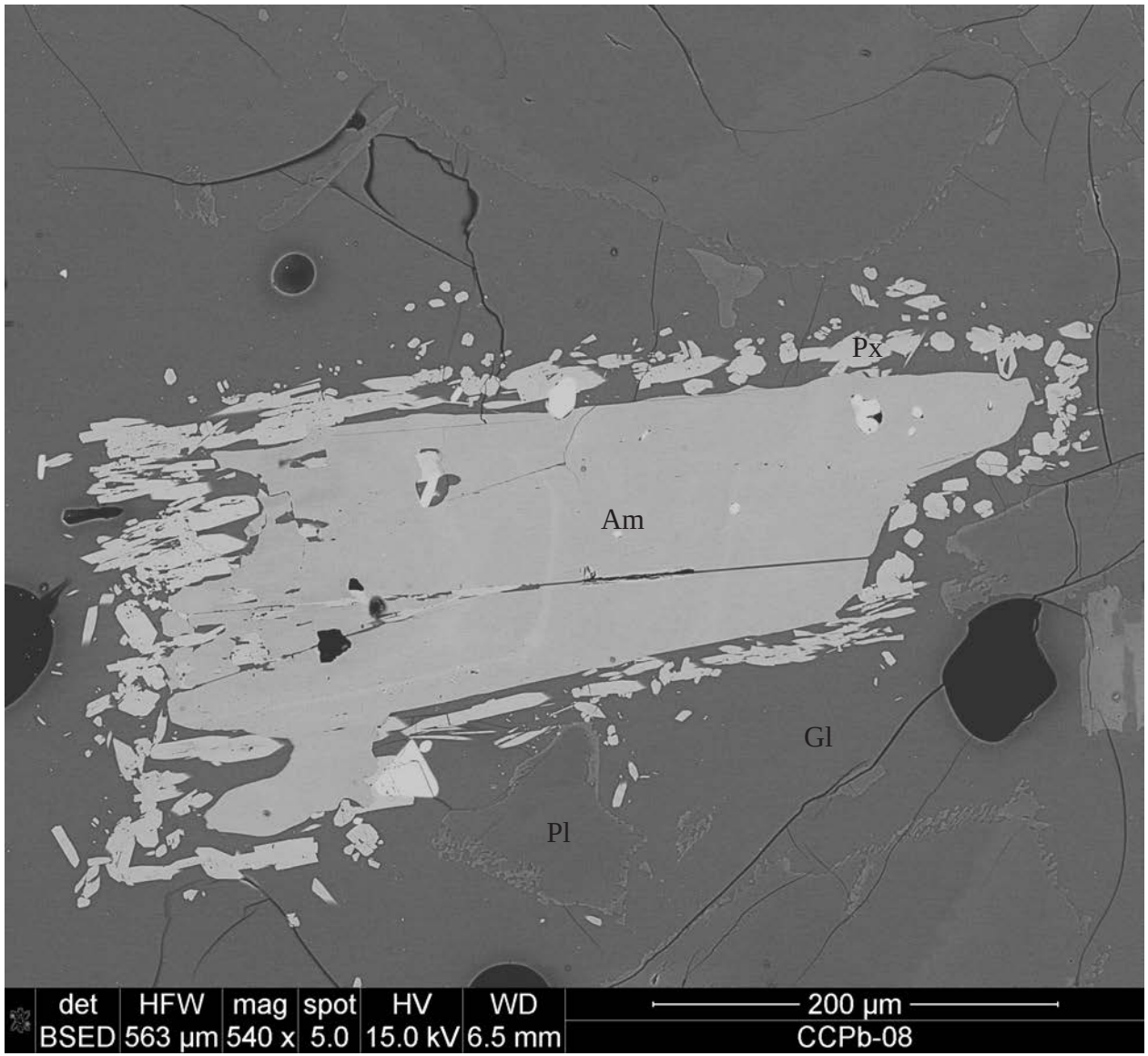


**Figure 17h.**

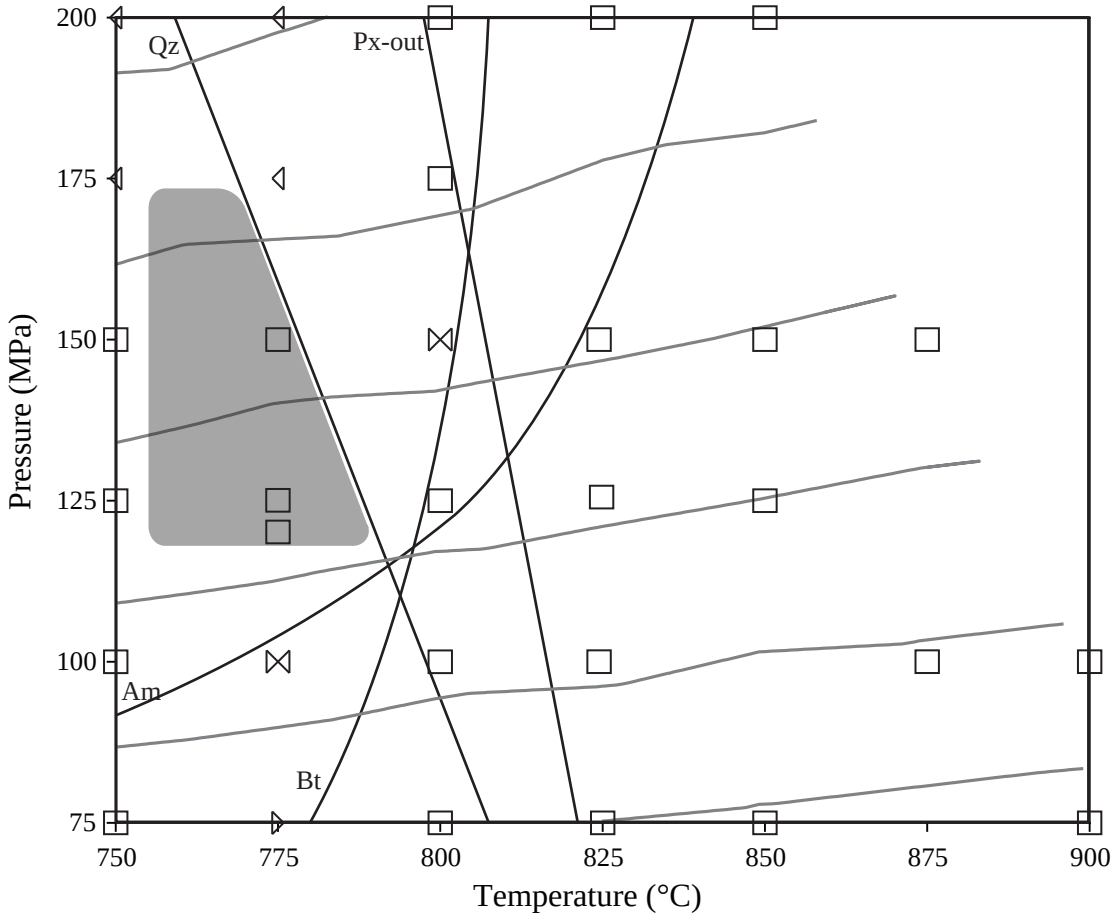
200
175
150
125
100
75
Pressure (MPa)
Qz
Px-out
Am
Bt
750
775
800
825
850
875
900
Temperature (°C)

**Figure 18.**

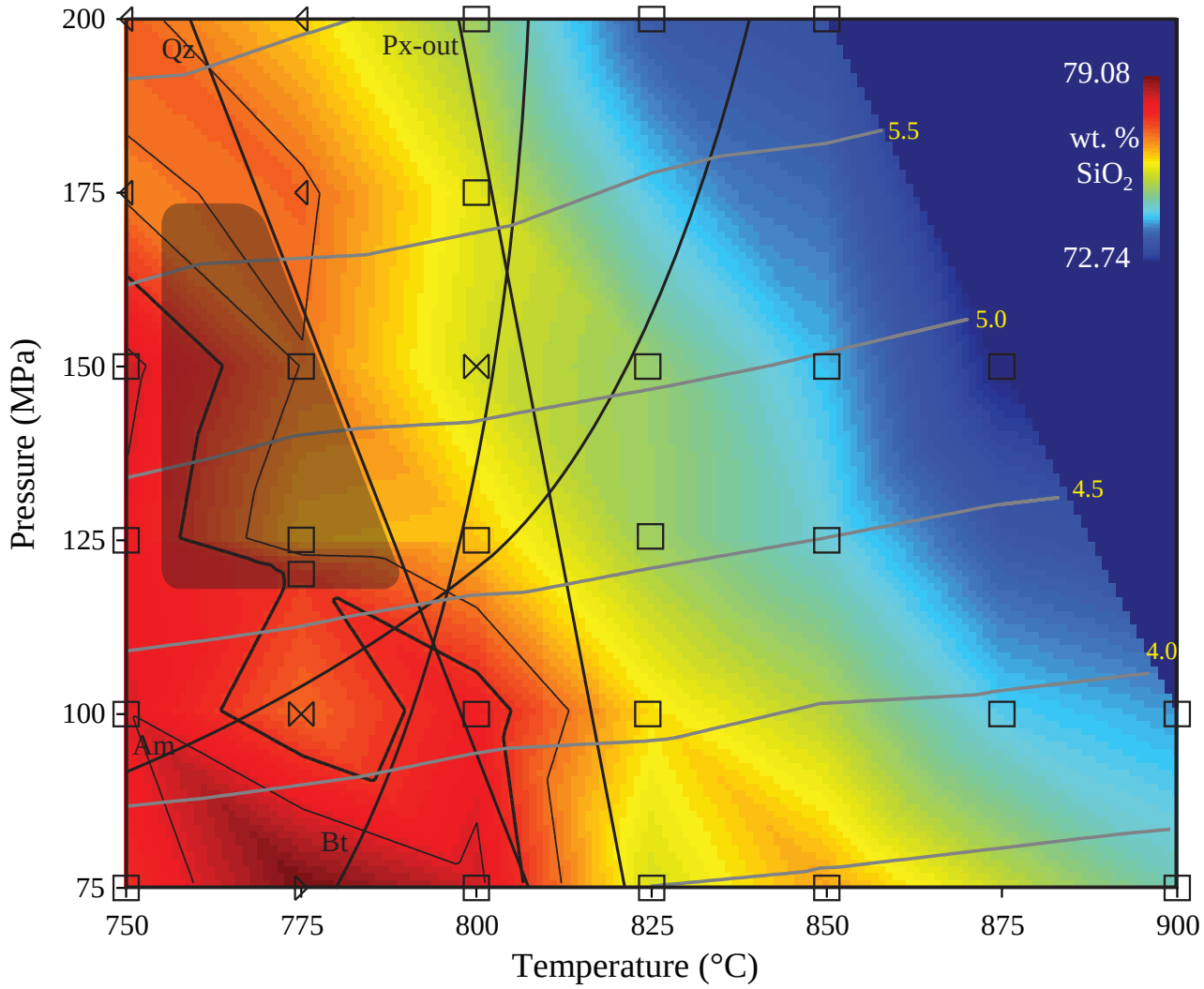


**Figure 19a.** $SiO_2$

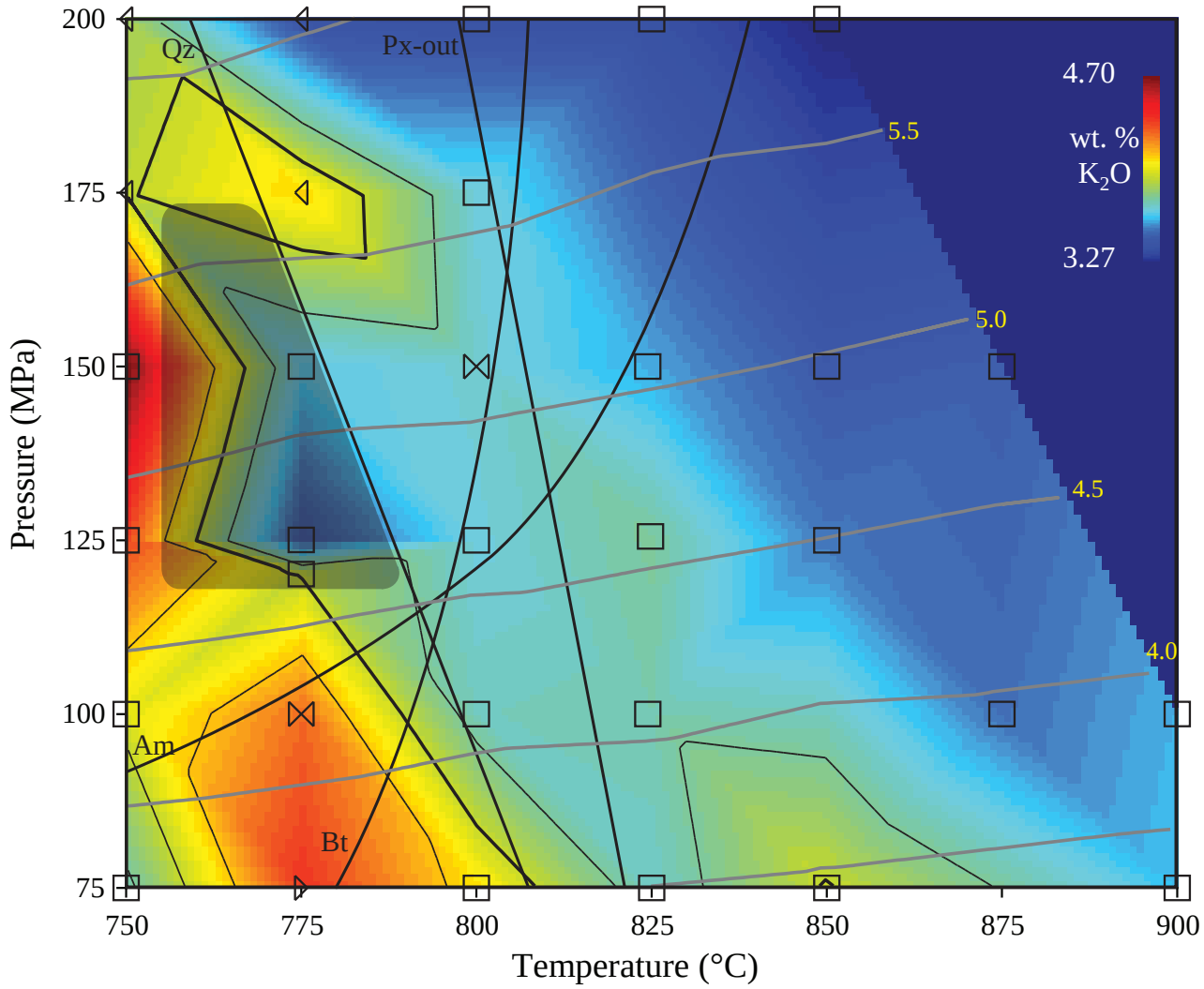


**Figure 19b.** $K_2O$

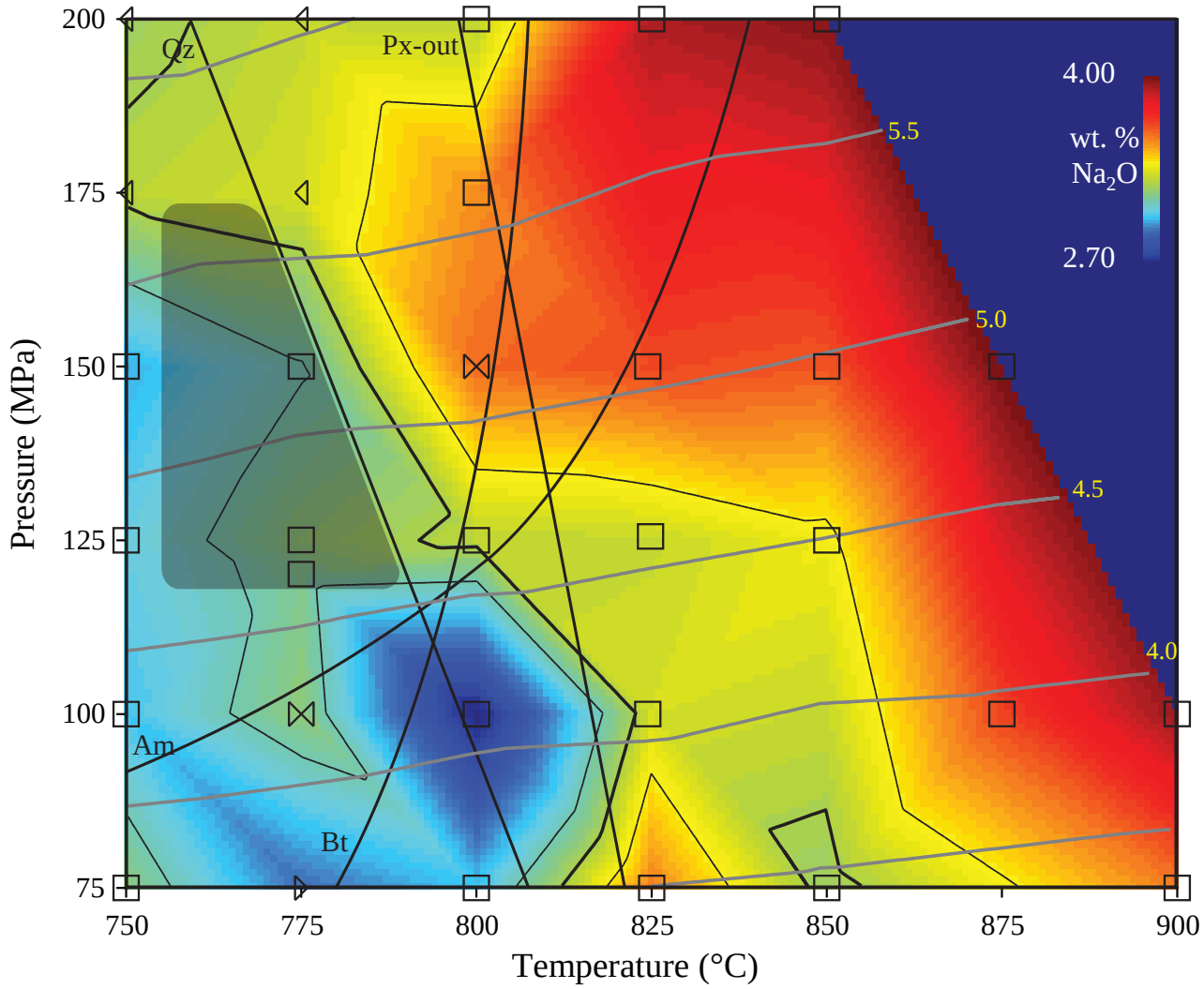


**Figure 19c.** $Na_2O$

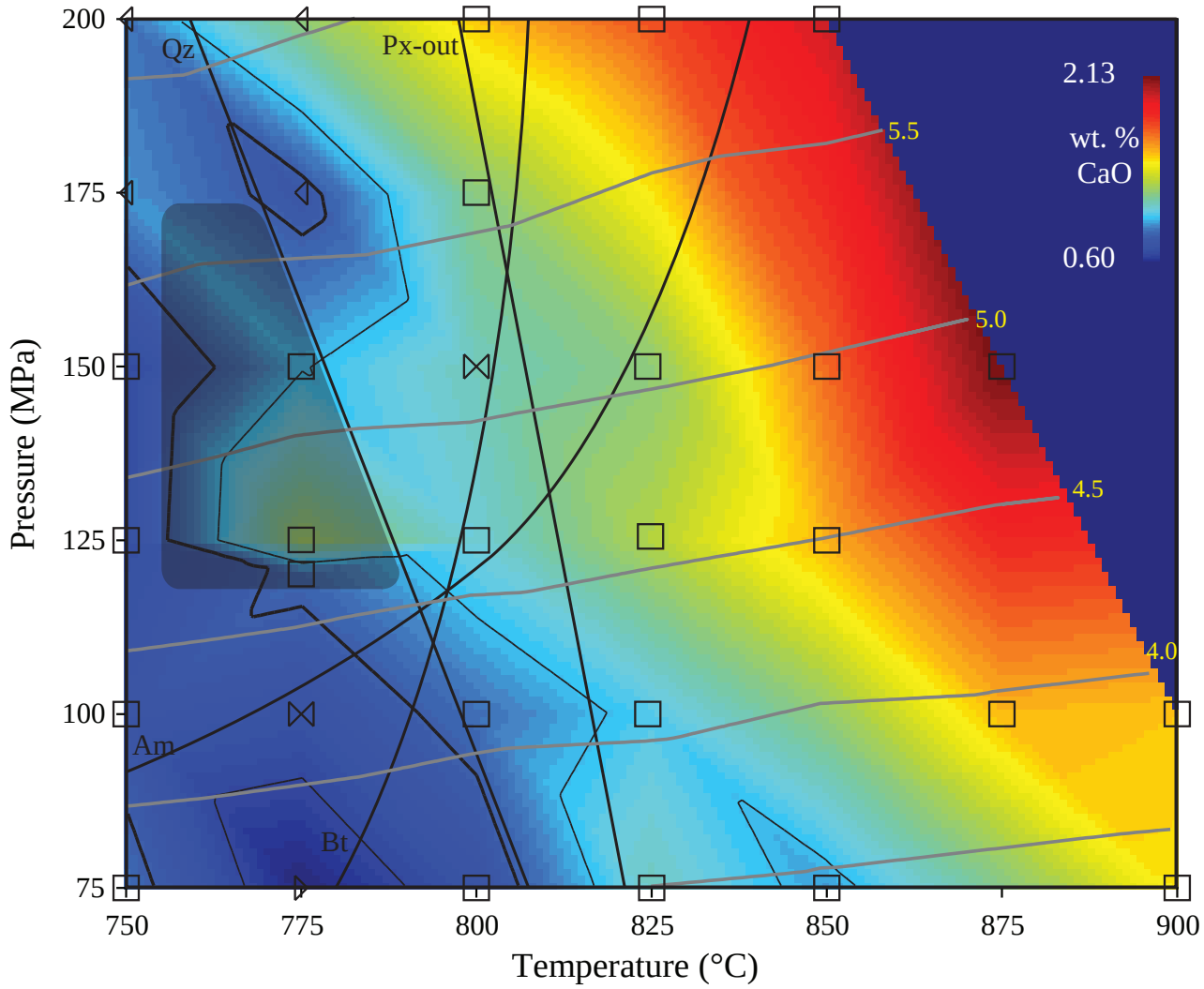


**Figure 19d.** CaO

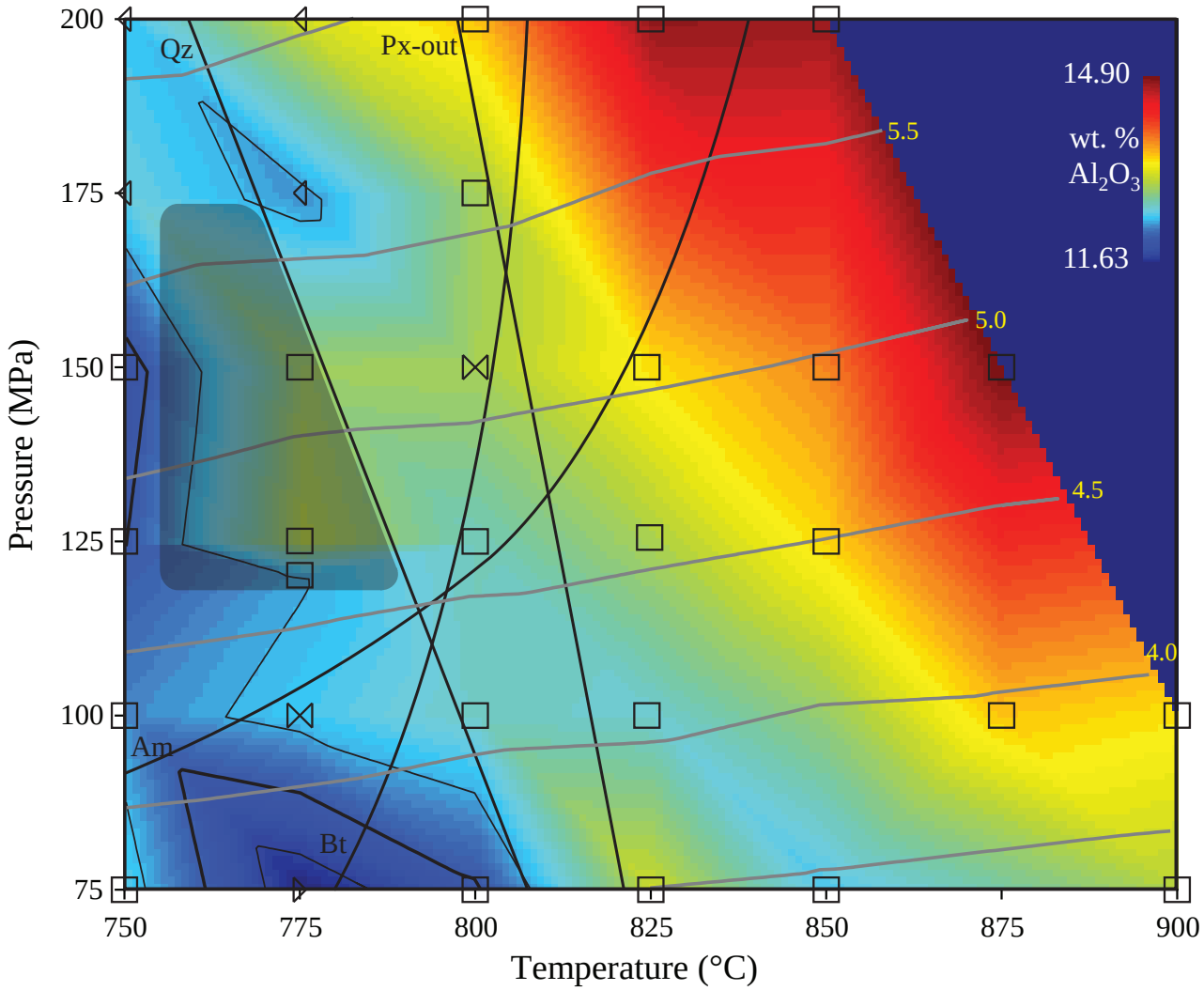


**Figure 19e.** $Al_2O_3$

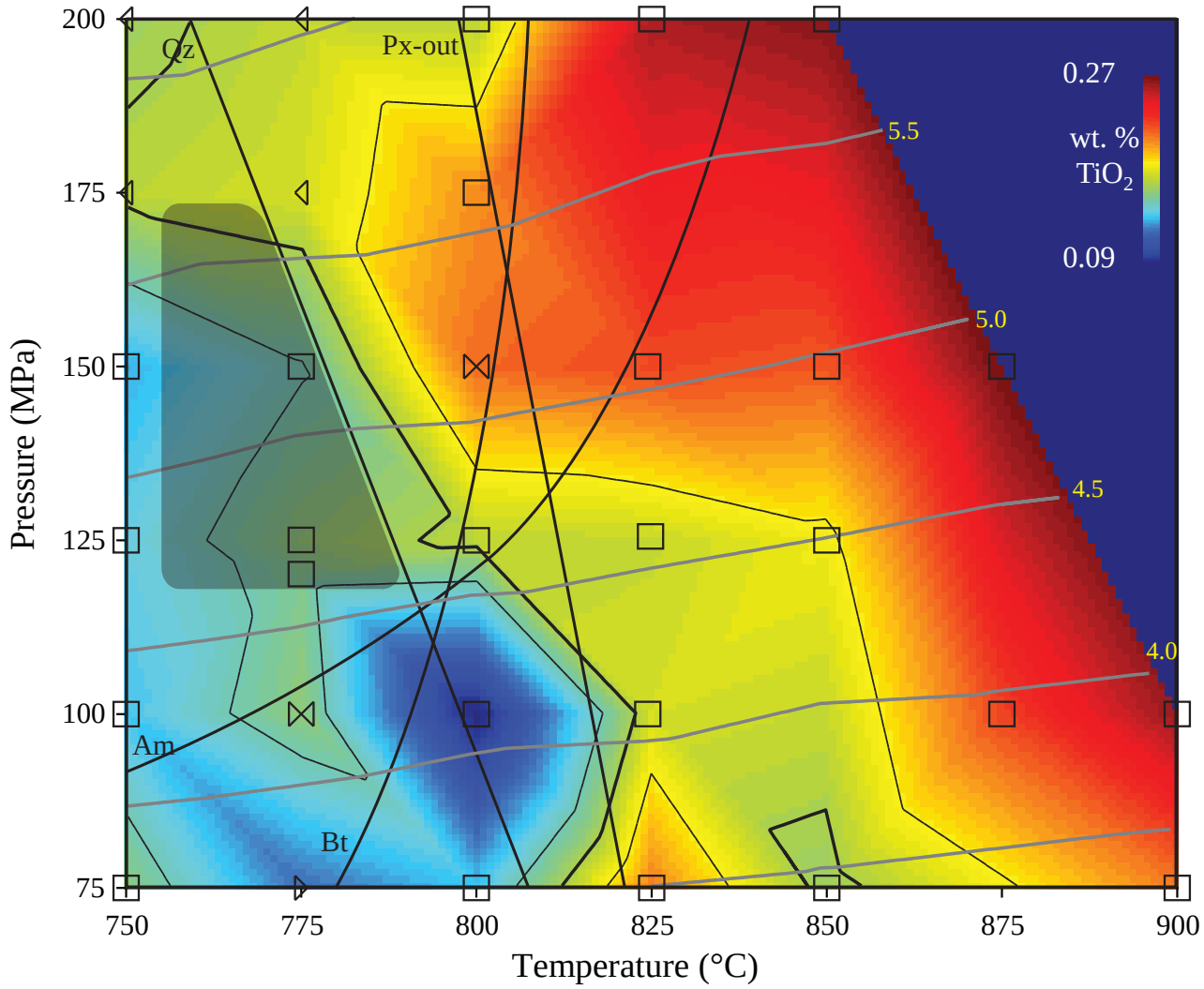


**Figure 19f.** $TiO_2$

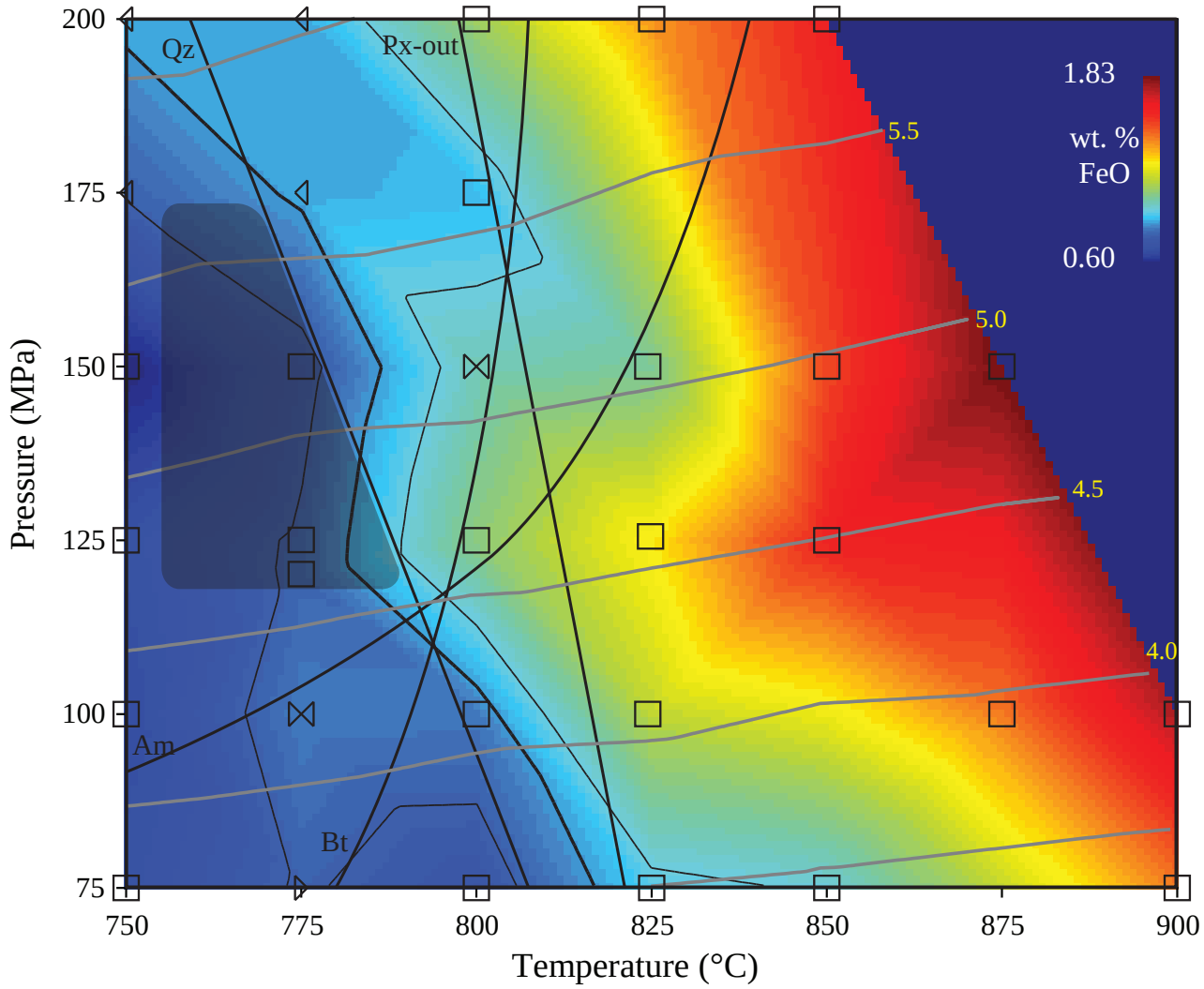


**Figure 19g.** FeO

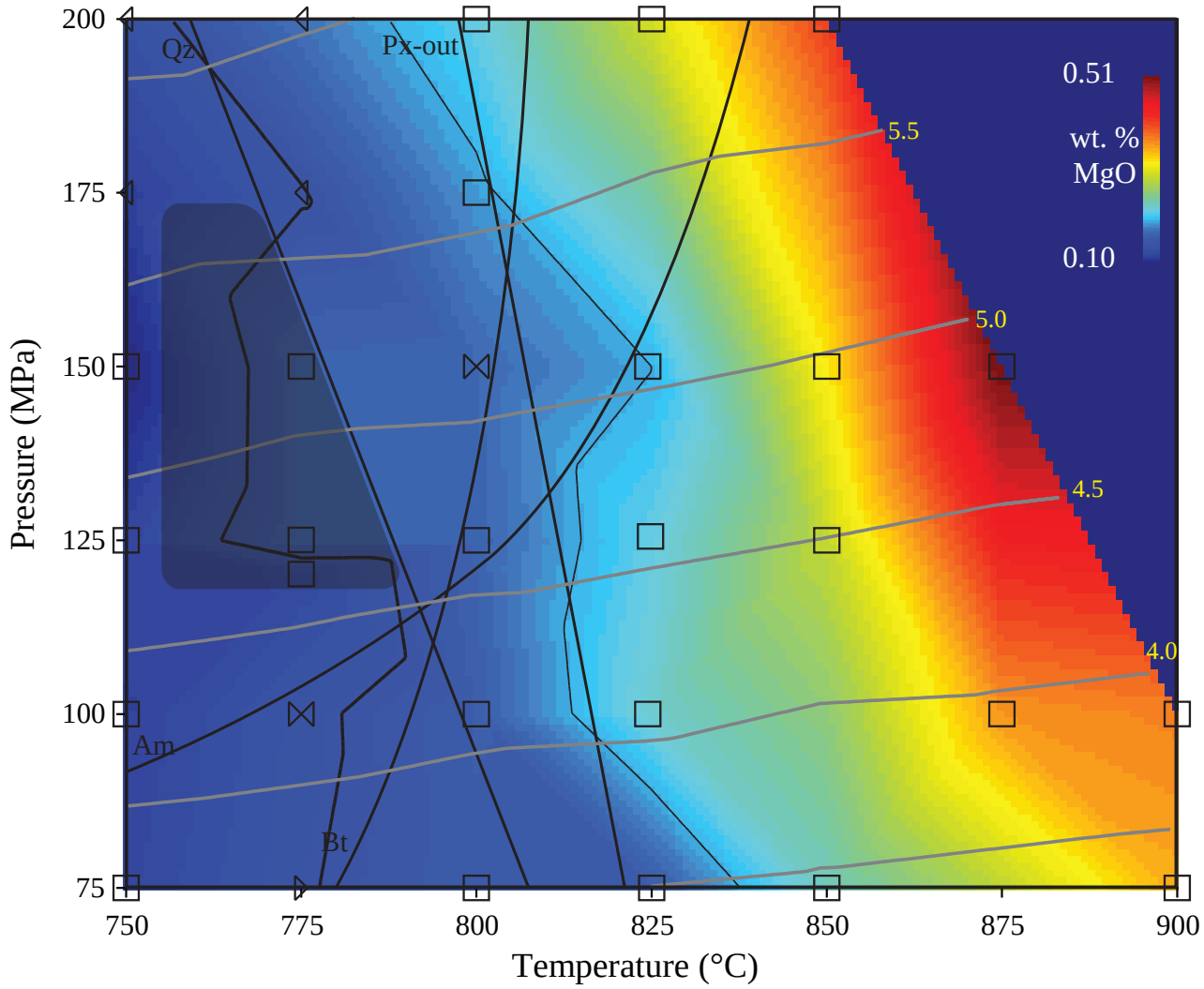


**Figure 19h.** MgO

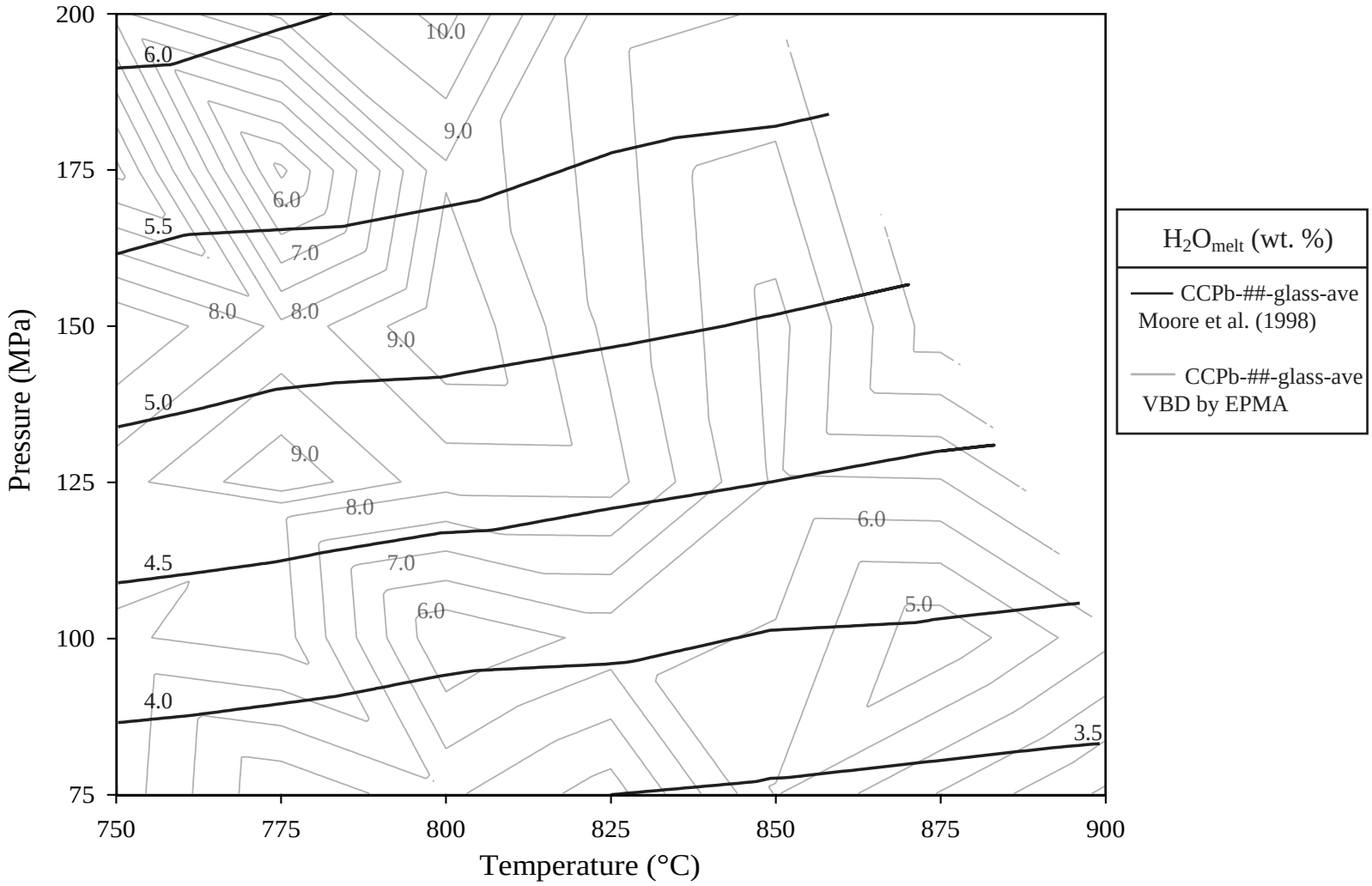
200
175
150
125
100
75
Pressure (MPa)
750
775
800
825
850
875
900
Temperature (°C)
10.0
9.0
6.0
5.5
7.0
8.0
8.0
9.0
5.0
9.0
8.0
6.0
4.5
7.0
6.0
5.0
4.0
3.5
H2Omelt (wt. %)
CCPb-##-glass-ave Moore et al. (1998)
CCPb-##-glass-ave VBD by EPMA

**Figure 20.**

CCPb-40

Rate:
8.5 MPa/hr

Run duration:
5.3 hrs

Final Pressure:
74.6 MPa

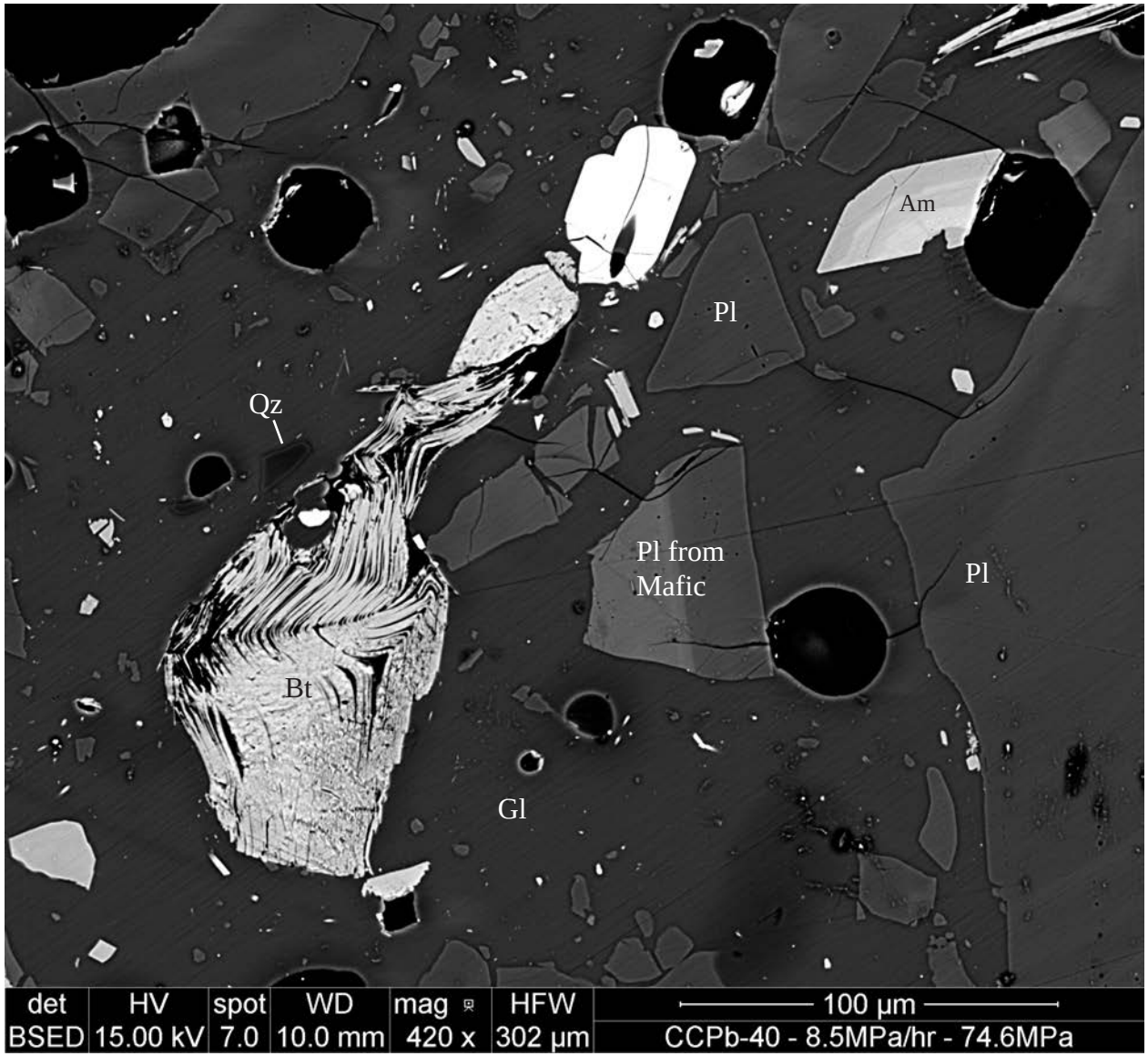


**Figure 21a.**

CCPb-41

Rate:
8.5 MPa/hr

Run duration:
8.0 hrs

Final Pressure:
51.8 MPa

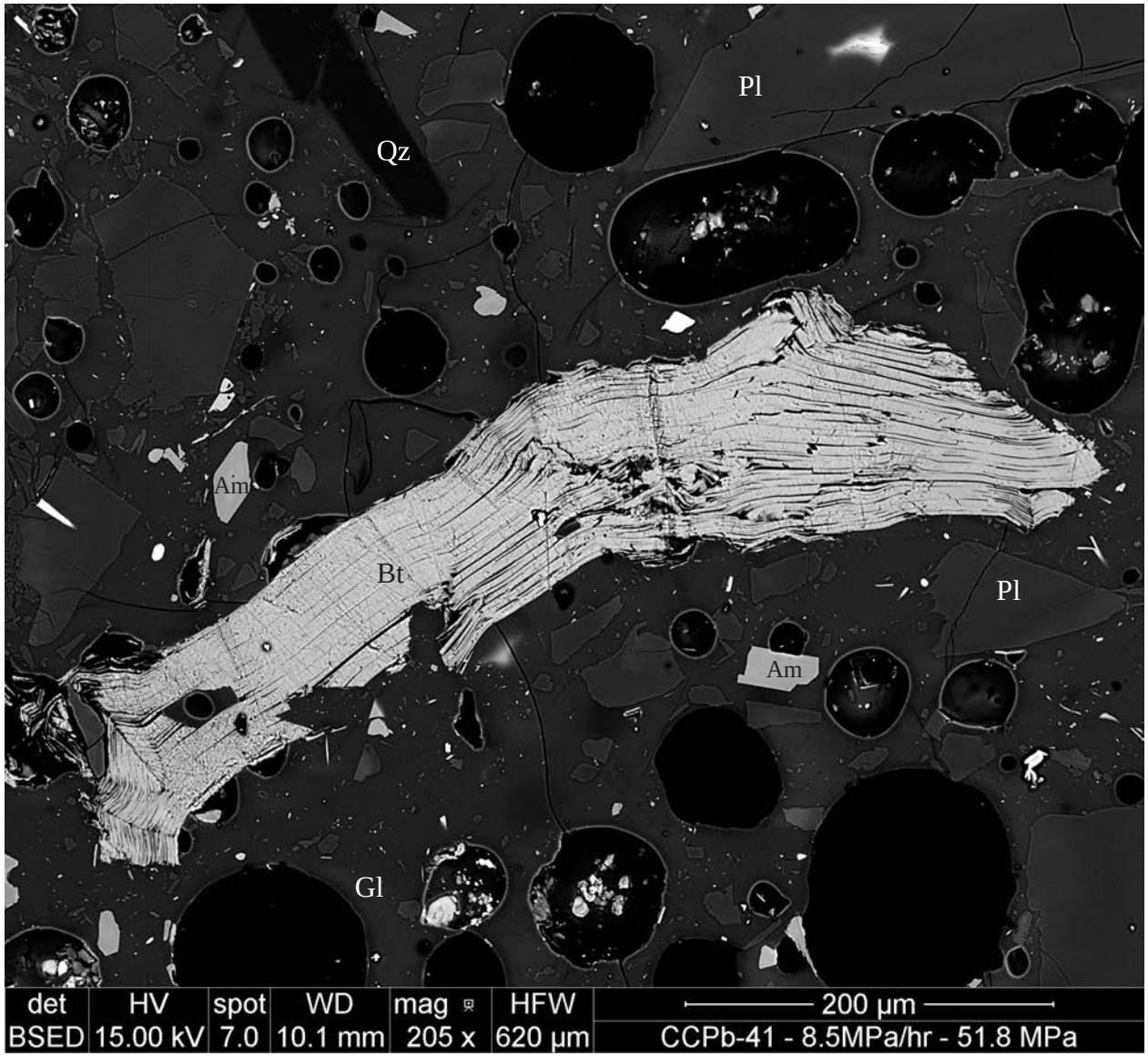


**Figure 21b.**

CCPb-38

Rate:
2.6 MPa/hr

Run duration:
16.0 hrs

Final Pressure:
78.3 MPa

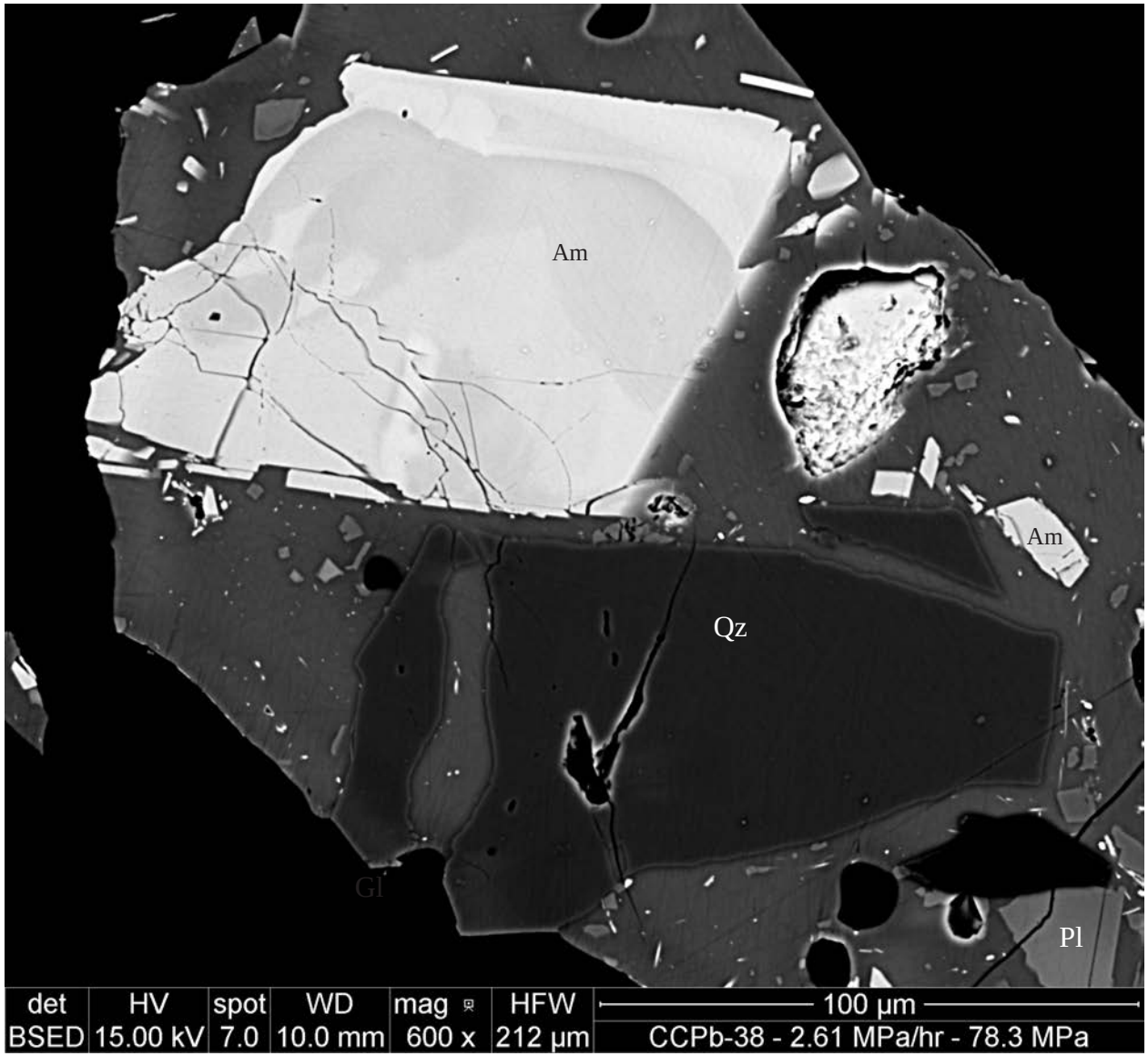


**Figure 21c.**

CCPb-39

Rate:
2.6 MPa/hr

Run duration:
24.0 hrs

Final Pressure:
57.6 MPa

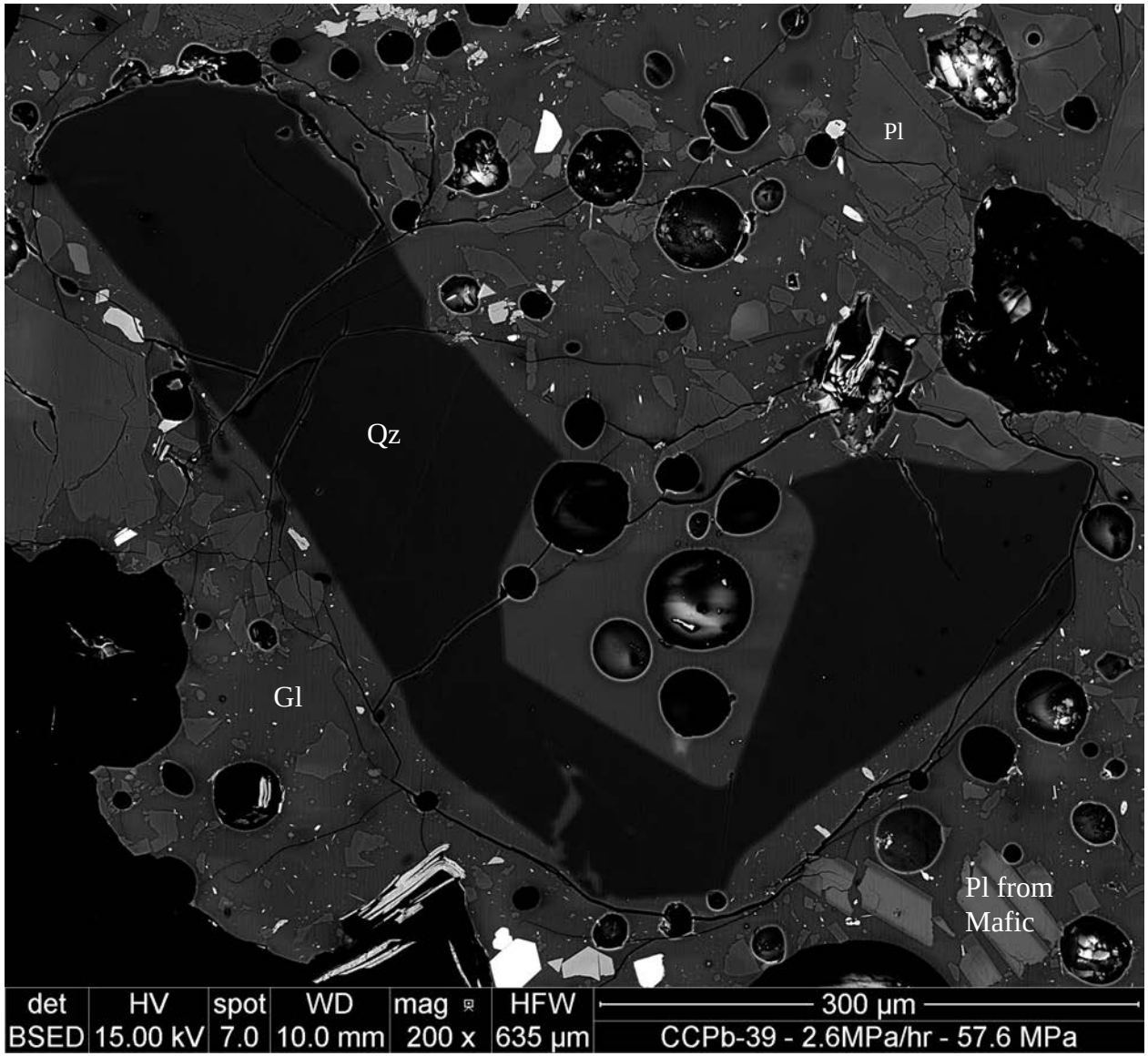


**Figure 21d.**

CCPb-35

Rate:
1.0 MPa/hr

Run duration:
24.0 hrs

Final Pressure:
96.3 MPa

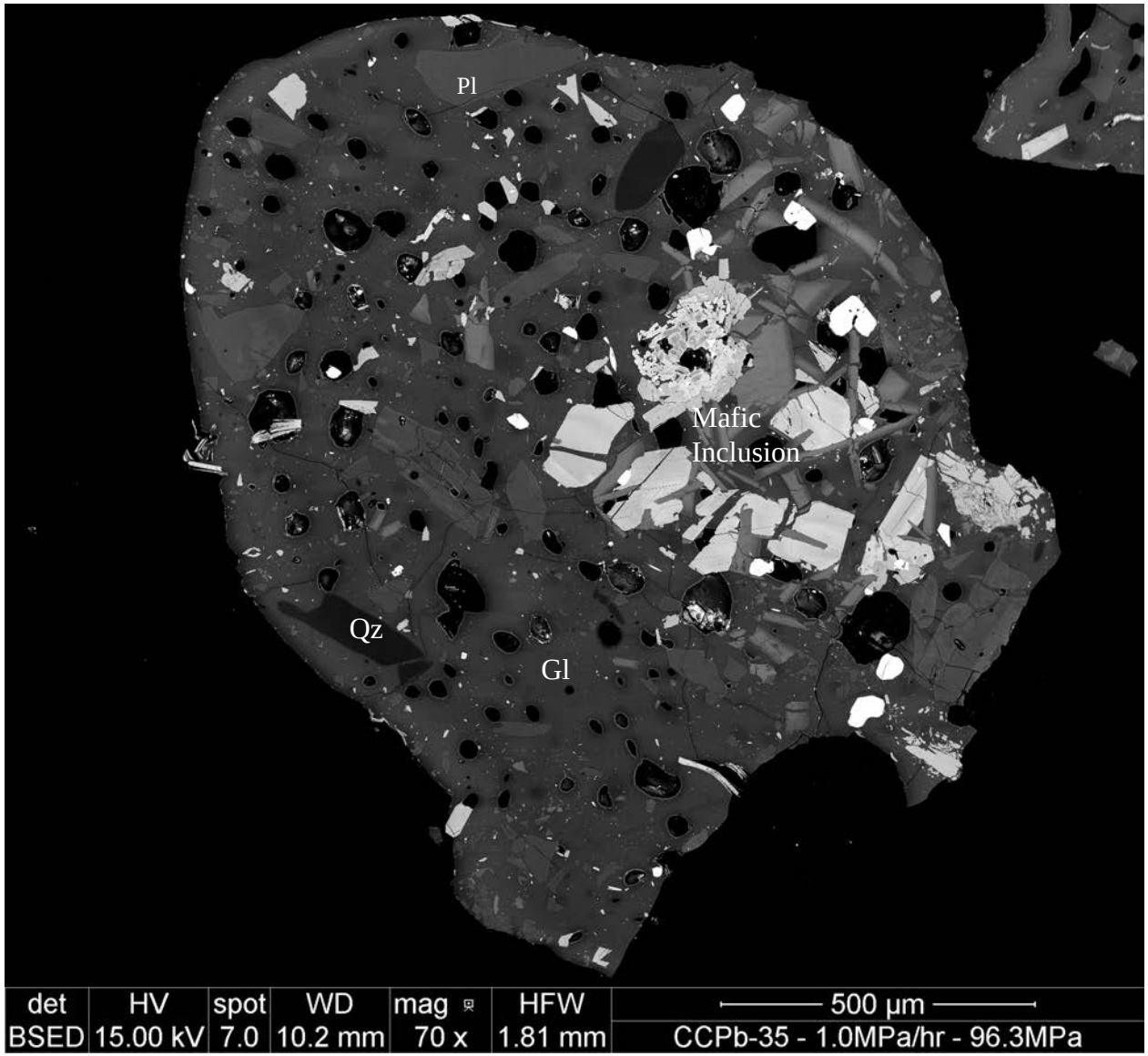


**Figure 21e.**

CCPb-36

Rate:
1.0 MPa/hr

Run duration:
48.0 hrs

Final Pressure:
72.5 MPa

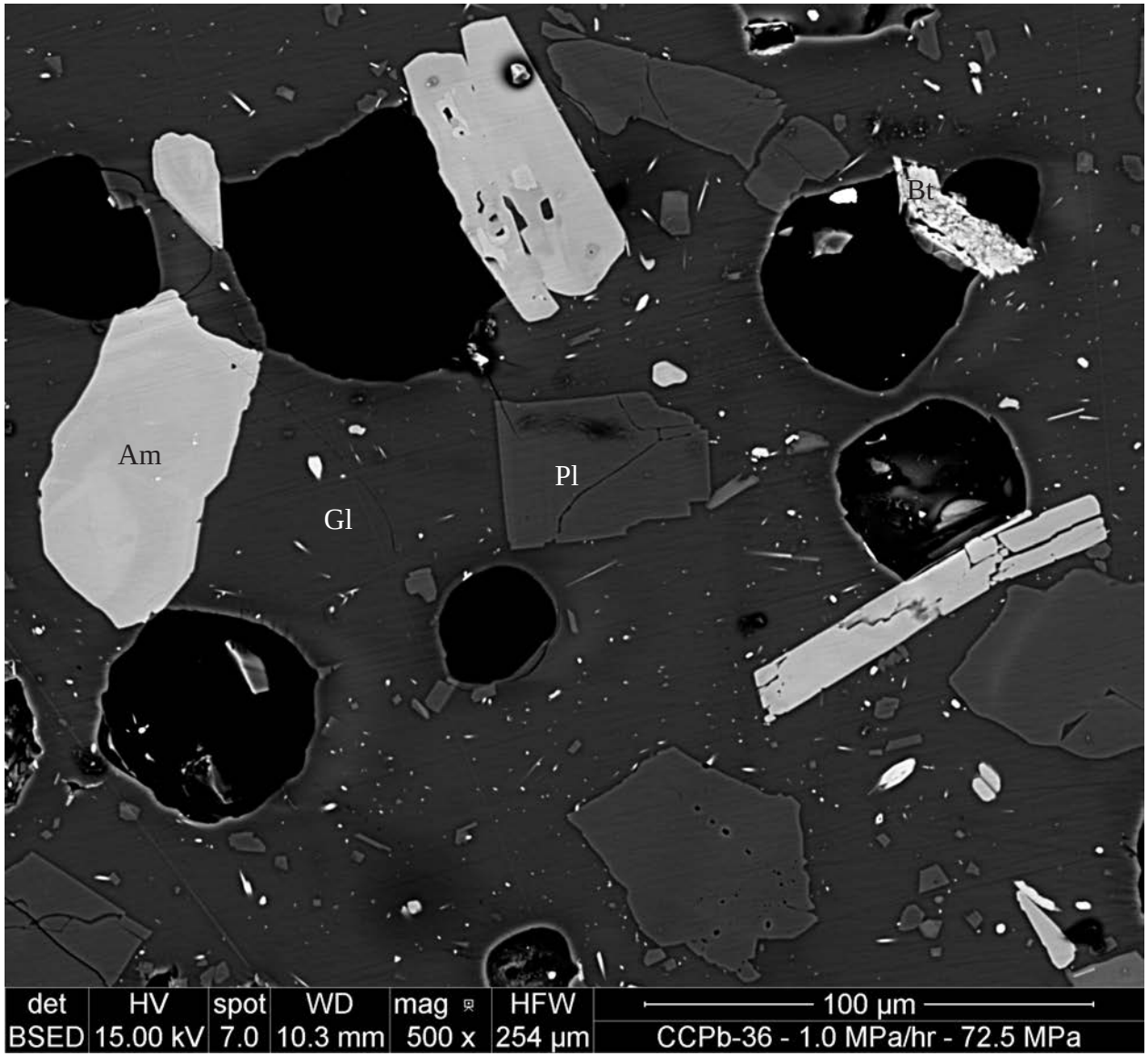


**Figure 21f.**

CCPb-37

Rate:
1.0 MPa/hr

Run duration:
72.0 hrs

Final Pressure:
50.0 MPa

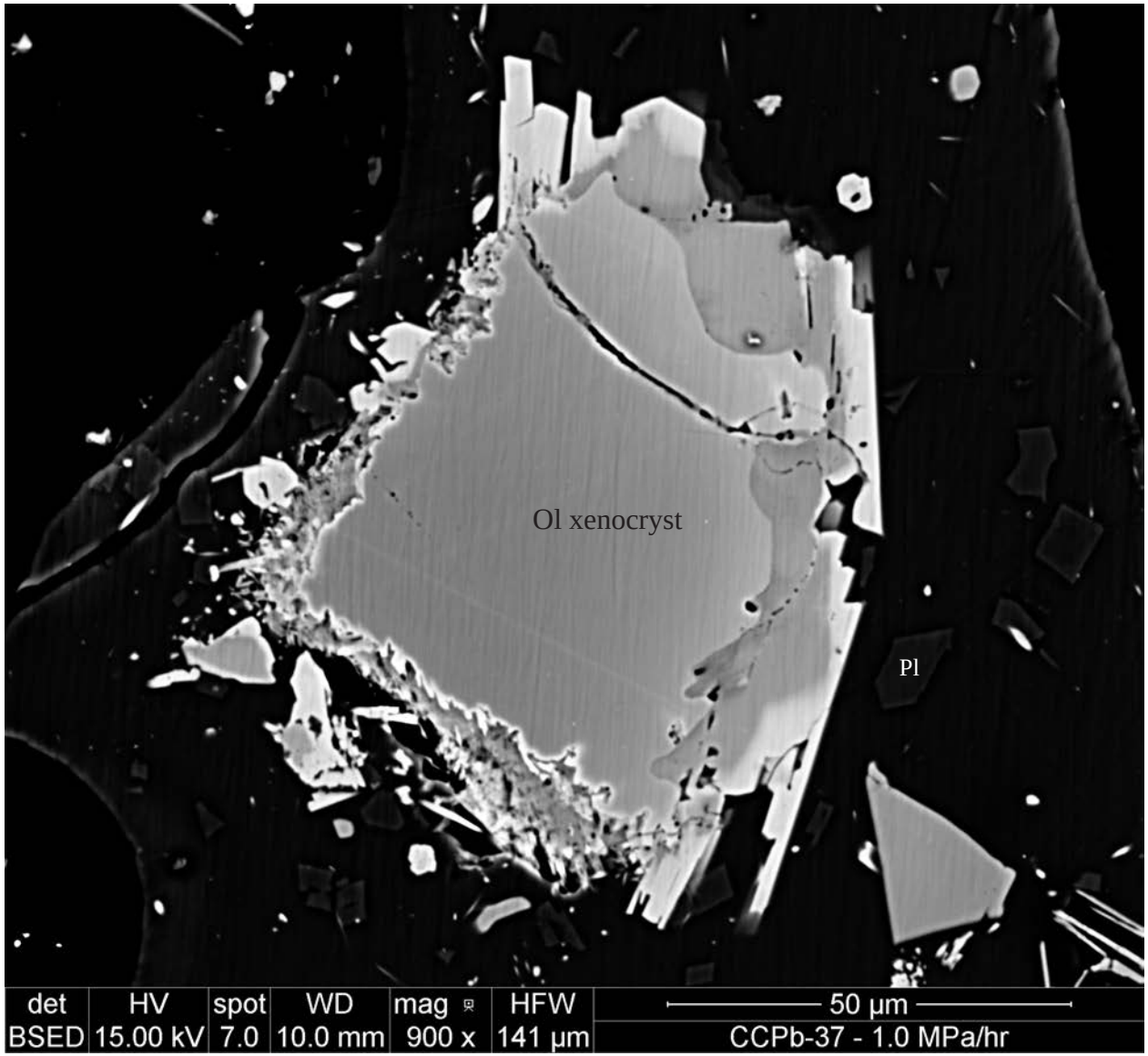


**Figure 21g.**

CCPb-37

Rate:
1.0 MPa/hr

Run duration:
72.0 hrs

Final Pressure:
50.0 MPa

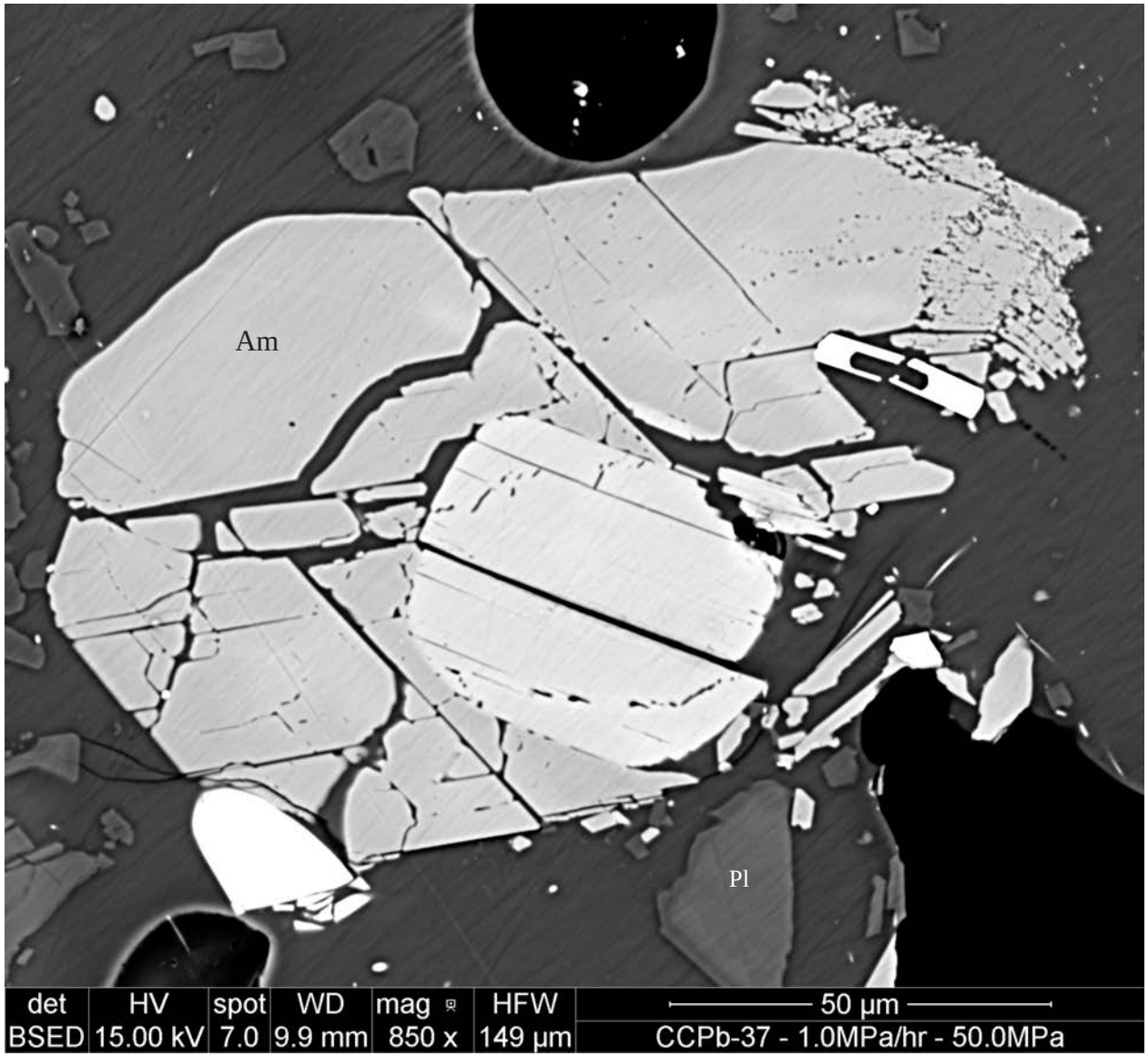


**Figure 21h.**

CCPb-42

Rate:
0.35 MPa/hr

Run duration:
145.0 hrs

Final Pressure:
69.0 MPa

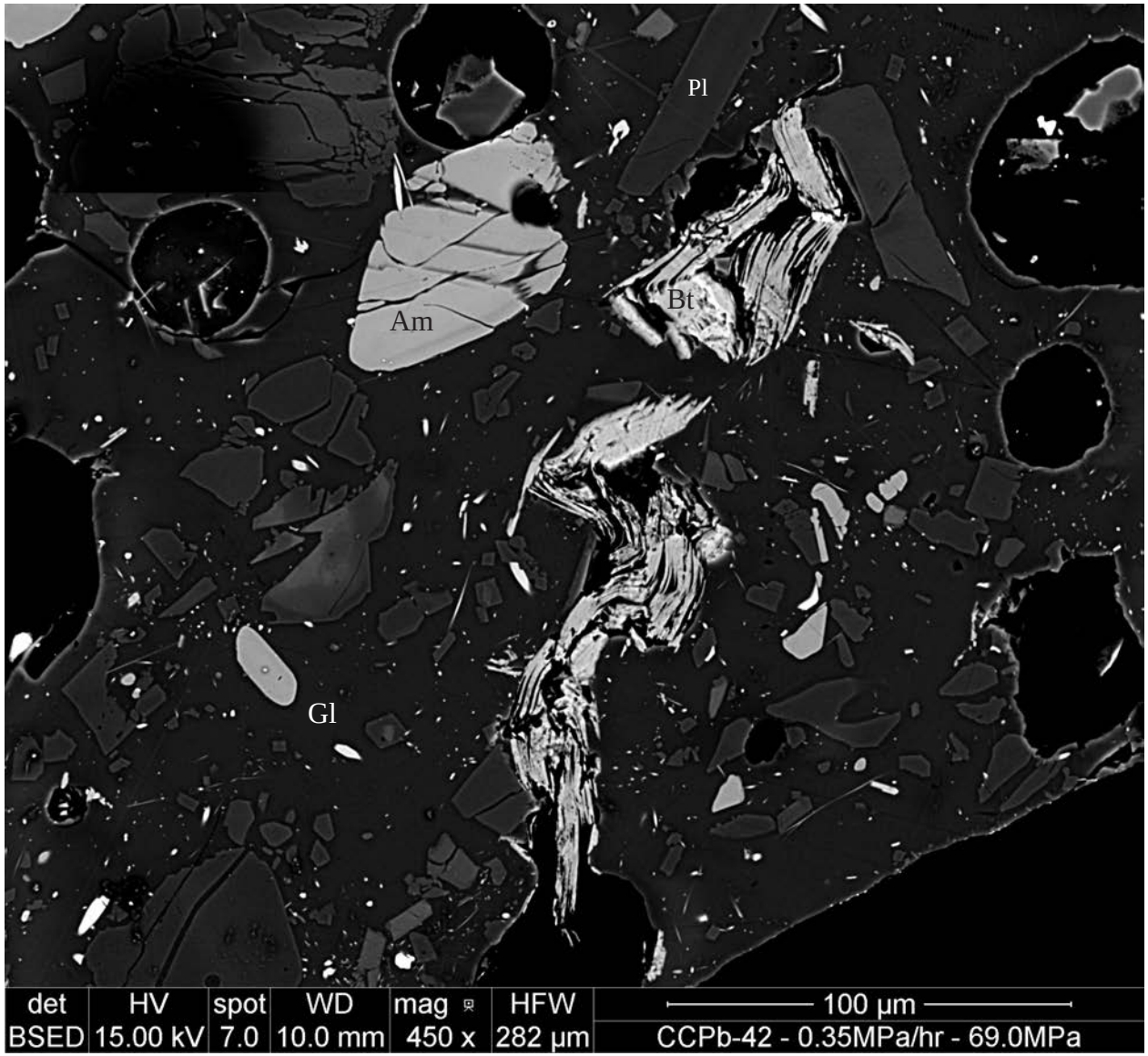


**Figure 21i.**

CCPb-43

Rate:
0.35 MPa/hr

Run duration:
213.8 hrs

Final Pressure:
47.3 MPa

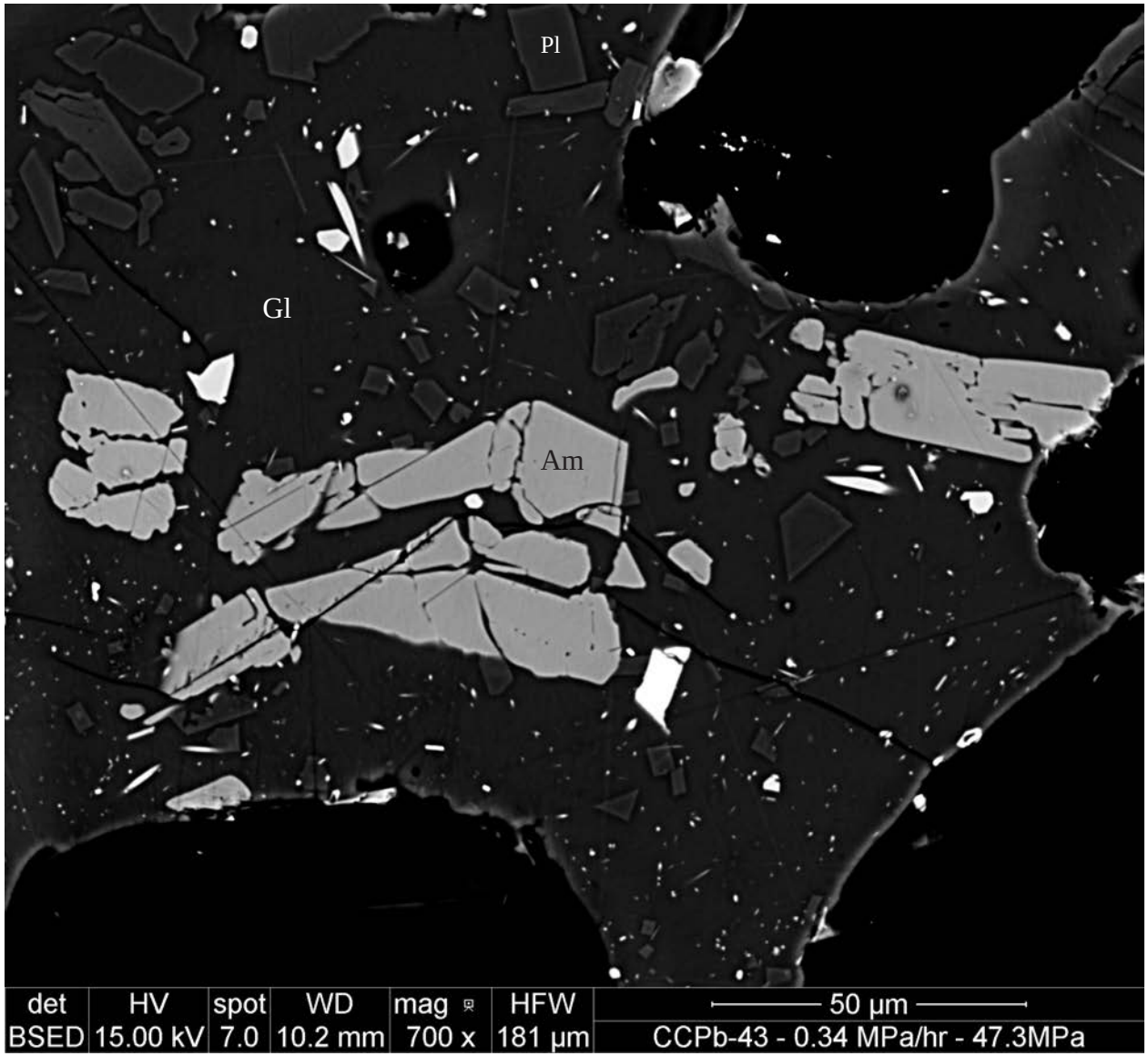


**Figure 21j.**

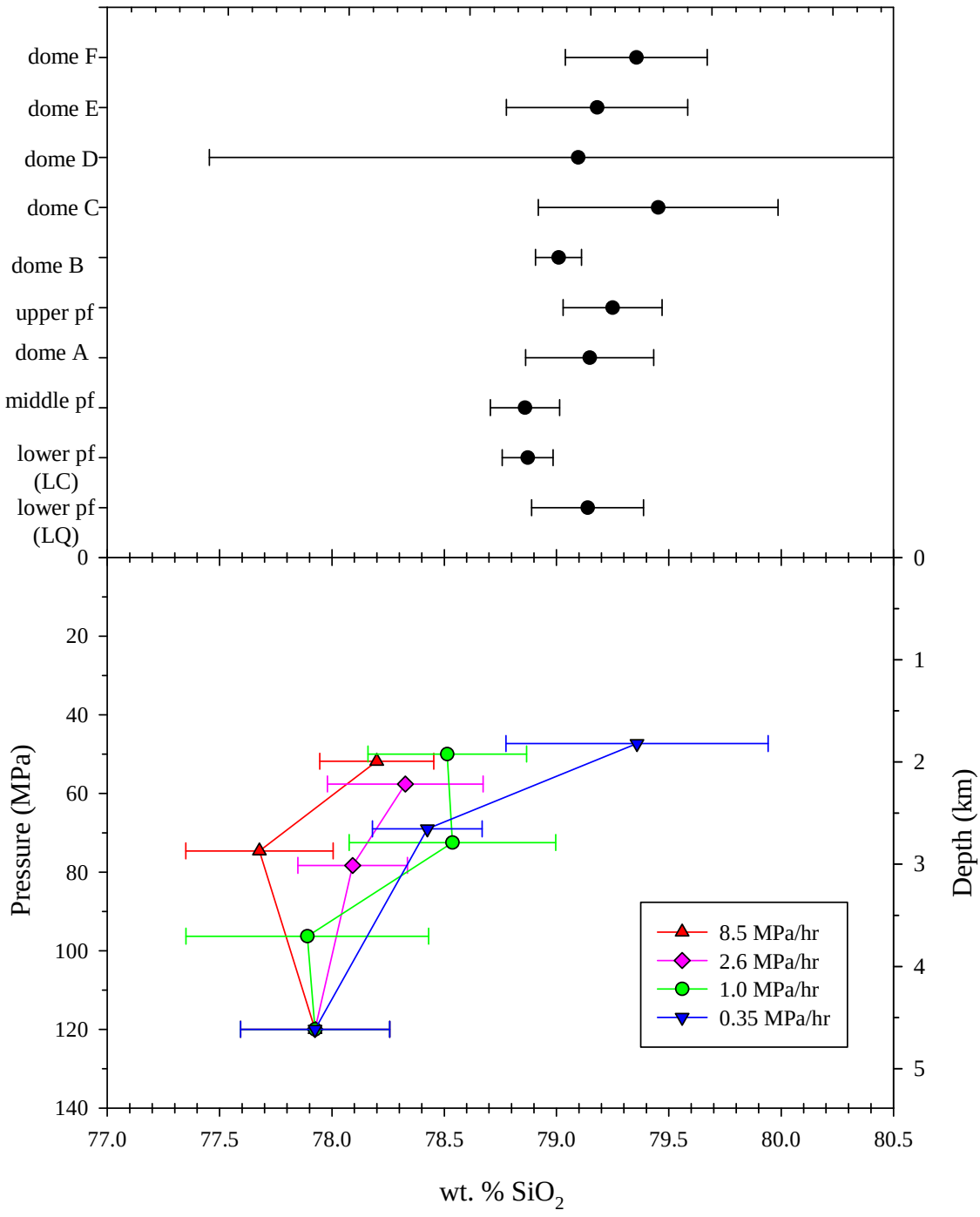
dome F
dome E
dome D
dome C
dome B
upper pf
dome A
middle pf
lower pf (LC)
lower pf (LQ)
0
20
40
60
80
100
120
140
Pressure (MPa)
0
1
2
3
4
5
Depth (km)
77.0
77.5
78.0
78.5
79.0
79.5
80.0
80.5
wt. % SiO2
8.5 MPa/hr
2.6 MPa/hr
1.0 MPa/hr
0.35 MPa/hr

**Figure 22a.**

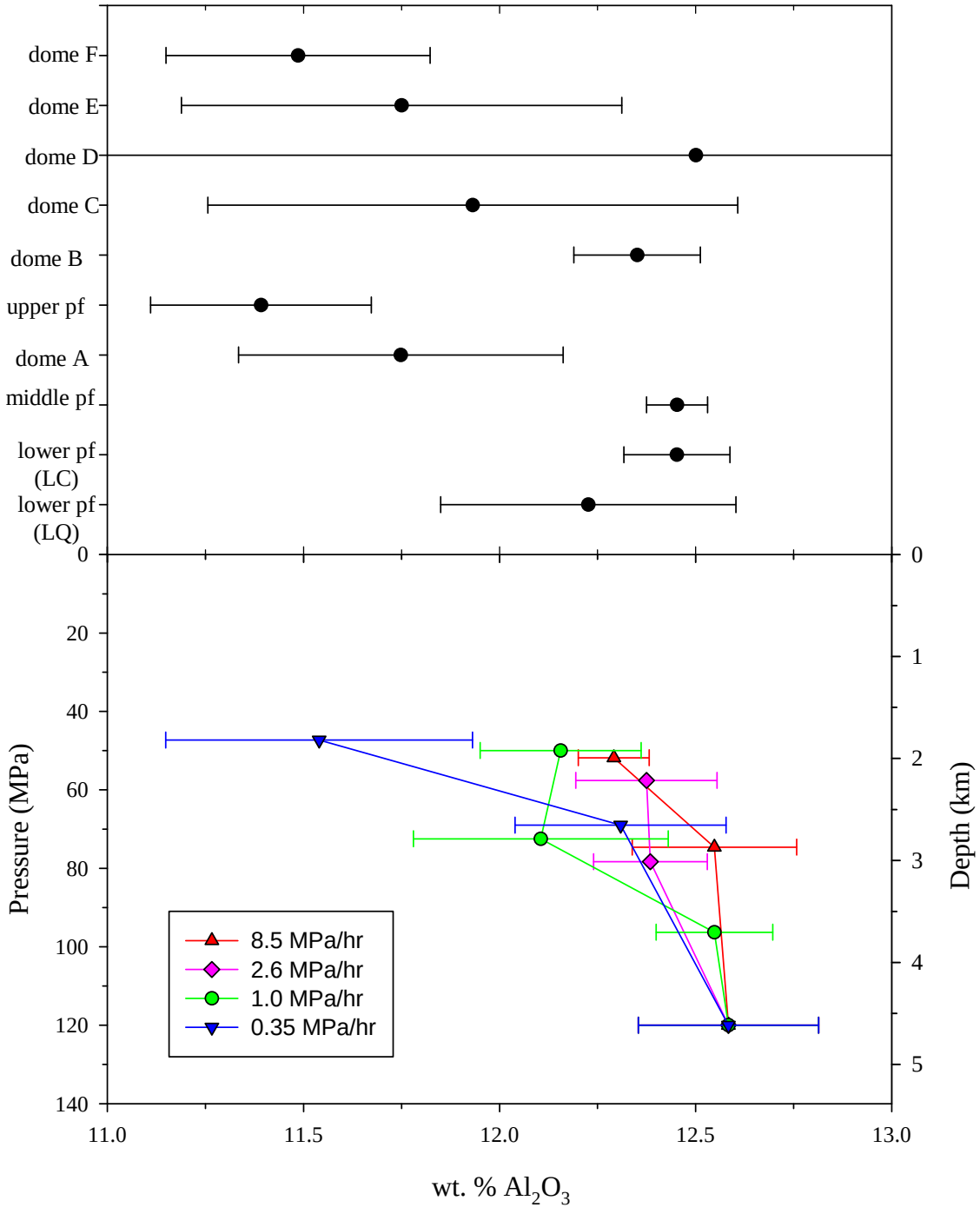
dome F
dome E
dome D
dome C
dome B
upper pf
dome A
middle pf
lower pf (LC)
lower pf (LQ)
0
20
40
60
80
100
120
140
Pressure (MPa)
0
1
2
3
4
5
Depth (km)
11.0
11.5
12.0
12.5
13.0
wt. % Al2O3
8.5 MPa/hr
2.6 MPa/hr
1.0 MPa/hr
0.35 MPa/hr

**Figure 22b.**

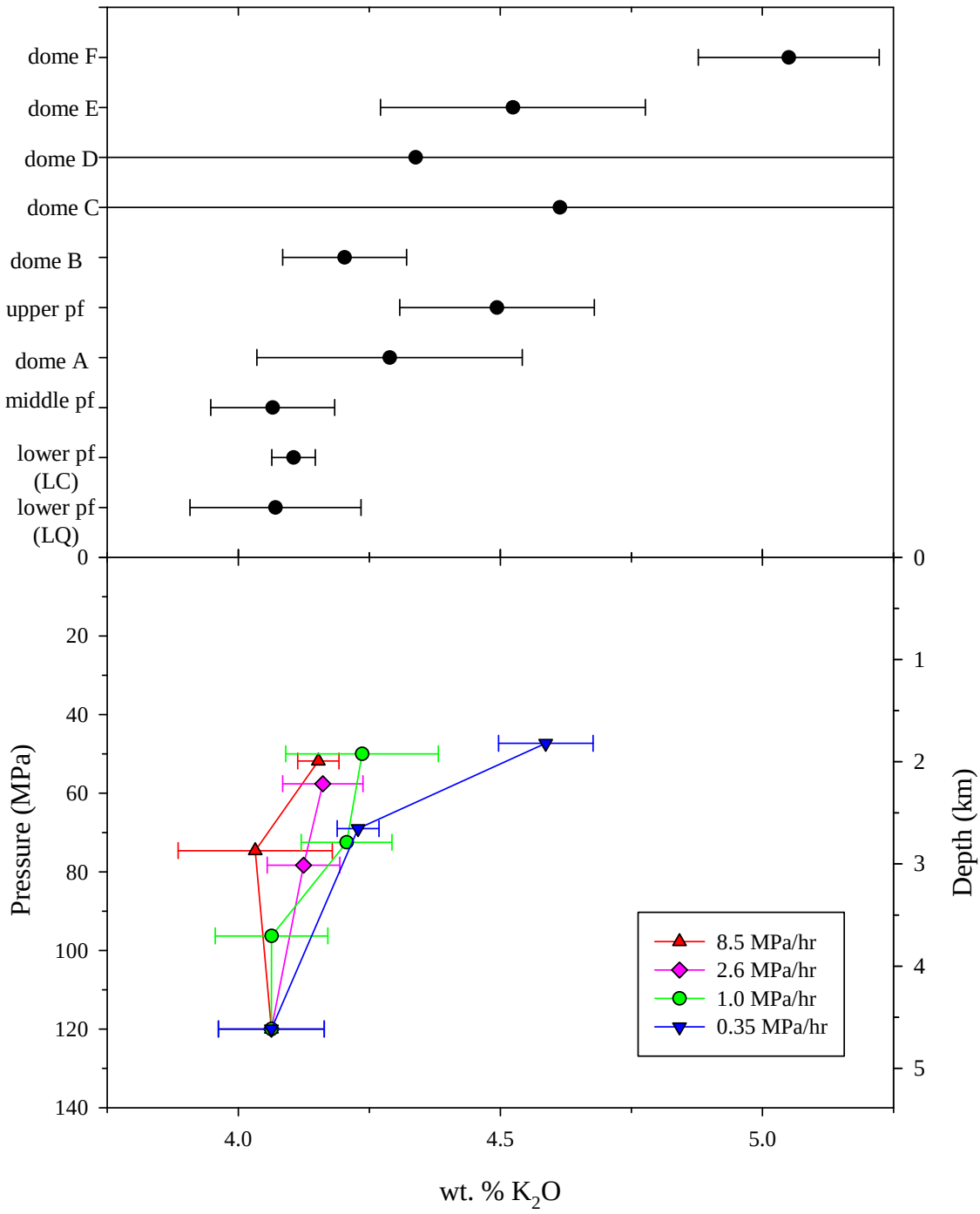
dome F
dome E
dome D
dome C
dome B
upper pf
dome A
middle pf
lower pf (LC)
lower pf (LQ)
0
20
40
60
80
100
120
140
Pressure (MPa)
0
1
2
3
4
5
Depth (km)
4.0
4.5
5.0
wt. % K2O
8.5 MPa/hr
2.6 MPa/hr
1.0 MPa/hr
0.35 MPa/hr

**Figure 22c.**

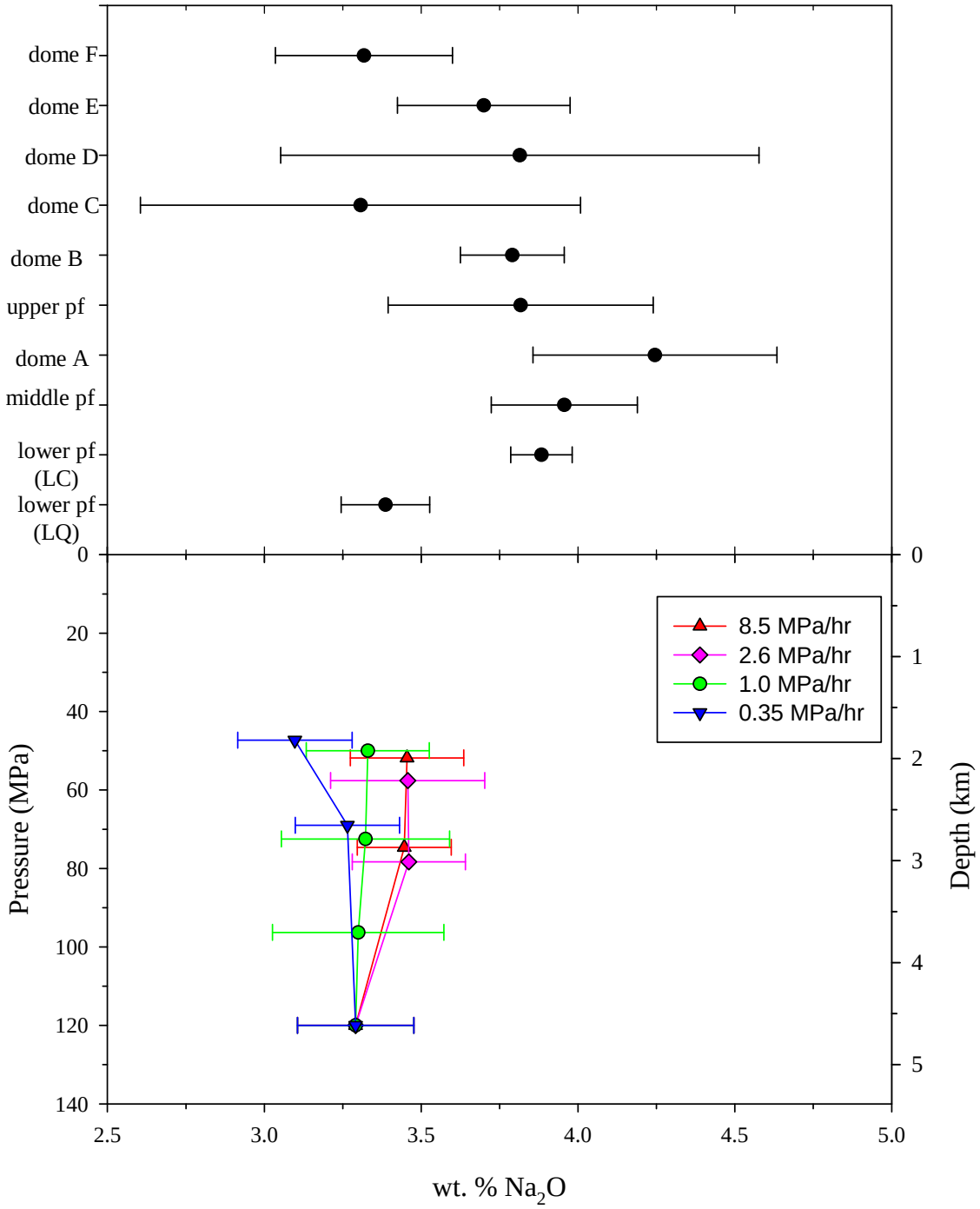
dome F
dome E
dome D
dome C
dome B
upper pf
dome A
middle pf
lower pf (LC)
lower pf (LQ)
0
20
40
60
80
100
120
140
Pressure (MPa)
0
1
2
3
4
5
Depth (km)
2.5
3.0
3.5
4.0
4.5
5.0
wt. % Na2O
8.5 MPa/hr
2.6 MPa/hr
1.0 MPa/hr
0.35 MPa/hr

**Figure 22d.**

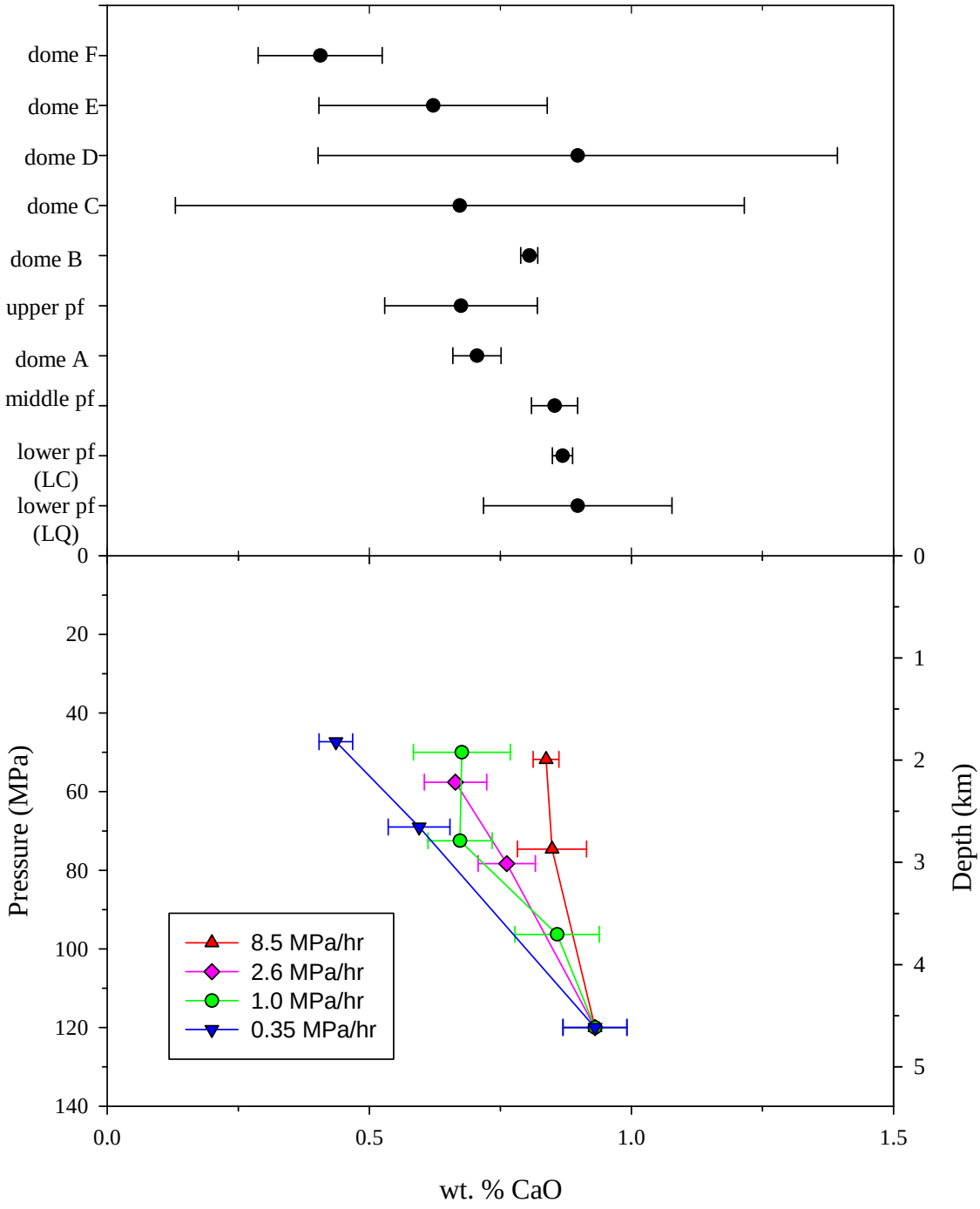
dome F
dome E
dome D
dome C
dome B
upper pf
dome A
middle pf
lower pf (LC)
lower pf (LQ)
0
20
40
60
80
100
120
140
Pressure (MPa)
0
1
2
3
4
5
Depth (km)
0.0
0.5
1.0
1.5
wt. % CaO
8.5 MPa/hr
2.6 MPa/hr
1.0 MPa/hr
0.35 MPa/hr

**Figure 22e.**

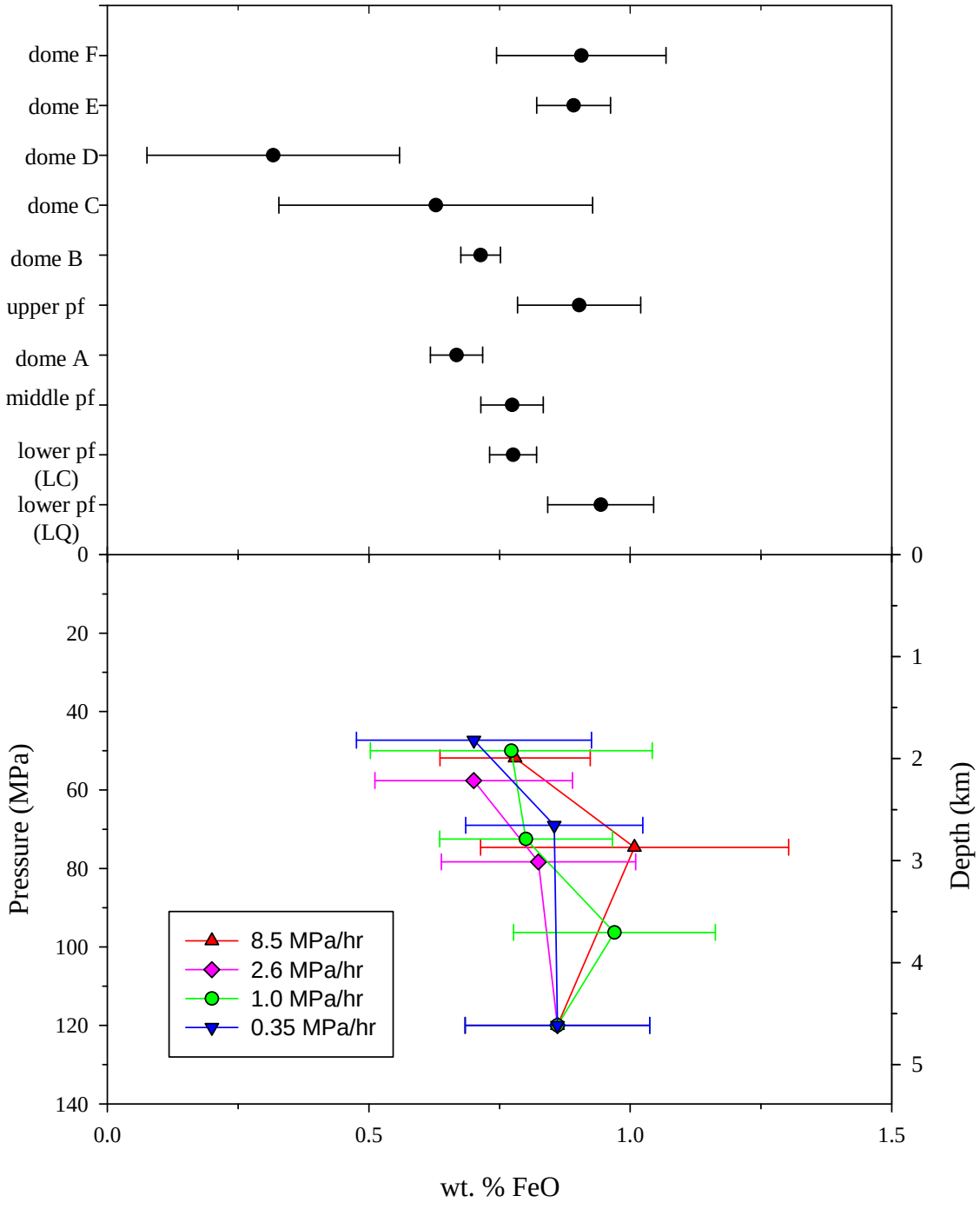
dome F
dome E
dome D
dome C
dome B
upper pf
dome A
middle pf
lower pf (LC)
lower pf (LQ)
0
20
40
60
80
100
120
140
Pressure (MPa)
0
1
2
3
4
5
Depth (km)
0.0
0.5
1.0
1.5
wt. % FeO
8.5 MPa/hr
2.6 MPa/hr
1.0 MPa/hr
0.35 MPa/hr

**Figure 22f.**

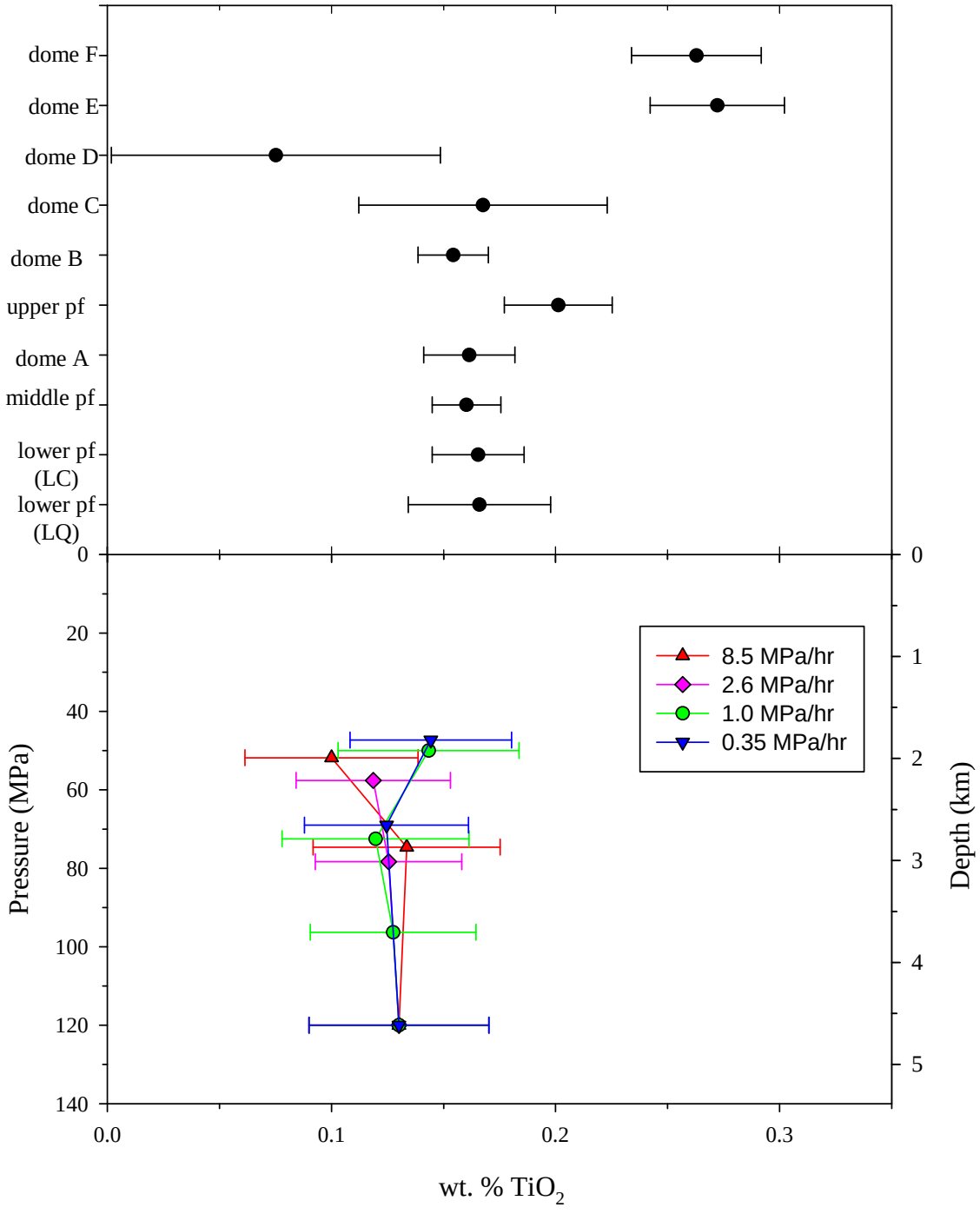
dome F
dome E
dome D
dome C
dome B
upper pf
dome A
middle pf
lower pf (LC)
lower pf (LQ)
8.5 MPa/hr
2.6 MPa/hr
1.0 MPa/hr
0.35 MPa/hr
Pressure (MPa)
Depth (km)
wt. % TiO2
0
20
40
60
80
100
120
140
0.0
0.1
0.2
0.3
1
2
3
4
5

**Figure 22g.**

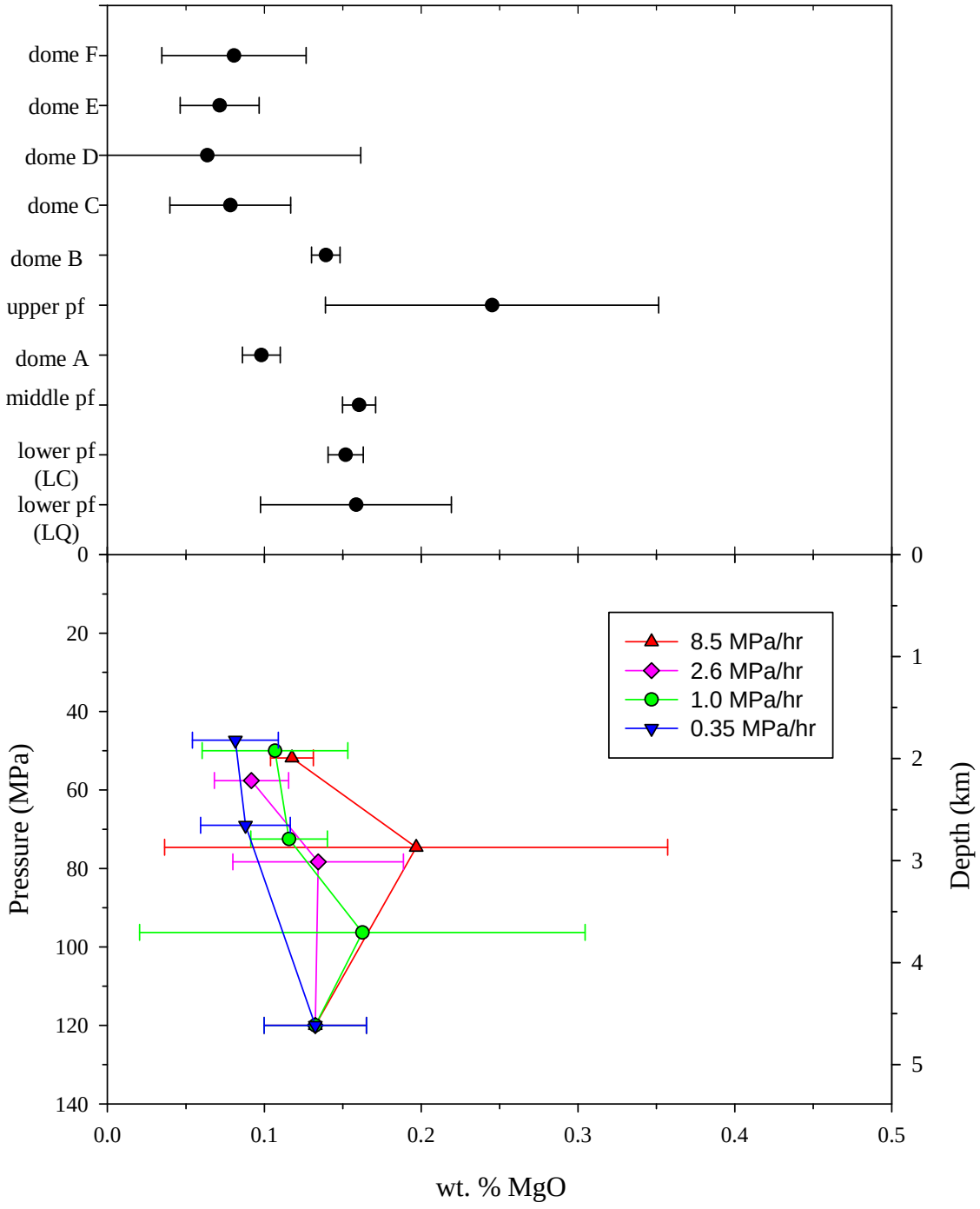
dome F
dome E
dome D
dome C
dome B
upper pf
dome A
middle pf
lower pf (LC)
lower pf (LQ)
0
20
40
60
80
100
120
140
Pressure (MPa)
0.0
0.1
0.2
0.3
0.4
0.5
wt. % MgO
0
1
2
3
4
5
Depth (km)
8.5 MPa/hr
2.6 MPa/hr
1.0 MPa/hr
0.35 MPa/hr

**Figure 22h.**

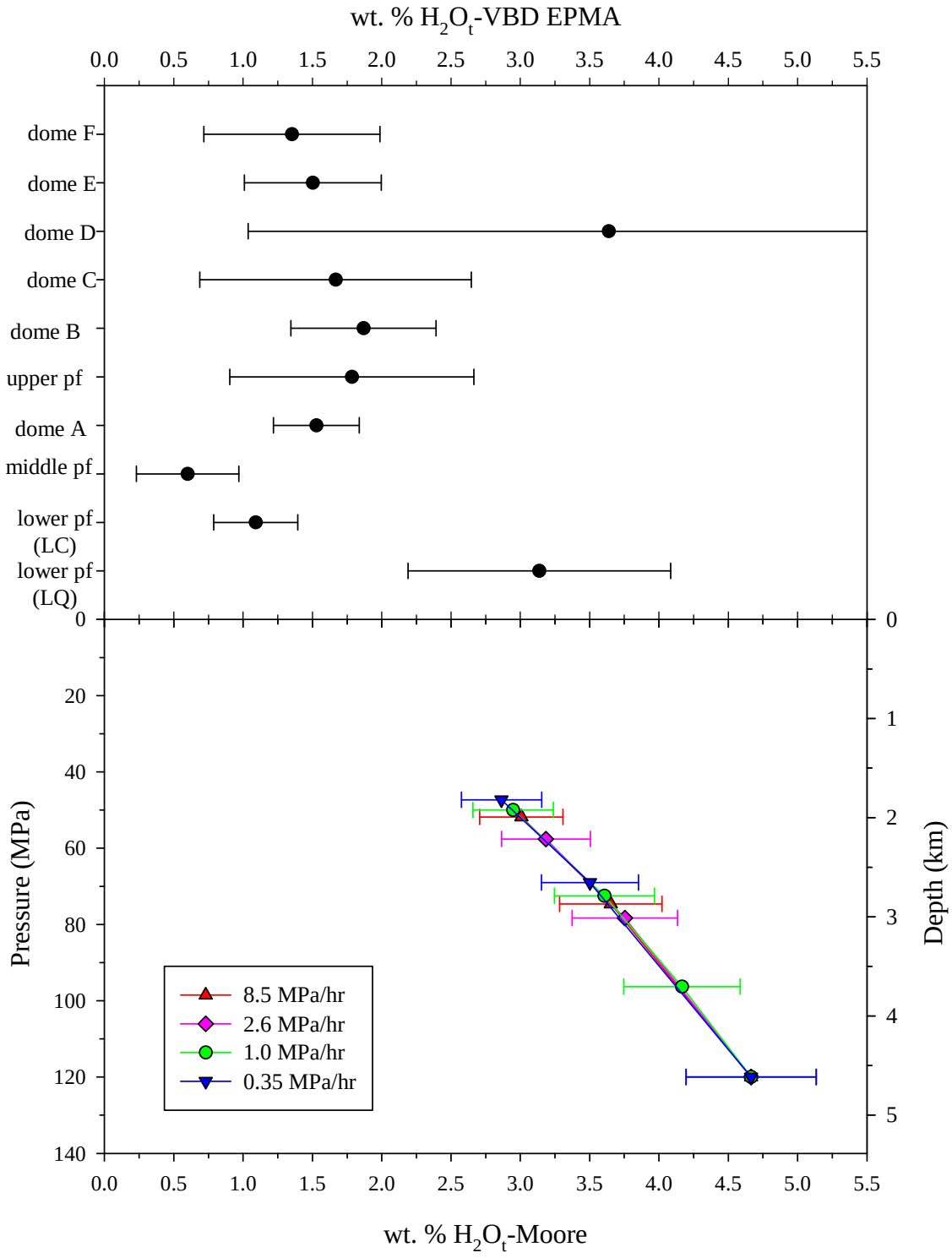
wt. % H2Ot-VBD EPMA
0.0
0.5
1.0
1.5
2.0
2.5
3.0
3.5
4.0
4.5
5.0
5.5
dome F
dome E
dome D
dome C
dome B
upper pf
dome A
middle pf
lower pf (LC)
lower pf (LQ)
0
20
40
60
80
100
120
140
Pressure (MPa)
Depth (km)
0
1
2
3
4
5
8.5 MPa/hr
2.6 MPa/hr
1.0 MPa/hr
0.35 MPa/hr
wt. % H2Ot-Moore

**Figure 22i.**

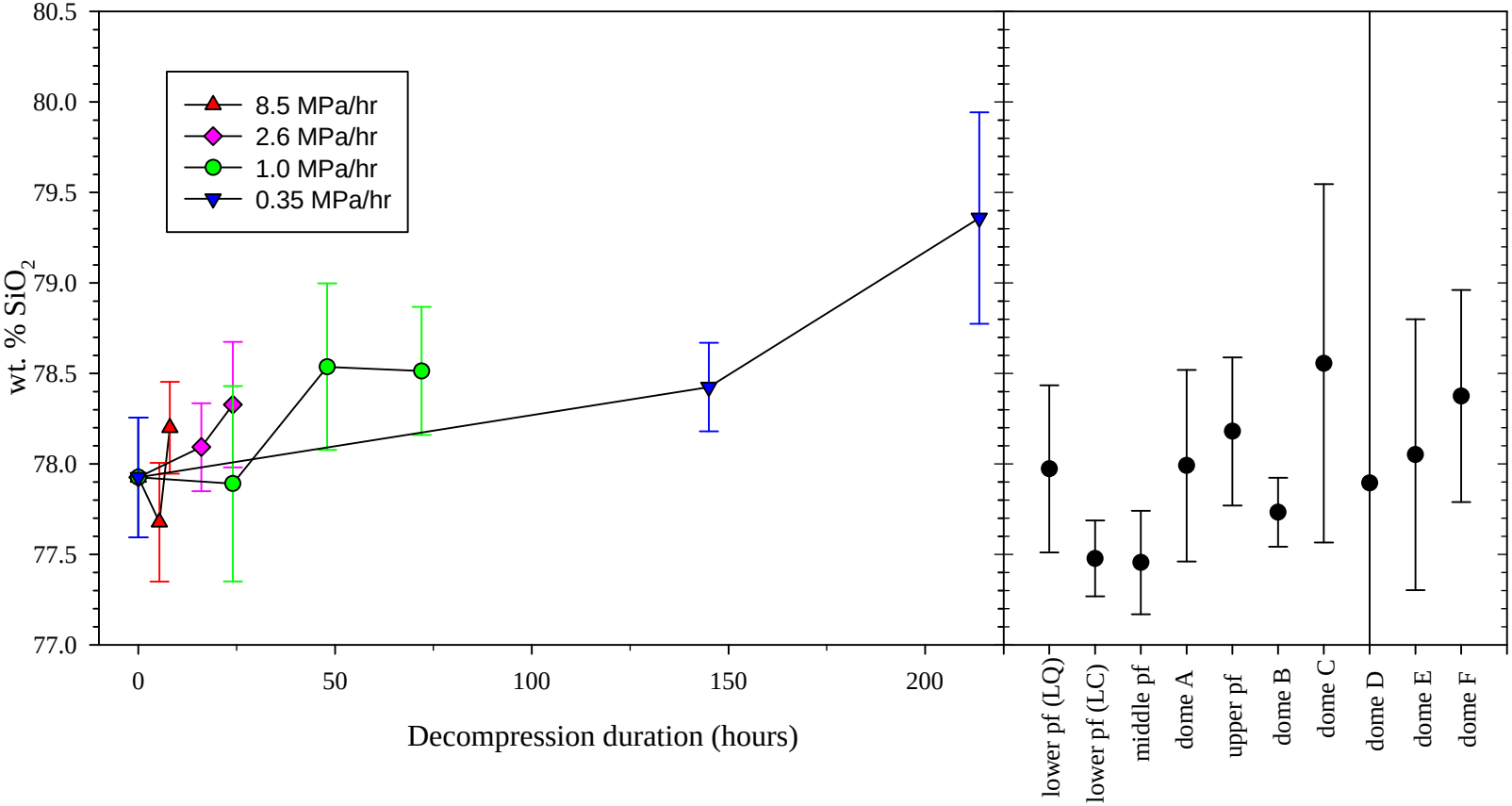
80.5
80.0
79.5
79.0
78.5
78.0
77.5
77.0
wt. % SiO2
8.5 MPa/hr
2.6 MPa/hr
1.0 MPa/hr
0.35 MPa/hr
0
50
100
150
200
Decompression duration (hours)
lower pf (LQ)
lower pf (LC)
middle pf
dome A
upper pf
dome B
dome C
dome D
dome E
dome F

**Figure 23a.**

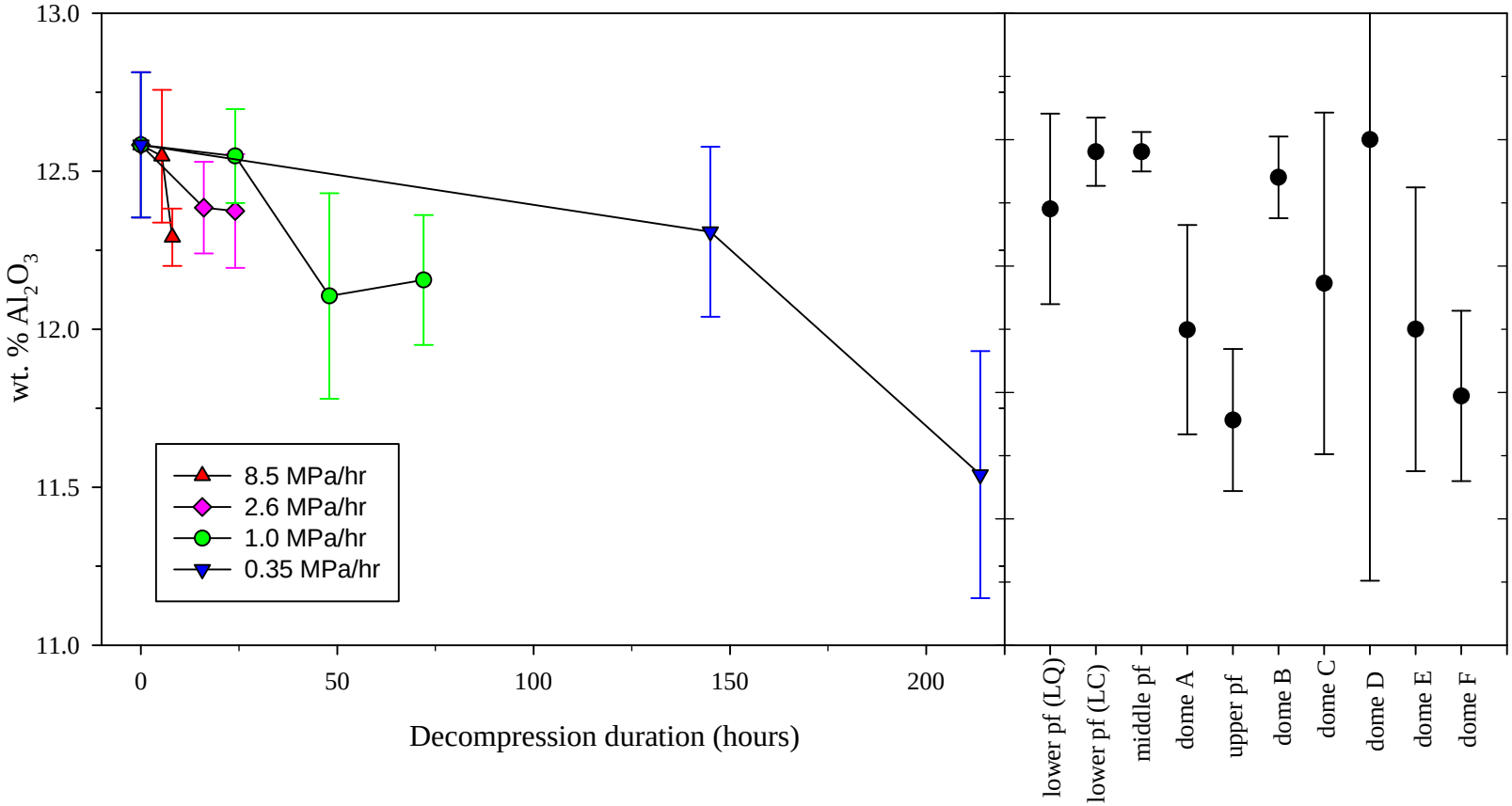
13.0
12.5
12.0
11.5
11.0
wt. % $Al_2O_3$
0
50
100
150
200
Decompression duration (hours)
8.5 MPa/hr
2.6 MPa/hr
1.0 MPa/hr
0.35 MPa/hr
lower pf (LQ)
lower pf (LC)
middle pf
dome A
upper pf
dome B
dome C
dome D
dome E
dome F

**Figure 23b.**

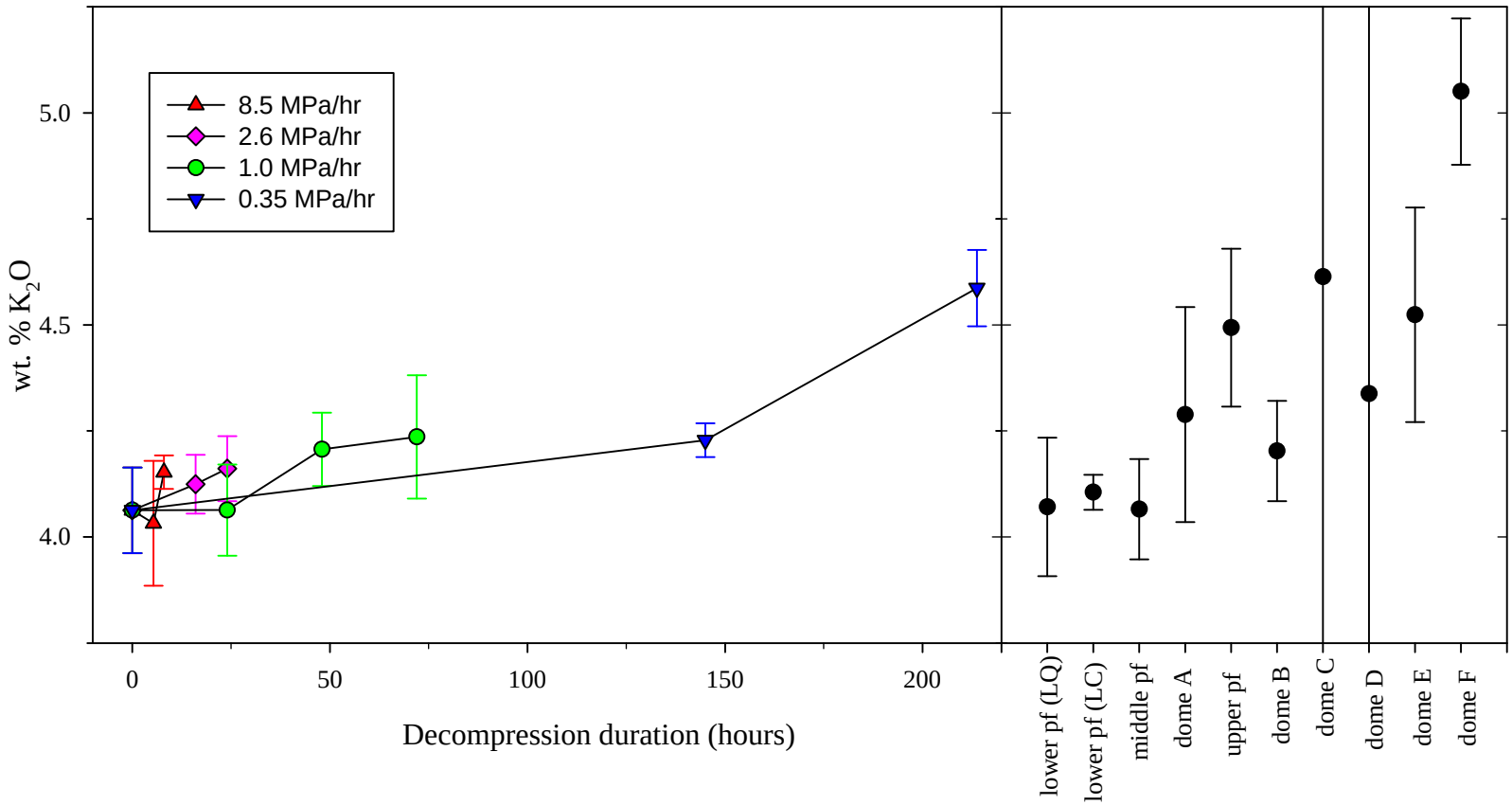
8.5 MPa/hr
2.6 MPa/hr
1.0 MPa/hr
0.35 MPa/hr
wt. % K2O
5.0
4.5
4.0
0
50
100
150
200
Decompression duration (hours)
lower pf (LQ)
lower pf (LC)
middle pf
dome A
upper pf
dome B
dome C
dome D
dome E
dome F

**Figure 23c.**

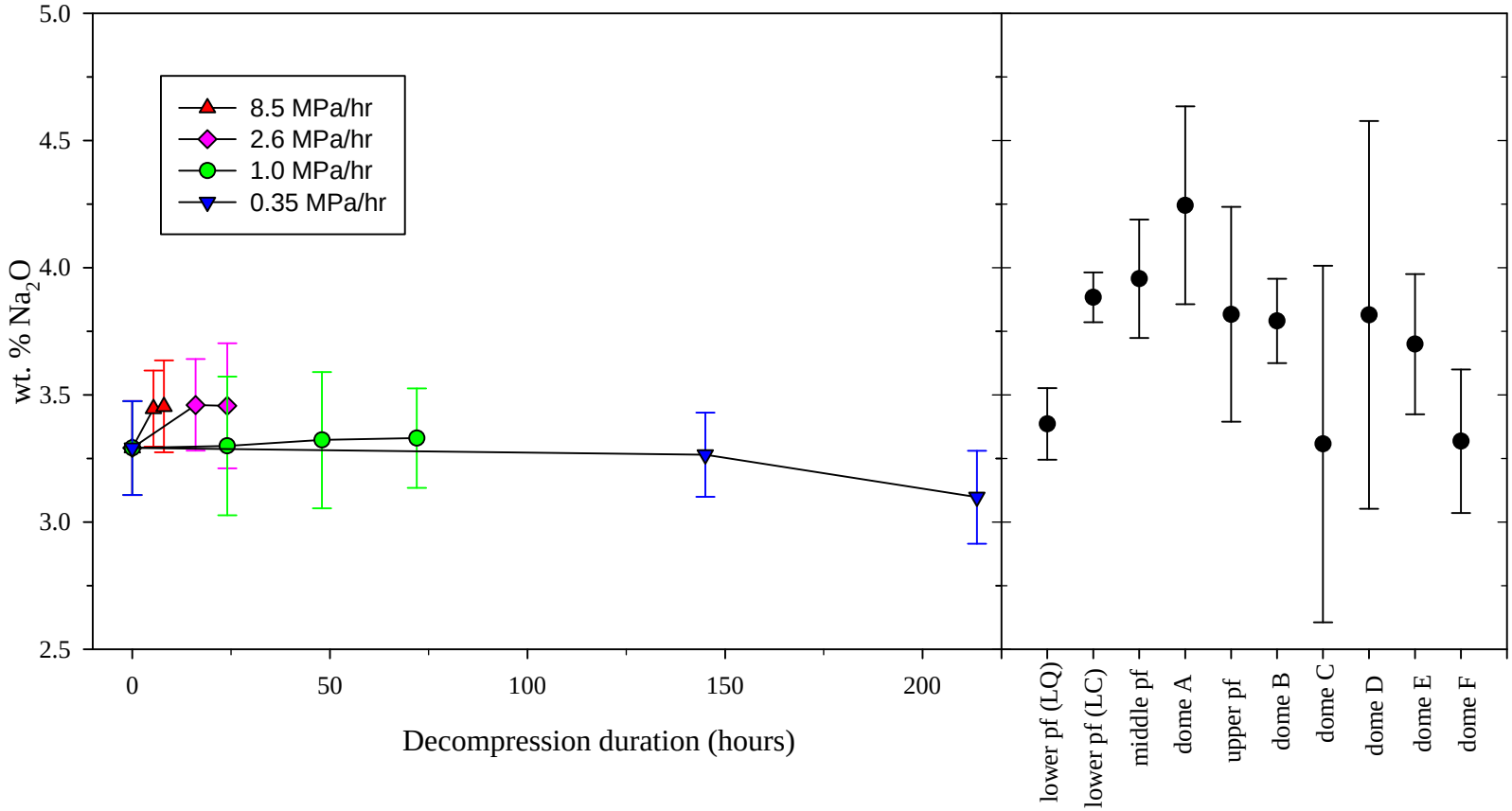
5.0
4.5
4.0
3.5
3.0
2.5
wt. % Na2O
8.5 MPa/hr
2.6 MPa/hr
1.0 MPa/hr
0.35 MPa/hr
0
50
100
150
200
Decompression duration (hours)
lower pf (LQ)
lower pf (LC)
middle pf
dome A
upper pf
dome B
dome C
dome D
dome E
dome F

**Figure 23d.**

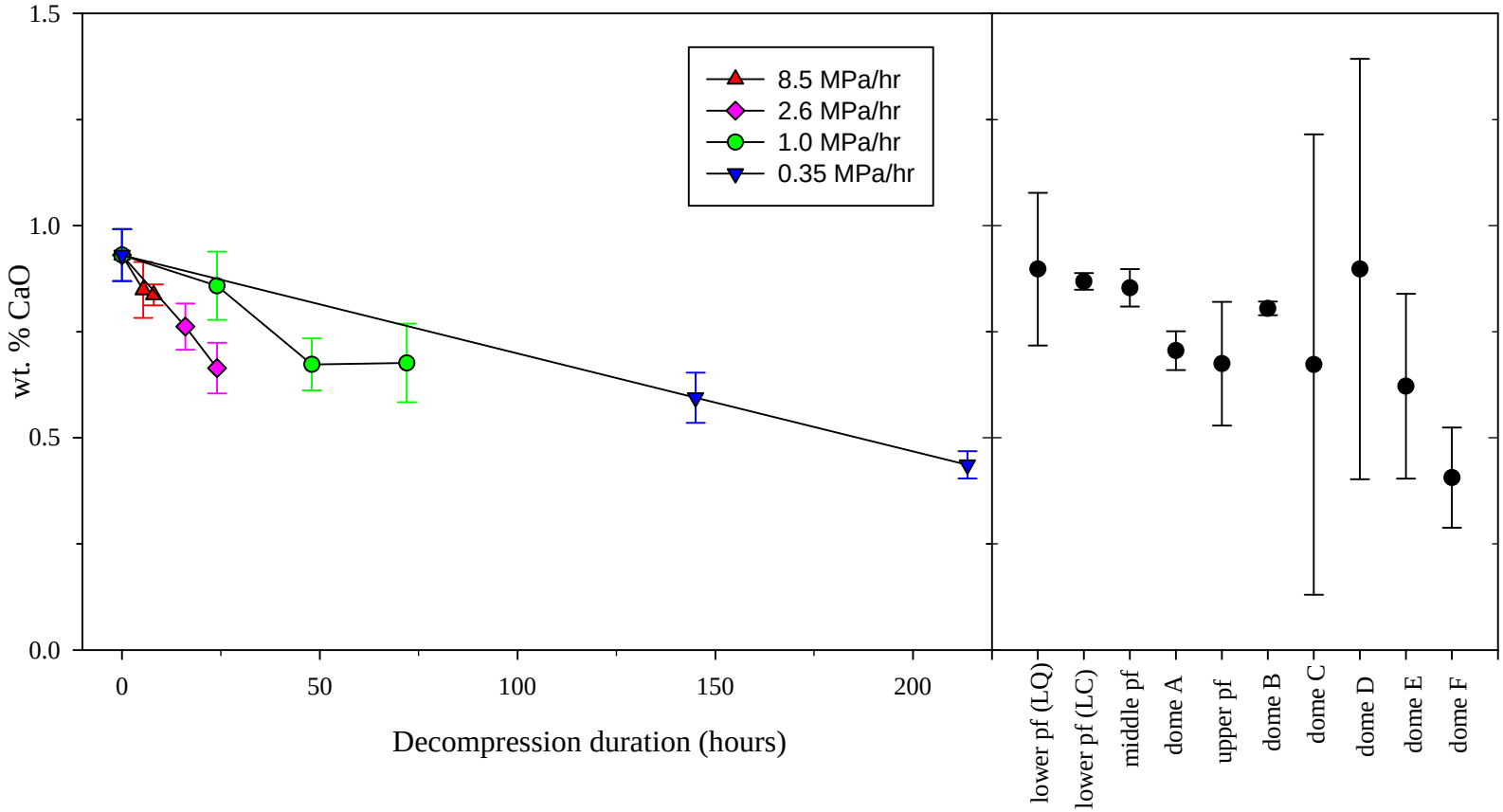
1.5
1.0
0.5
0.0
wt. % CaO
0
50
100
150
200
Decompression duration (hours)
8.5 MPa/hr
2.6 MPa/hr
1.0 MPa/hr
0.35 MPa/hr
lower pf (LQ)
lower pf (LC)
middle pf
dome A
upper pf
dome B
dome C
dome D
dome E
dome F

**Figure 23e.**

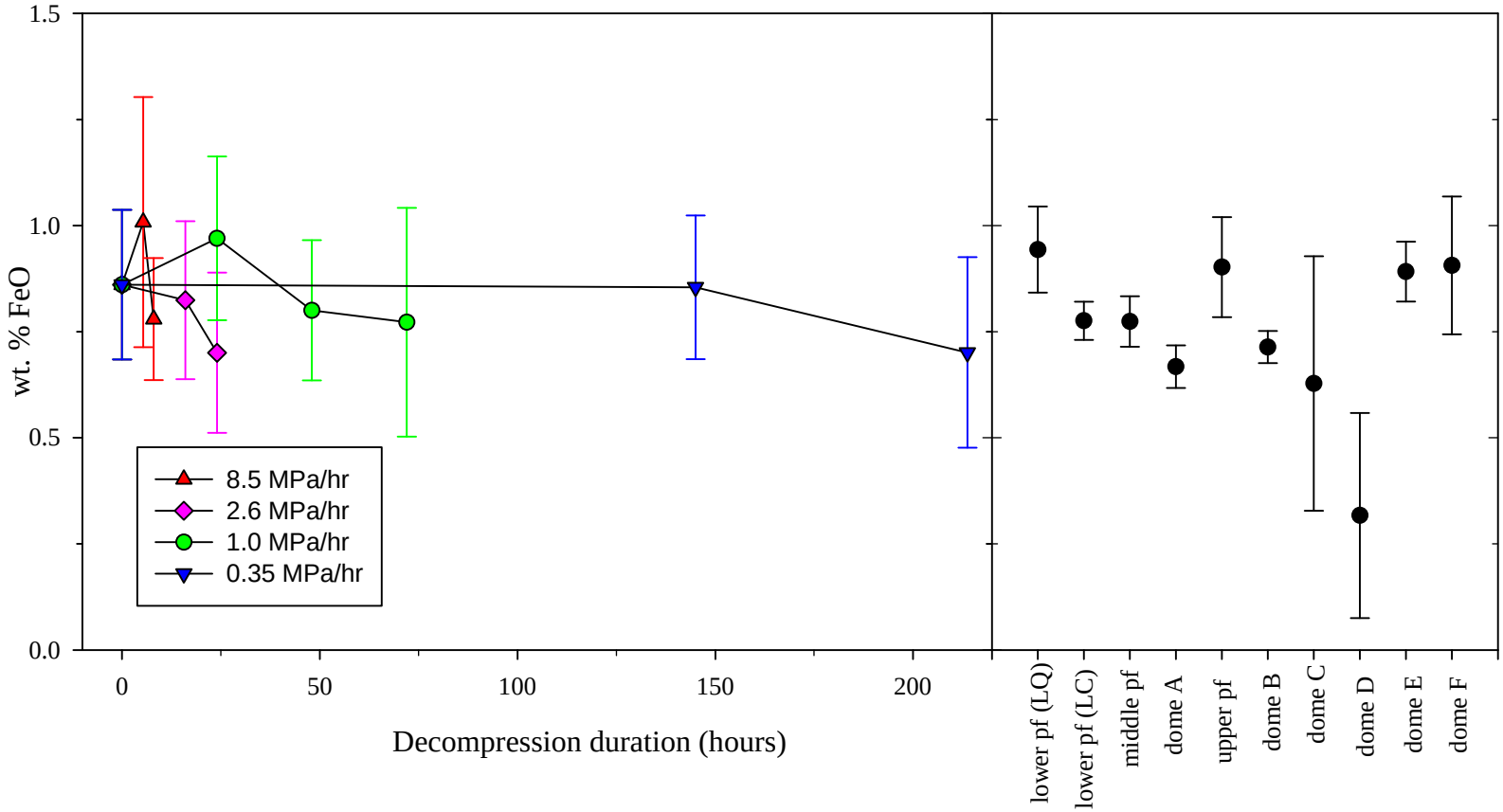
1.5
1.0
0.5
0.0
wt. % FeO
0
50
100
150
200
Decompression duration (hours)
8.5 MPa/hr
2.6 MPa/hr
1.0 MPa/hr
0.35 MPa/hr
lower pf (LQ)
lower pf (LC)
middle pf
dome A
upper pf
dome B
dome C
dome D
dome E
dome F

**Figure 23f.**

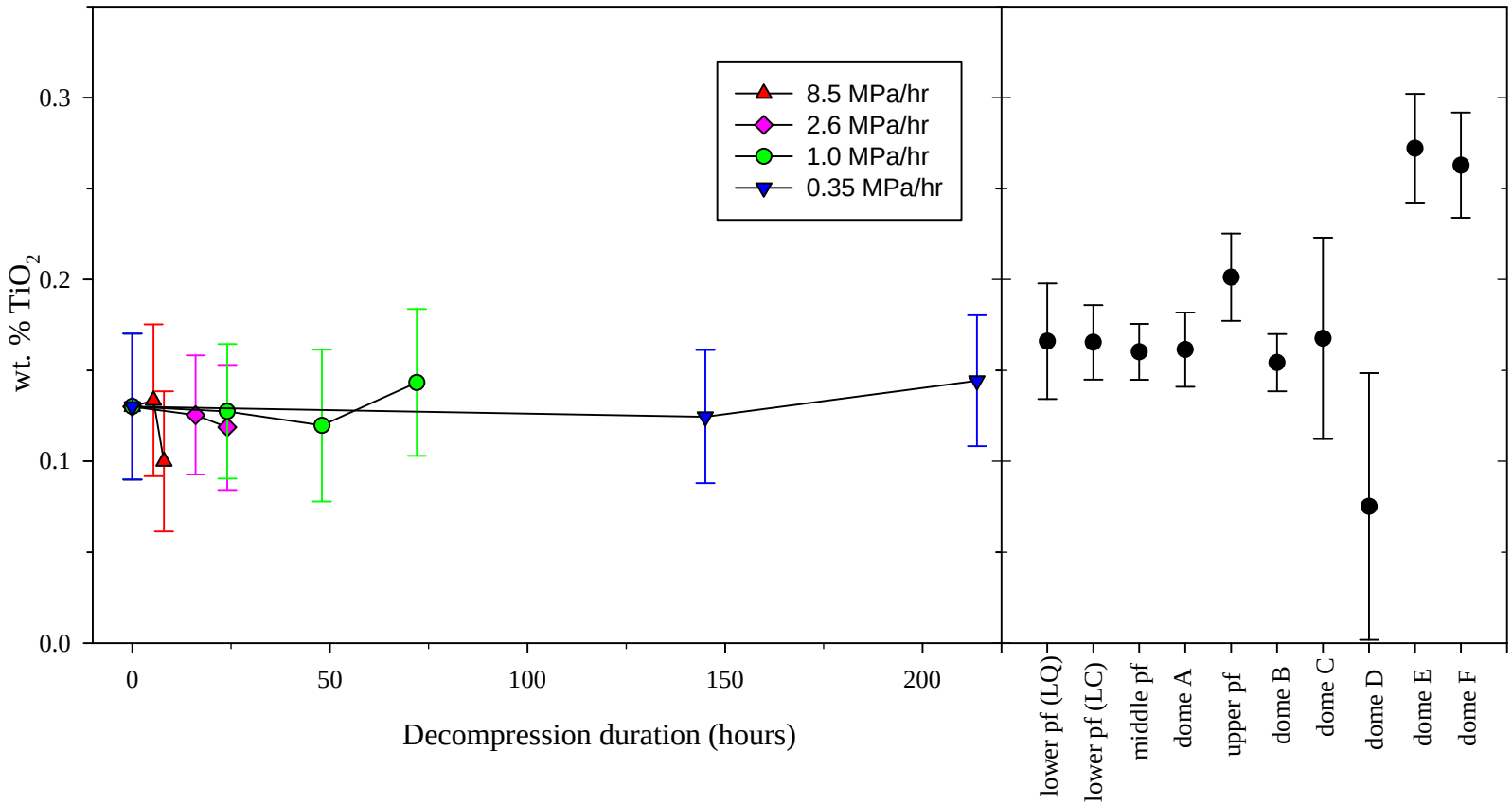
8.5 MPa/hr
2.6 MPa/hr
1.0 MPa/hr
0.35 MPa/hr
wt. % TiO2
0.0
0.1
0.2
0.3
0
50
100
150
200
Decompression duration (hours)
lower pf (LQ)
lower pf (LC)
middle pf
dome A
upper pf
dome B
dome C
dome D
dome E
dome F

**Figure 23g.**

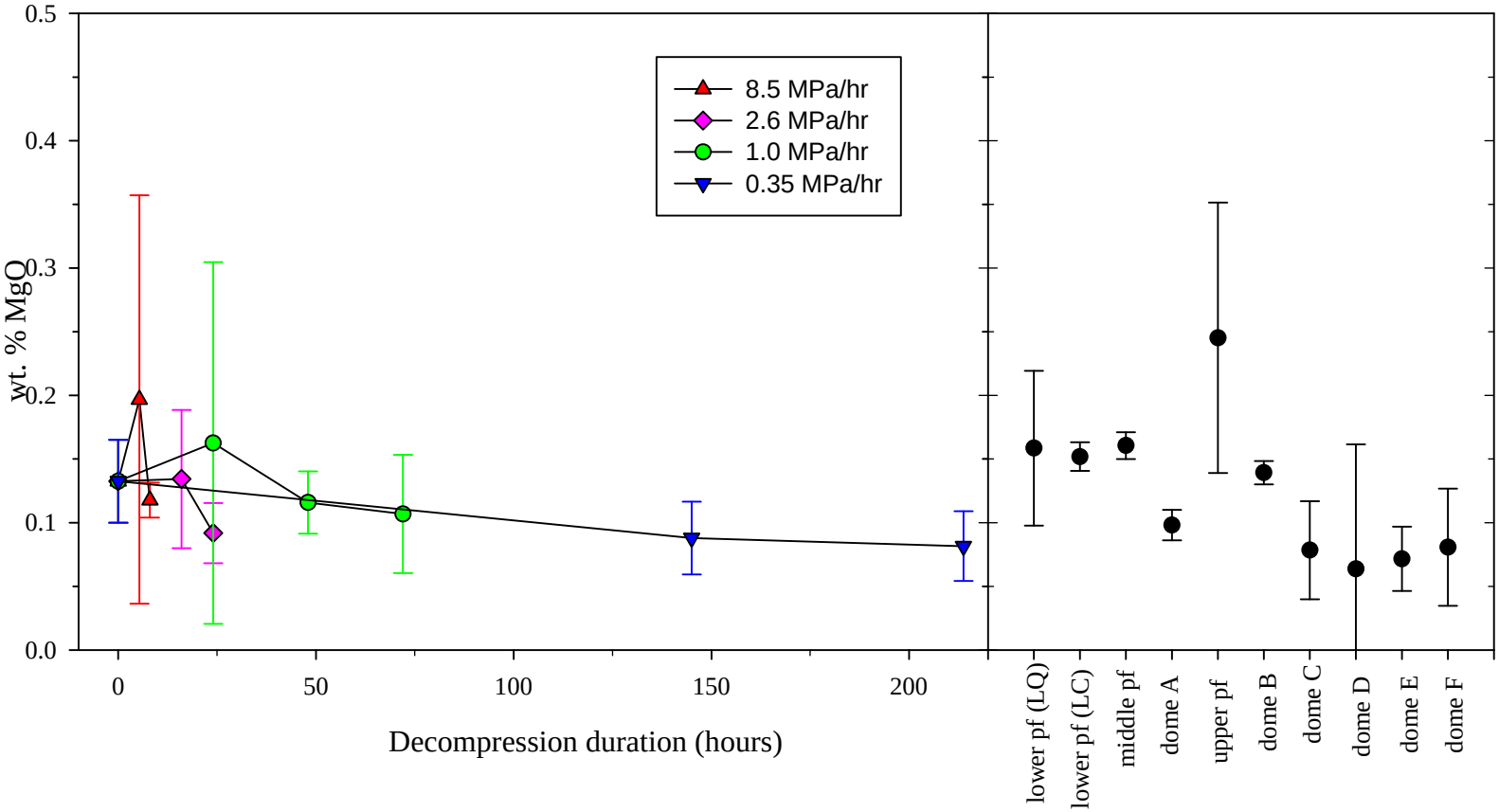
0.5
0.4
0.3
0.2
0.1
0.0
wt. % MgO
8.5 MPa/hr
2.6 MPa/hr
1.0 MPa/hr
0.35 MPa/hr
0
50
100
150
200
Decompression duration (hours)
lower pf (LQ)
lower pf (LC)
middle pf
dome A
upper pf
dome B
dome C
dome D
dome E
dome F

**Figure 23h.**

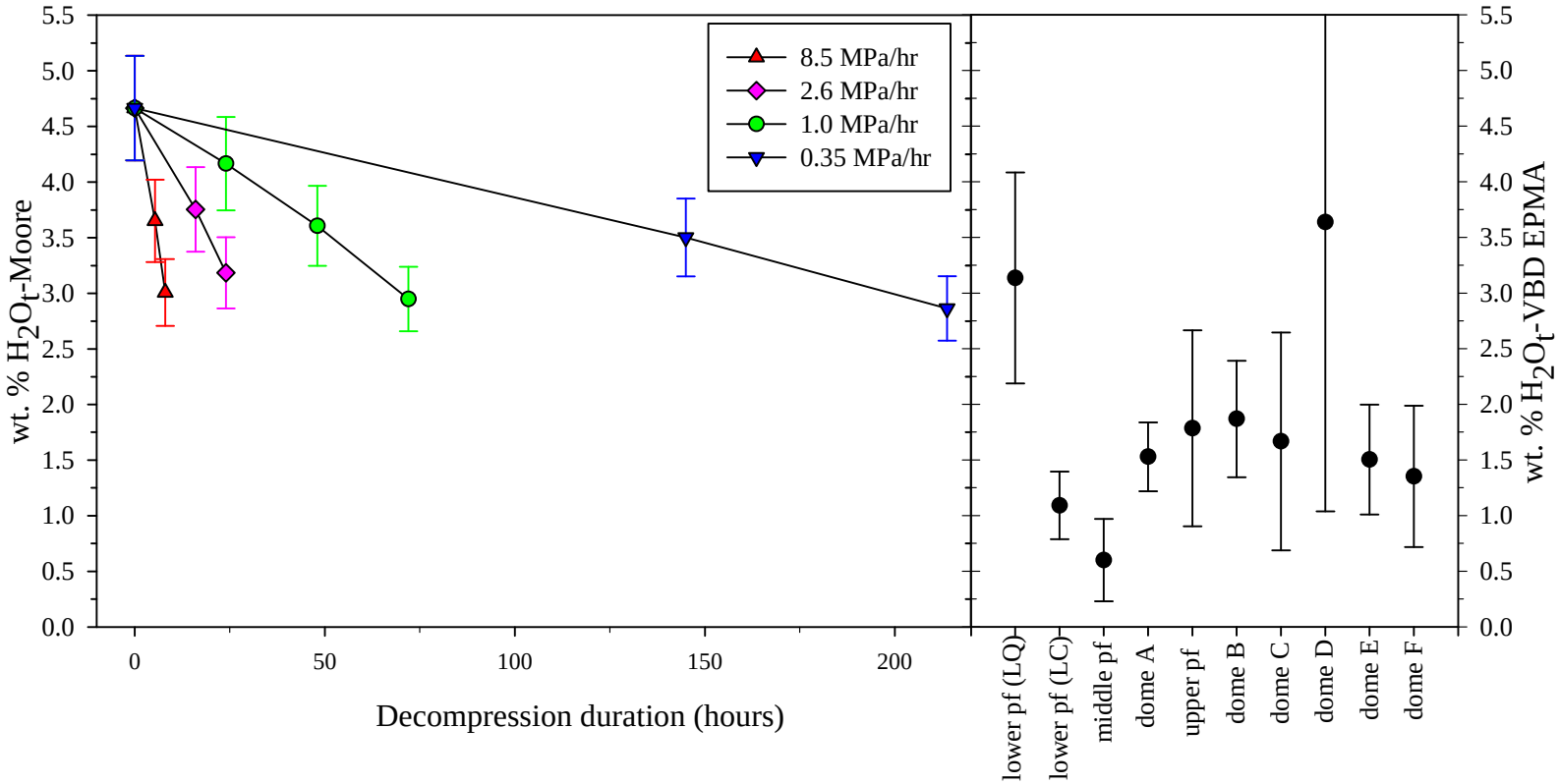
8.5 MPa/hr
2.6 MPa/hr
1.0 MPa/hr
0.35 MPa/hr
wt. % H2Ot-Moore
Decompression duration (hours)
wt. % H2Ot-VBD EPMA
lower pf (LQ)
lower pf (LC)
middle pf
dome A
upper pf
dome B
dome C
dome D
dome E
dome F

**Figure 23i.**

**Appendix A.** Natural sample bulk rock compositions (wt. %).

| Sample | Unit | $SiO_2$ | $Al_2O_3$ | $Fe_2O_3$ | FeO | FeOt | MgO | CaO | $Na_2O$ | $K_2O$ | $TiO_2$ | $P_2O_5$ | MnO | LOI | Total |
|---|---|---|---|---|---|---|---|---|---|---|---|---|---|---|---|
| LQ13-01 | lower pf | N/A | N/A | N/A | N/A | N/A | N/A | N/A | N/A | N/A | N/A | N/A | N/A | N/A | N/A |
| LC84-417 | lower pf | 69.58 | 15.37 | 0.61 | 2.21 | 2.76 | 1.39 | 3.34 | 4.22 | 2.71 | 0.40 | 0.12 | 0.05 | 1.22 | 97.83 |
| LC84-418 | middle pf | 69.30 | 15.47 | 0.62 | 2.25 | 2.81 | 1.43 | 3.44 | 4.23 | 2.66 | 0.41 | 0.12 | 0.06 | 0.92 | 98.51 |
| LC84-428 | dome A | 69.62 | 15.53 | 0.59 | 2.12 | 2.65 | 1.29 | 3.38 | 4.33 | 2.62 | 0.35 | 0.13 | 0.06 | 0.51 | 98.77 |
| LC84-419 | upper pf | 69.42 | 15.39 | 0.62 | 2.25 | 2.81 | 1.41 | 3.43 | 4.24 | 2.67 | 0.40 | 0.12 | 0.05 | 0.86 | 98.34 |
| LC84-443 | dome B | 69.81 | 15.60 | 0.56 | 2.03 | 2.54 | 1.20 | 3.31 | 4.30 | 2.64 | 0.35 | 0.12 | 0.06 | 0.76 | 98.91 |
| LC84-434 | dome C | 68.88 | 15.76 | 0.62 | 2.22 | 2.77 | 1.46 | 3.71 | 4.30 | 2.50 | 0.38 | 0.11 | 0.06 | 0.10 | 99.84 |
| Chaos D | dome D | N/A | N/A | N/A | N/A | N/A | N/A | N/A | N/A | N/A | N/A | N/A | N/A | N/A | N/A |
| LC84-435 | dome D | 67.78 | 15.81 | 0.74 | 2.67 | 3.34 | 1.77 | 4.08 | 4.01 | 2.52 | 0.42 | 0.12 | 0.07 | 0.18 | 99.58 |
| LC84-433 | dome E | 66.97 | 16.26 | 0.76 | 2.72 | 3.40 | 1.81 | 4.48 | 4.15 | 2.25 | 0.41 | 0.12 | 0.07 | 0.49 | 99.31 |
| LC84-455 | dome F | 68.17 | 16.10 | 0.66 | 2.38 | 2.98 | 1.50 | 4.16 | 4.23 | 2.25 | 0.36 | 0.11 | 0.06 | 0.40 | 98.99 |

Notes:

Determined by wavelength dispersive x-ray fluorescence. See Clynne et al. (2008) for additional details and locations. LQ13-01 and Chaos D not analyzed for bulk composition.

**Appendix B.** Raw individual natural sample glass compositions (wt. %) as determined by EPMA.

| Sample | line | $SiO_2$ | $TiO_2$ | $Al_2O_3$ | $FeO^*$ | MnO | MgO | CaO | $Na_2O$ | $K_2O$ | Cl | $SO_3$ | Total |
|---|---|---|---|---|---|---|---|---|---|---|---|---|---|
| LQ13-01-glass | 1 | 76.10 | 0.16 | 12.57 | 1.03 | 0.06 | 0.09 | 1.19 | 3.24 | 3.68 | 0.08 | 0.05 | 98.26 |
| LQ13-01-glass | 2 | 75.59 | 0.19 | 11.43 | 1.00 | 0.02 | 0.24 | 0.68 | 3.05 | 3.97 | 0.10 | MDL | 96.27 |
| LQ13-01-glass | 3 | 75.47 | 0.20 | 12.31 | 0.90 | 0.08 | 0.15 | 0.97 | 3.47 | 3.92 | 0.07 | 0.04 | 97.58 |
| LQ13-01-glass | 4 | 74.62 | 0.11 | 11.91 | 0.73 | 0.08 | 0.12 | 0.84 | 3.38 | 4.00 | 0.09 | 0.02 | 95.91 |
| LQ13-01-glass | 5 | 75.42 | 0.13 | 11.57 | 0.97 | 0.10 | 0.23 | 0.90 | 3.24 | 3.92 | 0.10 | 0.08 | 96.64 |
| LQ13-01-glass | 6 | 76.30 | 0.18 | 11.74 | 0.85 | 0.03 | 0.11 | 0.85 | 3.40 | 4.01 | 0.08 | 0.03 | 97.57 |
| LQ13-01-glass | 7 | 75.17 | 0.16 | 11.39 | 0.93 | 0.03 | 0.12 | 0.66 | 3.17 | 4.09 | 0.07 | 0.01 | 95.81 |
| LC84-417-glass | 8 | 76.20 | 0.18 | 12.39 | 0.71 | 0.05 | 0.14 | 0.84 | 3.88 | 4.05 | 0.09 | MDL | 98.53 |
| LC84-417-glass | 9 | 77.05 | 0.16 | 12.17 | 0.72 | 0.04 | 0.14 | 0.83 | 3.79 | 4.10 | 0.07 | MDL | 99.06 |
| LC84-417-glass | 10 | 77.19 | 0.15 | 12.26 | 0.78 | 0.02 | 0.14 | 0.87 | 3.80 | 4.05 | 0.08 | MDL | 99.36 |
| LC84-417-glass | 11 | 76.59 | 0.15 | 12.26 | 0.75 | 0.05 | 0.15 | 0.85 | 3.86 | 4.05 | 0.08 | MDL | 98.79 |
| LC84-417-glass | 12 | 76.27 | 0.16 | 12.32 | 0.80 | 0.01 | 0.15 | 0.89 | 3.77 | 4.09 | 0.09 | 0.01 | 98.56 |
| LC84-417-glass | 13 | 76.88 | 0.19 | 12.19 | 0.85 | 0.04 | 0.14 | 0.84 | 3.70 | 4.12 | 0.07 | MDL | 99.05 |
| LC84-417-glass | 14 | 76.64 | 0.14 | 12.54 | 0.76 | 0.04 | 0.16 | 0.87 | 3.95 | 4.02 | 0.08 | MDL | 99.21 |
| LC84-417-glass | 15 | 76.24 | 0.19 | 12.40 | 0.78 | 0.03 | 0.17 | 0.87 | 3.98 | 4.00 | 0.08 | MDL | 98.73 |
| LC84-418-glass | 16 | 76.71 | 0.14 | 12.23 | 0.78 | 0.04 | 0.15 | 0.79 | 3.64 | 4.14 | 0.08 | MDL | 98.68 |
| LC84-418-glass | 17 | 77.04 | 0.17 | 12.39 | 0.68 | 0.04 | 0.15 | 0.92 | 4.27 | 3.95 | 0.08 | MDL | 99.69 |
| LC84-418-glass | 18 | 77.38 | 0.15 | 12.39 | 0.83 | 0.02 | 0.15 | 0.84 | 3.87 | 4.07 | 0.08 | MDL | 99.78 |
| LC84-418-glass | 19 | 77.38 | 0.16 | 12.29 | 0.79 | 0.04 | 0.17 | 0.88 | 3.76 | 3.83 | 0.09 | MDL | 99.40 |
| LC84-418-glass | 20 | 76.78 | 0.17 | 12.49 | 0.85 | 0.04 | 0.18 | 0.90 | 3.68 | 3.99 | 0.08 | MDL | 99.17 |
| LC84-418-glass | 21 | 77.23 | 0.19 | 12.42 | 0.71 | 0.06 | 0.16 | 0.84 | 4.00 | 4.11 | 0.08 | 0.01 | 99.80 |
| LC84-418-glass | 22 | 77.00 | 0.16 | 12.52 | 0.74 | 0.02 | 0.15 | 0.83 | 3.93 | 4.16 | 0.08 | MDL | 99.59 |
| LC84-418-glass | 23 | 76.96 | 0.14 | 12.31 | 0.72 | 0.03 | 0.16 | 0.80 | 3.93 | 3.97 | 0.09 | MDL | 99.10 |
| LC84-418-glass | 24 | 76.43 | 0.16 | 12.37 | 0.82 | 0.04 | 0.17 | 0.84 | 4.32 | 4.17 | 0.09 | MDL | 99.40 |
| LC84-428-glass | 25 | 76.95 | 0.15 | 12.07 | 0.60 | 0.02 | 0.07 | 0.69 | 3.79 | 4.43 | 0.05 | MDL | 98.81 |
| LC84-428-glass | 26 | 77.08 | 0.16 | 11.02 | 0.67 | 0.03 | 0.10 | 0.63 | 3.97 | 4.39 | 0.06 | MDL | 98.12 |
| LC84-428-glass | 27 | 76.98 | 0.15 | 11.32 | 0.66 | 0.04 | 0.10 | 0.67 | 4.47 | 4.36 | 0.07 | MDL | 98.82 |
| LC84-428-glass | 28 | 76.07 | 0.20 | 12.29 | 0.76 | 0.03 | 0.11 | 0.78 | 4.71 | 3.78 | 0.06 | MDL | 98.79 |
| LC84-428-glass | 29 | 77.32 | 0.14 | 11.66 | 0.69 | 0.03 | 0.10 | 0.74 | 3.65 | 3.89 | 0.06 | MDL | 98.29 |
| LC84-428-glass | 30 | 76.53 | 0.14 | 11.18 | 0.61 | 0.03 | 0.09 | 0.67 | 4.43 | 4.31 | 0.06 | MDL | 98.06 |
| LC84-428-glass | 31 | 76.38 | 0.18 | 11.58 | 0.62 | 0.04 | 0.09 | 0.69 | 4.48 | 4.27 | 0.05 | MDL | 98.39 |
| LC84-428-glass | 32 | 77.07 | 0.15 | 11.43 | 0.66 | 0.02 | 0.10 | 0.68 | 3.96 | 4.36 | 0.07 | MDL | 98.50 |
| LC84-419-glass | 33 | 75.54 | 0.21 | 11.43 | 1.04 | 0.05 | 0.41 | 0.90 | 3.35 | 4.02 | 0.06 | MDL | 97.01 |
| LC84-419-glass | 34 | 77.46 | 0.19 | 10.86 | 1.04 | 0.03 | 0.34 | 0.60 | 4.06 | 4.48 | 0.05 | 0.01 | 99.12 |
| LC84-419-glass | 35 | 76.16 | 0.22 | 11.10 | 0.75 | 0.03 | 0.22 | 0.79 | 4.24 | 4.37 | 0.06 | MDL | 97.94 |
| LC84-419-glass | 36 | 77.66 | 0.16 | 11.05 | 0.81 | 0.02 | 0.15 | 0.51 | 4.03 | 4.59 | 0.06 | MDL | 99.06 |
| LC84-419-glass | 37 | 77.06 | 0.20 | 11.53 | 0.90 | 0.02 | 0.20 | 0.68 | 4.05 | 4.41 | 0.06 | MDL | 99.11 |
| LC84-419-glass | 38 | 76.57 | 0.22 | 11.19 | 0.88 | 0.02 | 0.23 | 0.60 | 3.21 | 4.39 | 0.06 | MDL | 97.38 |
| LC84-419-glass | 39 | 77.04 | 0.18 | 11.14 | 0.79 | 0.03 | 0.13 | 0.55 | 3.31 | 4.64 | 0.07 | MDL | 97.88 |

**Appendix B, continued.**

| Sample | line | $SiO_2$ | $TiO_2$ | $Al_2O_3$ | $FeO^*$ | MnO | MgO | CaO | $Na_2O$ | $K_2O$ | Cl | $SO_3$ | Total |
|---|---|---|---|---|---|---|---|---|---|---|---|---|---|
| LC84-443-glass | 40 | 75.73 | 0.14 | 12.06 | 0.73 | 0.04 | 0.15 | 0.79 | 3.46 | 4.32 | 0.07 | MDL | 97.49 |
| LC84-443-glass | 41 | 76.83 | 0.18 | 12.01 | 0.76 | 0.04 | 0.13 | 0.78 | 3.82 | 4.05 | 0.07 | MDL | 98.67 |
| LC84-443-glass | 42 | 75.77 | 0.17 | 11.99 | 0.69 | 0.02 | 0.12 | 0.82 | 3.71 | 4.05 | 0.07 | MDL | 97.41 |
| LC84-443-glass | 43 | 76.03 | 0.15 | 12.26 | 0.69 | 0.04 | 0.13 | 0.80 | 3.66 | 3.98 | 0.07 | MDL | 97.80 |
| LC84-443-glass | 44 | 76.55 | 0.13 | 11.96 | 0.65 | 0.02 | 0.13 | 0.79 | 3.75 | 4.26 | 0.08 | 0.01 | 98.35 |
| LC84-443-glass | 45 | 75.73 | 0.15 | 12.24 | 0.64 | 0.04 | 0.15 | 0.80 | 3.65 | 4.21 | 0.08 | MDL | 97.70 |
| LC84-443-glass | 46 | 75.96 | 0.16 | 12.27 | 0.77 | 0.07 | 0.14 | 0.81 | 3.62 | 4.09 | 0.07 | MDL | 97.95 |
| LC84-443-glass | 47 | 76.65 | 0.12 | 12.39 | 0.72 | 0.03 | 0.14 | 0.78 | 3.59 | 4.11 | 0.07 | MDL | 98.59 |
| LC84-443-glass | 48 | 76.73 | 0.17 | 12.27 | 0.70 | 0.01 | 0.14 | 0.80 | 3.96 | 4.12 | 0.07 | MDL | 98.97 |
| LC84-443-glass | 49 | 76.20 | 0.15 | 12.15 | 0.73 | 0.02 | 0.13 | 0.78 | 3.91 | 4.31 | 0.07 | MDL | 98.43 |
| LC84-443-glass | 50 | 76.29 | 0.15 | 11.97 | 0.65 | 0.03 | 0.14 | 0.80 | 3.74 | 4.11 | 0.07 | MDL | 97.94 |
| LC84-443-glass | 51 | 76.56 | 0.15 | 12.31 | 0.68 | 0.02 | 0.14 | 0.79 | 3.53 | 4.13 | 0.07 | MDL | 98.39 |
| LC84-443-glass | 52 | 76.96 | 0.16 | 11.91 | 0.73 | 0.04 | 0.14 | 0.79 | 3.82 | 4.22 | 0.07 | MDL | 98.83 |
| LC84-443-glass | 53 | 75.53 | 0.15 | 11.99 | 0.68 | 0.02 | 0.12 | 0.78 | 4.03 | 3.94 | 0.07 | MDL | 97.33 |
| LC84-443-glass | 54 | 76.68 | 0.15 | 12.03 | 0.70 | 0.05 | 0.14 | 0.77 | 3.55 | 3.97 | 0.07 | MDL | 98.11 |
| | | | | | | | | | | | | | |
| LC84-434-glass | 55 | 76.65 | 0.13 | 12.18 | 0.91 | 0.03 | 0.09 | 0.32 | 2.66 | 5.82 | 0.04 | MDL | 98.83 |
| LC84-434-glass | 56 | 75.38 | 0.16 | 12.19 | 1.00 | 0.04 | 0.09 | 0.29 | 2.24 | 5.64 | 0.03 | MDL | 97.06 |
| LC84-434-glass | 57 | 74.92 | 0.19 | 12.20 | 0.64 | 0.01 | 0.06 | 0.38 | 3.14 | 5.48 | 0.02 | MDL | 97.04 |
| LC84-434-glass | 58 | 76.93 | 0.23 | 10.69 | 0.71 | MDL | 0.07 | 0.14 | 2.79 | 5.58 | 0.04 | MDL | 97.17 |
| LC84-434-glass | 59 | 78.84 | 0.10 | 11.98 | 0.44 | 0.02 | 0.15 | 1.70 | 4.55 | 1.49 | MDL | MDL | 99.28 |
| LC84-434-glass | 60 | 77.37 | 0.21 | 12.26 | 0.46 | MDL | 0.04 | 0.67 | 3.59 | 4.65 | 0.03 | MDL | 99.27 |
| LC84-434-glass | 61 | 78.98 | 0.13 | 11.91 | 0.20 | 0.01 | 0.03 | 1.40 | 4.00 | 2.33 | 0.01 | 0.01 | 99.00 |
| LC84-434-glass | 62 | 77.23 | 0.10 | 11.62 | 0.26 | MDL | 0.06 | 0.37 | 2.97 | 5.61 | 0.02 | 0.02 | 98.25 |
| LC84-434-glass | 63 | 78.95 | 0.24 | 10.56 | 0.92 | 0.02 | 0.11 | 0.71 | 3.37 | 4.16 | 0.02 | 0.02 | 99.08 |

**Appendix B, continued.**

| Sample | line | $SiO_2$ | $TiO_2$ | $Al_2O_3$ | $FeO^*$ | MnO | MgO | CaO | $Na_2O$ | $K_2O$ | Cl | $SO_3$ | Total |
|---|---|---|---|---|---|---|---|---|---|---|---|---|---|
| ChaosD-glass | 64 | 72.64 | 0.02 | 11.22 | 0.57 | 0.04 | 0.34 | 1.00 | 3.04 | 3.99 | 0.12 | 0.11 | 93.09 |
| ChaosD-glass | 65 | 74.65 | 0.12 | 11.86 | 0.25 | 0.03 | 0.05 | 1.31 | 4.01 | 3.33 | 0.10 | 0.05 | 95.76 |
| ChaosD-glass | 66 | 75.28 | MDL | 14.00 | 0.33 | MDL | 0.00 | 1.99 | 4.63 | 3.10 | 0.02 | MDL | 99.36 |
| ChaosD-glass | 67 | 73.98 | 0.12 | 9.54 | 0.57 | 0.04 | 0.00 | 0.79 | 2.63 | 3.17 | 0.16 | 0.02 | 91.02 |
| ChaosD-glass | 68 | 79.71 | 0.08 | 11.03 | 0.59 | MDL | 0.08 | 0.42 | 3.10 | 4.76 | 0.04 | MDL | 99.81 |
| ChaosD-glass | 69 | 76.85 | 0.06 | 9.60 | 0.16 | 0.03 | 0.02 | 0.47 | 2.58 | 3.79 | 0.13 | 0.11 | 93.81 |
| ChaosD-glass | 70 | 76.53 | 0.03 | 10.45 | 0.21 | MDL | 0.01 | 1.01 | 3.33 | 3.12 | 0.10 | MDL | 94.80 |
| ChaosD-glass | 71 | 73.03 | MDL | 13.44 | 0.11 | MDL | 0.01 | 1.38 | 3.97 | 4.05 | 0.06 | MDL | 96.04 |
| ChaosD-glass | 72 | 72.27 | 0.02 | 12.94 | 0.21 | MDL | 0.00 | 0.65 | 4.31 | 5.62 | 0.09 | MDL | 96.11 |
| ChaosD-glass | 73 | 70.62 | 0.08 | 12.50 | 0.61 | MDL | 0.25 | 0.61 | 3.96 | 5.38 | 0.11 | MDL | 94.13 |
| ChaosD-glass | 74 | 76.70 | MDL | 12.99 | 0.23 | 0.03 | 0.00 | 1.70 | 4.91 | 2.78 | 0.06 | 0.07 | 99.46 |
| ChaosD-glass | 75 | 77.58 | 0.07 | 11.44 | 0.11 | 0.01 | 0.06 | 0.59 | 4.07 | 4.87 | 0.11 | 0.12 | 99.02 |
| ChaosD-glass | 76 | 76.90 | 0.01 | 11.14 | 0.60 | 0.07 | 0.11 | 0.85 | 3.73 | 4.30 | 0.07 | MDL | 97.79 |
| ChaosD-glass | 77 | 78.00 | 0.07 | 11.27 | 0.43 | 0.08 | 0.24 | 0.56 | 2.83 | 4.41 | 0.06 | MDL | 97.96 |
| ChaosD-glass | 78 | 77.41 | 0.06 | 10.02 | 0.11 | MDL | 0.07 | 0.57 | 2.90 | 3.75 | 0.15 | MDL | 95.05 |
| ChaosD-glass | 79 | 74.29 | 0.04 | 12.94 | 0.19 | MDL | 0.00 | 1.32 | 4.17 | 3.79 | 0.10 | MDL | 96.84 |
| ChaosD-glass | 80 | 74.42 | 0.03 | 13.79 | 0.11 | 0.02 | 0.02 | 0.88 | 4.57 | 5.08 | 0.06 | 0.02 | 99.00 |
| ChaosD-glass | 81 | 72.63 | 0.02 | 15.01 | 0.28 | 0.08 | 0.15 | 0.51 | 4.28 | 6.92 | 0.03 | 0.01 | 99.92 |
| ChaosD-glass | 82 | 78.60 | 0.08 | 10.02 | 0.14 | 0.02 | 0.00 | 0.35 | 2.29 | 4.93 | 0.07 | 0.06 | 96.55 |
| ChaosD-glass | 83 | 72.54 | 0.14 | 15.40 | 0.24 | MDL | 0.01 | 1.60 | 4.43 | 4.44 | 0.03 | 0.03 | 98.86 |
| ChaosD-glass | 84 | 75.69 | 0.27 | 13.37 | 0.36 | MDL | 0.00 | 0.53 | 3.83 | 5.88 | 0.01 | 0.04 | 99.98 |
| ChaosD-glass | 85 | 72.94 | 0.14 | 12.13 | 0.32 | 0.04 | 0.08 | 0.52 | 2.83 | 5.84 | 0.14 | 0.26 | 95.24 |
| ChaosD-glass | 86 | 72.11 | 0.32 | 15.00 | 0.50 | MDL | 0.13 | 0.53 | 3.95 | 6.71 | 0.02 | 0.03 | 99.31 |
| ChaosD-glass | 87 | 76.09 | 0.02 | 9.45 | 0.22 | MDL | 0.00 | 0.57 | 2.86 | 3.03 | 0.03 | MDL | 92.28 |
| ChaosD-glass | 88 | 73.08 | 0.16 | 12.74 | 0.23 | MDL | 0.06 | 0.50 | 2.95 | 5.35 | 0.05 | 0.01 | 95.14 |
| ChaosD-glass | 89 | 77.60 | 0.06 | 8.62 | 0.20 | 0.07 | 0.01 | 0.47 | 2.54 | 2.99 | 0.04 | 0.01 | 92.61 |
| ChaosD-glass | 90 | 77.81 | 0.03 | 9.18 | 0.15 | MDL | 0.00 | 0.66 | 3.71 | 2.67 | 0.02 | 0.02 | 94.24 |
| ChaosD-glass | 91 | 77.95 | MDL | 11.80 | 0.06 | MDL | 0.00 | 1.69 | 4.19 | 1.54 | MDL | MDL | 97.25 |
| ChaosD-glass | 92 | 78.21 | 0.03 | 11.36 | 0.17 | 0.05 | 0.00 | 0.53 | 3.88 | 4.10 | MDL | MDL | 98.32 |
| ChaosD-glass | 93 | 78.83 | 0.11 | 10.05 | 0.24 | 0.05 | 0.00 | 0.85 | 3.16 | 2.77 | 0.02 | MDL | 96.07 |
| ChaosD-glass | 94 | 76.84 | MDL | 12.54 | 0.18 | 0.05 | 0.00 | 1.04 | 4.50 | 3.00 | 0.02 | MDL | 98.16 |
| ChaosD-glass | 95 | 74.47 | 0.03 | 13.73 | 0.19 | 0.04 | 0.00 | 0.87 | 4.45 | 4.50 | MDL | MDL | 98.30 |
| ChaosD-glass | 96 | 77.34 | 0.02 | 11.20 | 0.11 | MDL | 0.00 | 0.54 | 2.92 | 4.19 | 0.04 | MDL | 96.35 |
| ChaosD-glass | 97 | 74.34 | 0.01 | 12.97 | 0.03 | 0.10 | 0.00 | 1.44 | 3.68 | 2.76 | MDL | 0.02 | 95.37 |
| ChaosD-glass | 98 | 72.88 | 0.07 | 12.27 | 0.37 | MDL | 0.03 | 1.04 | 4.42 | 2.96 | 0.02 | MDL | 94.06 |
| ChaosD-glass | 99 | 72.00 | 0.03 | 14.14 | 0.24 | MDL | 0.05 | 0.75 | 4.15 | 5.03 | 0.02 | MDL | 96.39 |
| ChaosD-glass | 100 | 74.71 | 0.11 | 12.67 | 0.39 | MDL | 0.16 | 0.99 | 5.02 | 3.17 | 0.02 | MDL | 97.24 |
| ChaosD-glass | 101 | 73.25 | 0.21 | 12.74 | 0.46 | 0.11 | 0.22 | 0.55 | 3.75 | 5.21 | MDL | MDL | 96.51 |
| ChaosD-glass | 102 | 77.44 | 0.10 | 9.23 | 0.89 | 0.01 | 0.05 | 0.31 | 2.73 | 3.75 | 0.02 | MDL | 94.52 |
| ChaosD-glass | 103 | 70.30 | 0.17 | 14.26 | 0.41 | MDL | 0.07 | 0.53 | 4.36 | 6.33 | 0.04 | MDL | 96.46 |
| ChaosD-glass | 104 | 73.99 | 0.06 | 13.00 | 0.04 | 0.07 | 0.00 | 1.60 | 3.34 | 2.78 | 0.02 | MDL | 94.91 |
| ChaosD-glass | 105 | 74.56 | 0.04 | 9.91 | 0.04 | 0.04 | 0.00 | 0.40 | 2.70 | 3.94 | 0.11 | MDL | 91.74 |
| ChaosD-glass | 106 | 70.16 | 0.33 | 12.19 | 0.80 | MDL | 0.19 | 0.35 | 3.09 | 5.35 | 0.04 | MDL | 92.50 |
| ChaosD-glass | 107 | 74.28 | 0.04 | 11.13 | 0.24 | MDL | 0.06 | 0.74 | 3.15 | 3.75 | 0.03 | 0.05 | 93.47 |

**Appendix B, continued.**

| Sample | line | $SiO_2$ | $TiO_2$ | $Al_2O_3$ | $FeO^*$ | MnO | MgO | CaO | $Na_2O$ | $K_2O$ | Cl | $SO_3$ | Total |
|---|---|---|---|---|---|---|---|---|---|---|---|---|---|
| ChaosD-glass | 108 | 71.40 | MDL | 15.36 | 0.15 | MDL | 0.03 | 1.80 | 5.11 | 3.74 | MDL | 0.03 | 97.62 |
| ChaosD-glass | 109 | 72.58 | 0.08 | 13.95 | 0.15 | 0.07 | 0.00 | 0.46 | 4.01 | 6.26 | 0.02 | MDL | 97.58 |
| ChaosD-glass | 110 | 75.97 | 0.08 | 8.57 | 0.20 | MDL | 0.09 | 0.40 | 2.30 | 3.54 | 0.02 | 0.03 | 91.21 |
| ChaosD-glass | 111 | 78.92 | 0.27 | 9.92 | 0.42 | 0.02 | 0.01 | 0.49 | 3.35 | 4.24 | MDL | MDL | 97.65 |
| ChaosD-glass | 112 | 77.53 | 0.12 | 10.34 | 0.39 | MDL | 0.11 | 0.22 | 2.56 | 5.26 | 0.03 | MDL | 96.56 |
| ChaosD-glass | 113 | 75.41 | 0.13 | 11.50 | 0.54 | MDL | 0.36 | 0.76 | 3.23 | 4.25 | 0.02 | MDL | 96.20 |
| ChaosD-glass | 114 | 79.78 | 0.06 | 10.22 | 0.27 | MDL | 0.00 | 0.56 | 3.43 | 3.69 | 0.02 | MDL | 98.02 |
| ChaosD-glass | 115 | 76.13 | 0.06 | 10.88 | 0.13 | MDL | 0.04 | 0.45 | 3.71 | 4.27 | 0.03 | MDL | 95.71 |
| ChaosD-glass | 116 | 72.47 | 0.04 | 14.62 | 0.28 | 0.07 | 0.00 | 1.73 | 4.74 | 3.10 | 0.03 | 0.02 | 97.11 |
| ChaosD-glass | 117 | 76.89 | 0.03 | 12.10 | 0.20 | MDL | 0.00 | 1.02 | 4.18 | 3.19 | 0.01 | MDL | 97.64 |
| ChaosD-glass | 118 | 73.43 | 0.12 | 12.34 | 0.38 | MDL | 0.03 | 0.45 | 3.32 | 5.59 | 0.01 | MDL | 95.69 |
| ChaosD-glass | 119 | 77.21 | 0.02 | 11.74 | 0.21 | 0.02 | 0.03 | 0.86 | 4.28 | 3.99 | MDL | 0.01 | 98.38 |
| ChaosD-glass | 120 | 74.02 | 0.05 | 9.90 | 0.22 | 0.02 | 0.07 | 1.46 | 3.43 | 1.75 | 0.15 | MDL | 91.07 |
| ChaosD-glass | 121 | 72.57 | 0.08 | 14.53 | 0.41 | 0.06 | 0.00 | 2.48 | 4.41 | 2.62 | MDL | 0.04 | 97.22 |
| ChaosD-glass | 122 | 72.99 | 0.09 | 13.92 | 1.19 | MDL | 0.04 | 1.13 | 3.37 | 4.32 | 0.02 | 0.13 | 97.20 |
| ChaosD-glass | 123 | 78.05 | MDL | 11.03 | 0.11 | 0.01 | 0.00 | 0.76 | 3.56 | 3.43 | 0.04 | MDL | 97.00 |
| ChaosD-glass | 124 | 76.09 | MDL | 13.28 | 0.18 | MDL | 0.00 | 1.36 | 4.27 | 3.26 | MDL | MDL | 98.45 |
| ChaosD-glass | 125 | 72.96 | 0.17 | 10.63 | 0.40 | 0.05 | 0.08 | 0.40 | 3.23 | 4.68 | 0.06 | MDL | 92.66 |
| ChaosD-glass | 126 | 76.70 | MDL | 11.14 | 0.26 | MDL | 0.04 | 0.81 | 2.88 | 3.89 | 0.02 | MDL | 95.75 |
| ChaosD-glass | 127 | 74.60 | 0.06 | 12.49 | 0.14 | MDL | 0.02 | 0.76 | 2.98 | 4.36 | 0.10 | 0.03 | 95.54 |
| ChaosD-glass | 128 | 78.58 | 0.04 | 10.00 | 0.49 | 0.05 | 0.07 | 0.32 | 2.45 | 5.20 | 0.12 | MDL | 97.32 |
| ChaosD-glass | 129 | 76.61 | MDL | 11.95 | 0.16 | MDL | 0.00 | 1.72 | 5.11 | 1.98 | 0.03 | MDL | 97.57 |
| ChaosD-glass | 130 | 76.64 | 0.06 | 11.70 | 0.21 | MDL | 0.04 | 0.48 | 3.06 | 5.27 | 0.05 | 0.07 | 97.58 |
| ChaosD-glass | 131 | 71.81 | 0.04 | 8.45 | 0.18 | 0.01 | 0.05 | 0.45 | 1.82 | 3.66 | 0.17 | 0.02 | 86.67 |
| ChaosD-glass | 132 | 79.62 | 0.09 | 10.41 | 0.57 | 0.02 | 0.52 | 0.76 | 3.35 | 3.50 | 0.05 | MDL | 98.91 |
| ChaosD-glass | 133 | 79.76 | 0.08 | 11.25 | 0.22 | MDL | 0.09 | 1.29 | 3.15 | 3.19 | 0.06 | MDL | 99.08 |
| ChaosD-glass | 134 | 71.07 | MDL | 12.91 | 0.23 | 0.07 | 0.01 | 1.20 | 4.88 | 3.78 | 0.08 | MDL | 94.23 |
| ChaosD-glass | 135 | 73.95 | 0.05 | 14.38 | 0.25 | 0.05 | 0.01 | 2.03 | 5.04 | 3.69 | 0.10 | 0.02 | 99.56 |
| ChaosD-glass | 136 | 77.74 | 0.04 | 10.05 | 0.20 | 0.01 | 0.10 | 0.59 | 3.17 | 3.83 | 0.13 | 0.06 | 95.91 |
| ChaosD-glass | 137 | 73.72 | 0.02 | 13.82 | 0.19 | 0.03 | 0.01 | 0.61 | 4.42 | 5.08 | 0.08 | 0.03 | 98.02 |
| ChaosD-glass | 138 | 73.22 | 0.14 | 14.80 | 0.25 | MDL | 0.00 | 1.79 | 4.66 | 3.71 | 0.02 | MDL | 98.58 |
| ChaosD-glass | 139 | 76.01 | 0.02 | 13.16 | 0.07 | MDL | 0.00 | 0.41 | 3.65 | 6.17 | 0.06 | 0.01 | 99.55 |
| ChaosD-glass | 140 | 75.28 | MDL | 12.52 | 0.27 | 0.05 | 0.00 | 0.52 | 3.50 | 5.08 | 0.09 | 0.02 | 97.32 |
| ChaosD-glass | 141 | 71.41 | 0.11 | 14.06 | 0.73 | 0.02 | 0.07 | 0.66 | 4.85 | 5.89 | 0.09 | 0.02 | 97.89 |
| ChaosD-glass | 142 | 73.44 | 0.10 | 14.97 | 0.17 | MDL | 0.17 | 0.56 | 3.74 | 6.68 | 0.03 | 0.11 | 99.95 |
| ChaosD-glass | 143 | 70.30 | 0.08 | 15.96 | 0.20 | 0.02 | 0.07 | 1.08 | 4.64 | 5.90 | 0.10 | 0.02 | 98.35 |
| ChaosD-glass | 144 | 71.47 | 0.14 | 14.98 | 1.36 | MDL | 0.31 | 1.02 | 4.88 | 5.18 | MDL | 0.07 | 99.42 |
| ChaosD-glass | 145 | 73.70 | 0.03 | 9.52 | 0.22 | MDL | 0.05 | 0.69 | 3.53 | 2.96 | 0.02 | MDL | 90.72 |

**Appendix B, continued.**

| Sample | line | $SiO_2$ | $TiO_2$ | $Al_2O_3$ | $FeO^*$ | MnO | MgO | CaO | $Na_2O$ | $K_2O$ | Cl | $SO_3$ | Total |
|---|---|---|---|---|---|---|---|---|---|---|---|---|---|
| LC84-433-glass | 146 | 77.16 | 0.28 | 11.54 | 0.83 | 0.04 | 0.06 | 0.69 | 3.50 | 4.46 | 0.08 | MDL | 98.64 |
| LC84-433-glass | 147 | 77.92 | 0.31 | 10.99 | 0.90 | 0.04 | 0.06 | 0.41 | 3.52 | 4.57 | 0.09 | MDL | 98.82 |
| LC84-433-glass | 148 | 75.57 | 0.23 | 12.44 | 0.81 | 0.02 | 0.05 | 0.96 | 4.03 | 4.14 | 0.08 | 0.01 | 98.35 |
| LC84-433-glass | 149 | 76.31 | 0.27 | 12.35 | 1.01 | 0.03 | 0.14 | 0.95 | 3.83 | 4.08 | 0.07 | MDL | 99.04 |
| LC84-433-glass | 150 | 77.28 | 0.22 | 11.77 | 0.86 | 0.03 | 0.06 | 0.68 | 3.99 | 4.25 | 0.08 | MDL | 99.22 |
| LC84-433-glass | 151 | 77.34 | 0.25 | 10.79 | 0.85 | 0.02 | 0.06 | 0.41 | 3.47 | 4.67 | 0.09 | MDL | 97.96 |
| LC84-433-glass | 152 | 76.45 | 0.28 | 11.31 | 0.84 | 0.02 | 0.06 | 0.47 | 3.29 | 4.74 | 0.08 | MDL | 97.55 |
| LC84-433-glass | 153 | 77.23 | 0.27 | 11.13 | 0.86 | 0.04 | 0.08 | 0.43 | 3.66 | 4.61 | 0.09 | MDL | 98.41 |
| LC84-433-glass | 154 | 76.05 | 0.27 | 12.09 | 0.83 | 0.02 | 0.06 | 0.70 | 3.90 | 4.38 | 0.08 | MDL | 98.38 |
| LC84-433-glass | 155 | 77.46 | 0.30 | 11.34 | 1.00 | 0.03 | 0.06 | 0.42 | 3.26 | 4.66 | 0.09 | MDL | 98.64 |
| | | | | | | | | | | | | | |
| LC84-455-glass | 156 | 79.15 | 0.25 | 11.00 | 0.80 | 0.02 | 0.05 | 0.40 | 3.16 | 4.88 | 0.06 | MDL | 99.79 |
| LC84-455-glass | 157 | 77.03 | 0.22 | 11.31 | 0.81 | 0.03 | 0.07 | 0.48 | 3.56 | 4.86 | 0.08 | MDL | 98.46 |
| LC84-455-glass | 158 | 77.39 | 0.29 | 11.00 | 0.95 | 0.03 | 0.06 | 0.30 | 3.22 | 5.08 | 0.09 | MDL | 98.41 |
| LC84-455-glass | 159 | 76.72 | 0.23 | 11.72 | 0.83 | 0.03 | 0.10 | 0.61 | 3.79 | 4.74 | 0.05 | MDL | 98.82 |
| LC84-455-glass | 160 | 77.40 | 0.25 | 11.02 | 0.81 | 0.04 | 0.06 | 0.28 | 3.14 | 5.18 | 0.08 | MDL | 98.27 |
| LC84-455-glass | 161 | 78.15 | 0.25 | 11.06 | 0.83 | 0.02 | 0.06 | 0.31 | 2.99 | 5.17 | 0.08 | MDL | 98.90 |
| LC84-455-glass | 162 | 77.33 | 0.25 | 11.02 | 0.89 | 0.02 | 0.04 | 0.28 | 3.01 | 4.79 | 0.09 | MDL | 97.72 |
| LC84-455-glass | 163 | 77.03 | 0.32 | 10.98 | 1.34 | 0.03 | 0.07 | 0.30 | 2.98 | 4.97 | 0.08 | MDL | 98.11 |
| LC84-455-glass | 164 | 78.14 | 0.27 | 11.46 | 0.68 | 0.01 | 0.04 | 0.45 | 3.08 | 5.14 | 0.08 | 0.01 | 99.36 |
| LC84-455-glass | 165 | 78.08 | 0.25 | 11.05 | 1.08 | 0.04 | 0.22 | 0.30 | 3.29 | 5.05 | 0.06 | MDL | 99.42 |
| LC84-455-glass | 166 | 76.69 | 0.25 | 11.68 | 0.82 | 0.02 | 0.08 | 0.42 | 3.28 | 4.98 | 0.07 | MDL | 98.31 |
| LC84-455-glass | 167 | 76.96 | 0.32 | 11.47 | 1.16 | 0.04 | 0.15 | 0.41 | 3.32 | 4.81 | 0.08 | 0.01 | 98.73 |
| LC84-455-glass | 168 | 76.81 | 0.26 | 11.92 | 0.86 | 0.03 | 0.09 | 0.57 | 3.34 | 4.87 | 0.08 | MDL | 98.84 |
| LC84-455-glass | 169 | 76.35 | 0.27 | 11.74 | 0.83 | 0.02 | 0.04 | 0.47 | 3.43 | 5.18 | 0.08 | MDL | 98.42 |
| LC84-455-glass | 170 | 78.56 | 0.26 | 11.37 | 0.81 | 0.04 | 0.06 | 0.29 | 3.01 | 5.17 | 0.11 | MDL | 99.70 |
| LC84-455-glass | 171 | 75.80 | 0.24 | 11.71 | 0.87 | 0.03 | 0.11 | 0.61 | 3.92 | 4.67 | 0.08 | MDL | 98.04 |
| LC84-455-glass | 172 | 76.78 | 0.23 | 11.09 | 0.83 | 0.05 | 0.04 | 0.33 | 3.11 | 5.15 | 0.08 | MDL | 97.71 |

**Appendix C.** Melt inclusion thickness and Absorbance values.

| Melt Inclusion ("n" thickness measurements) | Average thickness (mm) | Absorbance ($H_2O$; 5200 $cm^{-1}$ peak) | Absorbance $OH^-$ ($OH^-$; 4500 $cm^{-1}$ peak) | Absorbance $CO_2$ ($CO_2$; 2350 $cm^{-1}$ peak) |
|---|---|---|---|---|
| LQ13-01-mi-01-02 (n=2) | 0.061 | 0.063 | 0.015 | 0.077 |
| LQ13-01-mi-02-01 (n=2) | 0.051 | 0.042 | 0.005 | 0.011 |
| LQ13-01-mi-03-01 (n=2) | 0.031 | 0.019 | 0.010 | 0.043 |
| LQ13-01-mi-04-01 (n=3) | 0.060 | 0.041 | 0.014 | 0.060 |
| LQ13-01-mi-04-02 (n=3) | 0.060 | 0.035 | 0.015 | 0.056 |
| LQ13-01-mi-05-01 (n=3) | 0.082 | 0.059 | 0.023 | 0.077 |
| LQ13-01-mi-06-01 (n=3) | 0.047 | 0.036 | 0.018 | 0.073 |
| LQ13-01-mi-07-01 (n=3) | 0.052 | 0.038 | 0.014 | 0.077 |
| LQ13-01-mi-07-02 (n=3) | 0.052 | 0.039 | 0.014 | 0.045 |
| LQ13-01-mi-07-03 (n=3) | 0.052 | 0.034 | 0.014 | 0.036 |
| LQ13-01-mi-10-03 (n=3) | 0.061 | 0.037 | 0.020 | 0.063 |
| LQ13-01-mi-11-01 (n=2) | 0.041 | 0.036 | 0.019 | 0.057 |
| LQ13-01-mi-12-01 (n=3) | 0.074 | 0.059 | 0.033 | 0.070 |
| LQ13-01-mi-13-01 (n=3) | 0.055 | 0.044 | 0.018 | 0.052 |
| LQ13-01-mi-14-01 (n=2) | 0.083 | 0.065 | 0.028 | 0.099 |
| LQ13-01-mi-14-02 (n=2) | 0.083 | 0.057 | 0.023 | 0.030 |
| LQ13-01-mi-14-03 (n=2) | 0.083 | 0.045 | 0.024 | 0.037 |
| LQ13-01-mi-15-01 (n=3) | 0.059 | 0.045 | 0.018 | 0.088 |
| LQ13-01-mi-16-01 (n=3) | 0.068 | 0.051 | 0.023 | 0.084 |
| LQ13-01-mi-17-01 (n=3) | 0.083 | 0.064 | 0.023 | 0.064 |
| LQ13-01-mi-18-01 (n=3) | 0.072 | 0.049 | 0.018 | 0.063 |
| LQ13-01-mi-18-02 (n=3) | 0.072 | 0.053 | 0.020 | 0.080 |
| LQ13-01-mi-19-02 (n=3) | 0.085 | 0.058 | 0.023 | 0.060 |
| LQ13-01-mi-20-01 (n=3) | 0.082 | 0.060 | 0.022 | 0.137 |
| LQ13-01-mi-21-01 (n=3) | 0.072 | 0.050 | 0.020 | 0.123 |
| LQ13-01-mi-23-02 (n=3) | 0.072 | 0.054 | 0.019 | 0.102 |

**Appendix C, continued.**

| Melt Inclusion ("n" thickness measurements) | Average thickness (mm) | Absorbance ($H_2O$; 5200 $cm^{-1}$ peak) | Absorbance $OH^-$ ($OH^-$; 4500 $cm^{-1}$ peak) | Absorbance $CO_2$ ($CO_2$; 2350 $cm^{-1}$ peak) |
|---|---|---|---|---|
| LQ13-01-mi-23-03 (n=3) | 0.072 | 0.050 | 0.022 | 0.094 |
| LQ13-01-mi-24-01 (n=3) | 0.094 | 0.064 | 0.023 | 0.056 |
| LQ13-01-mi-25-01 (n=3) | 0.079 | 0.050 | 0.018 | 0.017 |
| LQ13-01-mi-26-02 (n=3) | 0.070 | 0.048 | 0.018 | 0.069 |
| LQ13-01-mi-27-01 (n=3) | 0.069 | 0.075 | 0.018 | 0.047 |
| LQ13-01-mi-28-01 (n=3) | 0.047 | 0.029 | 0.011 | 0.048 |
| LQ13-01-mi-28-02 (n=3) | 0.047 | 0.033 | 0.012 | 0.084 |
| LQ13-01-mi-29-01 (n=3) | 0.074 | 0.047 | 0.017 | 0.058 |
| LQ13-01-mi-01-01-leak (n=2) | 0.061 | 0.018 | 0.013 | 0.011 |
| LQ13-01-mi-02-02-leak (n=2) | 0.051 | 0.029 | 0.000 | 0.026 |
| LQ13-01-mi-10-01-leak (n=3) | 0.061 | 0.015 | 0.020 | 0.000 |
| LQ13-01-mi-15-02-leak (n=3) | 0.059 | 0.015 | 0.008 | 0.014 |
| LQ13-01-mi-18-03-leak (n=3) | 0.072 | 0.027 | 0.011 | 0.019 |
| LQ13-01-mi-19-01-leak (n=3) | 0.085 | 0.026 | 0.010 | 0.061 |
| LQ13-01-mi-24-02-leak (n=3) | 0.094 | 0.016 | 0.005 | 0.022 |
| LQ13-01-mi-26-01-leak (n=3) | 0.070 | 0.027 | 0.011 | 0.007 |

**Appendix D.** Raw individual melt inclusion glass compositions (wt. %) as determined by EPMA.

| | line | $SiO_2$ | $TiO_2$ | $Al_2O_3$ | $FeO^*$ | MnO | MgO | CaO | $Na_2O$ | $K_2O$ | Cl | $SO_3$ | Total |
|---|---|---|---|---|---|---|---|---|---|---|---|---|---|
| LQ13-01-mi-01-02-glass | 1 | 77.07 | 0.09 | 11.99 | 0.64 | MDL | 0.15 | 0.83 | 3.36 | 4.20 | 0.10 | MDL | 98.44 |
| LQ13-01-mi-01-02-glass | 2 | 75.60 | 0.12 | 12.02 | 0.69 | 0.05 | 0.12 | 0.81 | 3.48 | 4.13 | 0.09 | 0.03 | 97.15 |
| LQ13-01-mi-01-02-glass | 3 | 75.09 | 0.13 | 12.03 | 0.53 | MDL | 0.14 | 0.79 | 3.10 | 4.26 | 0.13 | MDL | 96.20 |
| LQ13-01-mi-02-01-glass | 4 | 75.64 | 0.07 | 12.09 | 0.63 | 0.04 | 0.12 | 0.73 | 3.29 | 4.17 | 0.08 | MDL | 96.85 |
| LQ13-01-mi-02-01-glass | 5 | 77.44 | 0.15 | 11.78 | 0.86 | MDL | 0.14 | 0.76 | 3.10 | 4.17 | 0.08 | 0.03 | 98.50 |
| LQ13-01-mi-02-01-glass | 6 | 77.47 | 0.11 | 11.93 | 0.75 | 0.01 | 0.13 | 0.73 | 3.29 | 4.26 | 0.08 | MDL | 98.75 |
| LQ13-01-mi-02-01-glass | 7 | 77.96 | 0.14 | 12.02 | 0.88 | 0.06 | 0.17 | 0.70 | 3.40 | 4.40 | 0.10 | MDL | 99.82 |
| LQ13-01-mi-04-01-glass | 8 | 74.46 | 0.09 | 10.65 | 0.64 | MDL | 0.09 | 0.65 | 3.07 | 3.82 | 0.11 | MDL | 93.56 |
| LQ13-01-mi-04-01-glass | 9 | 73.50 | 0.10 | 10.66 | 0.55 | 0.06 | 0.11 | 0.60 | 2.72 | 3.79 | 0.12 | 0.04 | 92.24 |
| LQ13-01-mi-04-01-glass | 10 | 73.82 | 0.07 | 10.73 | 0.57 | 0.01 | 0.08 | 0.70 | 3.01 | 3.86 | 0.09 | MDL | 92.94 |
| LQ13-01-mi-04-01-glass | 11 | 74.35 | 0.03 | 10.77 | 0.61 | 0.02 | 0.11 | 0.64 | 3.20 | 3.79 | 0.10 | 0.04 | 93.66 |
| LQ13-01-mi-04-02-glass | 12 | 75.03 | 0.12 | 10.55 | 0.72 | MDL | 0.05 | 0.63 | 3.20 | 3.81 | 0.09 | 0.01 | 94.22 |
| LQ13-01-mi-04-02-glass | 13 | 73.41 | 0.09 | 10.59 | 0.29 | MDL | 0.06 | 0.62 | 3.01 | 3.75 | 0.08 | MDL | 91.90 |
| LQ13-01-mi-04-02-glass | 14 | 73.63 | 0.04 | 10.80 | 0.72 | 0.07 | 0.09 | 0.68 | 2.99 | 3.78 | 0.10 | 0.09 | 92.99 |
| LQ13-01-mi-05-01-glass | 15 | 72.77 | 0.05 | 10.31 | 0.39 | 0.07 | 0.05 | 0.45 | 2.92 | 3.74 | 0.10 | MDL | 90.85 |
| LQ13-01-mi-05-01-glass | 16 | 74.48 | 0.08 | 10.31 | 0.46 | 0.03 | 0.06 | 0.53 | 3.00 | 3.69 | 0.11 | 0.02 | 92.76 |
| LQ13-01-mi-05-01-glass | 17 | 73.28 | 0.07 | 10.70 | 0.55 | 0.05 | 0.05 | 0.52 | 3.29 | 3.85 | 0.10 | 0.08 | 92.53 |
| LQ13-01-mi-05-01-glass | 18 | 72.20 | 0.08 | 10.74 | 0.58 | 0.05 | 0.05 | 0.54 | 3.05 | 3.79 | 0.12 | 0.03 | 91.23 |
| LQ13-01-mi-05-01-glass | 19 | 75.82 | 0.06 | 10.56 | 0.50 | 0.05 | MDL | 0.53 | 3.28 | 3.79 | 0.10 | MDL | 94.70 |
| LQ13-01-mi-05-01-glass | 20 | 75.53 | 0.10 | 10.40 | 0.62 | 0.05 | 0.04 | 0.49 | 3.13 | 3.75 | 0.09 | 0.02 | 94.22 |
| LQ13-01-mi-06-01-glass | 21 | 74.71 | 0.07 | 11.18 | 0.40 | 0.05 | 0.11 | 0.69 | 3.61 | 3.84 | 0.12 | 0.09 | 94.87 |
| LQ13-01-mi-06-01-glass | 22 | 73.69 | 0.08 | 10.85 | 0.52 | 0.03 | 0.06 | 0.68 | 2.97 | 3.88 | 0.13 | MDL | 92.90 |
| LQ13-01-mi-06-01-glass | 23 | 74.76 | 0.10 | 10.93 | 0.66 | 0.06 | 0.04 | 0.64 | 3.32 | 3.82 | 0.08 | 0.03 | 94.46 |
| LQ13-01-mi-06-01-glass | 24 | 73.25 | 0.07 | 10.81 | 0.41 | 0.07 | 0.07 | 0.72 | 3.14 | 3.88 | 0.08 | MDL | 92.50 |
| LQ13-01-mi-06-01-glass | 25 | 74.21 | 0.09 | 11.03 | 0.54 | 0.01 | 0.08 | 0.70 | 3.34 | 3.89 | 0.10 | MDL | 94.00 |
| LQ13-01-mi-07-01-glass | 26 | 73.90 | 0.02 | 11.11 | 0.57 | 0.08 | 0.07 | 0.59 | 3.23 | 3.87 | 0.10 | MDL | 93.55 |
| LQ13-01-mi-07-01-glass | 27 | 76.01 | 0.09 | 10.88 | 0.53 | 0.01 | 0.06 | 0.61 | 3.27 | 3.88 | 0.10 | MDL | 95.46 |
| LQ13-01-mi-07-01-glass | 28 | 74.25 | 0.08 | 10.96 | 0.57 | MDL | 0.04 | 0.62 | 3.17 | 3.87 | 0.11 | MDL | 93.68 |
| LQ13-01-mi-07-01-glass | 29 | 73.98 | 0.08 | 11.21 | 0.40 | MDL | 0.05 | 0.61 | 3.47 | 3.85 | 0.11 | MDL | 93.75 |
| LQ13-01-mi-07-01-glass | 30 | 73.99 | 0.10 | 10.70 | 0.67 | MDL | 0.11 | 0.60 | 3.36 | 3.85 | 0.10 | 0.06 | 93.55 |
| LQ13-01-mi-07-02-glass | 31 | 71.87 | 0.07 | 10.77 | 1.15 | 0.01 | 0.13 | 0.54 | 3.03 | 3.81 | 0.10 | 0.02 | 91.50 |
| LQ13-01-mi-07-02-glass | 32 | 73.94 | 0.05 | 10.88 | 0.51 | MDL | 0.05 | 0.54 | 3.02 | 3.84 | 0.13 | MDL | 92.98 |
| LQ13-01-mi-07-02-glass | 33 | 75.47 | 0.07 | 10.99 | 0.66 | 0.04 | 0.04 | 0.58 | 3.15 | 3.94 | 0.11 | 0.04 | 95.10 |
| LQ13-01-mi-07-02-glass | 34 | 73.60 | 0.07 | 11.04 | 0.36 | MDL | 0.05 | 0.60 | 3.30 | 3.90 | 0.12 | 0.02 | 93.05 |
| LQ13-01-mi-07-02-glass | 35 | 73.72 | 0.09 | 11.09 | 0.48 | 0.02 | 0.03 | 0.58 | 2.99 | 3.89 | 0.08 | MDL | 92.99 |

**Appendix D, continued.**

| | line | $SiO_2$ | $TiO_2$ | $Al_2O_3$ | $FeO^*$ | MnO | MgO | CaO | $Na_2O$ | $K_2O$ | Cl | $SO_3$ | Total |
|---|---|---|---|---|---|---|---|---|---|---|---|---|---|
| LQ13-01-mi-07-03-glass | 36 | 72.71 | 0.05 | 10.92 | 0.67 | 0.05 | 0.05 | 0.60 | 3.13 | 3.88 | 0.09 | MDL | 92.16 |
| LQ13-01-mi-07-03-glass | 37 | 74.24 | 0.10 | 10.99 | 0.48 | 0.07 | 0.03 | 0.68 | 2.95 | 3.90 | 0.08 | MDL | 93.52 |
| LQ13-01-mi-07-03-glass | 38 | 72.71 | 0.09 | 11.01 | 0.51 | 0.09 | 0.04 | 0.56 | 3.11 | 3.86 | 0.08 | MDL | 92.08 |
| LQ13-01-mi-07-03-glass | 39 | 74.52 | 0.06 | 11.15 | 0.51 | 0.00 | 0.07 | 0.55 | 3.37 | 3.92 | 0.11 | 0.03 | 94.29 |
| LQ13-01-mi-07-03-glass | 40 | 72.75 | 0.07 | 10.94 | 0.64 | 0.05 | 0.07 | 0.56 | 3.03 | 3.82 | 0.09 | 0.08 | 92.11 |
| LQ13-01-mi-07-03-glass | 41 | 73.92 | 0.05 | 10.90 | 0.63 | 0.06 | 0.07 | 0.67 | 3.19 | 3.85 | 0.07 | 0.01 | 93.43 |
| LQ13-01-mi-11-01-glass | 42 | 75.78 | 0.10 | 10.92 | 0.60 | MDL | 0.07 | 0.66 | 3.30 | 3.79 | 0.11 | MDL | 95.33 |
| LQ13-01-mi-12-01-glass | 43 | 74.64 | 0.05 | 10.52 | 0.58 | MDL | 0.08 | 0.64 | 2.96 | 3.82 | 0.11 | MDL | 93.39 |
| LQ13-01-mi-12-01-glass | 44 | 73.93 | 0.12 | 11.02 | 0.51 | 0.04 | 0.03 | 0.70 | 2.97 | 3.86 | 0.10 | 0.06 | 93.35 |
| LQ13-01-mi-12-01-glass | 45 | 75.51 | 0.10 | 10.84 | 0.62 | 0.07 | 0.07 | 0.63 | 3.19 | 3.91 | 0.11 | 0.01 | 95.06 |
| LQ13-01-mi-12-01-glass | 46 | 74.88 | 0.07 | 10.84 | 0.52 | 0.04 | 0.07 | 0.64 | 2.92 | 3.89 | 0.09 | 0.09 | 94.04 |
| LQ13-01-mi-12-01-glass | 47 | 73.67 | 0.08 | 10.70 | 0.59 | 0.05 | 0.07 | 0.65 | 3.01 | 3.85 | 0.10 | 0.01 | 92.78 |
| LQ13-01-mi-12-01-glass | 48 | 73.17 | 0.08 | 10.54 | 0.50 | 0.01 | 0.10 | 0.63 | 2.88 | 3.78 | 0.11 | MDL | 91.82 |
| LQ13-01-mi-12-01-glass | 49 | 74.53 | 0.08 | 10.70 | 0.78 | 0.08 | 0.09 | 0.61 | 3.02 | 3.78 | 0.09 | 0.01 | 93.79 |
| LQ13-01-mi-13-01-glass | 50 | 75.30 | 0.06 | 10.60 | 0.34 | 0.04 | 0.04 | 0.53 | 3.06 | 3.77 | 0.09 | MDL | 93.83 |
| LQ13-01-mi-13-01-glass | 51 | 74.18 | 0.05 | 10.66 | 0.44 | 0.04 | 0.06 | 0.55 | 3.07 | 3.76 | 0.09 | MDL | 92.89 |
| LQ13-01-mi-13-01-glass | 52 | 75.57 | 0.05 | 10.70 | 0.53 | 0.14 | 0.10 | 0.57 | 3.12 | 3.82 | 0.11 | MDL | 94.70 |
| LQ13-01-mi-13-01-glass | 53 | 74.39 | 0.06 | 10.79 | 0.33 | 0.05 | 0.08 | 0.57 | 3.15 | 3.82 | 0.13 | MDL | 93.38 |
| LQ13-01-mi-13-01-glass | 54 | 74.47 | 0.09 | 10.58 | 0.47 | MDL | 0.05 | 0.54 | 3.31 | 3.75 | 0.09 | 0.03 | 93.38 |
| LQ13-01-mi-14-01-glass | 55 | 73.25 | 0.14 | 11.04 | 0.54 | 0.05 | 0.07 | 0.71 | 2.99 | 3.85 | 0.09 | MDL | 92.73 |
| LQ13-01-mi-14-01-glass | 56 | 75.12 | 0.09 | 11.26 | 0.55 | 0.08 | 0.07 | 0.63 | 3.18 | 3.87 | 0.12 | MDL | 94.97 |
| LQ13-01-mi-14-01-glass | 57 | 73.97 | 0.07 | 11.16 | 0.54 | 0.07 | 0.08 | 0.70 | 3.14 | 3.88 | 0.09 | 0.01 | 93.71 |
| LQ13-01-mi-14-01-glass | 58 | 74.30 | 0.15 | 11.09 | 0.37 | 0.04 | 0.02 | 0.74 | 2.84 | 3.84 | 0.15 | MDL | 93.53 |
| LQ13-01-mi-14-01-glass | 59 | 73.27 | 0.14 | 11.01 | 0.58 | 0.02 | 0.08 | 0.78 | 3.15 | 3.83 | 0.09 | 0.02 | 92.97 |
| LQ13-01-mi-14-01-glass | 60 | 74.17 | 0.10 | 10.91 | 0.59 | MDL | 0.07 | 0.67 | 2.86 | 3.79 | 0.09 | MDL | 93.25 |
| LQ13-01-mi-14-01-glass | 61 | 73.59 | 0.09 | 10.89 | 0.40 | 0.06 | 0.04 | 0.71 | 3.01 | 3.87 | 0.10 | MDL | 92.77 |
| LQ13-01-mi-14-03-glass | 62 | 72.99 | 0.08 | 10.96 | 0.51 | MDL | 0.08 | 0.56 | 2.97 | 3.93 | 0.09 | 0.05 | 92.22 |
| LQ13-01-mi-14-03-glass | 63 | 73.19 | 0.11 | 10.92 | 0.62 | MDL | 0.09 | 0.58 | 3.01 | 3.97 | 0.10 | MDL | 92.60 |
| LQ13-01-mi-14-03-glass | 64 | 72.19 | 0.10 | 10.91 | 0.42 | MDL | 0.07 | 0.62 | 2.96 | 3.93 | 0.08 | MDL | 91.30 |
| LQ13-01-mi-14-03-glass | 65 | 74.02 | 0.09 | 10.87 | 0.73 | MDL | 0.08 | 0.58 | 3.21 | 3.98 | 0.12 | MDL | 93.70 |
| LQ13-01-mi-14-03-glass | 66 | 72.95 | 0.08 | 11.05 | 0.47 | 0.01 | 0.02 | 0.61 | 3.11 | 3.95 | 0.10 | 0.02 | 92.37 |
| LQ13-01-mi-14-03-glass | 67 | 73.08 | 0.01 | 10.84 | 0.55 | 0.03 | 0.06 | 0.59 | 2.88 | 4.00 | 0.10 | 0.02 | 92.16 |
| LQ13-01-mi-14-03-glass | 68 | 73.15 | 0.10 | 11.03 | 0.49 | 0.07 | 0.05 | 0.63 | 2.98 | 3.88 | 0.10 | MDL | 92.50 |
| LQ13-01-mi-14-03-glass | 69 | 75.12 | 0.08 | 11.73 | 0.64 | 0.07 | 0.15 | 0.82 | 3.26 | 3.72 | 0.11 | MDL | 95.70 |
| LQ13-01-mi-14-03-glass | 70 | 74.38 | 0.16 | 11.70 | 0.55 | 0.05 | 0.17 | 0.79 | 3.34 | 3.80 | 0.07 | 0.02 | 95.05 |
| LQ13-01-mi-14-03-glass | 71 | 75.38 | 0.16 | 11.57 | 0.59 | 0.07 | 0.13 | 0.81 | 3.04 | 3.77 | 0.09 | 0.04 | 95.65 |
| LQ13-01-mi-14-03-glass | 72 | 74.31 | 0.10 | 11.41 | 0.66 | 0.08 | 0.08 | 0.82 | 3.20 | 3.78 | 0.09 | MDL | 94.53 |
| LQ13-01-mi-14-03-glass | 73 | 75.51 | 0.14 | 11.71 | 1.10 | 0.05 | 0.13 | 0.84 | 3.24 | 3.74 | 0.08 | 0.04 | 96.57 |
| LQ13-01-mi-14-03-glass | 74 | 73.89 | 0.11 | 11.34 | 0.85 | 0.01 | 0.08 | 0.84 | 3.35 | 3.69 | 0.08 | 0.06 | 94.29 |

**Appendix D, continued.**

| | line | $SiO_2$ | $TiO_2$ | $Al_2O_3$ | $FeO^*$ | MnO | MgO | CaO | $Na_2O$ | $K_2O$ | Cl | $SO_3$ | Total |
|---|---|---|---|---|---|---|---|---|---|---|---|---|---|
| LQ13-01-mi-15-01-glass | 75 | 74.51 | 0.08 | 10.93 | 0.45 | 0.02 | 0.05 | 0.65 | 3.22 | 3.82 | 0.11 | MDL | 93.83 |
| LQ13-01-mi-15-01-glass | 76 | 73.94 | 0.10 | 10.59 | 0.59 | MDL | 0.08 | 0.69 | 3.26 | 3.68 | 0.08 | MDL | 93.02 |
| LQ13-01-mi-15-01-glass | 77 | 74.15 | 0.11 | 11.05 | 0.78 | 0.03 | 0.07 | 0.67 | 3.02 | 3.86 | 0.12 | MDL | 93.85 |
| LQ13-01-mi-15-01-glass | 78 | 75.36 | 0.04 | 10.99 | 0.79 | 0.06 | 0.06 | 0.63 | 3.03 | 3.88 | 0.08 | MDL | 94.93 |
| LQ13-01-mi-16-01-glass | 79 | 73.27 | 0.10 | 11.14 | 0.43 | 0.02 | 0.08 | 0.67 | 2.17 | 3.81 | 0.06 | 0.06 | 91.79 |
| LQ13-01-mi-16-01-glass | 80 | 73.69 | 0.07 | 11.38 | 0.41 | MDL | 0.03 | 0.67 | 2.95 | 3.88 | 0.10 | MDL | 93.19 |
| LQ13-01-mi-16-01-glass | 81 | 73.89 | 0.10 | 10.93 | 1.00 | 0.03 | 0.12 | 0.74 | 2.98 | 3.88 | 0.11 | 0.03 | 93.79 |
| LQ13-01-mi-16-01-glass | 82 | 74.18 | 0.06 | 11.21 | 0.66 | 0.03 | 0.07 | 0.69 | 3.21 | 3.93 | 0.07 | MDL | 94.12 |
| LQ13-01-mi-16-01-glass | 83 | 73.50 | 0.11 | 11.19 | 0.56 | 0.11 | 0.09 | 0.66 | 3.34 | 3.91 | 0.11 | 0.09 | 93.68 |
| LQ13-01-mi-17-01-glass | 84 | 73.48 | 0.04 | 10.97 | 0.51 | MDL | 0.10 | 0.62 | 3.02 | 3.93 | 0.13 | 0.01 | 92.82 |
| LQ13-01-mi-17-01-glass | 85 | 73.59 | 0.10 | 10.99 | 0.63 | 0.04 | 0.11 | 0.65 | 3.00 | 3.95 | 0.11 | 0.04 | 93.21 |
| LQ13-01-mi-17-01-glass | 86 | 73.37 | 0.09 | 11.09 | 0.72 | 0.09 | 0.05 | 0.69 | 3.09 | 3.88 | 0.09 | MDL | 93.16 |
| LQ13-01-mi-17-01-glass | 87 | 73.96 | 0.09 | 10.39 | 0.63 | 0.13 | 0.07 | 0.61 | 3.30 | 3.91 | 0.09 | MDL | 93.17 |
| LQ13-01-mi-17-01-glass | 88 | 73.76 | 0.06 | 10.70 | 0.81 | MDL | 0.08 | 0.65 | 3.21 | 3.88 | 0.12 | 0.03 | 93.29 |
| LQ13-01-mi-17-01-glass | 89 | 74.13 | 0.07 | 10.73 | 0.55 | 0.11 | 0.08 | 0.63 | 3.31 | 3.89 | 0.10 | MDL | 93.60 |
| LQ13-01-mi-17-01-glass | 90 | 74.77 | 0.11 | 10.97 | 0.39 | MDL | 0.05 | 0.64 | 3.02 | 3.95 | 0.09 | 0.01 | 94.00 |
| LQ13-01-mi-17-01-glass | 91 | 73.77 | 0.09 | 10.65 | 0.88 | 0.02 | 0.09 | 0.58 | 2.98 | 3.90 | 0.11 | MDL | 93.06 |
| LQ13-01-mi-18-01-glass | 92 | 74.36 | 0.05 | 10.87 | 0.24 | 0.02 | 0.05 | 0.53 | 3.38 | 3.72 | 0.11 | MDL | 93.32 |
| LQ13-01-mi-18-01-glass | 93 | 73.74 | 0.07 | 10.94 | 0.54 | 0.05 | 0.06 | 0.54 | 2.90 | 3.74 | 0.07 | MDL | 92.65 |
| LQ13-01-mi-18-01-glass | 94 | 74.46 | 0.08 | 10.83 | 0.37 | 0.03 | 0.04 | 0.51 | 3.51 | 3.79 | 0.11 | 0.02 | 93.75 |
| LQ13-01-mi-18-01-glass | 95 | 74.01 | 0.06 | 11.11 | 0.43 | 0.04 | 0.05 | 0.55 | 3.13 | 3.78 | 0.15 | 0.03 | 93.33 |
| LQ13-01-mi-18-01-glass | 96 | 75.48 | 0.06 | 10.78 | 0.49 | 0.03 | 0.08 | 0.57 | 3.71 | 3.74 | 0.10 | MDL | 95.03 |
| LQ13-01-mi-18-01-glass | 97 | 74.67 | 0.10 | 10.87 | 0.53 | MDL | 0.05 | 0.60 | 3.13 | 3.80 | 0.12 | 0.05 | 93.94 |
| LQ13-01-mi-18-02-glass | 98 | 74.41 | 0.07 | 10.91 | 0.65 | 0.07 | 0.05 | 0.61 | 3.12 | 3.79 | 0.10 | 0.01 | 93.79 |
| LQ13-01-mi-18-02-glass | 99 | 73.55 | 0.12 | 10.98 | 0.57 | 0.13 | 0.06 | 0.60 | 3.41 | 3.79 | 0.10 | 0.01 | 93.32 |
| LQ13-01-mi-18-02-glass | 100 | 73.82 | 0.07 | 10.88 | 0.79 | 0.10 | 0.04 | 0.58 | 3.30 | 3.81 | 0.10 | 0.02 | 93.51 |
| LQ13-01-mi-18-02-glass | 101 | 73.57 | 0.08 | 11.08 | 0.43 | 0.09 | 0.04 | 0.58 | 3.10 | 3.79 | 0.10 | MDL | 92.86 |
| LQ13-01-mi-18-02-glass | 102 | 73.93 | 0.07 | 11.08 | 0.42 | 0.02 | 0.04 | 0.63 | 3.38 | 3.83 | 0.10 | 0.06 | 93.56 |
| LQ13-01-mi-18-02-glass | 103 | 73.33 | 0.08 | 10.99 | 0.80 | MDL | 0.05 | 0.64 | 3.45 | 3.78 | 0.10 | 0.04 | 93.25 |
| LQ13-01-mi-18-02-glass | 104 | 74.88 | 0.05 | 10.89 | 0.51 | MDL | 0.08 | 0.57 | 3.28 | 3.81 | 0.11 | MDL | 94.18 |
| LQ13-01-mi-18-02-glass | 105 | 73.93 | 0.07 | 11.06 | 0.54 | 0.10 | 0.10 | 0.58 | 3.20 | 3.81 | 0.10 | 0.01 | 93.50 |
| LQ13-01-mi-18-02-glass | 106 | 73.57 | 0.07 | 11.21 | 0.55 | 0.03 | 0.11 | 0.68 | 3.24 | 3.83 | 0.10 | MDL | 93.38 |
| LQ13-01-mi-20-01-glass | 107 | 74.74 | 0.10 | 10.51 | 0.39 | 0.07 | 0.09 | 0.69 | 3.30 | 3.67 | 0.13 | 0.02 | 93.71 |
| LQ13-01-mi-20-01-glass | 108 | 74.88 | 0.09 | 10.61 | 0.76 | 0.06 | 0.04 | 0.68 | 3.31 | 3.84 | 0.11 | MDL | 94.38 |
| LQ13-01-mi-20-01-glass | 109 | 74.40 | 0.05 | 10.58 | 0.49 | MDL | 0.08 | 0.60 | 3.27 | 3.68 | 0.11 | 0.02 | 93.27 |
| LQ13-01-mi-20-01-glass | 110 | 75.32 | 0.07 | 10.65 | 0.55 | MDL | 0.09 | 0.66 | 3.16 | 3.80 | 0.10 | MDL | 94.39 |
| LQ13-01-mi-20-01-glass | 111 | 73.44 | 0.06 | 10.85 | 0.43 | 0.02 | 0.09 | 0.67 | 3.03 | 3.77 | 0.11 | MDL | 92.48 |
| LQ13-01-mi-20-01-glass | 112 | 74.74 | 0.09 | 10.50 | 0.86 | 0.07 | 0.09 | 0.69 | 3.11 | 3.75 | 0.09 | MDL | 94.00 |
| LQ13-01-mi-21-01-glass | 113 | 74.80 | 0.07 | 10.35 | 0.65 | 0.03 | 0.06 | 0.61 | 3.22 | 3.69 | 0.10 | MDL | 93.56 |
| LQ13-01-mi-21-01-glass | 114 | 75.02 | 0.08 | 10.36 | 0.34 | 0.10 | 0.04 | 0.63 | 3.32 | 3.73 | 0.07 | 0.02 | 93.71 |

**Appendix D, continued.**

| | line | $SiO_2$ | $TiO_2$ | $Al_2O_3$ | $FeO^*$ | MnO | MgO | CaO | $Na_2O$ | $K_2O$ | Cl | $SO_3$ | Total |
|---|---|---|---|---|---|---|---|---|---|---|---|---|---|
| LQ13-01-mi-23-02-glass | 115 | 75.48 | 0.07 | 10.60 | 0.58 | MDL | 0.07 | 0.59 | 3.02 | 3.70 | 0.09 | 0.01 | 94.21 |
| LQ13-01-mi-23-02-glass | 116 | 75.07 | 0.06 | 10.36 | 0.38 | MDL | MDL | 0.60 | 2.92 | 3.76 | 0.08 | MDL | 93.23 |
| LQ13-01-mi-23-03-glass | 117 | 74.28 | 0.11 | 10.91 | 0.55 | 0.08 | 0.07 | 0.67 | 3.12 | 3.84 | 0.12 | 0.04 | 93.78 |
| LQ13-01-mi-23-03-glass | 118 | 74.25 | 0.10 | 10.74 | 0.69 | 0.04 | 0.05 | 0.67 | 3.37 | 3.79 | 0.10 | MDL | 93.82 |
| LQ13-01-mi-23-03-glass | 119 | 74.31 | 0.07 | 10.85 | 0.50 | 0.05 | 0.05 | 0.71 | 3.29 | 3.85 | 0.13 | MDL | 93.82 |
| LQ13-01-mi-23-03-glass | 120 | 74.51 | 0.11 | 10.66 | 0.55 | 0.03 | 0.08 | 0.67 | 2.97 | 3.81 | 0.11 | MDL | 93.51 |
| LQ13-01-mi-23-03-glass | 121 | 74.10 | 0.10 | 11.06 | 0.67 | 0.05 | 0.07 | 0.69 | 3.37 | 3.88 | 0.12 | 0.01 | 94.11 |
| LQ13-01-mi-23-03-glass | 122 | 74.70 | 0.07 | 10.79 | 0.51 | MDL | 0.03 | 0.67 | 3.11 | 3.79 | 0.11 | MDL | 93.80 |
| LQ13-01-mi-25-01-glass | 123 | 74.67 | 0.06 | 10.53 | 0.60 | 0.06 | 0.08 | 0.58 | 3.14 | 3.74 | 0.09 | MDL | 93.56 |
| LQ13-01-mi-25-01-glass | 124 | 75.05 | 0.07 | 10.46 | 0.51 | 0.05 | 0.08 | 0.58 | 3.19 | 3.79 | 0.09 | MDL | 93.88 |
| LQ13-01-mi-25-01-glass | 125 | 75.36 | 0.11 | 10.19 | 0.51 | 0.04 | 0.07 | 0.55 | 3.33 | 3.76 | 0.11 | 0.02 | 94.04 |
| LQ13-01-mi-25-01-glass | 126 | 75.81 | 0.07 | 10.18 | 0.43 | 0.03 | 0.07 | 0.49 | 3.30 | 3.71 | 0.09 | 0.03 | 94.21 |
| LQ13-01-mi-25-01-glass | 127 | 73.98 | 0.05 | 10.62 | 0.48 | 0.05 | 0.09 | 0.56 | 3.43 | 3.77 | 0.11 | MDL | 93.14 |
| LQ13-01-mi-26-02-glass | 128 | 72.77 | 0.15 | 10.28 | 0.61 | 0.08 | 0.11 | 0.69 | 3.20 | 3.68 | 0.08 | 0.01 | 91.65 |
| LQ13-01-mi-26-02-glass | 129 | 72.87 | 0.10 | 10.63 | 0.40 | MDL | 0.11 | 0.62 | 3.23 | 3.73 | 0.11 | 0.03 | 91.81 |
| LQ13-01-mi-27-01-glass | 130 | 72.53 | 0.10 | 11.16 | 0.61 | 0.03 | 0.06 | 0.61 | 3.40 | 3.85 | 0.10 | 0.03 | 92.49 |
| LQ13-01-mi-27-01-glass | 131 | 71.71 | 0.06 | 10.78 | 0.46 | MDL | 0.06 | 0.55 | 3.21 | 3.73 | 0.11 | MDL | 90.67 |
| LQ13-01-mi-27-01-glass | 132 | 72.86 | 0.06 | 10.90 | 0.69 | 0.10 | 0.06 | 0.56 | 3.10 | 4.05 | 0.11 | MDL | 92.50 |
| LQ13-01-mi-27-01-glass | 133 | 71.26 | 0.08 | 11.04 | 0.57 | 0.08 | 0.07 | 0.60 | 3.08 | 4.18 | 0.10 | 0.08 | 91.13 |
| LQ13-01-mi-28-01-glass | 134 | 73.15 | 0.05 | 10.78 | 0.48 | MDL | 0.06 | 0.65 | 2.92 | 3.83 | 0.09 | 0.03 | 92.04 |
| LQ13-01-mi-28-01-glass | 135 | 73.58 | 0.08 | 10.69 | 0.80 | 0.05 | 0.10 | 0.66 | 3.32 | 3.83 | 0.09 | 0.04 | 93.24 |
| LQ13-01-mi-28-01-glass | 136 | 74.14 | 0.09 | 10.80 | 0.55 | 0.06 | 0.10 | 0.67 | 2.98 | 3.93 | 0.10 | MDL | 93.41 |
| LQ13-01-mi-28-01-glass | 137 | 74.05 | 0.07 | 10.74 | 0.47 | MDL | 0.07 | 0.64 | 3.20 | 3.86 | 0.10 | MDL | 93.22 |
| LQ13-01-mi-28-01-glass | 138 | 74.52 | 0.08 | 10.73 | 0.40 | 0.13 | 0.03 | 0.67 | 3.20 | 3.87 | 0.09 | MDL | 93.72 |
| LQ13-01-mi-28-01-glass | 139 | 74.23 | 0.09 | 10.58 | 0.54 | MDL | 0.11 | 0.66 | 3.28 | 3.89 | 0.10 | 0.03 | 93.50 |
| LQ13-01-mi-28-02-glass | 140 | 73.70 | 0.15 | 10.53 | 0.73 | 0.03 | 0.05 | 0.64 | 3.26 | 3.77 | 0.09 | MDL | 92.95 |
| LQ13-01-mi-28-02-glass | 141 | 74.20 | 0.09 | 10.51 | 0.69 | 0.02 | 0.07 | 0.67 | 3.07 | 3.75 | 0.10 | 0.02 | 93.19 |
| LQ13-01-mi-29-01-glass | 142 | 72.84 | 0.11 | 10.80 | 0.41 | MDL | 0.05 | 0.56 | 3.37 | 3.87 | 0.09 | 0.03 | 92.12 |
| LQ13-01-mi-29-01-glass | 143 | 73.41 | 0.09 | 10.82 | 0.36 | 0.03 | 0.05 | 0.56 | 3.26 | 3.87 | 0.11 | MDL | 92.57 |
| LQ13-01-mi-29-01-glass | 144 | 73.00 | 0.07 | 10.83 | 0.43 | 0.02 | 0.03 | 0.54 | 3.30 | 3.87 | 0.09 | MDL | 92.18 |
| LQ13-01-mi-29-01-glass | 145 | 72.37 | 0.06 | 10.82 | 0.61 | 0.03 | 0.09 | 0.51 | 2.93 | 3.85 | 0.10 | MDL | 91.36 |
| LQ13-01-mi-29-01-glass | 146 | 72.44 | 0.09 | 10.93 | 0.69 | 0.10 | 0.07 | 0.57 | 3.05 | 3.93 | 0.09 | 0.01 | 91.98 |
| LQ13-01-mi-29-01-glass | 147 | 74.17 | 0.05 | 10.85 | 0.47 | MDL | MDL | 0.56 | 3.39 | 3.96 | 0.10 | 0.05 | 93.60 |

Values marked MDL were below the minimum detection limit.

**Appendix E.** Raw individual titanomagnetite and ilmenite compositions (wt. %) as determined by EPMA.

| Sample | line | $SiO_2$ | $TiO_2$ | $Al_2O_3$ | $Cr_2O_3$ | $FeO^*$ | MnO | MgO | CaO | $Na_2O$ | Total |
|---|---|---|---|---|---|---|---|---|---|---|---|
| LQ13-01-ox-01-03-mag | 1 | 0.01 | 4.94 | 1.80 | 0.07 | 80.06 | 0.72 | 1.20 | 0.10 | 0.06 | 88.96 |
| LQ13-01-ox-01-03-mag | 2 | 0.03 | 5.24 | 1.70 | 0.08 | 80.61 | 0.61 | 1.25 | MDL | MDL | 89.51 |
| LQ13-01-ox-01-03-ilm | 3 | MDL | 38.86 | 0.25 | MDL | 51.11 | 0.83 | 2.25 | 0.04 | 0.03 | 93.36 |
| LQ13-01-ox-01-06-mag | 8 | MDL | 5.53 | 1.69 | 0.10 | 81.01 | 0.77 | 1.22 | MDL | 0.08 | 90.39 |
| LQ13-01-ox-01-06-mag | 9 | MDL | 5.42 | 1.85 | 0.08 | 81.69 | 0.66 | 1.21 | MDL | MDL | 90.91 |
| LQ13-01-ox-01-06-mag | 10 | 0.01 | 5.39 | 1.79 | 0.13 | 82.46 | 0.72 | 1.19 | MDL | MDL | 91.69 |
| LQ13-01-ox-01-06-ilm | 11 | 0.03 | 36.03 | 0.34 | MDL | 53.63 | 0.99 | 2.09 | 0.13 | MDL | 93.23 |
| LQ13-01-ox-01-08-mag | 12 | MDL | 5.33 | 1.77 | 0.07 | 81.48 | 0.75 | 1.18 | 0.05 | MDL | 90.62 |
| LQ13-01-ox-01-08-mag | 13 | MDL | 5.23 | 1.83 | 0.08 | 81.64 | 0.63 | 1.18 | 0.05 | MDL | 90.64 |
| LQ13-01-ox-01-08-ilm | 14 | MDL | 38.56 | 0.18 | MDL | 52.68 | 0.71 | 2.21 | 0.02 | MDL | 94.35 |
| LQ13-01-ox-01-08-ilm | 15 | MDL | 38.40 | 0.17 | 0.05 | 51.97 | 0.87 | 2.19 | 0.03 | 0.05 | 93.72 |
| LQ13-01-ox-01-09-mag | 16 | 0.01 | 5.28 | 1.80 | 0.09 | 81.68 | 0.76 | 1.25 | 0.10 | MDL | 90.96 |
| LQ13-01-ox-01-09-mag | 17 | MDL | 5.27 | 1.71 | 0.07 | 80.55 | 0.70 | 1.20 | 0.08 | MDL | 89.58 |
| LQ13-01-ox-01-09-mag | 18 | MDL | 5.07 | 1.81 | 0.08 | 81.23 | 0.62 | 1.21 | 0.01 | MDL | 90.04 |
| LQ13-01-ox-01-09-ilm | 19 | MDL | 39.33 | 0.15 | 0.03 | 52.10 | 0.81 | 2.13 | 0.01 | 0.01 | 94.58 |
| LQ13-01-ox-01-09-ilm | 20 | 0.11 | 38.41 | 0.17 | 0.06 | 50.57 | 0.98 | 2.10 | 0.11 | 0.02 | 92.54 |
| LQ13-01-ox-01-10-mag | 21 | 0.04 | 5.37 | 1.67 | 0.08 | 81.81 | 0.66 | 1.13 | MDL | 0.01 | 90.77 |
| LQ13-01-ox-01-10-mag | 22 | MDL | 5.29 | 1.83 | 0.09 | 82.58 | 0.71 | 1.24 | 0.01 | 0.05 | 91.80 |
| LQ13-01-ox-01-10-mag | 23 | MDL | 5.17 | 1.72 | 0.12 | 82.42 | 0.63 | 1.15 | 0.01 | MDL | 91.23 |
| LQ13-01-ox-01-10-ilm | 24 | MDL | 39.16 | 0.20 | MDL | 52.02 | 0.81 | 2.15 | 0.01 | MDL | 94.36 |
| LQ13-01-ox-01-10-ilm | 25 | MDL | 38.44 | 0.17 | MDL | 51.82 | 0.89 | 2.17 | 0.01 | 0.02 | 93.51 |
| LQ13-01-ox-01-12-mag | 26 | MDL | 5.20 | 1.75 | 0.04 | 80.51 | 0.67 | 1.23 | 0.16 | 0.03 | 89.61 |
| LQ13-01-ox-01-12-mag | 27 | MDL | 5.16 | 1.74 | 0.09 | 82.04 | 0.67 | 1.24 | 0.08 | 0.04 | 91.08 |
| LQ13-01-ox-01-12-mag | 28 | MDL | 5.19 | 1.75 | 0.07 | 81.15 | 0.61 | 1.35 | 0.13 | MDL | 90.24 |
| LQ13-01-ox-01-12-ilm | 29 | 0.01 | 38.44 | 0.23 | 0.01 | 50.75 | 0.92 | 2.30 | 0.06 | MDL | 92.72 |
| LQ13-01-ox-01-13-mag | 30 | MDL | 5.07 | 1.72 | 0.04 | 82.70 | 0.71 | 1.18 | 0.01 | 0.01 | 91.44 |
| LQ13-01-ox-01-13-mag | 31 | MDL | 5.13 | 1.66 | 0.11 | 82.34 | 0.71 | 1.25 | 0.02 | 0.08 | 91.31 |
| LQ13-01-ox-01-13-ilm | 32 | MDL | 38.19 | 0.18 | MDL | 52.59 | 0.84 | 2.08 | 0.02 | 0.01 | 93.90 |
| LQ13-01-ox-01-13-ilm | 33 | 0.01 | 38.30 | 0.15 | 0.07 | 53.33 | 0.93 | 2.22 | 0.01 | MDL | 95.03 |
| LQ13-01-ox-01-13-ilm | 34 | MDL | 38.21 | 0.14 | 0.02 | 52.98 | 0.92 | 2.14 | 0.01 | 0.10 | 94.51 |
| LQ13-01-ox-01-14-mag | 35 | MDL | 5.24 | 1.81 | 0.13 | 81.76 | 0.74 | 1.20 | 0.18 | MDL | 91.06 |
| LQ13-01-ox-01-14-mag | 36 | 0.03 | 5.25 | 1.79 | 0.05 | 82.12 | 0.69 | 1.14 | 0.03 | 0.01 | 91.10 |
| LQ13-01-ox-01-14-mag | 37 | MDL | 5.31 | 1.87 | 0.09 | 81.86 | 0.57 | 1.25 | 0.02 | 0.02 | 90.99 |
| LQ13-01-ox-01-14-mag | 38 | 0.03 | 5.30 | 1.70 | 0.10 | 81.21 | 0.71 | 1.24 | 0.02 | MDL | 90.32 |
| LQ13-01-ox-01-14-ilm | 39 | MDL | 39.06 | 0.17 | 0.02 | 51.48 | 0.85 | 2.29 | 0.04 | MDL | 93.91 |
| LQ13-01-ox-01-14-ilm | 40 | MDL | 38.46 | 0.19 | MDL | 51.77 | 0.90 | 2.24 | 0.09 | MDL | 93.66 |

**Appendix E, continued.**

| Sample | line | $SiO_2$ | $TiO_2$ | $Al_2O_3$ | $Cr_2O_3$ | $FeO^*$ | MnO | MgO | CaO | $Na_2O$ | Total |
|---|---|---|---|---|---|---|---|---|---|---|---|
| LQ13-01-ox-01-16-mag | 47 | MDL | 5.57 | 1.80 | 0.06 | 81.65 | 0.70 | 1.26 | 0.01 | 0.04 | 91.07 |
| LQ13-01-ox-01-16-mag | 48 | MDL | 5.18 | 1.98 | 0.05 | 82.39 | 0.60 | 1.24 | 0.02 | MDL | 91.45 |
| LQ13-01-ox-01-16-ilm | 49 | MDL | 37.51 | 0.18 | MDL | 53.89 | 0.80 | 2.12 | 0.09 | 0.02 | 94.62 |
| LQ13-01-ox-01-16-ilm | 50 | MDL | 37.56 | 0.19 | 0.04 | 53.91 | 0.89 | 2.03 | MDL | MDL | 94.61 |
| LQ13-01-ox-01-16-ilm | 51 | MDL | 37.18 | 0.16 | 0.03 | 53.82 | 0.78 | 2.05 | 0.02 | MDL | 94.05 |
| LQ13-01-ox-01-16-ilm | 52 | MDL | 37.64 | 0.23 | 0.03 | 52.90 | 0.94 | 2.07 | 0.02 | 0.02 | 93.85 |
| LQ13-01-ox-01-17-mag | 53 | 0.02 | 5.27 | 1.76 | 0.12 | 81.65 | 0.65 | 1.12 | 0.01 | MDL | 90.59 |
| LQ13-01-ox-01-17-mag | 54 | MDL | 5.35 | 1.78 | 0.10 | 82.67 | 0.75 | 1.24 | MDL | 0.03 | 91.92 |
| LQ13-01-ox-01-17-mag | 55 | MDL | 5.20 | 1.68 | 0.09 | 83.06 | 0.79 | 1.29 | 0.02 | 0.01 | 92.13 |
| LQ13-01-ox-01-17-mag | 56 | MDL | 5.22 | 1.69 | 0.07 | 83.14 | 0.77 | 1.18 | 0.01 | MDL | 92.08 |
| LQ13-01-ox-01-17-ilm | 57 | MDL | 38.50 | 0.23 | 0.00 | 51.97 | 1.02 | 2.11 | MDL | MDL | 93.83 |
| LQ13-01-ox-01-17-ilm | 58 | MDL | 39.67 | 0.16 | 0.02 | 52.52 | 0.79 | 2.24 | MDL | MDL | 95.41 |
| LQ13-01-ox-01-17-ilm | 59 | MDL | 38.80 | 0.15 | 0.03 | 52.60 | 0.76 | 2.32 | 0.05 | MDL | 94.72 |
| LQ13-01-ox-01-17-ilm | 60 | MDL | 38.84 | 0.17 | 0.03 | 52.65 | 0.89 | 2.22 | 0.04 | MDL | 94.84 |
| LQ13-01-ox-01-18-mag | 61 | 0.06 | 5.24 | 1.86 | 0.07 | 82.03 | 0.60 | 1.21 | 0.02 | 0.02 | 91.12 |
| LQ13-01-ox-01-18-mag | 62 | MDL | 5.27 | 1.70 | 0.01 | 83.36 | 0.71 | 1.14 | 0.05 | MDL | 92.25 |
| LQ13-01-ox-01-18-mag | 63 | 0.07 | 5.15 | 1.62 | 0.04 | 82.26 | 0.63 | 1.18 | 0.03 | MDL | 90.98 |
| LQ13-01-ox-01-18-mag | 64 | MDL | 5.29 | 1.77 | 0.05 | 82.71 | 0.58 | 1.28 | 0.01 | MDL | 91.69 |
| LQ13-01-ox-01-18-ilm | 65 | MDL | 38.50 | 0.23 | MDL | 51.97 | 1.02 | 2.11 | MDL | MDL | 93.83 |
| LQ13-01-ox-01-18-ilm | 66 | MDL | 39.67 | 0.16 | 0.02 | 52.52 | 0.79 | 2.24 | MDL | MDL | 95.41 |
| LQ13-01-ox-01-18-ilm | 67 | MDL | 38.80 | 0.15 | 0.03 | 52.60 | 0.76 | 2.32 | 0.05 | MDL | 94.72 |
| LQ13-01-ox-01-18-ilm | 68 | MDL | 38.84 | 0.17 | 0.03 | 52.65 | 0.89 | 2.22 | 0.04 | MDL | 94.84 |
| LQ13-01-ox-02-01-mag | 75 | MDL | 5.29 | 1.65 | 0.07 | 83.80 | 0.78 | 1.17 | MDL | MDL | 92.76 |
| LQ13-01-ox-02-01-mag | 76 | MDL | 5.22 | 1.62 | 0.07 | 82.74 | 0.72 | 1.21 | 0.06 | MDL | 91.64 |
| LQ13-01-ox-02-01-mag | 77 | 0.01 | 5.27 | 1.77 | 0.08 | 83.24 | 0.62 | 1.19 | 0.02 | MDL | 92.20 |
| LQ13-01-ox-02-01-mag | 78 | MDL | 5.16 | 1.71 | 0.09 | 82.45 | 0.63 | 1.21 | 0.01 | 0.06 | 91.30 |
| LQ13-01-ox-02-01-mag | 79 | MDL | 5.22 | 1.74 | 0.06 | 83.94 | 0.73 | 1.08 | 0.02 | MDL | 92.78 |
| LQ13-01-ox-02-01-mag | 80 | 0.03 | 5.09 | 1.70 | 0.02 | 83.80 | 0.60 | 1.19 | 0.02 | 0.01 | 92.46 |
| LQ13-01-ox-02-01-ilm | 81 | MDL | 39.25 | 0.15 | 0.05 | 52.64 | 0.69 | 2.17 | 0.03 | 0.12 | 95.09 |
| LQ13-01-ox-02-01-ilm | 82 | 0.01 | 39.25 | 0.19 | 0.04 | 52.46 | 0.88 | 2.17 | 0.01 | 0.05 | 95.05 |
| LQ13-01-ox-02-01-ilm | 83 | MDL | 38.69 | 0.15 | 0.03 | 53.10 | 0.85 | 2.06 | 0.07 | MDL | 94.96 |
| LQ13-01-ox-02-02-mag | 84 | MDL | 5.29 | 1.65 | 0.07 | 83.80 | 0.78 | 1.17 | MDL | MDL | 92.76 |
| LQ13-01-ox-02-02-mag | 85 | MDL | 5.22 | 1.62 | 0.07 | 82.74 | 0.72 | 1.21 | 0.06 | MDL | 91.64 |
| LQ13-01-ox-02-02-mag | 86 | 0.01 | 5.27 | 1.77 | 0.08 | 83.24 | 0.62 | 1.19 | 0.02 | MDL | 92.20 |
| LQ13-01-ox-02-02-mag | 87 | MDL | 5.16 | 1.71 | 0.09 | 82.45 | 0.63 | 1.21 | 0.01 | 0.06 | 91.30 |
| LQ13-01-ox-02-02-mag | 88 | MDL | 5.22 | 1.74 | 0.06 | 83.94 | 0.73 | 1.08 | 0.02 | MDL | 92.78 |
| LQ13-01-ox-02-02-mag | 89 | 0.03 | 5.09 | 1.70 | 0.02 | 83.80 | 0.60 | 1.19 | 0.02 | 0.01 | 92.46 |
| LQ13-01-ox-02-02-ilm | 90 | MDL | 39.05 | 0.16 | 0.04 | 52.62 | 0.87 | 2.05 | MDL | MDL | 94.80 |

**Appendix E, continued.**

| Sample | line | $SiO_2$ | $TiO_2$ | $Al_2O_3$ | $Cr_2O_3$ | $FeO^*$ | MnO | MgO | CaO | $Na_2O$ | Total |
|---|---|---|---|---|---|---|---|---|---|---|---|
| LQ13-01-ox-02-03-mag | 91 | MDL | 5.29 | 1.65 | 0.07 | 83.80 | 0.78 | 1.17 | MDL | MDL | 92.76 |
| LQ13-01-ox-02-03-mag | 92 | MDL | 5.22 | 1.62 | 0.07 | 82.74 | 0.72 | 1.21 | 0.06 | MDL | 91.64 |
| LQ13-01-ox-02-03-mag | 93 | 0.01 | 5.27 | 1.77 | 0.08 | 83.24 | 0.62 | 1.19 | 0.02 | MDL | 92.20 |
| LQ13-01-ox-02-03-mag | 94 | MDL | 5.16 | 1.71 | 0.09 | 82.45 | 0.63 | 1.21 | 0.01 | 0.06 | 91.30 |
| LQ13-01-ox-02-03-mag | 95 | MDL | 5.22 | 1.74 | 0.06 | 83.94 | 0.73 | 1.08 | 0.02 | MDL | 92.78 |
| LQ13-01-ox-02-03-mag | 96 | 0.03 | 5.09 | 1.70 | 0.02 | 83.80 | 0.60 | 1.19 | 0.02 | 0.01 | 92.46 |
| LQ13-01-ox-02-03-ilm | 97 | 0.03 | 38.47 | 0.12 | 0.06 | 53.21 | 0.82 | 2.01 | 0.07 | 0.03 | 94.83 |
| LQ13-01-ox-02-04-mag | 98 | MDL | 6.46 | 1.95 | 0.06 | 82.03 | 0.71 | 1.20 | 0.02 | 0.04 | 92.48 |
| LQ13-01-ox-02-04-mag | 99 | MDL | 5.88 | 1.88 | 0.03 | 81.88 | 0.71 | 1.23 | 0.02 | 0.02 | 91.65 |
| LQ13-01-ox-02-04-mag | 100 | MDL | 5.95 | 1.93 | 0.01 | 81.73 | 0.74 | 1.26 | 0.01 | 0.04 | 91.68 |
| LQ13-01-ox-02-04-ilm | 101 | MDL | 37.38 | 0.25 | 0.06 | 54.28 | 0.81 | 2.02 | MDL | MDL | 94.80 |
| LQ13-01-ox-02-04-ilm | 102 | MDL | 37.90 | 0.30 | MDL | 54.55 | 0.94 | 2.00 | 0.01 | MDL | 95.71 |
| LQ13-01-ox-02-04-ilm | 103 | MDL | 37.73 | 0.30 | 0.03 | 53.85 | 0.79 | 1.89 | MDL | 0.02 | 94.61 |
| LQ13-01-ox-02-04-ilm | 104 | MDL | 37.43 | 0.25 | 0.01 | 53.39 | 0.70 | 1.96 | 0.02 | MDL | 93.77 |
| LQ13-01-ox-02-04-ilm | 105 | MDL | 37.11 | 0.23 | 0.03 | 54.21 | 0.78 | 1.87 | 0.04 | 0.02 | 94.29 |
| LQ13-01-ox-02-05-mag | 106 | MDL | 5.21 | 1.70 | 0.09 | 83.23 | 0.70 | 1.07 | 0.03 | 0.01 | 92.03 |
| LQ13-01-ox-02-05-mag | 107 | MDL | 5.20 | 1.67 | 0.10 | 84.10 | 0.71 | 1.11 | 0.02 | MDL | 92.91 |
| LQ13-01-ox-02-05-ilm | 108 | MDL | 38.78 | 0.13 | 0.02 | 53.22 | 0.88 | 2.04 | 0.01 | 0.01 | 95.08 |
| LQ13-01-ox-02-05-ilm | 109 | MDL | 38.94 | 0.13 | 0.03 | 54.76 | 0.87 | 2.07 | 0.06 | 0.01 | 96.87 |

Values marked MDL were below the minimum detection limit.

**Appendix F.** Raw individual phase equilibrium experimental run product glass compositions (wt. %) as determined by EPMA.

| Sample | line | $SiO_2$ | $TiO_2$ | $Al_2O_3$ | $FeO^*$ | MnO | MgO | CaO | $Na_2O$ | $K_2O$ | Cl | $SO_3$ | Total |
|---|---|---|---|---|---|---|---|---|---|---|---|---|---|
| CCPb-01-glass | 1 | 72.22 | 0.16 | 12.54 | 0.63 | 0.04 | 0.18 | 1.00 | 2.64 | 2.32 | 0.01 | 0.02 | 91.76 |
| CCPb-01-glass | 2 | 71.44 | 0.06 | 12.16 | 0.60 | 0.05 | 0.13 | 0.95 | 3.25 | 3.62 | MDL | MDL | 92.28 |
| CCPb-01-glass | 3 | 71.68 | 0.17 | 12.02 | 0.71 | 0.04 | 0.18 | 0.94 | 3.04 | 3.72 | MDL | MDL | 92.52 |
| CCPb-01-glass | 4 | 70.82 | 0.05 | 12.19 | 0.77 | MDL | 0.21 | 0.96 | 3.06 | 3.69 | MDL | MDL | 91.76 |
| CCPb-01-glass | 5 | 70.43 | 0.04 | 12.41 | 0.77 | 0.05 | 0.17 | 0.96 | 3.06 | 3.62 | MDL | 0.03 | 91.53 |
| CCPb-01-glass | 6 | 69.93 | 0.09 | 11.98 | 0.90 | 0.06 | 0.14 | 1.10 | 2.96 | 3.58 | 0.01 | MDL | 90.75 |
| CCPb-01-glass | 7 | 71.92 | 0.03 | 12.13 | 0.81 | 0.10 | 0.18 | 0.96 | 2.81 | 3.64 | MDL | MDL | 92.59 |
| CCPb-02-glass | 8 | 71.14 | 0.18 | 13.00 | 1.68 | 0.06 | 0.35 | 1.61 | 3.52 | 3.37 | 0.05 | MDL | 94.95 |
| CCPb-02-glass | 9 | 69.91 | 0.19 | 12.63 | 1.43 | MDL | 0.32 | 1.65 | 3.60 | 3.28 | 0.04 | MDL | 93.05 |
| CCPb-02-glass | 10 | 70.58 | 0.19 | 13.39 | 1.38 | 0.08 | 0.36 | 1.64 | 3.71 | 3.26 | 0.02 | MDL | 94.61 |
| CCPb-02-glass | 11 | 69.38 | 0.22 | 13.51 | 1.45 | MDL | 0.33 | 1.73 | 3.51 | 3.34 | 0.03 | 0.03 | 93.52 |
| CCPb-02-glass | 12 | 69.20 | 0.16 | 13.01 | 1.77 | MDL | 0.33 | 1.64 | 3.51 | 3.28 | 0.01 | 0.02 | 92.93 |
| CCPb-02-glass | 13 | 69.65 | 0.24 | 12.81 | 1.37 | 0.10 | 0.32 | 1.56 | 3.50 | 3.31 | 0.02 | 0.02 | 92.91 |
| CCPb-02-glass | 14 | 70.13 | 0.18 | 13.63 | 1.37 | 0.10 | 0.28 | 1.75 | 3.74 | 3.35 | 0.03 | 0.02 | 94.59 |
| CCPb-02-glass | 15 | 70.02 | 0.19 | 13.68 | 2.04 | 0.02 | 0.34 | 1.79 | 3.30 | 3.32 | 0.02 | MDL | 94.72 |
| CCPb-02-glass | 16 | 68.95 | 0.10 | 13.17 | 1.41 | 0.04 | 0.37 | 1.68 | 3.37 | 3.24 | 0.04 | MDL | 92.35 |
| CCPb-02-glass | 17 | 69.22 | 0.18 | 13.18 | 1.50 | 0.03 | 0.30 | 1.74 | 3.52 | 3.26 | 0.03 | MDL | 92.96 |
| CCPb-02-glass | 18 | 71.71 | 0.30 | 13.08 | 1.54 | 0.18 | 0.39 | 1.61 | 3.74 | 3.29 | 0.02 | MDL | 95.86 |
| CCPb-02-glass | 19 | 71.05 | 0.19 | 13.07 | 1.67 | MDL | 0.30 | 1.53 | 3.20 | 3.32 | 0.04 | MDL | 94.36 |
| CCPb-02-glass | 20 | 69.44 | 0.19 | 12.76 | 0.84 | 0.16 | 0.35 | 1.58 | 3.13 | 3.29 | 0.03 | MDL | 91.76 |
| CCPb-02-glass | 21 | 69.31 | 0.25 | 13.14 | 1.37 | MDL | 0.33 | 1.66 | 3.41 | 3.31 | 0.04 | MDL | 92.83 |
| CCPb-03-glass | 22 | 72.86 | 0.26 | 12.15 | 1.15 | MDL | 0.26 | 1.04 | 3.10 | 3.09 | 0.04 | 0.07 | 94.01 |
| CCPb-03-glass | 23 | 70.71 | 0.18 | 11.98 | 0.95 | 0.04 | 0.21 | 1.14 | 3.30 | 3.66 | 0.04 | MDL | 92.19 |
| CCPb-03-glass | 24 | 70.95 | 0.12 | 11.99 | 1.35 | MDL | 0.17 | 1.03 | 2.89 | 3.71 | 0.04 | MDL | 92.25 |
| CCPb-03-glass | 25 | 73.09 | 0.14 | 12.39 | 1.33 | 0.08 | 0.39 | 1.02 | 3.41 | 3.70 | 0.03 | MDL | 95.58 |
| CCPb-03-glass | 26 | 72.59 | 0.23 | 12.00 | 1.27 | 0.03 | 0.22 | 1.06 | 3.33 | 3.80 | 0.02 | MDL | 94.55 |
| CCPb-03-glass | 27 | 71.86 | 0.17 | 12.12 | 1.11 | MDL | 0.22 | 1.06 | 3.38 | 3.71 | 0.06 | 0.04 | 93.72 |
| CCPb-03-glass | 28 | 72.62 | 0.19 | 11.99 | 1.26 | 0.04 | 0.22 | 1.02 | 3.26 | 3.79 | 0.05 | 0.01 | 94.43 |
| CCPb-04-glass | 29 | 71.58 | 0.21 | 13.21 | 1.46 | MDL | 0.40 | 1.52 | 3.45 | 3.46 | 0.03 | MDL | 95.32 |
| CCPb-04-glass | 30 | 71.34 | 0.18 | 13.03 | 1.29 | 0.01 | 0.31 | 1.53 | 3.38 | 3.50 | 0.02 | MDL | 94.60 |
| CCPb-04-glass | 31 | 72.57 | 0.23 | 13.14 | 1.61 | 0.12 | 0.46 | 1.47 | 3.63 | 3.51 | 0.03 | MDL | 96.78 |
| CCPb-04-glass | 32 | 71.69 | 0.26 | 13.14 | 1.59 | 0.09 | 0.39 | 1.54 | 3.40 | 3.47 | 0.05 | 0.09 | 95.71 |
| CCPb-04-glass | 33 | 72.65 | 0.21 | 13.63 | 1.37 | 0.03 | 0.34 | 1.59 | 3.38 | 3.50 | 0.03 | 0.02 | 96.74 |
| CCPb-04-glass | 34 | 69.23 | 0.13 | 13.12 | 1.13 | 0.09 | 0.41 | 1.64 | 3.56 | 3.39 | 0.03 | 0.01 | 92.73 |
| CCPb-04-glass | 35 | 71.29 | 0.22 | 13.31 | 1.48 | 0.06 | 0.37 | 1.70 | 3.72 | 3.46 | 0.03 | 0.08 | 95.71 |
| CCPb-04-glass | 36 | 72.66 | 0.31 | 13.45 | 1.59 | MDL | 0.37 | 1.56 | 3.59 | 3.44 | 0.03 | 0.08 | 97.08 |
| CCPb-04-glass | 37 | 71.37 | 0.21 | 13.04 | 1.94 | 0.05 | 0.37 | 1.63 | 3.63 | 3.41 | 0.03 | 0.05 | 95.73 |
| CCPb-04-glass | 38 | 71.65 | 0.22 | 13.10 | 1.48 | 0.03 | 0.36 | 1.56 | 3.68 | 3.25 | 0.03 | 0.02 | 95.37 |
| CCPb-04-glass | 39 | 70.71 | 0.33 | 12.84 | 1.28 | MDL | 0.34 | 1.56 | 3.82 | 3.42 | 0.03 | MDL | 94.33 |
| CCPb-04-glass | 40 | 70.41 | 0.32 | 13.36 | 1.24 | 0.07 | 0.37 | 1.59 | 3.63 | 3.42 | 0.04 | 0.05 | 94.51 |

**Appendix F, continued.**

| Sample | line | $SiO_2$ | $TiO_2$ | $Al_2O_3$ | $FeO^*$ | MnO | MgO | CaO | $Na_2O$ | $K_2O$ | Cl | $SO_3$ | Total |
|---|---|---|---|---|---|---|---|---|---|---|---|---|---|
| CCPb-05-glass | 41 | 69.25 | 0.23 | 12.90 | 1.33 | 0.07 | 0.33 | 1.62 | 3.81 | 2.96 | 0.03 | MDL | 92.53 |
| CCPb-05-glass | 42 | 68.04 | 0.24 | 13.13 | 1.16 | 0.05 | 0.42 | 1.77 | 3.66 | 2.97 | 0.04 | 0.03 | 91.49 |
| CCPb-05-glass | 43 | 67.63 | 0.22 | 13.01 | 1.36 | 0.04 | 0.35 | 1.68 | 3.44 | 3.09 | 0.03 | MDL | 90.86 |
| CCPb-05-glass | 44 | 69.91 | 0.20 | 13.44 | 1.89 | MDL | 0.42 | 1.78 | 3.48 | 3.01 | 0.02 | MDL | 94.17 |
| CCPb-05-glass | 45 | 68.25 | 0.22 | 13.84 | 1.92 | 0.15 | 0.39 | 1.82 | 3.75 | 3.05 | 0.02 | MDL | 93.40 |
| CCPb-05-glass | 46 | 69.38 | 0.21 | 13.79 | 1.29 | MDL | 0.37 | 1.78 | 3.84 | 3.05 | 0.02 | MDL | 93.74 |
| CCPb-05-glass | 47 | 63.79 | 0.17 | 13.25 | 1.53 | MDL | 0.35 | 2.03 | 3.38 | 3.03 | 0.10 | 0.06 | 87.69 |
| CCPb-05-glass | 48 | 68.51 | 0.24 | 13.72 | 1.29 | 0.02 | 0.38 | 1.67 | 3.62 | 3.07 | 0.01 | MDL | 92.52 |
| CCPb-05-glass | 49 | 68.82 | 0.24 | 13.35 | 1.78 | 0.07 | 0.42 | 1.90 | 3.71 | 2.96 | 0.01 | MDL | 93.27 |
| CCPb-05-glass | 50 | 68.30 | 0.18 | 13.73 | 1.39 | 0.03 | 0.42 | 1.85 | 3.59 | 3.03 | MDL | MDL | 92.53 |
| CCPb-05-glass | 51 | 67.33 | 0.28 | 14.78 | 2.04 | 0.21 | 0.46 | 2.14 | 4.07 | 3.02 | 0.03 | MDL | 94.36 |
| CCPb-05-glass | 52 | 68.74 | 0.24 | 14.53 | 1.70 | 0.17 | 0.41 | 1.94 | 3.91 | 3.11 | 0.05 | 0.01 | 94.81 |
| CCPb-05-glass | 53 | 66.59 | 0.30 | 14.36 | 1.26 | 0.04 | 0.42 | 2.07 | 3.57 | 3.02 | 0.01 | MDL | 91.65 |
| CCPb-06-glass | 54 | 71.18 | 0.18 | 12.74 | 1.21 | MDL | 0.23 | 1.28 | 3.14 | 2.45 | 0.02 | MDL | 92.44 |
| CCPb-06-glass | 55 | 70.30 | 0.14 | 12.91 | 1.08 | 0.07 | 0.20 | 1.29 | 3.72 | 3.53 | 0.02 | MDL | 93.25 |
| CCPb-06-glass | 56 | 69.32 | 0.16 | 12.85 | 1.27 | MDL | 0.21 | 1.23 | 3.63 | 3.56 | 0.03 | MDL | 92.25 |
| CCPb-06-glass | 57 | 69.30 | 0.18 | 12.53 | 0.85 | 0.07 | 0.20 | 1.17 | 3.47 | 3.61 | MDL | MDL | 91.39 |
| CCPb-06-glass | 58 | 69.49 | 0.21 | 13.00 | 0.93 | 0.03 | 0.23 | 1.36 | 3.65 | 3.56 | 0.02 | 0.02 | 92.51 |
| CCPb-06-glass | 59 | 69.96 | 0.13 | 12.44 | 0.94 | 0.06 | 0.18 | 1.12 | 3.31 | 3.51 | 0.02 | MDL | 91.67 |
| CCPb-06-glass | 60 | 69.88 | 0.11 | 12.18 | 1.17 | 0.08 | 0.16 | 1.18 | 3.20 | 3.55 | 0.02 | MDL | 91.53 |
| CCPb-07-glass | 61 | 68.36 | 0.23 | 12.98 | 1.42 | 0.04 | 0.42 | 1.75 | 3.78 | 3.21 | 0.01 | MDL | 92.18 |
| CCPb-07-glass | 62 | 66.28 | 0.26 | 13.80 | 1.80 | 0.06 | 0.50 | 1.93 | 3.77 | 3.30 | 0.02 | 0.02 | 91.74 |
| CCPb-07-glass | 63 | 66.52 | 0.21 | 13.84 | 1.64 | 0.06 | 0.48 | 2.01 | 3.58 | 3.27 | 0.02 | MDL | 91.63 |
| CCPb-07-glass | 64 | 66.83 | 0.25 | 13.75 | 1.76 | 0.06 | 0.45 | 1.95 | 3.56 | 3.29 | MDL | 0.05 | 91.94 |
| CCPb-07-glass | 65 | 66.40 | 0.29 | 13.97 | 1.73 | 0.02 | 0.47 | 2.12 | 3.58 | 3.20 | 0.02 | 0.04 | 91.85 |
| CCPb-07-glass | 66 | 66.60 | 0.24 | 13.62 | 1.63 | 0.04 | 0.51 | 1.90 | 3.61 | 3.28 | 0.02 | MDL | 91.46 |
| CCPb-07-glass | 67 | 65.86 | 0.23 | 13.66 | 1.79 | 0.03 | 0.41 | 2.00 | 3.78 | 3.23 | 0.02 | 0.01 | 91.03 |
| CCPb-08-glass | 68 | 70.52 | 0.31 | 12.81 | 1.84 | 0.02 | 0.37 | 1.37 | 3.64 | 3.47 | 0.03 | MDL | 94.38 |
| CCPb-08-glass | 69 | 70.66 | 0.27 | 12.50 | 1.47 | MDL | 0.33 | 1.36 | 3.64 | 3.51 | 0.03 | MDL | 93.77 |
| CCPb-08-glass | 70 | 71.18 | 0.20 | 12.17 | 1.67 | MDL | 0.32 | 1.44 | 3.75 | 3.41 | MDL | 0.03 | 94.17 |
| CCPb-08-glass | 71 | 70.65 | 0.27 | 12.57 | 1.59 | 0.02 | 0.33 | 1.31 | 3.28 | 3.48 | 0.02 | MDL | 93.51 |
| CCPb-08-glass | 72 | 71.08 | 0.31 | 12.85 | 1.78 | 0.02 | 0.40 | 1.54 | 3.92 | 3.54 | MDL | 0.01 | 95.47 |
| CCPb-08-glass | 73 | 70.07 | 0.19 | 12.60 | 1.74 | 0.04 | 0.36 | 1.49 | 3.68 | 3.49 | 0.02 | MDL | 93.70 |
| CCPb-08-glass | 74 | 69.99 | 0.21 | 13.22 | 1.55 | 0.02 | 0.43 | 1.75 | 3.82 | 3.45 | 0.01 | 0.03 | 94.48 |
| CCPb-08-glass | 75 | 69.66 | 0.22 | 13.54 | 1.91 | MDL | 0.37 | 1.68 | 4.02 | 3.50 | 0.02 | MDL | 94.93 |
| CCPb-08-glass | 76 | 67.97 | 0.20 | 13.44 | 1.66 | MDL | 0.42 | 1.73 | 3.73 | 3.43 | 0.02 | MDL | 92.60 |
| CCPb-08-glass | 77 | 69.60 | 0.21 | 13.67 | 1.43 | 0.08 | 0.42 | 1.67 | 3.77 | 3.52 | MDL | 0.07 | 94.46 |

**Appendix F, continued.**

| Sample | line | $SiO_2$ | $TiO_2$ | $Al_2O_3$ | $FeO^*$ | MnO | MgO | CaO | $Na_2O$ | $K_2O$ | Cl | $SO_3$ | Total |
|---|---|---|---|---|---|---|---|---|---|---|---|---|---|
| CCPb-09-glass | 78 | 68.33 | 0.20 | 13.07 | 1.08 | 0.08 | 0.22 | 1.59 | 2.70 | 2.14 | 0.04 | MDL | 89.45 |
| CCPb-09-glass | 79 | 67.79 | 0.10 | 12.51 | 0.88 | 0.13 | 0.22 | 1.55 | 3.16 | 3.30 | 0.05 | MDL | 89.69 |
| CCPb-09-glass | 80 | 67.83 | 0.14 | 12.10 | 1.25 | 0.10 | 0.21 | 1.36 | 3.04 | 3.28 | 0.03 | 0.03 | 89.36 |
| CCPb-09-glass | 81 | 67.70 | 0.16 | 12.20 | 1.14 | 0.04 | 0.23 | 1.46 | 2.92 | 3.30 | 0.04 | MDL | 89.18 |
| CCPb-09-glass | 82 | 69.22 | 0.16 | 12.64 | 1.07 | MDL | 0.24 | 1.51 | 3.22 | 3.28 | 0.04 | MDL | 91.38 |
| CCPb-09-glass | 83 | 68.51 | 0.13 | 12.15 | 1.04 | 0.09 | 0.21 | 1.38 | 3.16 | 3.26 | 0.04 | 0.05 | 90.01 |
| CCPb-09-glass | 84 | 67.91 | 0.14 | 12.33 | 1.19 | MDL | 0.20 | 1.37 | 3.28 | 3.22 | 0.03 | MDL | 89.67 |
| CCPb-10-glass | 85 | 70.16 | 0.15 | 12.51 | 0.93 | 0.06 | 0.18 | 1.27 | 3.29 | 3.45 | MDL | MDL | 92.00 |
| CCPb-10-glass | 86 | 70.20 | 0.14 | 12.21 | 0.97 | MDL | 0.19 | 1.23 | 3.64 | 3.52 | 0.02 | MDL | 92.12 |
| CCPb-10-glass | 87 | 69.09 | 0.13 | 12.16 | 0.86 | 0.09 | 0.22 | 1.29 | 3.40 | 3.43 | MDL | MDL | 90.67 |
| CCPb-10-glass | 88 | 70.41 | 0.17 | 11.44 | 0.84 | 0.06 | 0.16 | 1.04 | 3.19 | 3.45 | 0.01 | 0.02 | 90.79 |
| CCPb-10-glass | 89 | 69.68 | 0.15 | 12.01 | 0.73 | MDL | 0.19 | 1.23 | 3.26 | 3.47 | MDL | MDL | 90.73 |
| CCPb-10-glass | 90 | 68.70 | 0.13 | 12.36 | 1.01 | MDL | 0.22 | 1.16 | 3.14 | 3.45 | MDL | 0.01 | 90.18 |
| CCPb-11-glass | 91 | 70.44 | 0.25 | 13.10 | 1.70 | MDL | 0.32 | 1.56 | 3.41 | 3.41 | 0.03 | 0.04 | 94.26 |
| CCPb-11-glass | 92 | 71.48 | 0.29 | 13.07 | 1.61 | 0.02 | 0.32 | 1.49 | 2.25 | 3.32 | 0.06 | MDL | 93.92 |
| CCPb-11-glass | 93 | 69.48 | 0.18 | 12.98 | 1.55 | 0.09 | 0.35 | 1.51 | 3.48 | 3.41 | 0.03 | MDL | 93.08 |
| CCPb-11-glass | 94 | 71.07 | 0.26 | 12.98 | 1.49 | 0.02 | 0.33 | 1.51 | 3.65 | 3.41 | 0.06 | 0.01 | 94.79 |
| CCPb-11-glass | 95 | 70.51 | 0.15 | 13.27 | 1.20 | 0.08 | 0.24 | 1.46 | 3.23 | 3.47 | 0.05 | MDL | 93.65 |
| CCPb-11-glass | 96 | 69.25 | 0.20 | 12.54 | 1.81 | 0.07 | 0.26 | 1.51 | 3.29 | 3.42 | 0.04 | 0.03 | 92.43 |
| CCPb-11-glass | 97 | 70.24 | 0.28 | 12.54 | 1.62 | MDL | 0.22 | 1.55 | 3.14 | 3.27 | 0.03 | 0.03 | 92.90 |
| CCPb-11-glass | 98 | 71.19 | 0.22 | 12.26 | 1.33 | 0.07 | 0.33 | 1.52 | 3.02 | 3.36 | 0.05 | 0.03 | 93.37 |
| CCPb-11-glass | 99 | 71.42 | 0.26 | 12.80 | 1.72 | 0.05 | 0.27 | 1.47 | 3.45 | 3.35 | 0.04 | 0.03 | 94.85 |
| CCPb-11-glass | 100 | 69.91 | 0.24 | 12.97 | 1.49 | 0.04 | 0.34 | 1.54 | 3.17 | 3.42 | 0.04 | MDL | 93.16 |
| CCPb-11-glass | 101 | 71.98 | 0.22 | 12.99 | 1.46 | 0.01 | 0.34 | 1.59 | 3.57 | 3.47 | 0.04 | MDL | 95.67 |
| CCPb-11-glass | 102 | 67.42 | 0.27 | 12.90 | 1.41 | 0.06 | 0.29 | 1.63 | 3.13 | 3.24 | 0.04 | MDL | 90.41 |
| CCPb-11-glass | 103 | 69.33 | 0.29 | 13.20 | 1.69 | 0.01 | 0.35 | 1.85 | 3.82 | 3.46 | 0.08 | MDL | 94.07 |
| CCPb-12-glass | 104 | 71.06 | 0.19 | 12.41 | 1.12 | MDL | 0.20 | 1.20 | 2.98 | 2.74 | 0.06 | MDL | 91.96 |
| CCPb-12-glass | 105 | 71.58 | 0.16 | 11.65 | 0.94 | MDL | 0.14 | 1.06 | 3.21 | 3.62 | 0.05 | MDL | 92.40 |
| CCPb-12-glass | 106 | 71.19 | 0.15 | 11.71 | 1.06 | MDL | 0.16 | 1.07 | 3.09 | 3.54 | 0.04 | MDL | 92.01 |
| CCPb-12-glass | 107 | 69.89 | 0.13 | 11.82 | 1.04 | 0.09 | 0.13 | 1.11 | 3.15 | 3.64 | 0.05 | MDL | 91.06 |
| CCPb-12-glass | 108 | 71.02 | 0.14 | 11.86 | 1.28 | 0.06 | 0.20 | 1.06 | 3.17 | 3.67 | 0.05 | 0.02 | 92.52 |
| CCPb-12-glass | 109 | 69.93 | 0.15 | 12.08 | 1.31 | MDL | 0.18 | 1.02 | 3.19 | 3.58 | 0.04 | MDL | 91.48 |
| CCPb-12-glass | 110 | 70.38 | 0.17 | 11.84 | 0.88 | 0.07 | 0.17 | 1.06 | 3.14 | 3.63 | 0.04 | MDL | 91.37 |
| CCPb-13-glass | 111 | 73.08 | 0.06 | 11.66 | 0.64 | MDL | 0.11 | 0.77 | 3.06 | 3.81 | 0.05 | 0.01 | 93.25 |
| CCPb-13-glass | 112 | 72.42 | 0.07 | 11.39 | 0.60 | 0.11 | 0.09 | 0.76 | 2.90 | 3.78 | 0.03 | 0.02 | 92.19 |
| CCPb-13-glass | 113 | 72.24 | 0.12 | 11.58 | 0.77 | 0.07 | 0.19 | 0.71 | 2.78 | 3.79 | 0.04 | MDL | 92.29 |
| CCPb-13-glass | 114 | 71.44 | 0.08 | 11.28 | 0.66 | 0.03 | 0.11 | 0.74 | 2.71 | 3.79 | 0.05 | 0.03 | 90.91 |
| CCPb-13-glass | 115 | 71.91 | 0.06 | 11.50 | 0.71 | MDL | 0.11 | 0.72 | 2.92 | 3.77 | 0.04 | MDL | 91.74 |
| CCPb-13-glass | 116 | 72.38 | 0.06 | 11.47 | 0.60 | MDL | 0.08 | 0.78 | 2.96 | 3.83 | 0.03 | MDL | 92.18 |
| CCPb-13-glass | 117 | 71.91 | 0.10 | 11.57 | 0.65 | 0.06 | 0.10 | 0.85 | 2.83 | 3.78 | 0.05 | MDL | 91.90 |

**Appendix F, continued.**

| Sample | line | $SiO_2$ | $TiO_2$ | $Al_2O_3$ | $FeO^*$ | MnO | MgO | CaO | $Na_2O$ | $K_2O$ | Cl | $SO_3$ | Total |
|---|---|---|---|---|---|---|---|---|---|---|---|---|---|
| CCPb-14-glass | 118 | 74.25 | 0.20 | 12.20 | 0.94 | MDL | 0.20 | 1.08 | 3.07 | 3.45 | 0.03 | MDL | 95.41 |
| CCPb-14-glass | 119 | 75.08 | 0.18 | 12.23 | 0.93 | MDL | 0.19 | 1.01 | 3.15 | 3.92 | 0.04 | MDL | 96.72 |
| CCPb-14-glass | 120 | 73.19 | 0.17 | 12.13 | 0.77 | 0.06 | 0.22 | 1.01 | 3.09 | 3.84 | 0.02 | MDL | 94.48 |
| CCPb-14-glass | 121 | 71.77 | 0.19 | 11.86 | 0.97 | MDL | 0.15 | 0.92 | 3.14 | 3.89 | MDL | MDL | 92.89 |
| CCPb-14-glass | 122 | 72.04 | 0.26 | 12.37 | 1.06 | 0.04 | 0.35 | 0.94 | 3.46 | 3.97 | MDL | MDL | 94.49 |
| CCPb-14-glass | 123 | 72.70 | 0.17 | 11.64 | 1.03 | 0.07 | 0.24 | 0.90 | 3.33 | 3.91 | MDL | 0.03 | 94.02 |
| CCPb-14-glass | 124 | 72.01 | 0.23 | 11.74 | 1.30 | 0.02 | 0.40 | 0.98 | 2.95 | 4.01 | MDL | 0.06 | 93.70 |
| CCPb-15-glass | 125 | 73.24 | 0.11 | 11.62 | 0.66 | 0.05 | 0.13 | 0.77 | 2.92 | 3.40 | 0.02 | MDL | 92.91 |
| CCPb-15-glass | 126 | 71.52 | 0.14 | 11.17 | 0.71 | 0.03 | 0.11 | 0.68 | 2.76 | 3.93 | MDL | MDL | 91.06 |
| CCPb-15-glass | 127 | 72.92 | 0.18 | 11.64 | 0.61 | 0.04 | 0.13 | 0.84 | 3.09 | 3.99 | 0.03 | 0.01 | 93.48 |
| CCPb-15-glass | 128 | 73.49 | 0.16 | 11.35 | 0.77 | MDL | 0.18 | 0.80 | 2.76 | 4.05 | 0.02 | MDL | 93.57 |
| CCPb-15-glass | 129 | 73.04 | 0.12 | 11.27 | 0.89 | 0.08 | 0.22 | 0.69 | 2.84 | 4.02 | 0.03 | 0.02 | 93.21 |
| CCPb-15-glass | 130 | 71.89 | 0.14 | 11.09 | 0.71 | MDL | 0.19 | 0.75 | 2.80 | 3.93 | MDL | MDL | 91.49 |
| CCPb-15-glass | 131 | 75.76 | 0.13 | 11.23 | 0.82 | 0.05 | 0.20 | 0.67 | 3.19 | 3.99 | 0.01 | MDL | 96.04 |
| CCPb-16-glass | 132 | 66.46 | 0.17 | 12.19 | 1.48 | 0.09 | 0.38 | 1.50 | 3.36 | 3.48 | 0.02 | MDL | 89.13 |
| CCPb-16-glass | 133 | 65.61 | 0.26 | 11.80 | 1.32 | 0.11 | 0.34 | 1.44 | 3.34 | 3.38 | 0.03 | MDL | 87.64 |
| CCPb-16-glass | 134 | 70.69 | 0.32 | 12.89 | 1.40 | MDL | 0.37 | 1.57 | 3.44 | 3.46 | 0.03 | 0.03 | 94.20 |
| CCPb-16-glass | 135 | 72.33 | 0.31 | 12.87 | 1.27 | 0.06 | 0.34 | 1.57 | 3.24 | 3.50 | 0.03 | MDL | 95.52 |
| CCPb-16-glass | 136 | 69.59 | 0.30 | 12.65 | 1.45 | 0.12 | 0.42 | 1.51 | 3.52 | 3.45 | 0.03 | 0.05 | 93.09 |
| CCPb-16-glass | 137 | 68.59 | 0.26 | 12.35 | 1.48 | MDL | 0.38 | 1.53 | 3.35 | 3.41 | 0.03 | 0.06 | 91.43 |
| CCPb-16-glass | 138 | 71.28 | 0.22 | 13.01 | 1.75 | MDL | 0.34 | 1.41 | 3.73 | 3.42 | 0.04 | 0.01 | 95.22 |
| CCPb-16-glass | 139 | 68.41 | 0.19 | 11.61 | 1.47 | 0.02 | 0.34 | 1.38 | 3.14 | 3.40 | 0.04 | MDL | 89.98 |
| CCPb-16-glass | 140 | 73.90 | 0.23 | 11.98 | 0.98 | MDL | 0.26 | 1.29 | 3.40 | 3.42 | 0.04 | 0.02 | 95.51 |
| CCPb-17-glass | 141 | 70.68 | 0.19 | 12.33 | 1.08 | MDL | 0.25 | 1.35 | 3.25 | 3.64 | 0.04 | 0.05 | 92.86 |
| CCPb-17-glass | 142 | 70.23 | 0.20 | 12.22 | 1.33 | 0.10 | 0.22 | 1.22 | 3.15 | 3.61 | 0.06 | MDL | 92.34 |
| CCPb-17-glass | 143 | 69.42 | 0.13 | 12.38 | 1.44 | 0.11 | 0.19 | 1.33 | 3.43 | 3.61 | 0.05 | 0.03 | 92.12 |
| CCPb-17-glass | 144 | 69.96 | 0.19 | 11.94 | 1.32 | 0.02 | 0.21 | 1.25 | 3.20 | 3.55 | 0.03 | MDL | 91.68 |
| CCPb-17-glass | 145 | 69.16 | 0.17 | 12.19 | 1.10 | 0.01 | 0.21 | 1.35 | 3.07 | 3.57 | 0.05 | 0.01 | 90.88 |
| CCPb-17-glass | 146 | 69.89 | 0.22 | 12.30 | 1.39 | MDL | 0.19 | 1.26 | 2.86 | 3.61 | 0.03 | 0.18 | 91.93 |
| CCPb-17-glass | 147 | 68.69 | 0.19 | 12.35 | 1.26 | 0.04 | 0.29 | 1.35 | 3.07 | 3.51 | 0.06 | MDL | 90.81 |
| CCPb-18-glass | 148 | 70.18 | 0.09 | 12.53 | 0.86 | 0.07 | 0.12 | 1.28 | 2.88 | 2.02 | 0.03 | 0.03 | 90.07 |
| CCPb-18-glass | 149 | 71.14 | 0.11 | 12.15 | 0.85 | MDL | 0.20 | 1.17 | 2.86 | 3.41 | 0.03 | 0.06 | 91.97 |
| CCPb-18-glass | 150 | 70.63 | 0.12 | 11.95 | 0.74 | 0.04 | 0.15 | 1.22 | 3.01 | 3.34 | 0.04 | 0.03 | 91.27 |
| CCPb-18-glass | 151 | 68.54 | 0.12 | 12.11 | 0.77 | 0.06 | 0.17 | 1.29 | 2.80 | 3.44 | 0.01 | MDL | 89.31 |
| CCPb-18-glass | 152 | 69.38 | 0.11 | 12.03 | 0.83 | 0.09 | 0.14 | 1.28 | 3.26 | 3.37 | 0.03 | MDL | 90.52 |
| CCPb-18-glass | 153 | 69.94 | 0.10 | 12.17 | 0.68 | 0.03 | 0.16 | 1.28 | 3.14 | 3.37 | 0.02 | MDL | 90.88 |
| CCPb-18-glass | 154 | 69.37 | 0.09 | 12.01 | 0.70 | 0.02 | 0.23 | 1.21 | 3.20 | 3.43 | 0.02 | MDL | 90.28 |

**Appendix F, continued.**

| Sample | line | $SiO_2$ | $TiO_2$ | $Al_2O_3$ | $FeO^*$ | MnO | MgO | CaO | $Na_2O$ | $K_2O$ | Cl | $SO_3$ | Total |
|---|---|---|---|---|---|---|---|---|---|---|---|---|---|
| CCPb-19-glass | 155 | 73.02 | 0.16 | 12.44 | 0.74 | MDL | 0.15 | 0.93 | 2.52 | 3.52 | 0.04 | 0.01 | 93.52 |
| CCPb-19-glass | 156 | 74.03 | 0.13 | 12.45 | 0.89 | MDL | 0.15 | 0.92 | 2.65 | 3.59 | 0.03 | 0.06 | 94.91 |
| CCPb-19-glass | 157 | 74.18 | 0.10 | 12.57 | 0.61 | 0.03 | 0.18 | 0.90 | 2.55 | 3.57 | 0.05 | MDL | 94.74 |
| CCPb-19-glass | 158 | 74.81 | 0.15 | 12.62 | 0.97 | MDL | 0.17 | 0.92 | 2.80 | 3.58 | 0.02 | MDL | 96.04 |
| CCPb-19-glass | 159 | 73.67 | 0.14 | 11.99 | 0.70 | 0.02 | 0.18 | 0.91 | 2.28 | 3.63 | 0.05 | MDL | 93.56 |
| CCPb-19-glass | 160 | 74.42 | 0.14 | 12.08 | 0.57 | MDL | 0.14 | 0.85 | 2.22 | 3.65 | 0.03 | MDL | 94.11 |
| CCPb-19-glass | 161 | 73.52 | 0.18 | 12.10 | 0.78 | 0.02 | 0.16 | 0.91 | 2.13 | 3.64 | 0.04 | 0.02 | 93.50 |
| CCPb-19-glass | 162 | 73.36 | 0.22 | 11.75 | 0.96 | 0.11 | 0.23 | 0.94 | 2.29 | 3.72 | 0.06 | MDL | 93.64 |
| CCPb-19-glass | 163 | 74.32 | 0.15 | 12.04 | 1.27 | MDL | 0.14 | 0.84 | 2.98 | 3.76 | 0.05 | 0.02 | 95.57 |
| CCPb-19-glass | 164 | 73.87 | 0.10 | 12.16 | 1.03 | 0.02 | 0.16 | 0.89 | 3.15 | 3.71 | 0.04 | MDL | 95.14 |
| CCPb-20-glass | 165 | 72.57 | 0.12 | 10.21 | 0.72 | 0.04 | 0.18 | 0.66 | 3.00 | 4.04 | 0.05 | MDL | 91.59 |
| CCPb-20-glass | 166 | 72.49 | 0.12 | 11.44 | 0.73 | 0.11 | 0.12 | 0.64 | 2.88 | 4.01 | 0.05 | MDL | 92.58 |
| CCPb-20-glass | 167 | 71.32 | 0.08 | 11.69 | 0.84 | 0.04 | 0.15 | 0.73 | 2.96 | 4.02 | 0.03 | MDL | 91.84 |
| CCPb-20-glass | 168 | 71.60 | 0.16 | 11.56 | 0.80 | MDL | 0.12 | 0.64 | 2.83 | 4.14 | 0.05 | MDL | 91.89 |
| CCPb-20-glass | 169 | 71.11 | 0.12 | 11.64 | 0.62 | MDL | 0.14 | 0.80 | 3.00 | 3.95 | 0.05 | 0.03 | 91.45 |
| CCPb-20-glass | 170 | 72.23 | 0.13 | 11.36 | 0.51 | 0.02 | 0.08 | 0.66 | 2.93 | 4.20 | 0.05 | MDL | 92.16 |
| CCPb-20-glass | 171 | 72.50 | 0.06 | 11.02 | 0.66 | 0.07 | 0.06 | 0.66 | 3.01 | 4.07 | 0.05 | 0.04 | 92.21 |
| CCPb-20-glass | 172 | 70.69 | 0.11 | 10.70 | 0.64 | 0.07 | 0.07 | 0.62 | 2.59 | 3.99 | 0.04 | MDL | 89.54 |
| CCPb-20-glass | 173 | 72.08 | 0.07 | 11.30 | 0.61 | MDL | 0.14 | 0.83 | 2.98 | 4.08 | 0.04 | 0.02 | 92.16 |
| CCPb-21-glass | 174 | 72.67 | 0.08 | 11.34 | 0.81 | 0.08 | 0.11 | 0.66 | 2.80 | 4.43 | 0.01 | 0.02 | 93.02 |
| CCPb-21-glass | 175 | 73.62 | 0.06 | 11.15 | 0.50 | 0.07 | 0.08 | 0.65 | 2.98 | 4.45 | 0.02 | MDL | 93.58 |
| CCPb-21-glass | 176 | 73.61 | 0.05 | 10.83 | 0.41 | 0.09 | 0.04 | 0.45 | 2.63 | 4.62 | 0.02 | MDL | 92.77 |
| CCPb-21-glass | 177 | 71.58 | 0.09 | 12.29 | 0.53 | MDL | 0.08 | 0.95 | 3.12 | 4.21 | 0.02 | MDL | 92.87 |
| CCPb-21-glass | 178 | 73.67 | 0.12 | 10.54 | 0.53 | 0.02 | 0.16 | 0.66 | 2.82 | 4.14 | 0.01 | MDL | 92.67 |
| CCPb-22-glass | 179 | 69.07 | 0.21 | 13.12 | 1.15 | 0.05 | 0.23 | 1.42 | 3.31 | 3.14 | MDL | 0.01 | 91.71 |
| CCPb-22-glass | 180 | 68.13 | 0.13 | 14.00 | 1.20 | 0.03 | 0.34 | 1.73 | 3.68 | 3.19 | MDL | MDL | 92.44 |
| CCPb-22-glass | 181 | 69.11 | 0.20 | 13.34 | 1.59 | 0.08 | 0.30 | 1.66 | 3.65 | 3.15 | MDL | 0.01 | 93.13 |
| CCPb-22-glass | 182 | 69.60 | 0.20 | 13.62 | 1.58 | 0.08 | 0.29 | 1.64 | 3.52 | 3.18 | MDL | 0.02 | 93.74 |
| CCPb-22-glass | 183 | 68.68 | 0.23 | 13.67 | 1.47 | MDL | 0.28 | 1.67 | 3.79 | 3.10 | 0.02 | MDL | 92.91 |
| CCPb-22-glass | 184 | 67.11 | 0.14 | 13.72 | 1.27 | MDL | 0.34 | 1.62 | 3.71 | 3.26 | MDL | 0.06 | 91.24 |
| CCPb-22-glass | 185 | 68.18 | 0.20 | 13.90 | 1.64 | 0.14 | 0.24 | 1.73 | 3.63 | 3.18 | MDL | 0.17 | 93.03 |
| CCPb-22-glass | 186 | 68.10 | 0.20 | 13.84 | 1.48 | MDL | 0.29 | 1.71 | 3.66 | 3.16 | 0.03 | MDL | 92.47 |
| CCPb-22-glass | 187 | 68.46 | 0.17 | 14.25 | 1.42 | 0.06 | 0.37 | 1.71 | 3.96 | 3.21 | MDL | MDL | 93.63 |
| CCPb-22-glass | 188 | 66.86 | 0.21 | 13.62 | 1.27 | 0.01 | 0.35 | 1.73 | 3.63 | 3.18 | 0.02 | MDL | 90.88 |
| CCPb-22-glass | 189 | 68.42 | 0.22 | 13.45 | 1.07 | 0.07 | 0.32 | 1.72 | 3.31 | 3.23 | 0.03 | MDL | 91.84 |
| CCPb-22-glass | 190 | 67.22 | 0.24 | 13.51 | 1.32 | MDL | 0.33 | 1.72 | 3.69 | 3.20 | 0.03 | 0.02 | 91.28 |

**Appendix F, continued.**

| Sample | line | $SiO_2$ | $TiO_2$ | $Al_2O_3$ | $FeO^*$ | MnO | MgO | CaO | $Na_2O$ | $K_2O$ | Cl | $SO_3$ | Total |
|---|---|---|---|---|---|---|---|---|---|---|---|---|---|
| CCPb-23-glass | 191 | 72.33 | 0.11 | 11.74 | 0.84 | MDL | 0.11 | 0.89 | 3.25 | 3.56 | 0.01 | MDL | 92.84 |
| CCPb-23-glass | 192 | 72.96 | 0.10 | 11.72 | 0.65 | 0.03 | 0.10 | 0.92 | 3.11 | 3.55 | 0.05 | MDL | 93.18 |
| CCPb-23-glass | 193 | 73.06 | 0.10 | 11.51 | 0.65 | 0.02 | 0.11 | 0.88 | 2.93 | 3.62 | 0.03 | MDL | 92.92 |
| CCPb-23-glass | 194 | 71.97 | 0.11 | 11.53 | 0.58 | MDL | 0.12 | 0.90 | 3.05 | 3.60 | 0.03 | MDL | 91.89 |
| CCPb-23-glass | 195 | 71.85 | 0.09 | 11.74 | 0.86 | 0.05 | 0.10 | 0.84 | 3.03 | 3.56 | 0.03 | 0.03 | 92.19 |
| CCPb-23-glass | 196 | 70.94 | 0.08 | 11.79 | 0.58 | 0.07 | 0.15 | 0.81 | 3.19 | 3.60 | 0.03 | MDL | 91.25 |
| CCPb-23-glass | 197 | 70.53 | 0.11 | 12.07 | 0.65 | 0.14 | 0.14 | 0.87 | 2.88 | 3.59 | 0.03 | MDL | 91.00 |
| CCPb-24-glass | 198 | 72.43 | 0.12 | 11.59 | 0.73 | 0.03 | 0.14 | 0.85 | 3.23 | 3.69 | 0.06 | MDL | 92.86 |
| CCPb-24-glass | 199 | 72.82 | 0.12 | 11.76 | 1.10 | 0.02 | 0.14 | 0.86 | 3.07 | 3.71 | 0.04 | MDL | 93.64 |
| CCPb-24-glass | 200 | 70.03 | 0.15 | 11.87 | 0.98 | MDL | 0.11 | 0.88 | 3.11 | 3.67 | 0.05 | MDL | 90.83 |
| CCPb-24-glass | 201 | 72.67 | 0.12 | 11.56 | 0.90 | 0.05 | 0.14 | 0.93 | 3.13 | 3.72 | 0.07 | 0.07 | 93.36 |
| CCPb-24-glass | 202 | 71.29 | 0.11 | 11.65 | 1.03 | 0.03 | 0.17 | 0.85 | 3.21 | 3.65 | 0.05 | MDL | 92.03 |
| CCPb-24-glass | 203 | 71.36 | 0.12 | 11.42 | 0.77 | MDL | 0.12 | 0.94 | 3.08 | 3.67 | 0.04 | 0.02 | 91.55 |
| CCPb-24-glass | 204 | 70.19 | 0.16 | 11.82 | 0.69 | 0.05 | 0.13 | 0.91 | 2.86 | 3.73 | 0.05 | MDL | 90.60 |
| CCPb-25-glass | 205 | 75.37 | 0.16 | 11.69 | 0.64 | MDL | 0.12 | 0.67 | 2.96 | 3.14 | 0.05 | MDL | 94.79 |
| CCPb-25-glass | 206 | 73.86 | 0.12 | 11.63 | 0.64 | 0.01 | 0.12 | 0.72 | 3.03 | 3.90 | 0.04 | 0.03 | 94.09 |
| CCPb-25-glass | 207 | 74.77 | 0.07 | 11.47 | 0.73 | 0.02 | 0.11 | 0.73 | 2.90 | 3.88 | 0.04 | MDL | 94.72 |
| CCPb-25-glass | 208 | 74.04 | 0.15 | 11.57 | 0.71 | 0.03 | 0.10 | 0.91 | 3.01 | 3.90 | 0.01 | 0.02 | 94.45 |
| CCPb-25-glass | 209 | 73.52 | 0.13 | 11.77 | 0.66 | 0.03 | 0.10 | 0.79 | 2.97 | 3.90 | 0.03 | MDL | 93.90 |
| CCPb-25-glass | 210 | 73.45 | 0.17 | 11.30 | 0.73 | 0.07 | 0.11 | 0.70 | 2.90 | 3.84 | 0.05 | MDL | 93.33 |
| CCPb-25-glass | 211 | 73.81 | 0.13 | 11.36 | 0.76 | 0.05 | 0.11 | 0.71 | 2.84 | 4.01 | 0.04 | 0.01 | 93.83 |
| CCPb-26-glass | 212 | 70.16 | 0.10 | 11.56 | 0.71 | MDL | 0.05 | 0.64 | 2.77 | 2.93 | MDL | 0.01 | 88.94 |
| CCPb-26-glass | 213 | 70.57 | 0.13 | 12.31 | 0.74 | MDL | 0.20 | 0.72 | 3.18 | 4.53 | 0.01 | MDL | 92.39 |
| CCPb-26-glass | 214 | 70.14 | 0.07 | 12.49 | 1.09 | MDL | 0.16 | 0.72 | 3.51 | 4.52 | MDL | 0.02 | 92.73 |
| CCPb-26-glass | 215 | 69.57 | 0.13 | 11.56 | 1.38 | MDL | 0.29 | 0.69 | 3.33 | 4.61 | MDL | MDL | 91.55 |
| CCPb-27-glass | 216 | 74.75 | 0.11 | 11.42 | 0.56 | 0.07 | 0.11 | 0.43 | 2.61 | 3.86 | 0.03 | 0.01 | 93.95 |
| CCPb-27-glass | 217 | 74.17 | 0.07 | 11.17 | 0.55 | 0.03 | 0.08 | 0.62 | 2.99 | 4.32 | 0.05 | MDL | 94.04 |
| CCPb-27-glass | 218 | 73.61 | 0.10 | 11.04 | 0.67 | 0.06 | 0.12 | 0.59 | 2.94 | 4.25 | 0.04 | MDL | 93.42 |
| CCPb-27-glass | 219 | 73.59 | 0.12 | 11.00 | 1.88 | 0.11 | 0.37 | 0.63 | 2.69 | 4.43 | 0.06 | MDL | 94.87 |
| CCPb-27-glass | 220 | 75.41 | 0.13 | 10.36 | 0.63 | 0.02 | 0.07 | 0.67 | 2.98 | 3.90 | 0.01 | 0.02 | 94.21 |
| CCPb-27-glass | 221 | 74.25 | 0.13 | 10.58 | 0.53 | 0.06 | 0.14 | 0.46 | 2.70 | 4.35 | 0.03 | MDL | 93.22 |
| CCPb-28-glass | 222 | 69.38 | 0.12 | 12.72 | 0.95 | 0.03 | 0.31 | 1.23 | 2.68 | 2.02 | MDL | MDL | 89.46 |
| CCPb-28-glass | 223 | 69.91 | 0.05 | 12.33 | 0.86 | MDL | 0.17 | 1.26 | 2.90 | 3.41 | MDL | 0.01 | 90.92 |
| CCPb-28-glass | 224 | 70.10 | 0.08 | 12.37 | 0.80 | 0.09 | 0.14 | 1.21 | 3.28 | 3.34 | 0.01 | MDL | 91.43 |
| CCPb-28-glass | 225 | 70.44 | 0.09 | 12.13 | 0.88 | 0.02 | 0.17 | 1.23 | 3.13 | 3.37 | MDL | 0.04 | 91.51 |
| CCPb-28-glass | 226 | 70.52 | 0.12 | 12.12 | 0.84 | MDL | 0.19 | 1.19 | 3.18 | 3.41 | MDL | 0.01 | 91.59 |
| CCPb-28-glass | 227 | 69.94 | 0.08 | 12.06 | 0.98 | 0.06 | 0.14 | 1.18 | 3.51 | 3.34 | 0.02 | 0.03 | 91.33 |
| CCPb-28-glass | 228 | 69.35 | 0.12 | 12.19 | 0.72 | 0.02 | 0.11 | 1.18 | 3.12 | 3.31 | 0.02 | MDL | 90.14 |

**Appendix F, continued.**

| Sample | line | $SiO_2$ | $TiO_2$ | $Al_2O_3$ | $FeO^*$ | MnO | MgO | CaO | $Na_2O$ | $K_2O$ | Cl | $SO_3$ | Total |
|---|---|---|---|---|---|---|---|---|---|---|---|---|---|
| CCPb-29-glass | 229 | 70.49 | 0.14 | 12.48 | 1.26 | 0.04 | 0.19 | 1.18 | 3.07 | 2.61 | 0.01 | MDL | 91.49 |
| CCPb-29-glass | 230 | 68.70 | 0.15 | 12.18 | 1.22 | 0.03 | 0.17 | 1.15 | 3.40 | 3.61 | MDL | MDL | 90.63 |
| CCPb-29-glass | 231 | 70.22 | 0.13 | 11.48 | 0.86 | 0.06 | 0.19 | 1.10 | 3.08 | 3.59 | 0.02 | MDL | 90.72 |
| CCPb-29-glass | 232 | 68.66 | 0.13 | 12.27 | 1.04 | 0.05 | 0.17 | 1.18 | 3.25 | 3.60 | 0.02 | MDL | 90.37 |
| CCPb-29-glass | 233 | 68.78 | 0.14 | 12.18 | 1.02 | 0.03 | 0.19 | 1.08 | 3.52 | 3.63 | MDL | MDL | 90.57 |
| CCPb-29-glass | 234 | 68.43 | 0.17 | 12.20 | 0.79 | 0.06 | 0.19 | 1.17 | 3.34 | 3.57 | 0.01 | MDL | 89.93 |
| CCPb-29-glass | 235 | 69.62 | 0.15 | 12.06 | 0.87 | 0.02 | 0.17 | 1.17 | 3.14 | 3.61 | 0.01 | 0.07 | 90.88 |
| CCPb-30-glass | 236 | 69.60 | 0.19 | 12.30 | 0.86 | 0.06 | 0.15 | 1.04 | 3.19 | 2.34 | 0.01 | MDL | 89.74 |
| CCPb-30-glass | 237 | 67.87 | 0.15 | 12.05 | 1.03 | 0.05 | 0.17 | 1.12 | 3.64 | 3.61 | 0.02 | MDL | 89.70 |
| CCPb-30-glass | 238 | 67.54 | 0.16 | 12.19 | 0.87 | 0.10 | 0.16 | 1.12 | 3.25 | 3.68 | MDL | 0.03 | 89.10 |
| CCPb-30-glass | 239 | 69.50 | 0.15 | 11.43 | 0.92 | 0.03 | 0.16 | 0.95 | 3.32 | 3.60 | 0.01 | MDL | 90.07 |
| CCPb-30-glass | 240 | 71.54 | 0.19 | 11.97 | 1.13 | 0.03 | 0.15 | 1.04 | 3.51 | 3.66 | MDL | MDL | 93.21 |
| CCPb-30-glass | 241 | 68.25 | 0.16 | 11.90 | 1.19 | 0.07 | 0.15 | 1.13 | 3.60 | 3.61 | MDL | 0.02 | 90.09 |
| CCPb-30-glass | 242 | 68.83 | 0.20 | 12.09 | 0.98 | 0.06 | 0.17 | 1.10 | 3.45 | 3.69 | 0.02 | 0.03 | 90.62 |
| CCPb-31-glass | 243 | 69.88 | 0.10 | 11.58 | 0.84 | 0.07 | 0.12 | 0.94 | 3.08 | 3.66 | 0.01 | MDL | 90.28 |
| CCPb-31-glass | 244 | 69.69 | 0.39 | 11.48 | 0.79 | 0.02 | 0.12 | 0.94 | 3.00 | 3.59 | MDL | 0.01 | 90.04 |
| CCPb-31-glass | 245 | 68.97 | 0.11 | 11.49 | 0.96 | 0.13 | 0.12 | 0.87 | 3.16 | 3.66 | MDL | MDL | 89.48 |
| CCPb-31-glass | 246 | 69.90 | 0.10 | 11.74 | 0.73 | 0.09 | 0.11 | 0.90 | 3.02 | 3.68 | 0.01 | MDL | 90.28 |
| CCPb-31-glass | 247 | 68.70 | 0.14 | 11.38 | 0.54 | 0.09 | 0.10 | 0.91 | 3.15 | 3.56 | MDL | MDL | 88.57 |
| CCPb-31-glass | 248 | 70.16 | 0.12 | 11.59 | 0.69 | 0.05 | 0.10 | 0.98 | 3.20 | 3.72 | MDL | 0.03 | 90.62 |
| CCPb-31-glass | 249 | 69.75 | 0.18 | 11.32 | 0.82 | 0.11 | 0.11 | 0.88 | 2.84 | 3.68 | 0.01 | 0.01 | 89.70 |
| CCPb-32-glass | 250 | 73.57 | 0.19 | 11.86 | 0.88 | 0.06 | 0.14 | 0.77 | 2.96 | 3.89 | 0.01 | 0.03 | 94.36 |
| CCPb-32-glass | 251 | 74.17 | 0.14 | 11.59 | 0.90 | 0.04 | 0.13 | 0.72 | 2.98 | 4.02 | MDL | 0.03 | 94.72 |
| CCPb-32-glass | 252 | 73.69 | 0.15 | 11.91 | 1.45 | 0.02 | 0.21 | 0.85 | 3.02 | 4.06 | MDL | 0.03 | 95.40 |
| CCPb-32-glass | 253 | 72.52 | 0.19 | 11.78 | 0.86 | 0.02 | 0.20 | 0.83 | 3.38 | 3.98 | MDL | MDL | 93.75 |
| CCPb-32-glass | 254 | 71.92 | 0.21 | 11.56 | 0.79 | MDL | 0.14 | 0.79 | 3.11 | 3.99 | 0.01 | 0.05 | 92.57 |
| CCPb-32-glass | 255 | 71.97 | 0.18 | 11.71 | 0.72 | MDL | 0.11 | 0.80 | 3.07 | 4.01 | MDL | MDL | 92.57 |
| CCPb-32-glass | 256 | 72.49 | 0.21 | 12.47 | 1.05 | 0.06 | 0.10 | 1.16 | 3.68 | 3.95 | MDL | 0.01 | 95.19 |
| CCPb-32-glass | 257 | 74.89 | 0.19 | 12.03 | 1.08 | MDL | 0.17 | 0.77 | 3.19 | 3.97 | MDL | MDL | 96.30 |
| CCPb-32-glass | 258 | 72.95 | 0.13 | 12.17 | 0.51 | 0.01 | 0.13 | 0.72 | 3.45 | 4.06 | 0.15 | MDL | 94.29 |
| CCPb-32-glass | 259 | 72.85 | 0.11 | 11.12 | 0.97 | 0.04 | 0.15 | 0.68 | 3.39 | 3.86 | 0.03 | 0.03 | 93.22 |
| CCPb-32-glass | 260 | 74.48 | 0.12 | 11.95 | 0.95 | 0.04 | 0.17 | 0.74 | 3.49 | 4.09 | 0.02 | MDL | 96.06 |
| CCPb-32-glass | 261 | 75.88 | 0.16 | 11.85 | 0.73 | 0.08 | 0.13 | 0.77 | 3.51 | 3.98 | MDL | 0.03 | 97.12 |

**Appendix F, continued.**

| Sample | line | $SiO_2$ | $TiO_2$ | $Al_2O_3$ | $FeO^*$ | MnO | MgO | CaO | $Na_2O$ | $K_2O$ | Cl | $SO_3$ | Total |
|---|---|---|---|---|---|---|---|---|---|---|---|---|---|
| CCPb-33-glass | 262 | 70.19 | 0.09 | 12.38 | 0.77 | 0.13 | 0.15 | 1.13 | 3.09 | 3.53 | MDL | 0.05 | 91.52 |
| CCPb-33-glass | 263 | 70.16 | 0.19 | 12.79 | 1.48 | MDL | 0.23 | 1.18 | 3.63 | 3.55 | MDL | MDL | 93.21 |
| CCPb-33-glass | 264 | 69.90 | 0.08 | 12.64 | 0.76 | 0.10 | 0.16 | 1.09 | 3.28 | 3.50 | MDL | 0.01 | 91.53 |
| CCPb-33-glass | 265 | 71.50 | 0.12 | 12.82 | 1.17 | 0.11 | 0.16 | 1.13 | 3.75 | 3.47 | MDL | 0.02 | 94.25 |
| CCPb-33-glass | 266 | 70.54 | 0.15 | 12.84 | 0.91 | MDL | 0.23 | 1.11 | 3.84 | 3.58 | MDL | 0.04 | 93.26 |
| CCPb-33-glass | 267 | 71.37 | 0.11 | 12.50 | 0.96 | 0.17 | 0.18 | 1.04 | 3.28 | 3.52 | MDL | MDL | 93.13 |
| CCPb-33-glass | 268 | 71.01 | 0.08 | 12.41 | 0.62 | 0.02 | 0.16 | 1.07 | 3.38 | 3.52 | MDL | MDL | 92.28 |
| CCPb-33-glass | 269 | 71.00 | 0.09 | 12.50 | 0.76 | MDL | 0.19 | 1.14 | 3.29 | 3.49 | 0.01 | MDL | 92.46 |
| CCPb-33-glass | 270 | 70.39 | 0.12 | 12.75 | 0.91 | 0.06 | 0.15 | 1.07 | 3.68 | 3.53 | MDL | MDL | 92.67 |
| CCPb-33-glass | 271 | 70.34 | 0.12 | 12.20 | 0.88 | MDL | 0.13 | 1.14 | 3.52 | 3.56 | MDL | 0.01 | 91.91 |
| CCPb-33-glass | 272 | 69.72 | 0.12 | 12.13 | 0.89 | 0.03 | 0.13 | 1.11 | 3.23 | 3.55 | MDL | MDL | 90.90 |
| CCPb-33-glass | 273 | 69.41 | 0.15 | 11.99 | 1.04 | MDL | 0.18 | 1.08 | 3.38 | 3.54 | MDL | 0.04 | 90.81 |
| CCPb-33-glass | 274 | 70.69 | 0.09 | 12.10 | 1.03 | 0.05 | 0.17 | 1.16 | 3.23 | 3.51 | MDL | 0.04 | 92.05 |
| CCPb-33-glass | 275 | 70.27 | 0.17 | 12.26 | 1.16 | MDL | 0.17 | 1.11 | 3.33 | 3.59 | MDL | MDL | 92.05 |
| CCPb-33-glass | 276 | 70.73 | 0.10 | 12.22 | 1.00 | 0.03 | 0.12 | 1.14 | 3.16 | 3.50 | MDL | MDL | 92.00 |
| CCPb-33-glass | 277 | 70.67 | 0.12 | 12.46 | 0.90 | MDL | 0.12 | 1.21 | 3.32 | 3.59 | MDL | MDL | 92.40 |
| CCPb-33-glass | 278 | 70.78 | 0.13 | 12.46 | 0.89 | MDL | 0.14 | 1.12 | 3.20 | 3.55 | 0.01 | 0.01 | 92.29 |
| CCPb-33-glass | 279 | 70.28 | 0.10 | 12.53 | 0.78 | MDL | 0.12 | 1.11 | 3.29 | 3.58 | MDL | MDL | 91.80 |
| | | | | | | | | | | | | | |
| CCPb-34-glass | 280 | 72.28 | 0.14 | 11.21 | 0.91 | 0.02 | 0.10 | 0.81 | 2.92 | 3.82 | 0.03 | 0.03 | 92.28 |
| CCPb-34-glass | 281 | 70.15 | 0.11 | 11.46 | 0.80 | MDL | 0.13 | 0.82 | 2.95 | 3.73 | 0.01 | 0.02 | 90.20 |
| CCPb-34-glass | 282 | 70.79 | 0.18 | 11.40 | 0.90 | 0.01 | 0.18 | 0.80 | 2.89 | 3.75 | MDL | 0.05 | 90.96 |
| CCPb-34-glass | 283 | 71.32 | 0.10 | 11.49 | 0.62 | 0.05 | 0.14 | 0.87 | 2.86 | 3.71 | 0.04 | MDL | 91.23 |
| CCPb-34-glass | 284 | 71.53 | 0.10 | 11.31 | 0.61 | 0.06 | 0.12 | 0.80 | 2.88 | 3.75 | 0.03 | 0.02 | 91.21 |
| CCPb-34-glass | 285 | 71.07 | 0.12 | 11.00 | 0.67 | MDL | 0.12 | 0.85 | 2.97 | 3.73 | 0.03 | 0.05 | 90.62 |
| CCPb-34-glass | 286 | 70.82 | 0.13 | 11.45 | 0.67 | 0.05 | 0.12 | 0.85 | 3.09 | 3.84 | 0.02 | MDL | 91.04 |
| CCPb-34-glass | 287 | 68.54 | 0.15 | 11.33 | 0.78 | 0.05 | 0.15 | 0.82 | 2.93 | 3.76 | 0.02 | MDL | 88.54 |
| CCPb-34-glass | 288 | 71.69 | 0.15 | 11.36 | 0.84 | MDL | 0.11 | 0.85 | 2.92 | 3.82 | 0.02 | MDL | 91.74 |
| CCPb-34-glass | 289 | 72.65 | 0.18 | 11.57 | 0.88 | 0.05 | 0.11 | 0.84 | 3.22 | 3.74 | 0.02 | MDL | 93.26 |
| CCPb-34-glass | 290 | 70.59 | 0.11 | 11.78 | 0.61 | 0.18 | 0.10 | 0.89 | 2.79 | 3.53 | 0.03 | 0.03 | 90.65 |
| CCPb-34-glass | 291 | 70.95 | 0.04 | 11.84 | 1.28 | 0.01 | 0.09 | 0.85 | 3.03 | 3.79 | 0.02 | 0.03 | 91.92 |
| CCPb-34-glass | 292 | 72.80 | 0.15 | 11.69 | 0.99 | 0.05 | 0.08 | 0.82 | 3.18 | 3.75 | 0.01 | MDL | 93.53 |
| CCPb-34-glass | 293 | 70.69 | 0.10 | 11.50 | 0.90 | MDL | 0.09 | 0.84 | 3.20 | 3.74 | 0.03 | MDL | 91.09 |
| CCPb-34-glass | 294 | 72.47 | 0.11 | 11.82 | 0.78 | 0.05 | 0.12 | 0.82 | 3.27 | 3.74 | 0.02 | 0.03 | 93.24 |
| CCPb-34-glass | 295 | 71.75 | 0.09 | 11.73 | 0.79 | 0.04 | 0.18 | 0.87 | 3.19 | 3.70 | 0.02 | 0.02 | 92.38 |
| CCPb-34-glass | 296 | 72.45 | 0.19 | 11.78 | 0.81 | MDL | 0.08 | 0.91 | 2.83 | 3.72 | 0.01 | 0.04 | 92.83 |
| CCPb-34-glass | 297 | 72.05 | 0.14 | 11.58 | 0.64 | 0.07 | 0.16 | 0.78 | 3.02 | 3.71 | MDL | MDL | 92.17 |
| CCPb-34-glass | 298 | 72.78 | 0.09 | 12.31 | 0.71 | MDL | 0.12 | 1.05 | 3.37 | 3.61 | 0.02 | 0.01 | 94.08 |
| CCPb-34-glass | 299 | 71.59 | 0.14 | 11.64 | 0.67 | 0.02 | 0.08 | 0.89 | 3.08 | 3.73 | 0.03 | 0.02 | 91.88 |
| CCPb-34-glass | 300 | 72.58 | 0.09 | 11.47 | 1.02 | 0.07 | 0.14 | 0.95 | 2.95 | 3.62 | 0.02 | MDL | 92.91 |
| CCPb-34-glass | 301 | 72.10 | 0.08 | 11.54 | 0.59 | 0.06 | 0.14 | 0.92 | 3.07 | 3.86 | 0.02 | MDL | 92.38 |
| CCPb-34-glass | 302 | 73.17 | 0.13 | 11.82 | 0.90 | 0.05 | 0.14 | 0.77 | 2.64 | 3.75 | MDL | MDL | 93.36 |
| CCPb-34-glass | 303 | 72.39 | 0.05 | 11.53 | 0.62 | 0.04 | 0.12 | 0.85 | 3.36 | 3.70 | 0.04 | MDL | 92.71 |

Values marked MDL were below the minimum detection limit.

**Appendix G.** Raw individual continuous decompression experimental run product glass compositions (wt. %) as determined by EPMA.

| Sample | line | $SiO_2$ | $TiO_2$ | $Al_2O_3$ | $FeO^*$ | MnO | MgO | CaO | $Na_2O$ | $K_2O$ | Cl | $SO_3$ | Total |
|---|---|---|---|---|---|---|---|---|---|---|---|---|---|
| CCPb-35-glass | 1 | 72.28 | 0.16 | 11.50 | 0.99 | MDL | 0.08 | 0.92 | 3.16 | 3.77 | 0.02 | MDL | 92.89 |
| CCPb-35-glass | 2 | 73.53 | 0.10 | 11.86 | 0.82 | MDL | 0.06 | 0.76 | 3.31 | 3.82 | 0.03 | MDL | 94.28 |
| CCPb-35-glass | 3 | 74.44 | 0.12 | 12.02 | 0.81 | MDL | 0.14 | 0.81 | 2.47 | 3.83 | 0.04 | 0.02 | 94.69 |
| CCPb-35-glass | 4 | 72.71 | 0.14 | 11.88 | 0.85 | 0.04 | 0.09 | 0.76 | 3.21 | 3.78 | 0.03 | MDL | 93.48 |
| CCPb-35-glass | 5 | 73.19 | 0.09 | 11.76 | 1.08 | MDL | 0.13 | 0.79 | 3.17 | 3.85 | 0.02 | MDL | 94.09 |
| CCPb-35-glass | 6 | 74.37 | 0.11 | 11.68 | 0.56 | MDL | 0.10 | 0.73 | 3.03 | 3.84 | MDL | MDL | 94.43 |
| CCPb-35-glass | 7 | 75.14 | 0.10 | 11.93 | 0.82 | MDL | 0.12 | 0.84 | 3.26 | 3.82 | MDL | 0.01 | 96.04 |
| CCPb-35-glass | 8 | 73.04 | 0.13 | 11.46 | 0.82 | 0.18 | 0.11 | 0.76 | 2.85 | 3.88 | 0.02 | 0.04 | 93.29 |
| CCPb-35-glass | 9 | 72.72 | 0.07 | 11.75 | 1.20 | 0.04 | 0.18 | 0.77 | 3.04 | 3.81 | 0.02 | 0.02 | 93.62 |
| CCPb-35-glass | 10 | 74.55 | 0.19 | 12.07 | 1.15 | 0.14 | 0.12 | 0.74 | 3.30 | 3.84 | 0.02 | 0.02 | 96.14 |
| CCPb-35-glass | 11 | 71.91 | 0.18 | 11.94 | 1.03 | 0.14 | 0.58 | 0.96 | 3.50 | 3.59 | MDL | MDL | 93.85 |
| CCPb-35-glass | 12 | 70.84 | 0.09 | 11.61 | 1.00 | 0.03 | 0.15 | 0.78 | 3.08 | 3.81 | 0.02 | MDL | 91.39 |
| CCPb-35-glass | 13 | 69.86 | 0.10 | 11.36 | 0.69 | 0.04 | 0.12 | 0.85 | 2.78 | 3.83 | 0.01 | MDL | 89.63 |
| CCPb-36-glass | 14 | 74.75 | 0.16 | 11.26 | 0.72 | 0.11 | 0.12 | 0.53 | 3.29 | 3.93 | MDL | MDL | 94.89 |
| CCPb-36-glass | 15 | 73.87 | 0.06 | 11.29 | 0.59 | 0.01 | 0.12 | 0.56 | 2.94 | 3.95 | 0.03 | MDL | 93.42 |
| CCPb-36-glass | 16 | 72.97 | 0.08 | 11.21 | 0.63 | 0.04 | 0.12 | 0.65 | 2.81 | 4.01 | 0.02 | 0.10 | 92.62 |
| CCPb-36-glass | 17 | 75.30 | 0.20 | 11.63 | 0.63 | 0.03 | 0.11 | 0.65 | 3.08 | 3.96 | 0.02 | 0.10 | 95.71 |
| CCPb-36-glass | 18 | 73.77 | 0.13 | 11.15 | 1.01 | 0.02 | 0.08 | 0.70 | 3.59 | 3.93 | 0.02 | MDL | 94.39 |
| CCPb-36-glass | 19 | 71.63 | 0.10 | 10.99 | 0.66 | 0.09 | 0.12 | 0.70 | 3.24 | 3.93 | 0.04 | MDL | 91.50 |
| CCPb-36-glass | 20 | 73.28 | 0.08 | 11.47 | 0.96 | 0.12 | 0.08 | 0.64 | 3.32 | 4.01 | 0.01 | 0.03 | 94.01 |
| CCPb-36-glass | 21 | 75.45 | 0.11 | 10.78 | 0.90 | 0.10 | 0.08 | 0.54 | 3.10 | 3.93 | 0.02 | MDL | 94.99 |
| CCPb-36-glass | 22 | 74.60 | 0.07 | 11.61 | 0.97 | 0.04 | 0.15 | 0.69 | 3.55 | 3.92 | 0.03 | MDL | 95.62 |
| CCPb-36-glass | 23 | 72.40 | 0.13 | 11.72 | 0.56 | 0.01 | 0.12 | 0.61 | 2.86 | 4.05 | 0.02 | 0.16 | 92.64 |
| CCPb-36-glass | 24 | 73.67 | 0.15 | 11.84 | 0.60 | 0.13 | 0.12 | 0.66 | 3.13 | 3.94 | 0.02 | 0.06 | 94.32 |
| CCPb-36-glass | 25 | 74.84 | 0.10 | 11.61 | 0.77 | MDL | 0.13 | 0.66 | 2.98 | 4.01 | 0.02 | 0.03 | 95.15 |
| CCPb-36-glass | 26 | 74.48 | 0.10 | 11.55 | 0.82 | 0.02 | 0.08 | 0.64 | 2.77 | 3.89 | MDL | MDL | 94.35 |
| CCPb-37-glass | 27 | 75.37 | 0.11 | 11.69 | 0.61 | MDL | 0.08 | 0.68 | 3.48 | 3.97 | 0.03 | MDL | 96.04 |
| CCPb-37-glass | 28 | 75.74 | 0.19 | 11.45 | 0.49 | 0.04 | 0.09 | 0.64 | 3.22 | 4.12 | 0.02 | 0.03 | 96.03 |
| CCPb-37-glass | 29 | 75.34 | 0.13 | 11.31 | 1.18 | MDL | 0.15 | 0.62 | 3.02 | 4.09 | 0.02 | 0.01 | 95.86 |
| CCPb-37-glass | 30 | 76.37 | 0.17 | 11.71 | 0.98 | MDL | 0.19 | 0.70 | 3.41 | 4.17 | 0.02 | 0.03 | 97.75 |
| CCPb-37-glass | 31 | 75.68 | 0.12 | 11.76 | 0.54 | 0.06 | 0.12 | 0.52 | 3.12 | 4.04 | 0.03 | MDL | 95.98 |
| CCPb-37-glass | 32 | 73.89 | 0.10 | 11.77 | 0.77 | MDL | 0.04 | 0.64 | 3.21 | 4.17 | 0.03 | MDL | 94.62 |
| CCPb-37-glass | 33 | 75.67 | 0.12 | 11.86 | 0.54 | 0.07 | 0.08 | 0.61 | 3.34 | 4.21 | 0.03 | 0.04 | 96.56 |
| CCPb-37-glass | 34 | 76.43 | 0.15 | 12.09 | 1.15 | 0.05 | 0.06 | 0.87 | 3.32 | 3.80 | 0.02 | 0.02 | 97.98 |
| CCPb-37-glass | 35 | 74.39 | 0.20 | 11.61 | 0.53 | MDL | 0.12 | 0.65 | 2.76 | 4.07 | 0.03 | 0.04 | 94.41 |
| CCPb-37-glass | 36 | 75.97 | 0.08 | 11.62 | 0.66 | MDL | 0.09 | 0.57 | 3.14 | 4.08 | MDL | MDL | 96.22 |

**Appendix G, continued.**

| Sample | line | $SiO_2$ | $TiO_2$ | $Al_2O_3$ | $FeO^*$ | MnO | MgO | CaO | $Na_2O$ | $K_2O$ | Cl | $SO_3$ | Total |
|---|---|---|---|---|---|---|---|---|---|---|---|---|---|
| CCPb-38-glass | 37 | 73.94 | 0.15 | 11.76 | 0.62 | 0.10 | 0.09 | 0.72 | 3.34 | 4.03 | 0.03 | 0.02 | 94.80 |
| CCPb-38-glass | 38 | 74.33 | 0.16 | 11.92 | 0.84 | 0.06 | 0.12 | 0.81 | 3.01 | 3.91 | 0.02 | 0.01 | 95.20 |
| CCPb-38-glass | 39 | 74.12 | 0.09 | 11.95 | 0.64 | 0.03 | 0.18 | 0.64 | 3.17 | 3.94 | 0.02 | 0.03 | 94.81 |
| CCPb-38-glass | 40 | 73.45 | 0.07 | 11.74 | 1.06 | MDL | 0.12 | 0.68 | 3.50 | 3.83 | 0.03 | MDL | 94.50 |
| CCPb-38-glass | 41 | 73.95 | 0.11 | 11.59 | 0.96 | MDL | 0.10 | 0.77 | 3.36 | 3.94 | 0.02 | MDL | 94.79 |
| CCPb-38-glass | 42 | 73.62 | 0.11 | 11.80 | 0.65 | 0.14 | 0.06 | 0.69 | 3.20 | 3.92 | 0.01 | 0.08 | 94.29 |
| CCPb-38-glass | 43 | 75.31 | 0.13 | 11.78 | 0.68 | MDL | 0.17 | 0.73 | 3.14 | 3.88 | 0.02 | 0.05 | 95.88 |
| CCPb-38-glass | 44 | 73.39 | 0.15 | 11.68 | 0.57 | 0.05 | 0.08 | 0.67 | 3.31 | 3.92 | 0.01 | MDL | 93.84 |
| CCPb-38-glass | 45 | 73.93 | 0.13 | 11.57 | 0.99 | MDL | 0.23 | 0.80 | 3.55 | 3.83 | 0.03 | MDL | 95.07 |
| CCPb-38-glass | 46 | 74.52 | 0.08 | 11.66 | 0.81 | 0.04 | 0.11 | 0.72 | 3.24 | 3.91 | 0.04 | 0.02 | 95.15 |
| CCPb-39-glass | 47 | 74.70 | 0.13 | 11.79 | 0.65 | 0.02 | 0.07 | 0.68 | 3.08 | 4.08 | 0.01 | MDL | 95.22 |
| CCPb-39-glass | 48 | 74.90 | 0.06 | 11.98 | 0.57 | 0.07 | 0.13 | 0.66 | 3.25 | 4.00 | 0.03 | MDL | 95.64 |
| CCPb-39-glass | 49 | 76.20 | 0.14 | 12.05 | 0.91 | 0.07 | 0.10 | 0.61 | 3.62 | 3.93 | 0.02 | MDL | 97.64 |
| CCPb-39-glass | 50 | 75.54 | 0.08 | 11.97 | 0.86 | MDL | 0.08 | 0.60 | 3.07 | 3.99 | MDL | 0.02 | 96.21 |
| CCPb-39-glass | 51 | 74.14 | 0.13 | 11.81 | 0.57 | 0.03 | 0.12 | 0.60 | 3.30 | 3.97 | MDL | MDL | 94.68 |
| CCPb-39-glass | 52 | 76.51 | 0.12 | 11.65 | 0.54 | 0.06 | 0.09 | 0.63 | 2.99 | 4.06 | 0.04 | 0.05 | 96.74 |
| CCPb-39-glass | 53 | 76.25 | 0.08 | 11.71 | 0.77 | 0.06 | 0.08 | 0.56 | 3.54 | 3.94 | 0.04 | MDL | 97.02 |
| CCPb-39-glass | 54 | 75.45 | 0.08 | 12.07 | 0.64 | 0.20 | 0.08 | 0.59 | 3.35 | 3.98 | 0.02 | MDL | 96.47 |
| CCPb-39-glass | 55 | 74.93 | 0.14 | 11.70 | 1.04 | 0.09 | 0.06 | 0.61 | 3.26 | 3.93 | 0.03 | MDL | 95.80 |
| CCPb-39-glass | 56 | 75.30 | 0.13 | 11.95 | 0.41 | 0.08 | 0.10 | 0.75 | 3.23 | 3.99 | 0.02 | 0.09 | 96.06 |
| CCPb-39-glass | 57 | 73.89 | 0.13 | 11.82 | 0.61 | 0.09 | 0.08 | 0.66 | 3.81 | 4.07 | 0.03 | MDL | 95.19 |
| CCPb-39-glass | 58 | 75.12 | 0.16 | 12.13 | 0.51 | MDL | 0.06 | 0.72 | 3.34 | 4.02 | 0.01 | MDL | 96.09 |
| CCPb-40-glass | 59 | 73.67 | 0.21 | 11.98 | 0.74 | 0.16 | 0.09 | 0.80 | 3.32 | 3.84 | 0.01 | MDL | 94.82 |
| CCPb-40-glass | 60 | 70.49 | 0.11 | 11.37 | 0.76 | MDL | 0.13 | 0.76 | 3.40 | 3.38 | 0.02 | MDL | 90.43 |
| CCPb-40-glass | 61 | 74.23 | 0.15 | 11.95 | 0.90 | MDL | 0.13 | 0.94 | 3.30 | 3.78 | MDL | 0.03 | 95.42 |
| CCPb-40-glass | 62 | 74.33 | 0.12 | 11.74 | 0.79 | 0.15 | 0.15 | 0.73 | 3.36 | 3.79 | MDL | MDL | 95.17 |
| CCPb-40-glass | 63 | 72.81 | 0.11 | 11.62 | 0.71 | 0.05 | 0.16 | 0.81 | 3.13 | 3.91 | MDL | MDL | 93.33 |
| CCPb-40-glass | 64 | 74.01 | 0.10 | 12.05 | 1.33 | 0.03 | 0.18 | 0.73 | 3.09 | 3.86 | 0.03 | 0.03 | 95.45 |
| CCPb-40-glass | 65 | 72.51 | 0.14 | 11.45 | 1.48 | 0.07 | 0.58 | 0.83 | 3.20 | 3.73 | 0.02 | 0.08 | 94.09 |
| CCPb-40-glass | 66 | 71.72 | 0.13 | 11.86 | 1.06 | 0.04 | 0.10 | 0.75 | 3.07 | 3.80 | 0.02 | 0.03 | 92.60 |
| CCPb-40-glass | 67 | 70.49 | 0.06 | 11.66 | 0.74 | 0.07 | 0.13 | 0.78 | 3.13 | 3.86 | 0.05 | MDL | 90.96 |

**Appendix G, continued.**

| Sample | line | $SiO_2$ | $TiO_2$ | $Al_2O_3$ | $FeO^*$ | MnO | MgO | CaO | $Na_2O$ | $K_2O$ | Cl | $SO_3$ | Total |
|---|---|---|---|---|---|---|---|---|---|---|---|---|---|
| CCPb-41-glass | 68 | 74.44 | 0.15 | 11.72 | 1.05 | 0.04 | 0.11 | 0.79 | 3.57 | 3.90 | MDL | MDL | 95.77 |
| CCPb-41-glass | 69 | 74.45 | 0.09 | 11.69 | 0.78 | 0.03 | 0.12 | 0.77 | 3.12 | 3.97 | 0.01 | 0.01 | 95.03 |
| CCPb-41-glass | 70 | 74.33 | 0.14 | 11.79 | 0.75 | 0.06 | 0.13 | 0.84 | 3.36 | 3.92 | 0.02 | 0.01 | 95.34 |
| CCPb-41-glass | 71 | 74.19 | 0.13 | 11.65 | 0.56 | 0.10 | 0.10 | 0.81 | 3.01 | 3.93 | 0.01 | 0.06 | 94.56 |
| CCPb-41-glass | 72 | 74.01 | 0.08 | 11.57 | 0.84 | MDL | 0.13 | 0.78 | 3.05 | 3.93 | 0.01 | MDL | 94.40 |
| CCPb-41-glass | 73 | 75.14 | 0.08 | 11.71 | 0.75 | 0.02 | 0.11 | 0.81 | 3.44 | 3.96 | 0.02 | MDL | 96.03 |
| CCPb-41-glass | 74 | 74.34 | 0.07 | 11.49 | 0.70 | MDL | 0.11 | 0.79 | 3.19 | 3.95 | 0.01 | MDL | 94.66 |
| CCPb-41-glass | 75 | 74.34 | 0.02 | 11.69 | 0.68 | 0.03 | 0.10 | 0.75 | 3.45 | 3.95 | 0.02 | MDL | 95.05 |
| CCPb-41-glass | 76 | 73.41 | 0.10 | 11.68 | 0.57 | 0.04 | 0.09 | 0.79 | 3.29 | 3.94 | 0.01 | MDL | 93.94 |
| CCPb-41-glass | 77 | 73.37 | 0.08 | 11.65 | 0.72 | 0.05 | 0.11 | 0.80 | 3.33 | 3.95 | 0.03 | MDL | 94.11 |
| CCPb-42-glass | 78 | 76.81 | 0.13 | 12.05 | 0.72 | 0.11 | 0.08 | 0.55 | 3.02 | 4.10 | 0.04 | MDL | 97.60 |
| CCPb-42-glass | 79 | 74.14 | 0.15 | 11.90 | 0.56 | MDL | 0.08 | 0.60 | 3.23 | 4.06 | 0.03 | 0.09 | 94.84 |
| CCPb-42-glass | 80 | 76.33 | 0.09 | 11.87 | 0.69 | 0.11 | 0.13 | 0.67 | 3.05 | 4.13 | 0.03 | MDL | 97.10 |
| CCPb-42-glass | 81 | 74.10 | 0.13 | 11.66 | 0.77 | 0.02 | 0.11 | 0.53 | 3.02 | 3.99 | 0.02 | 0.09 | 94.44 |
| CCPb-42-glass | 82 | 75.79 | 0.16 | 11.59 | 0.93 | 0.07 | 0.06 | 0.50 | 3.38 | 4.02 | 0.03 | 0.03 | 96.59 |
| CCPb-42-glass | 83 | 74.32 | 0.10 | 11.55 | 1.04 | 0.03 | 0.09 | 0.60 | 3.04 | 4.02 | 0.01 | MDL | 94.80 |
| CCPb-42-glass | 84 | 76.69 | 0.13 | 11.73 | 0.96 | MDL | 0.07 | 0.52 | 3.37 | 4.09 | MDL | MDL | 97.57 |
| CCPb-42-glass | 85 | 72.85 | 0.05 | 11.97 | 0.89 | 0.05 | 0.05 | 0.60 | 2.90 | 3.99 | 0.02 | 0.07 | 93.43 |
| CCPb-43-glass | 86 | 73.87 | 0.12 | 10.73 | 0.63 | 0.09 | 0.07 | 0.44 | 2.94 | 4.37 | MDL | MDL | 93.26 |
| CCPb-43-glass | 87 | 75.44 | 0.19 | 11.53 | 0.80 | 0.08 | 0.10 | 0.42 | 3.08 | 4.44 | MDL | MDL | 96.10 |
| CCPb-43-glass | 88 | 77.88 | 0.12 | 11.18 | 0.45 | MDL | 0.06 | 0.37 | 2.99 | 4.44 | MDL | MDL | 97.49 |
| CCPb-43-glass | 89 | 76.27 | 0.15 | 10.84 | 0.53 | MDL | 0.06 | 0.43 | 2.85 | 4.30 | MDL | 0.01 | 95.44 |
| CCPb-43-glass | 90 | 74.92 | 0.14 | 10.81 | 0.90 | MDL | 0.09 | 0.37 | 2.88 | 4.33 | 0.02 | MDL | 94.45 |
| CCPb-43-glass | 91 | 77.30 | 0.11 | 10.62 | 1.03 | 0.04 | 0.12 | 0.40 | 2.71 | 4.38 | 0.02 | MDL | 96.73 |
| CCPb-43-glass | 92 | 74.99 | 0.14 | 11.47 | 0.59 | 0.02 | 0.08 | 0.44 | 3.33 | 4.53 | MDL | 0.04 | 95.64 |
| CCPb-43-glass | 93 | 75.35 | 0.19 | 10.47 | 0.73 | 0.10 | 0.08 | 0.41 | 2.89 | 4.20 | MDL | MDL | 94.43 |
| CCPb-43-glass | 94 | 75.45 | 0.09 | 11.45 | 0.36 | MDL | 0.04 | 0.45 | 2.92 | 4.39 | MDL | MDL | 95.15 |

Values marked MDL were below the minimum detection limit.